Numerical and Experimental Study of Personalized Ventilation

Gao Naiping

Department of Building Services Engineering,
The Hong Kong Polytechnic University

A thesis submitted in partial fulfillment of the requirements for the
Degree of Doctor of Philosophy

August, 2006

Certificate of Originality

I hereby declare that this thesis is my own work and that, to the best of my knowledge and belief, it reproduces no material previously published or written, nor material that has been accepted for the award of any other degree or diploma, except where due acknowledgement has been made in the text.

Gao Naiping

Department of Building Services Engineering
The Hong Kong Polytechnic University
Hong Kong SAR, China
August, 2006

Abstract

Abstract of thesis entitled: Numerical and experimental study of personalized

ventilation

Submitted by   :   Gao Naiping

For the degree of   :   Doctor of Philosophy

at The Hong Kong Polytechnic University in August, 2006.

Conventional air conditioning systems in buildings are designed to create a uniform environment across the entire occupied zone. Individual thermal preferences cannot be accommodated, and the fresh supply air is polluted by indoor contaminants before its inhalation by the occupants. Personalized ventilation (PV) is a novel development in the field of heating, ventilation, and air conditioning (HVAC) that has the potential to eliminate the deficiencies of conventional systems. The primary aim of this work is to measure the ventilation effectiveness of PV, to find out the human response to PV, and to develop a numerical thermal manikin (NTM) for the evaluation of the non-uniform thermal environment that is generated by PV. Experimental and numerical studies are reported in this thesis. The work that is presented consists of five parts: 1) a review of PV and computational fluid dynamics (CFD) studies of the thermal environment around a human body, 2) an experimental study of the ventilation seat type of PV, 3) the development of an NTM and its application to investigate the micro-environment that surrounds a human body and the performance of the ventilation seat, 4) the coupling of CFD and an inner-body thermoregulation model to predict local thermal sensation and comfort in the non-uniform thermal environments that are created by three different PV systems, and 5) a comparison of PV performance in a displacement ventilated room and a mixing ventilated room and a discussion of some significant issues of PV.

Experiments using tracer gas and a heated, breathing thermal manikin with an artificial lung are carried out to measure the pollutant exposure reduction effectiveness (PER) of a chair-based PV system (a ventilation seat) that has an air supply nozzle that is located at the microphone position and serves cool, fresh air directly to the nose and mouth. The personalized airflow rate and temperature are maintained at 0.4-2.5 l/s and 15-22℃, respectively. The PER is found to increase when the air supply flow rate and temperature increase. At an operating ventilation rate of 2.5 l/s, the pollutant level in the air that the user inhales can be reduced by around 76%.

Subjective measurements are taken to evaluate human responses to the chair-based PV, and the perceived air quality; irritation at the eyes, nose, and lips; thermal sensation in different body parts; and overall thermal comfort are surveyed. In the personalized air temperature range of 15-22℃, the perceived air quality is greatly improved without any facial discomfort, such as eye irritation and the sensation of a local draft feelings through correct design. Personalized air with a temperature that is below the air temperature in a room creates a "cool head" and increases the thermal comfort level in comparison to conventional mixing ventilation. People are found to be more sensitive to the flow rate of personalized air than to its temperature. To enrich thermal comfort theory, it is highlighted that the perceived air quality is significantly affected by the velocity of air on the face.

Based on a review of existing work on the simulation of the micro-environment around a human body, an NTM with a realistic geometry of the body is developed to visualize the airflow in the breathing zone. This NTM, the skin surface of which is composed of small patches, is obtained by the laser scanning of a thermal manikin. In a CFD simulation using a commercial code (Fluent), the NTM surface is

discretized into triangular elements with an average length scale of 4 mm. With the help of the NTM, the interaction between PA, respiration airflow, and the thermal plume around the body is clarified. The PER values from the simulation are compared to the experimental values, and a reasonable agreement is found. Parametric studies are conducted to investigate the effects of room air movement, personalized air temperature, and the turbulence intensity of personalized air on the performance of PV.

Equipped with an up-to-date thermoregulation model that was developed at the University of California at Berkeley, the NTM, which mimics a real person in terms of heat and mass loss to the surrounding environment, is integrated into the CFD model for the evaluation of thermal comfort. The NTM is divided into 16 segments. The local air conditions, that is, the air velocity and air temperature, are input into the thermoregulation model manually to calculate the various skin temperatures, which are then fed back to the CFD as the body boundary conditions. A new set of local air conditions is created and the process is repeated until convergence. This coupling simulation is validated against some experimental data from the literature. In further steps, the facial thermal comfort level and ventilation effectiveness are comprehensively assessed using a state of the art local thermal comfort prediction model. The developed NTM may also be applied in other fields, such as the evaluation of airborne infection control technologies and thermal comfort levels in non-uniform and transient environments in vehicle HVAC engineering.

The performance of PV in displacement ventilation and mixing ventilation systems is modeled and compared. In general, it is found that the combination of PV systems with displacement ventilation systems provides better indoor air quality and more opportunities for energy saving than the combination of PV with mixing ventilation

systems. In the both modes, the inhaled air quality and overall thermal comfort level are determined by the conditions of the personalized air and the room air. With the head cooling function of PV, the limitation on the vertical temperature difference in the occupied zone of a building can be increased by up to 6℃.

Acknowledgements

Table of Contents

List of Figures

List of Tables

Nomenclature

Variable	Description	Unit
a	Turbulence coefficient, 0.076 for circular jet flows	ND
ACE	Air change efficiency	ND
c_P	Specific heat of air	J/(kg℃)
C	Mass fraction of sneezed air in inhaled air	ND
C_a	Tracer gas concentration of ambient air	ppm
C_{ex}	Tracer gas concentration of exhaled air	ppm
C_f	Tracer gas concentration of personalized air	ppm
C_{floor}	Contaminant concentration at floor level	ppm
$C_{inhalation}$	Contaminant concentration of inhaled air	ppm
C_L	Tracer gas concentration of inhaled air	ppm
C_{ref}	Contaminant concentration at breathing height	ppm
C_{room}	Mean indoor contaminant concentration	ppm
C_s	Pollutant level in the air supply	ppm
d_0	Diameter of the circular air outlet	m
D_t	Temperature difference between personalized and room air	℃
E	Emission rate of indoor pollutants	kg/s
E_s	Latent heat loss from a human body	W
f	Mass fraction	ND
g	Gravitational acceleration	m/s^2
g_i	Gravitational acceleration in the direction x_i	m/s^2
Gr	Grashof number	ND
h_c	Convective heat transfer coefficient	W/(m^2℃)
k	Turbulence kinetic energy	J/kg
L	Characteristic length	m
M	Metabolic heat production	W
P	Pressure	pa

P_a	Vapor pressure in the room air	pa
PER	Pollutant exposure reduction	ND
PPD	Predicted percentage of dissatisfaction	ND
PS	Predicted percentage of satisfaction	ND
q_c	Heat flux	W/m^2
Q	Energy source term	W/m^3
Q_c	Convective heat loss from a human body	W
Q_m	Total heat loss from a human body	W
Q_r	Radiative heat loss from a human body	W
Q_{res}	Heat loss caused by respiration	W
Q_s	Heat loss from the skin surface	W
Q_t	Sensible heat loss from a human body	W
Q_{vent}	Room ventilation rate	L/s
r_0	Radius of the circular air outlet	m
Ra	Rayleigh number	ND
Re	Reynolds number	ND
s	Axial distance from the nose to the air terminal device	m
s_n	Length of the jet flow development region	m
Sc	Schmidt number	ND
Sh	Sherwood number	ND
S_φ	Source term of φ for transport equation	ND
t	Time	s
t_a	Ambient air temperature	℃
t_{in}	Room air supply temperature	℃
t_s	Human body mean skin temperature	℃
T	Temperature	℃
T_f	Local temperature of personalized air	℃
T_{op}	Operative temperature	℃
T_u	Turbulence intensity	ND

U_i U_j	Velocity component in direction x_i x_j	m/s
v	Average air speed at the heat-height, mid-body, and foot-levels	m/s
v_f	Local air speed forced by personalized ventilation	m/s
V	Local mean air speed	m/s
V_1	Mean personalized air speed at the face	m/s
V_f	Personalized air supply rate	L/s
$V_{F,L}$	Volume of personalized air in inhaled air	L/s
V_L	Inhaled air volume	L/s
x_i x_j	Direction of velocity component	ND
y	Normal distance from the wall at the cell centers	m

Greek symbols

α	Thermal diffusivity	m²/s
β	Coefficient of gas thermal expansion	℃⁻¹
ε	Dissipation rate of turbulence energy	W/kg
φ	Scalar quantity for concentration	ND
η	Infection index	ND
η_e	Effective entrainment ratio	ND
η_{PER}	Pollutant exposure reduction index	ND
η_u	Utilization efficiency	ND
λ	Thermal conductivity	W/(m℃)
μ	Dynamic viscosity	kg/(ms)
ν	Kinematic viscosity	m²/s
$\widehat{\nu}$	Effective viscosity ratio	ND
θ'	Instantaneous temperature	℃
ρ	Air density	kg/m³
τ_n	Nominal ventilation time constant	s
τ_{avg}	Average age of air in the breathing zone	s
Γ_φ	Diffusion coefficient for φ	

Note: ND = No dimensions.

Chapter 1
Introduction

The primary aim of heating, ventilation, and air conditioning (HVAC) is to provide outdoor air and to maintain comfortable conditions for building occupants in terms of air quality and thermal comfort. The thermal comfort zone, which is defined by ASHRAE Standard 55 (1992) and an ISO Standard (1993), is the set of environmental conditions that 80% or more of the occupants regard as being thermally acceptable. A field survey of the response of occupants to the indoor environment that is created by displacement ventilation found that almost one half of the occupants reported being bothered daily by uncomfortable room temperatures (Melikov et al. 2005). Ventilation constitutes the major energy use in building heating and cooling. Currently, ventilation rate specifications are based on ASHRAE Standard 69, which is a *de facto* international standard that promulgates a minimum value of 5 to 10 l/s per person. However, the human physiological respiration rate is only 0.08 l/s. This 100-fold difference between supply and demand is caused by the fact that the fresh supply air is mixed with indoor air before inhalation by the occupants in the indoor environment. This clearly indicates that the conventional air supply method that is based on the full-mixing ventilation principle is inherently inefficient.

Personalized ventilation (PV) has been proposed as a possible solution to these problems, and is expected to greatly improve inhaled air quality. The basis of PV is that a person will inhale air from the unpolluted core of a supply jet. In principle, this means that a much-reduced fresh air supply rate is required compared to diluting the air in an entire space, as is normally practiced.

However, there are a number of fundamental issues that need to be investigated before such a system can be widely used. Human subjects are the objects of service in air conditioning systems, but the thermal flow and transient respiration flow that are induced by the human body are poorly understood, particularly in relation to their interaction with different air supply methods in built or man-made environments. Further in-depth investigation of these airflows and their interaction is the focus of this study. The first issue with PV is that although the average respiration air requirement is 0.08 l/s for the average adult, the actual inhalation and exhalation processes are transient, and the peak airflow rate is likely to be much higher than this average time value. Second, a buoyancy-driven natural convection plume flow is naturally formed around the human body that interacts with the respiration flow. Third, the direct fresh air supply jet that serves cool, dry air creates a thermal sensation on the surface of the body. Finally, a background climate system must be provided to control the global thermal environment in the building space. Ultimately, under the influence of all of these factors, the minimum ventilation air supply rate and the velocity, temperature, humidity, turbulence level, direction, and distance to the occupants of the personalized air must be optimized to achieve the most cost-effective design. The two key physical phenomena – the transient respiratory flow and the thermal flow that is induced by the human body due to buoyancy effects – and their fluid-dynamic interaction are seldom studied, and a limited amount of experimental and numerical investigations can be found in the scientific literature.

This study has four outcomes. First, in the experimental work the performance of one air terminal device that is installed in a PV system is evaluated, and the human

response to a particular kind of PV (a ventilation seat) is surveyed. Second, in the simulation work an effort has been made to develop a generic numerical tool – a three-dimensional numerical thermal manikin (NTM) with a thermoregulation model and realistic geometry – that is able to provide further insight into human thermal comfort. Third, the NTM is used to investigate the technical feasibilities of using PV to reduce human exposure to indoor pollutants through respiration at a reduced ventilation rate and using local air movement to achieve individual thermal comfort control. Fourth, the possible parameters of a PV system, including distance and direction relative to the facial area, flow rate, velocity, temperature, and turbulence level, are assessed.

The work in this thesis is presented in the following order.

- Chapter 2 presents a review of PV technology and the state of the art CFD simulation of the micro-environment around a human body.

- Chapter 3 describes the experimental work and survey of human subjects.

- Chapter 4 presents the development of the numerical thermal manikin and a parametric study of PV and indoor personal exposure to exhaled air.

- Chapter 5 presents the coupling of CFD with a whole-body thermo-regulation model and its application to the evaluation of PV.

- Chapter 6 gives the overall conclusions and some recommendations for future work.

Chapter 2
Literature Review

2.1 Personalized ventilation

2.1.1 Introduction

In modern buildings, the never-ending complaints of occupants about thermal comfort and indoor air quality call for new ventilation techniques. Task/ambient air conditioning (TAC) and personalized ventilation (PV) are two systems that have been developed to provide individual control, accommodate individual preferences for thermal environment, improve inhaled and perceived air quality, and offer the potential for increased work performance. TAC, which is analogous to task/ambient lighting, aims to establish a non-uniform thermal environment to improve the thermal comfort level of building occupants, and has been investigated since under-floor air distribution (UFAD) was introduced (Matsunawa et al. 1995; Sodec and Craig 1990). PV, which was proposed by Fanger (1999; 2000; 2001), is analogous to a personal computer, and gently supplies fresh air close to the nose so that the user can inhale clean, cool, and dry air from the core of the jet flow. Fanger (2001) pointed out that "we would hesitate to drink water from a swimming pool polluted by human bio-effluent. Still we accept consuming indoor air that has previously been in the lungs of the other persons and is polluted by human bio-effluent and other contaminants generated in the space." Although some researchers regard TAC and PV to be synonymous, their original intent is not the same.

However, TAC and PV do have two key features in common: the air outlet is installed close to the occupant and is under the control of the user. Users are

provided with a broad menu of thermal environments, as distinct from the conventional one-for-all service. In summary then, with total volume (TV) ventilation and air conditioning systems building occupants must passively accept what they are given, whereas with TAC or PV they can actively design the air conditions that they desire. The release of the control of the thermal environment around the human body from facilities managers to individual users with TAC or PV systems may eliminate the thermostat wars that occur in modern offices (Heinemeier et al. 1990).

With PV systems, each user is equipped with one or more air outlets, which can be called personalized air diffusers. Normally, the distance between the personalized air diffuser and the occupant is less than 0.8 m, except in cases in which the diffuser is mounted at floor level. As personalized air diffusers are positioned closer the human body, and especially the head region, the air conditioning ability attenuates and the improvement of the quality of the inhaled air becomes much more significant, which consequently modifies the emphasis of the "task" from thermal comfort to inhaled air quality. For example, the temperature level at a single workstation can be regulated over a sizeable range of 7℃ by desktop personalized air diffusers (Bauman and Webster 2001), but the improvement in the ventilation effectiveness is not remarkable (Fisk et al. 1990). In contrast, Bolashikov et al. (2003) reported that inhaled air that is composed of 100% personalized air can be achieved with a round movable panel (RMP) diffuser, and that air that is up to 80% personalized air can be attained with a headset-incorporated supply (Headset) system. The cooling capacities of these systems as expressed by the change in the whole-body equivalent temperature range from less than 0.5-2.2℃ for the RMP to almost 0℃ for the

Headset system. With a desk-edge-mounted personalized ventilation system operating at a flow rate of 3.5-6.5 l/s, it has been found that it is possible to obtain an air change effectiveness (ACE) of approximate 1.5, which represents a 50% increase in the effective ventilation rate in the breathing zone (Faulkner et al. 2004). An ACE of 1.5 implies a reduced outdoor air supply rate and reduced energy use based on the current ASHRAE ventilation standard (ASHRAE 2001). The survey results of Bauman et al. (1998) showed that in office buildings the installation of a desktop personalized ventilation system leads to a great increase in the overall occupant satisfaction with thermal quality, acoustical quality, and air quality. Kaczmarczyk (2003) proved that supplying outdoor air by means of personalized ventilation reduced complaints of headaches and improved the ability of occupants to think and concentrate. Tham et al. (2003) compared the energy consumed at an indoor ambient temperature of 26℃ and a personalized air supply temperature of 20℃ or 23℃ with that in a mixing ventilation system in which the indoor temperature was maintained at 23℃. They found that a PV system with a flow rate of 7-11 l/s/person in conjunction with a background mixing ventilation system that operated to maintain an ambient temperature of 26 ℃ had a 29.5% smaller cooling load and consumed 27% less electricity than the mixing ventilation system at an ambient temperature of 23℃.

In this thesis, all of the aforementioned systems in which the air diffuser is located close to the human body and is under the control of the user are referred to as personalized ventilation (PV) systems.

2.1.2 Various types of personalized ventilation

Due to the limited cooling capacity of PV, it must be integrated into a background total volume ventilation and air conditioning system. In many cases, personalized air is supplied from the underfloor plenum, with an ambient zone that is conditioned by a UFAD system (Hiwatashi et al. 2000; Bauman et al. 1995; Cermak and Melikov 2003). Nakamura and Mizuno (1996) combined PV with mixing ventilation by serving personalized air from the underfloor plenum. Tamblyn (1995) released personalized air through a large ducted adjustable ceiling nozzle in a mixing ventilation system. Loomans (1999) studied the feasibility of combining displacement ventilation with PV, which he called desk displacement ventilation (DDV), to create a micro-climate by supplying air below the desk close to the occupant over a relatively large area at a low velocity (0.1-0.2 m/s) and a relatively high temperature (20-22℃). The DDV system is intended to "combine the positive features of displacement ventilation e.g., higher ventilation effectiveness when compared to normal mixing ventilation, with those for task conditioning, e.g. control of thermal comfort conditions" (Loomans 1999). DDV differs from underfloor task/ambient air conditioning in that cool air is supplied at a low momentum to weaken the entrainment function (Loomans et al. 1996; Loomans and Rutten 1997; Roos 1998). However, because the room air diffuser and personalized air diffuser are combined into one by locating the diffuser close to the occupant, the boundary of the personal micro-climate is not clear. Furthermore, under normal conditions additional cooling is required, such as a cooled ceiling, because of the limited cooling capacity of DDV. Chang et al. (2004) studied the characteristics of an indoor environment that utilizes hybrid ventilation (natural and mechanical ventilation) and personalized

ventilation, and found that energy savings could be made and human thermal comfort increased.

PV systems can be classified into desk-based, partition-based, and chair-based types according to the position of the personalized air diffuser. Melikov et al. (2002) investigated a desk-based PV with the air outlet at five locations: 0.2 m in front of the occupant's face, on the monitor at a distance of 0.4 m from the edge of the desk; a vertical grill on the edge of the desk; a horizontal grill on the edge of the desk, and two nozzles on the desk 0.8 m from the occupant that generated air jets toward the occupant's face (Figure 2.1). Personalized air diffusers can also be mounted on the partitions in modern offices. Conditioned air is then supplied toward the face of the occupant from the front side (Jeong 2003; Hiwatashi et al. 2000), or is blown upward from a wide-cover outlet to fall down over the body as a result of the different density of the cool fresh air (Figure 2.2).
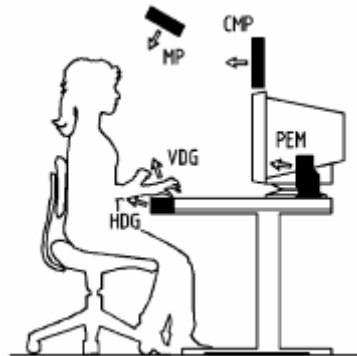
Figure 2.1 Five types of desk-based personalized ventilation system: movable panel (MP), computer monitor panel (CMP), vertical desk grill (VDG), horizontal desk grill (HDG), and personal environmental module (PEM) (Melikov et al. 2002)
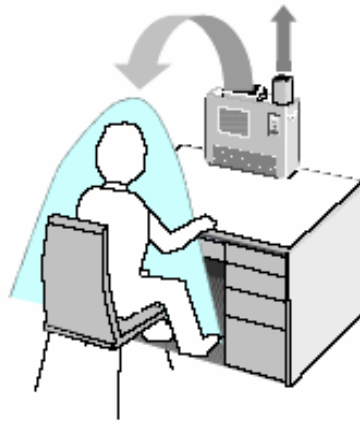
Figure 2.2 A wide-cover partition-based personalized ventilation system (Chikamoto et al. 2004)

Other personalized air diffusers are mounted on chairs, with the position of the fresh air supply nozzle being adjustable by the seated user (Niu 2005; Nobe et al. 2003). Fresh air is ducted from the bottom of the seat (Figure 2.3), which means that an occupant who is seated for a prolonged period, such as on a long-distance commercial flight, can enjoy inhaled air that is much purer than the current standards. Should the occupant need to move around, the ventilation nozzle can be conveniently moved aside to function as a normal air supply outlet. This ventilation seat is expected to be applicable in many other built environments, such as seats in theatres, cinemas, lecture halls, and auditoriums; passenger seats on commercial airplanes, and driver seats in taxis and buses. If the principle of chair-based personalized air is used, then it is essential that a separate HVAC system be established for thermal comfort. "It should be remembered that the idea of the personalized air system is to provide clean air to inhale, while the task of the individual thermal control system is to provide thermal neutrality for the entire human body" (Fanger 2001).
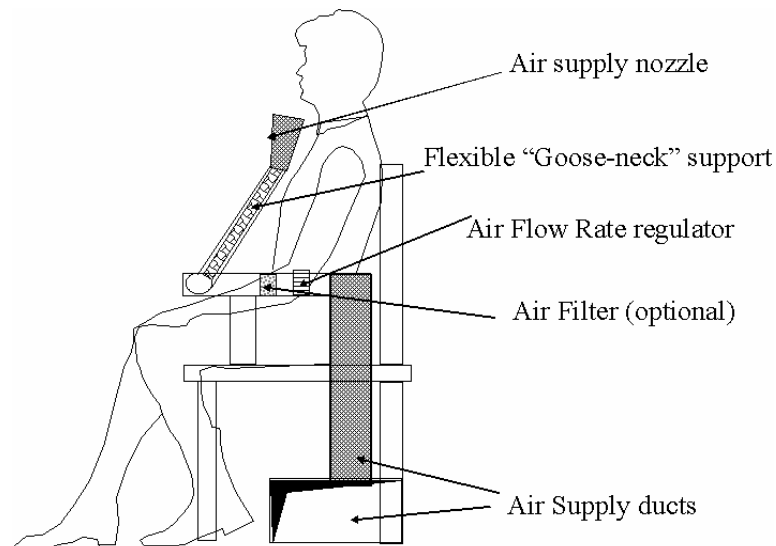
Figure 2.3 Ventilation seat with an adjustable personalized air supply nozzle (Niu 2005)

PV systems can be divided into two types depending on how they are integrated with the total volume ventilation and air conditioning system (Bauman and Arens 1996). In the first type, the personal micro-climate and ambient environment are controlled by two distinct air distribution systems. The air conditioning system of the ambient environment operates in the same manner as in a conventional HVAC system, and the ambient air of the room is conditioned without consideration of the PV system, which is used only when the occupant desires a local micro-climate that is different from the ambient condition. The cost of this arrangement is high, because it means that a supplementary ventilation system must be added to the conventional HVAC system, which involves retrofit installation. In the second type, the personal and ambient environment is controlled in a single air distribution system. Personalized air responds to the removal of part of the building heat load. The cost of this configuration is lower than that of the first type, but the individual adjustment of the PV system may affect the operation of the whole HVAC system and the temperature and airflow in the ambient space. Therefore compensating measures or limits to the amount of individual control should be incorporated in the design of such systems.

A pollutant exposure reduction index (PER) η_{PER}, which is equal to the fraction of personalized air in inhaled air, is used to express the effectiveness of personalized air in reducing exposure to pollutants (Zuo 2003). η_{PER} equals one if the inhaled air is totally composed by personalized air. The personalized air utilization efficiency η_u is determined as the ratio of actual personalized air in the inhaled air to the total supplied personalized air. η_{PER} quantifies the quality of the inhaled air, and η_u quantifies the efficiency of the personalized ventilation system. η_{PER} and η_u can be calculated from the following equations.

$$\eta_{PER} = \frac{V_{F,L}}{V_L} = \frac{C_L - C_a}{C_f - C_a} \tag{2.1}$$

$$\eta_u = \eta_{PER} \times \frac{V_L}{V_f}, \tag{2.2}$$

where

C_L = the CO_2 concentration of the inhaled air,

C_f = the CO_2 concentration of the personalized air,

C_a = the CO_2 concentration of the ambient air,

V_L = the volume of the inhaled air,

$V_{F,L}$ = the volume of personalized air in the inhaled air V_L, and

V_f = the total supplied personalized air volume.

2.1.3 Key parameters of personalized ventilation

Some parameters of PV that have been investigated by researchers are listed in Table 2.1. It is obvious there is a large difference between them. The important factors of

11

PV include the distance between the air outlet and the human body, airflow direction, cross-section area, air outlet geometry, air supply temperature, humidity, velocity, and turbulence intensity. These factors determine the characteristics of personalized airflow and its interaction with the respiratory flow and hot plume flow that exists around the human body, and therefore the performance of PV. Comprehensive analyses of this interaction and detailed reviews of PV have been conducted, and readers are directed to Melikov (2004) and Kaczmarczyk (2003) for more information.

Table 2.1 Parameters of various types of PV

Authors	Position	Geometry (cm)	Outlet numbers	Temperature (℃)	Flow rate (l/s)
Akimoto et al. 2003	Desktop-based	Rectangular	2	23-26	3-22
Bauman et al. 1993	Desktop-based	Rectangular	2	18-20	20-70
Bolashikov et al. 2003	Head set, 2-6 cm to the nose	Rectangular 3.5×0.8	1	20-23	0.18-0.5
Bolashikov et al. 2003	Desktop-based movable	Circular A = 268 cm^2	1	20-23	5-15
Cermak and Melikov 2003	On the desk surface, 45cm from the face	Rectangular	1	20	10-15
Cho et al. 2001	Desktop-based	Rectangular	2	24	30-160
Faulkner et al. 1993	Desktop-based	Rectangular 10×5.8 or 23×7.8	2	15.5-22	22-95
Fisk et al. 1990	On a raised access floor	Circular grilles D =12.7	4	18	40-90
Niu et al. 2004	Beneath the chin	Circular and Rectangular nozzle	1	20	0.1-3.0
Hayashi et al. 2003	Desktop-based	Rectangular	2	23-30	Jet velocity

					1.0-3.4 m/s
Jeong 2003	Partition-based	Rectangular	2-3	24	Air velocity in breathing zone 0.1-0.7m/s
Kaczmarczyk 2003	On the desk surface, 30-40cm from the face	Rectangular	1	20-23	3-15
Loomans 1999	At the bottom of the desk	Rectangular	1	20-22	10-47
Melikov et al. 2002	Desktop-based, five locations	Rectangular	1-2	20	Less than 5-23
Sekhar et al. 2005	Desktop-based	Rectangular	1	20-26	7-15
Tsuzuki et al. 1999	On the desk surface	Rectangular	2	19-25	6-71
Tsuzuki et al. 1999	At the front edge under the desk surface	Rectangular	2	19-25	0-7
Tsuzuki et al. 1999	On a raised access floor	Circular grilles D =12.7	4	19-25	43-85

The air temperature in PV systems typically ranges from 20-23℃, with the lowest value being 18℃ and the highest 26℃. The temperature should not be higher than the room air temperature, because people find the inhalation of cool air to be pleasant (Fang et al. 1998a). Due to the temperature difference, the flow of personalized air is a non-isothermal jet flow, and therefore the bent trajectory of the personalized airflow must be taken into account so that the core of the supply flow occurs in the nose zone. In some systems, the personalized air temperature is adjustable through an

electric pre-heater, or by mixing with the room return air. In the latter type of system, an increase in the temperature of the personalized air decreases the ratio of fresh outdoor air in the supply air.

To reach the breathing zone, a minimum flow rate is required to ensure a certain target air velocity. Assuming that an air terminal device (ATD) with a circular outlet is set in front of the face at a distance of s in the range of 30~50 cm, which has been proved to be preferred by building occupants (Kaczmarczyk 2003), and that the personalized airflow is a circular turbulent jet flow. To achieve high ventilation efficiency, the human face, and especially the nose, should be located in the jet flow development region where there is a core of flow with an undiminished velocity that is equal to U_0. In an experiment by Melikov and Zhou (1996), it was found that an invading flow at a mean speed of 0.1 m/s and a turbulence intensity of 10% was able to penetrate the enclosing free convection flow. Here, the target velocity V_1 is expected to exceed 0.15 m/s. The relationship between the personalized airflow rate and the radius of the circular outlet in isothermal conditions can be derived (Figure 2.4) according to the following empirical equations (Xu 1995).

$$s_n = 0.672 \frac{r_0}{a} > s \qquad (2.3)$$

$$\frac{V_1}{U_0} = \frac{1 + 0.76 \frac{as}{r_0} + 1.32 \left(\frac{as}{r_0}\right)^2}{1 + 6.8 \frac{as}{r_0} + 11.56 \left(\frac{as}{r_0}\right)^2} \ (V_1 \geq 0.15, U_0 = 4V_f /(\pi d_0^2)), \qquad (2.4)$$

where

U_0 = the outlet air velocity of the ATD in m/s,

V_1 = the mean personalized air velocity at the face in m/s,

s_n = the length of the jet flow development region in m,

s = the axial distance from the nose to the ATD,

r_0 = the radius of the circular outlet of the ATD in m,

d_0 = the diameter of the circular outlet of the ATD in m,

a = the turbulence coefficient of 0.076 for the circular jet flow, and

V_f = the personalized airflow rate at l/s.

Setting the ATD far from the face or enlarging the ATD outlet demands a higher personalized airflow rate. If all of the fresh air, that is, 10 l/s/person (ASHRAE 62-2001), is supplied by PV, then the radius of the ATD should be less than 7~9 cm.
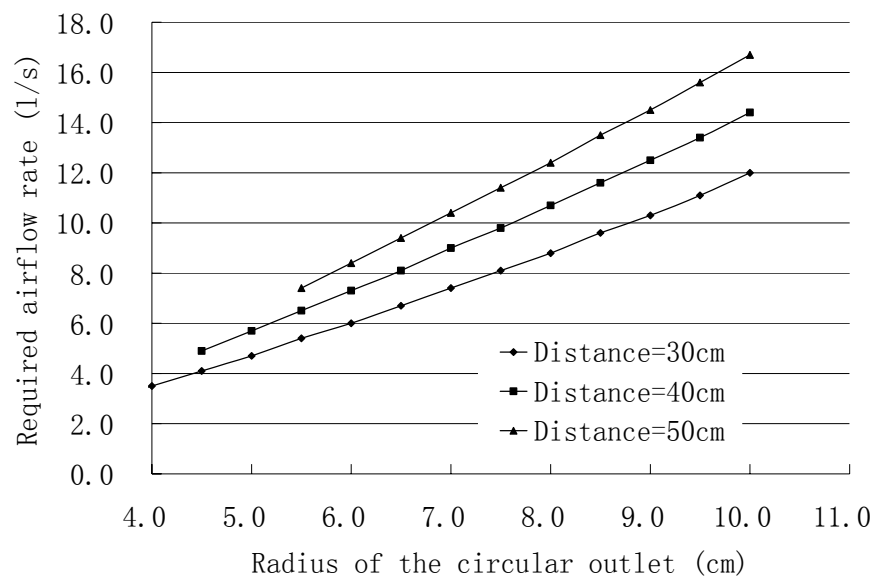
Figure 2.4 Minimum personalized airflow rate required to ensure a target air velocity of no less than 0.15 m/s at different radii of the circular outlet

According to Fanger's draft equation, assuming the PPD to be 20, t_a 23℃, and T_u 25%, the maximum mean air speed in the facial region should be no greater than 0.23

m/s. Fortunately, the speed that is required to penetrate the thermal plume that is created by body heat (0.1 m/s) is much lower than 0.23 m/s, which indicates that no local draft is present. The foregoing calculations demonstrate in a simple way that a personalized air supply is able to improve the inhaled air quality without sacrificing thermal comfort.

Theoretically, there should be an optimum air outlet area that maintains the best ventilation performance at a fixed personalized airflow rate. Melikov et al. (2002) decreased the cross-section area of an ATD that was located at the edge of the desk (named VDG) by 50% and increased that of another ATD that was set in front of the face (named CMP) by 50% (see Figure 2.1 for the definitions of VDG and CMP). The change in the VDG had almost no impact on the ventilation effectiveness, whereas the change in the CMP decreased the ventilation effectiveness at low flow rates and increased it at high flow rates. When fresh air was supplied from the desk edge by the VDG device, it impinged on the body, mixed with the warm free convection flow, and was then drawn up to breathing level. The flow rate was thus found to be more important than the cross-section area of the airflow. When fresh air was supplied from the front by the CMP device, the increased outlet area led to a larger cross-section area of the jet flow and consequently a purer core region, as long as the flow rate was high enough to extend the jet flow to the nose. Therefore, the optimum area of an ATD is related to its position.

2.1.4 Factors affecting personalized ventilation performance
To date, knowledge on the design or selection of PV is scarce. No related standards provide guidelines on the design of PV systems. Designing such systems is not an easy job, as many factors must be considered, such as the background total-volume-

air-conditioning system, the application situation, and human responses or preferences. Some of the primary considerations based on a literature review that was undertaken by the author are listed in the following.

- Most PV systems in practice are combined with UFAD systems that take advantage of an air plenum. This means that supply air can easily be ducted to the task zones.

- An important requirement for the installation of a PV system is that the occupant is seated in a certain place for a prolonged time. Desk-mounted or partition-mounted PV systems are recommended for modern offices, whereas chair-mounted PV systems are best for vehicles, airplanes, theatres, and cinemas.

- An occupancy sensor can monitor the presence and absence of the user and turn the PV system on and off accordingly, which allows energy savings. The delay time of the on/off action is of essential importance to the stability of the air conditioning system. If occupants repeatedly leave and return to their seats over a short time, the delay time should be long. Nobe et al. (2003) surveyed the seat occupancy characteristics in an actual office in Japan, and found that the occupancy rate of an individual work space was below 40%, and that workers tended to leave their seats frequently over a short time. The optimal delay time of the occupancy sensor requires further study.

- Individual preferences for temperature can vary by as much as 10 ℃ in offices (Grivel and Candas 1991; Jones 1998). Wyon (1996) estimated that 99% of occupants will be thermally comfortable if the control range of the whole-body equivalent operative temperature is 6℃, 95% will be comfortable if it is 4.6℃, and 90% will be comfortable if it is 3.9℃. Therefore, PV systems should have a certain cooling capacity to fulfill individual preferences. The adjustable range of

the temperature and velocity of personalized air should be considered together.

- A fluctuating airflow has the effect of reducing the perception of thermal asymmetry (Arens et al. 1998, Zhu et al. 1995). Yang et al. (2002) compared the human response to three periodically fluctuating airflows with frequencies of 0.1 Hz, 0.2 Hz, and 0.3 Hz, and found that air movement with a frequency of 0.2 Hz was preferred by the subjects. However, the subjects felt more distracted when the airflow was fluctuating than when it was constant. Jia (2000) found that people prefer a natural airflow with a flow pattern that is similar to that of outdoor air to other fluctuating or constant airflow types. Personalized airflow that simulates a natural flow may thus be favorable.

- Movable air outlets provide the opportunity to change the distance between the outlet and the human body and the personalized airflow direction. Their control can be manual or automatic, and can be set by occupants according to their preference. The position of the human body should be automatically monitored and the air outlet adjusted accordingly to ensure that the nose is in the core region of the personalized airflow, as the ventilation effectiveness of PV is sensitive to the relative position of the outlet nozzle and the body.

- A long response time of a PV system will lead to over-adjustment and oscillations in the individual environment. The response action should therefore be as quick as possible.

- Cutting down the noise of a PV system is essential. Experiments indicate that the overall degree of subjective comfort will increase if each change of 1℃ in the operative temperature in the desired direction can be realized with an increase in noise level of less than 3.9 dBA (Wyon 1996). A noise level of 40 dBA will cause 5% of occupants to be dissatisfied, and a level of 45 dBA will cause 10%

of occupants to be dissatisfied.

2.1.5 Energy consumption

The energy consumption of PV systems can be higher or lower than that of conventional air conditioning systems, depending on the system design and operation strategy (Bauman and Arens 1996). The integration of the PV system with the secondary air conditioning system is of most relevance to energy use. In general, the greater energy efficiency potential of PV systems is a result of the increased ambient air temperature and higher ventilation efficiency. An increased ambient air temperature can bring the benefits of extended periods of "free cooling," an increased chiller COP, and a diminished skin load. Greater ventilation efficiency can lead to a decrease in the fresh air load (Sekhar et al. 2005). Niu (2003) demonstrated that an equivalent inhaled air quality could be achieved with PV at a total ventilation rate of 30% that of a conventional system. In a room with well-mixed conventional ventilation, the indoor air pollutant level is

$$C_{room} = C_s + E / Q_{vent} , \tag{2.5}$$

where C_s is the pollutant level in the supplied air, E is the emission rate of the indoor pollutants, and Q_{vent} is the total ventilation rate. With the introduction of PV, the total ventilation rate can be reduced to $\alpha_{PV} \times Q_{vent}$ ($0 < \alpha_{PV} < 1$). The pollutant level of the room air is then raised to $C_{room}' = C_s + E /(\alpha_{PV} \times Q_{vent})$, and the pollutant concentration in the inhaled air is

$$C_{inhalation} - C_s = (1 - PER)(C_{room}' - C_s) = \frac{(1 - PER)}{\alpha_{PV}} \times \frac{E}{Q_{vent}} , \tag{2.6}$$

where PER is the proportion of personalized air in the inhaled air.

Equation (2.6) indicates that $(1-PER)\times 100\%$ of the conventional ventilation rate will achieve the same inhaled air quality ($C_{inhalation} = C_{room}$), which means a significant saving of the energy that is expended through air conditioning, especially in hot-humid climates and cold climates, where cooling or heating and the dehumidification and humidification of outdoor air constitute a large percentage of the total energy use.

The main drawback of PV in terms of energy consumption is the use of local fans with a small capacity. Bauman et al. (1994) simulated the annual energy consumption of an office in two California climates, and concluded that a desktop-based PV system with occupancy sensor control could achieve an annual saving of as much as 18% of the cooling energy and 9% of the total electricity cost. Seem and Braun (1992) compared the energy use characteristics of PV systems with those of conventional designs through computer simulation, and reported that the energy consumption of PV was more sensitive to the temperature set-point in the occupied individual zones than the temperature set-point in the unoccupied ambient zone, as in their simulation the occupied floor area was greater than the unoccupied area. PV systems without small local fans and radiant panels can save 6% of energy over conventional VAV ceiling-supply systems.

2.2 CFD study of the thermal environment around a human body

2.2.1 Fundamentals of CFD

The governing equations of indoor air flow in a Cartesian and time averaged version could be written as:

Continuity equation

$$\frac{\partial U_i}{\partial x_i} = 0 \tag{2.7}$$

Momentum equation

$$\rho \frac{\partial U_i}{\partial t} + \rho U_j \frac{\partial U_i}{\partial x_j} = -\frac{\partial P}{\partial x_i} + \mu \frac{\partial^2 U_i}{\partial x_j x_j} + \frac{\partial}{\partial x_j}(-\rho \overline{u_i' u_j'}) - \rho g_i \beta \Delta T \tag{2.8}$$

Energy equation

$$\rho c_p \frac{\partial T}{\partial t} + \rho c_p U_j \frac{\partial T}{\partial x_j} = \lambda \frac{\partial^2 T}{\partial x_j \partial x_j} + \frac{\partial}{\partial x_j}(-\rho c_p \overline{u_j' \theta'}) + Q \tag{2.9}$$

In these equations the Reynolds stress terms $\overline{u_i' u_j'}$ and the turbulence heat flux $\overline{u_j' \theta'}$

evoke the requirement for the introduction of a turbulence model.

2.2.2 Turbulence modeling approaches

Basically indoor air flow can be viewed as turbulent flow, which can be characterized by irregularity, three-dimensionality, dissipativity, and diffusivity. Turbulence appears at high Reynolds numbers and it is not a property of the particular fluid itself. Analytical solutions to the Navier-Stokes equations are not available for most practical flows. In engineering calculations the mean flow is an approximating solution to real turbulence problem (Figure 2.5). During the growth of turbulence modeling, a series of approaches has been proposed and developed: large-eddy simulation, and simulation by turbulence transport models. Depending on how to determine the Reynolds stress and whether or not the Boussinesq concept is used, turbulence transport models can be classified into eddy viscosity models and Reynolds stress models. The eddy viscosity models can further be divided into zero equation model, one equation model, and two equation models. At present the two equation models are the main models applied in the HVAC engineering.
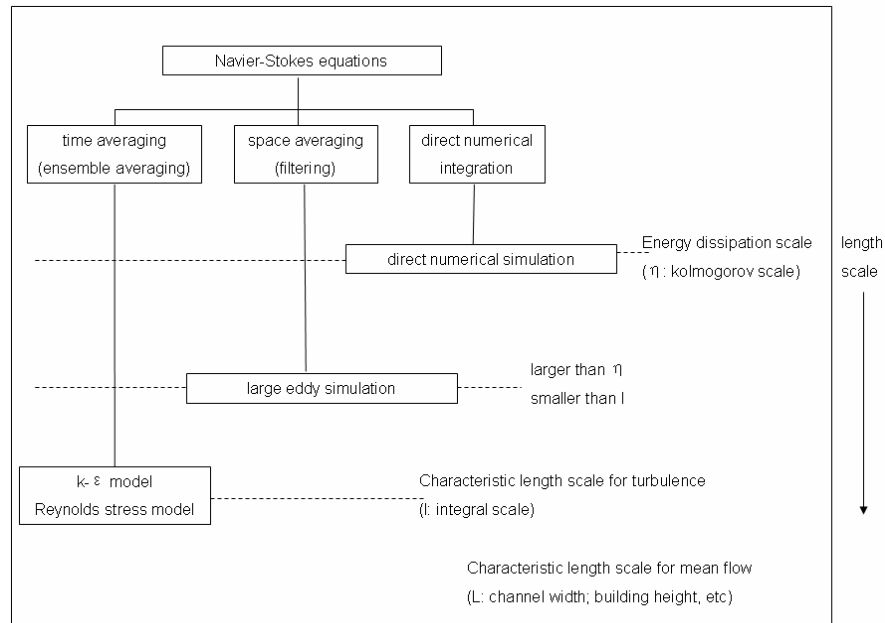
Figure 2.5 The concept of different turbulence models (Heiselberg et al. 1998)

Airflow in buildings is characterized by a display of various flow elements. For example, the air movements at the supply opening and the exhaust can be described as jet flow and potential flow respectively, and the airflow in a room can be divided into natural convection, forced convection, or mixed convection according to the driving force. One kind of turbulence model is good at dealing with certain flow elements. It is almost impossible so far to find out a model to solve room air flow economically and accurately.

The performances of different turbulence models in modeling indoor air flows have been continuously evaluated by many researchers (Chen 1995; Lai and Yang 1997; Nielsen 1998; Murakami 1998; Walsh and Leong 2004). Nielsen (1998) showed that a k-ε model with buoyancy term was important for the simulation of flow in the case of thermal stratification and a low Reynolds number k-ε model was suitable for predicting mass transfer coefficients at solid surfaces such as in the case of emission

of volatile organic compounds (VOCs). Up to the present moment, the k-ε models are still most commonly used in practical engineering applications. Strictly speaking the standard k-ε model is only applicable for fully turbulent flows. Since in the region near a solid surface this model is applied in conjunction with wall functions considering the dominant effects of viscosity, the simulation accuracy is greatly impacted by the location of first grids close to the wall boundaries (Niu and Kooi 1992). Low Reynolds number k-ε models differ from the standard k-ε model by using damping functions in the viscous sub-layer in place of wall functions which brings the benefit of more accurate modeling of transport phenomena in boundary layers and the penalty of finer grids near the wall at the same time. The renormalized group k- ε model has the same form as the standard k-ε model except that the model coefficients are derived from renormalization group theory (Yakhot and Orszag 1986), not from experiments. However all these three kinds of k-ε models mentioned above have their shortcomings. The turbulent energy, k, is over-predicted by the standard k-ε model (Wright and Easom 1999; Murakami 1998). Very fine grids should be located near the wall and computational stability probably is a problem if a low Reynolds number k-ε model is employed. The RNG k-ε model still requires to be used in conjunction with wall functions. All the k-ε models have their deficiencies for adverse pressure gradient flows.

As to the selection of models, generally speaking, complex turbulence models such as Reynolds-stress models produce better accuracy with the penalties in regard to computational stability and CPU time. In most cases the standard k-ε model and the RNG k-ε model are able to predict room air flow satisfactorily (Chen and Srebric

2002). Some previous comparison results of different models are listed in Table 2.2 and Table 2.3.

Table 2.2 Comparison of various turbulence models for practical modeling of indoor air flows (Murakami 1992)

Turbulence model	Standard k- ε	Low Re k- ε	Standard RSM (ASM)	Low Re RSM (ASM)	LES (Standard)	LES (dynamic)
Wall boundary condition	Wall function	Non-slip	Wall function	Non-slip	-	-
1. Simple flow (channel flow, pipe flow) (local equilibrium is valid)	O	O	O	O	O	O
2. Flow with streamline curvature 1) weak curvature, convection is dominate (usually in room)	O	O	O	O	O	O
2) strong curvature (flow around bluff body)	X Δ	X Δ	O	O	O	O
3. Jet 1) normal	O	O	O	O	O	O
2) swirl	X	X	O	O	O	O
4. Impinging flow	X Δ	X Δ	O	O	O	O
5. Non-isothermal flow 1) weak stratification	O	O	O	O	O	O
2) strong stratification	X Δ	X Δ	O	O	O	O
6. Convection heat transfer at wall	X Δ	O	X Δ	O	X Δ	O
7. Flowfield with low Reynolds No.	X Δ	Δ O	X Δ	Δ O	O	O

8. unsteady flow,						
unsteady diffusion	X	X	X	X	O	O
1) highly unsteady	X	Δ	Δ	O	O	O
2) vortex shedding						

O : functions well   Δ : insufficiently functional   X : functions poorly

Table 2.3 Summary of performance of the k-ε models for predicting indoor air flow[a]

(Chen 1995)

Flow type	Parameters	k-ε [b]	LB k-ε [c]	2L k-ε [d]	2S k-ε [e]	RNG k-ε [f]
Natural convection	Mean velocity	B	A	B	B	B
	Turbulence	C	C	D	D	C
	Temperature	B	D	B	B	B
	Heat transfer	C	B	A	C	C
Forced convection	Mean velocity	C	C	C	E	C
	Turbulence	D	D	D	D	D
Mixed convection	Temperature	A	A	C	A	A
Impinging jet	Mean velocity	C	C	C	A	A
	Turbulence	D	D	D	C	C

[a]A=excellent, B=good, C=fair, D=poor, E=unacceptable; [b]the standard k-ε model from Launder and Spalding (1974); [c]a low-Reynolds-number k-ε model from Lam and Bremhorst (1981); [d]a two-layer k-ε model from Rodi (1991); [e]a two-scale k-ε model from Kim and Chen (1989); [f]a k-ε model based on a renormalization group (RNG) method from Yakhot et al.. (1992).

2.2.3 Simulation of the micro-environment around a human body

An important goal in research on indoor air quality (IAQ) and thermal comfort is an enhanced understanding of the relationship between the human body and the surrounding environment. Human bodies, in this respect play a central role in indoor environment. To facilitate studies thermal manikins were introduced at least a half century ago. Thermal manikins are heated dummies which were originally developed

to measure the thermal insulation of clothing. In 1977, Mihira et al. (1977) developed a thermal manikin not only for clothing insulation measurement but also for the evaluation of thermal environments. Later more complex thermal manikins were used to study thermal reactions of human bodies in the indoor environment (Fanger et al. 1980; 1986; Tanabe et al. 1989).

During the last few years CFD technique has progressed and made it possible to numerically analyze the micro-climate around a human body. A growing number of numerical thermal manikins (NTMs) have been proposed with the purpose of determining indices that are not able, at least very difficult, to be obtained from experiments. A lot of work on CFD calculation of NTMs has been done in Japan (University of Tokyo) and Denmark (Aalborg University and Technical University of Denmark). The intention behind CFD simulations of modeled human bodies is various. Hayashi et al. (2002a ; 2002b), Murakami et al. (1998), BjØrn and Nielsen (1998), Xing et al. (2001) simulated the contaminant distribution around modelled human bodies and its impact on inhaled air quality. SØrensen (2002) tabulated view factors between different body segments and between the outer surfaces and the body segments by numerical method. Murakami et al. (1995; 1996; 1997), SØrensen and Voigt (2003) investigated the airflow velocity field and convective and radiative heat loss from a human body through CFD. However, very few researches have been carried out to evaluate thermal comfort using NTMs. At the present time such work has reached the stage where the CFD simulation firstly generates the environment data to input into a thermal comfort model, and then the thermal comfort model calculates the whole body thermal sensation and local sensation. Such thermal comfort simulations are regarded as preliminary because they do not reach the degree

of combined simulation which bridges analysis of the indoor air environment with thermoregulation of the human body.

The development of NTMs is step by step. Two-dimensional simplified geometry was used in earlier studies to simulate the air flow field around a human body without consideration of temperature difference. Then a temperature field and radiation was calculated through simplified 3-dimensional geometry. More complicated simulations take account of inhalation and exhalation process, and an unsteady state may be modeled (Murakami 2002).

The following sections summarize some issues in CFD simulations of thermal manikins. Geometric complexity, turbulence model, boundary conditions, grid generation, and simulation results from various studies are reviewed. Finally the author gives out some suggestions and discusses the future outlook for these simulations.

2.2.4 Geometry of NTMs

NTMs differ in size, posture, and their level of geometric complexity. Although there are no standards for the size of NTMs the skin surface area and body volume are based on those of real human bodies. The height of most NTMs is about 1.65m and the surface area ranges from 1.594m^2 (SØrensen and Voigt 2003) to 1.688m^2 (Murakami et al. 1995). According to different situations that are selected, three postures of NTMs are normally applied: sleeping, seated, and standing.

The level of geometric complexity of NTMs depends on the purpose of simulations involving them. Dunnett (1994) proposed an elliptical cylinder to simulate a standing

person, and Niwa et al. (1996) applied a heated box representing a seated person. Davidson and Nielsen (1995) simulated the air flow in facial regions and nasal cavity by means of two-dimensional simulations with a detailed model of a human head. Heinsohn (1991) used a cuboid (parallelepiped) to model the exposure of a standing person. Tjelflaat and Knott (1996) proposed a cuboid suspended from the floor to calculate thermal comfort indices. Other researchers have used a three-dimensional cuboid in rectangular geometry to model either a seated person (Iwamoto 1996) or a standing person (Bluyssen and Lemaire 1992; Gan et al. 1993; Gan 1994; Brohus and Nielsen 1995; 1996; Awbi 1996).

The geometries discussed above are obtained from computer aided design. The latest and most complicated NTM geometry is obtained using the laser scanning technique. The hair and clothes are usually not included since correct description of them is a difficult task. SØrensen and Voigt (2003) extract the geometrical details of a thermal manikin in a seated position using a laser scanning technique in their simulation. The surface of a human body was represented by approximately 125,000, 250,000, and 500,000 triangular elements for coarse, medium, and fine surface descriptions (Figure 2.6). This model is especially useful in some cases, such as in calculation of segment-to-segment view factors and inhaled air quality under the influence of facial geometry characteristics.
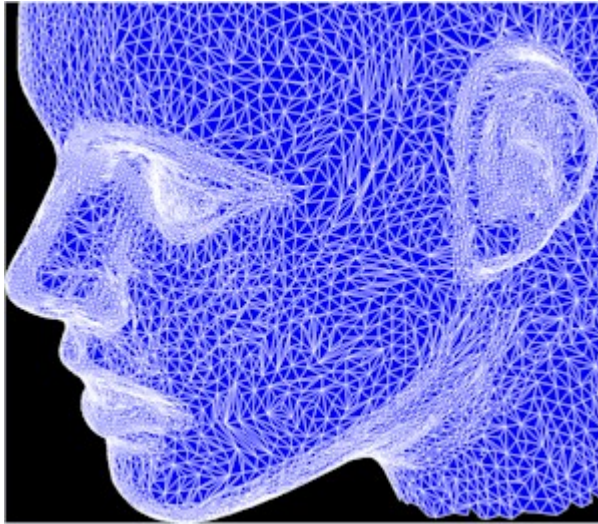
Figure 2.6 Close-up of the numerical thermal manikin's face (from the website of the International Center for Indoor Environment and Energy, Denmark Technical University, www.ie.dtu.dk/manikin/)

As in the case, say, of modeling an air diffuser, the key problem is the large difference in the scale between the detail of body extremities and the room size ranging in magnitude from centimeters to meters. Calculation of NTMs with simple geometry requires fewer computational resources and less time for modeling and grid generation. However using a detailed representation of a human body is closer to practical situations and so able to provide better local results. From the view point of computational expense, the geometry of NTMs should be as simple as possible. From the view point of simulation accuracy, it should be as real as possible. Therefore, it is necessary to know how complex a shape of the NTMs is required to obtain the desired CFD results. Topp et al. (2002a; 2002b) investigated numerically the difference between different shapes of NTMs with respect to both local and global air distributions as well as convective transfer. Two seated NTMs with different levels of geometric complexity were placed in a unidirectional flow field. The simulated human body geometries are illustrated in Figure 2.7. The one on the

left is a simple rectangular model of a seated person and the others (middle and right) are accurate representations of a human body.
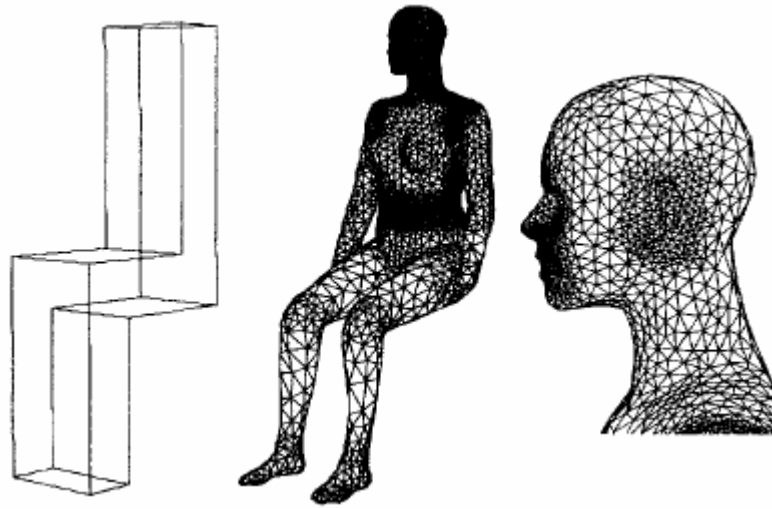
Figure 2.7 Geometry of the numerical thermal manikins from Topp et al. (2002b)

Topp et al. (2002a) found that the geometry of the NTM had an influence only in the region very close where it was located. It had no influence on the airflow at some distance from it. An accurate geometric model of NTMs is necessary for the numerical studies of thermal plume around the human body, thermal comfort, and inhaled air quality since the geometry of the human body plays a role in the measurement of draft and contaminant transport. In their studies of heat transfer from a human body to its surroundings in which the convective heat flow rate was fixed at 38.0W, the convective heat transfer coefficient of the complicated NTM model (7.4W/m^2℃) was higher than that of the simple NTM model (5.0 W/m^2℃). It was calculated from the following equation.

$$h_c = \frac{q_c}{t_s - t_{in}} \tag{2.10}$$

where

h_c = convective heat transfer coefficient, W/(m^2℃)

q_c = heat flux, W/m^2

t_s = human body mean skin temperature, ℃

t_{in} = room air supply temperature, ℃

The higher value for the complicated NTM model was the result of the higher local air velocity due to the geometric configuration of the figures.

From this study we can see that when numerical research focuses on global airflow pattern in a ventilated room a less detailed geometry is enough, however an accurate geometry of the human body is necessary when we are interested in local flow pattern around human body. Two examples are given here. One case is in the vehicle HVAC industry. In the simulation of airflow and evaluate the thermal comfort condition in a car, a NTM with detailed body surface characteristics is needed since the length scale of a car compartment is close to the boundary layer thickness of air around the human body. The other is in the numerical simulations of the inhaled air quality provided by personalized ventilation systems in which the air supply jet is located very close to the face. All facial extremities should be addressed by the NTM since large field gradient is expected at the head region and the inhaled air quality is very sensitive to the interaction of different airflows, such as the warm rising airflow caused by natural convection, the personalized airflow, the respiration airflow, and the room ambient airflow (Gao and Niu 2004).

2.2.5 Turbulence models selection

Although there are many turbulence models it is an unfortunate fact that no single turbulence model is universally accepted as being superior to the others for all classes of problems. The choice of a turbulence model is a compromise, which

depends on considerations such as the physics encompassed in the flow, the established practice for a specific class of problems, the level of accuracy required, the available computational resources, and the amount of time available for the simulation. In the simulations of airflow around human body, the most frequently used turbulence models are the RNG k-ε model and the low Reynolds number k-ε model. Murakami et al. (1995) pointed out that since no wall functions had been applicable for the standard k- ε turbulence model to simulate the airflow around thermal manikins the low Reynolds number k- ε model with locally-fine grids at the human body surface is the only way to calculate the convective heat transfer. However in the simulations using the low Reynolds number k-ε model and an accurate geometric model of the human body, it is difficult to achieve convergence due to the extremely fine grids near the human body (Voigt 2001). In the simulation by SØrensen and Voigt (2003) using the low Reynolds number k-ε model, in order to tackle the boundary layer around the NTM, 20 layers of extruded triangular prisms were created at the surface of the manikin with an initial height of 0.2mm and a growth rate of 1.13 between layers. In present work a standard k-ε model and the RNG k-ε model are applied. Detailed descriptions are in Chapter 4.

Due to the temperature difference between the human body and its surroundings, the airflow pattern close to the body can be mixed convection flow or natural convection flow which depends on whether the human body is placed in a stagnant air or not. The importance of buoyancy forces in a mixed convection flow can be measured by the ratio of the Grashof and Reynolds numbers:

$$\frac{Gr}{\text{Re}^2} = \frac{g\beta\Delta TL}{v^2} \qquad\qquad (2.11)$$

When this number approaches or exceeds unity, this means strong buoyancy contributions to the flow. Conversely, if it is very small, buoyancy forces may be ignored in simulations. In pure natural convection, the strength of the buoyancy-induced flow is measured by the Rayleigh number:

$$Ra = \frac{g\beta\Delta T L^3 \rho}{\mu\alpha} \tag{2.12}$$

Where β is the thermal expansion coefficient:

$$\beta = -\frac{1}{\rho}\left(\frac{\partial\rho}{\partial T}\right)_P \tag{2.13}$$

and α is the thermal diffusivity:

$$\alpha = \frac{\lambda}{\rho c_P} \tag{2.14}$$

Rayleigh numbers less than 10^8 indicate a buoyancy-induced laminar flow, with transition to turbulence occurring over the range of $10^8 < Ra < 10^{10}$.

If we assume the human body to be a cylinder with the height of 1.65m and radius of 0.15m, the Reynolds number will exceed 2500 based on the equivalent diameter of 0.3m as the characteristic length of a human body if the air velocity is more than 0.13m/s. When a human body is sitting in stagnant air, the Ra number will reach about 4.1×10^9 at the head level, assuming the temperature difference is 9 ℃. Therefore in most cases the airflow around the human body is turbulent or is in the transition zone from laminar flow to turbulent flow. However, strictly speaking, the k-ε model is only applicable in the fully developed turbulent flow. It is difficult to reproduce the transition from laminar to turbulent with the k- ε model. Furthermore the k- ε model is not accurate enough for simulating the air flow field around a bluff body. Murakami et al. (1997) used a contrived method on a k- ε model to simulate

this transition flow by adding a slight turbulence generation term to the k-equation and ε-equation throughout the whole computational domain.

Since there may be many typical flow elements, such as jet flow, buoyancy driven flow, laminar flow, and potential flow, in the simulation of air flow in a ventilated room with a human body, no turbulence model which is now available can deal perfectly with this complex flow pattern. The k- ε model is the best choice by now among various turbulence models in view of its simulation accuracy and computational expense. The low Reynolds number k-ε model performs better in the prediction of heat loss from human body while the standard k-ε model and RNG k-ε model are sufficient if the emphasis is on airflow field.

2.2.6 Grid generation

Since the human body has an extremely complex geometry, grid generation for its simulation has special requirements. The correctness and accuracy of a simulation result depends very much on grid quality. Ordinarily for complex configurations the grid generation takes up most of the time and human labor in the whole process of CFD calculation. The accuracy is influenced by a number of grid factors, such as grid size, grid topology, grid shape, consistency of the grids with the geometry, etc.

The space can be discretized into Cartesian coordinates, cylinder coordinates, body-fitted coordinates, and unstructured grids. In the simulation of airflow around complicated geometries, body-fitted coordinates and unstructured grids are often used to present the complex boundaries. Body-fitted coordinates are suitable for internal or external flows with smoothly varying irregular boundaries. An unstructured grids method is more flexible in grid distribution than the body-fitted

coordinates. Because structured grids have higher quality than unstructured grids, the ventilated room is usually divided into two parts: a cuboid enclosing the human body and the remaining room space. The cuboid is broken with unstructured grids due to the complex geometry while the remaining room space is discretized with structured grids (Figure 2.8).
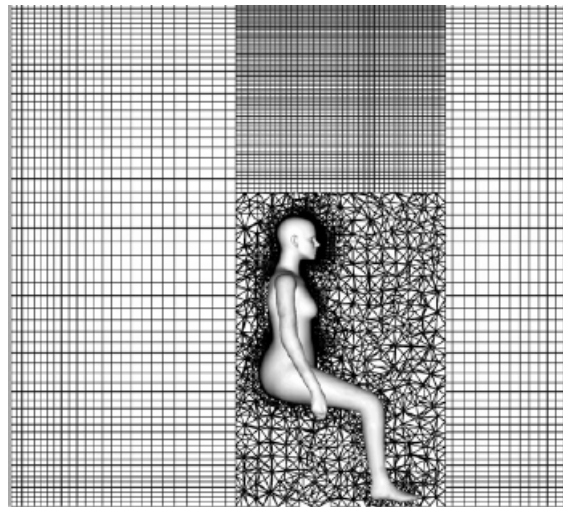
Figure 2.8 Grid configuration of the computational domain from SØrensen and Voigt (2003)

The number of cells is very large especially in a simulation using an accurate representation of the human body. The three-dimensional computational domain is discretized into 125,568 cells in Murakami et al. (1995), 292,421 in Topp et al. (2002b) and more than one million in SØrensen and Voigt (2003). This is because to discretize the region close the complicated boundary of human body requires very fine cells.

If the NTM is obtained from a laser scanning technique, the surface is composed by a huge number of elements. For example, the number of triangular elements of body

surface reaches 500,000 in (SØrensen and Voigt 2003). A large number of surface elements has its advantages for the view factors calculation of body segments. However this number, which is at the quantitative magnitude of one hundred thousand, means almost impossible to use in calculations of view factor using commercial CFD codes. Thus the elements on body surface should be coarsened to calculate the view factors.

2.2.7 Boundary conditions specification

Two methods are usually applied to describe the boundary condition of the human body: fixed surface temperature or fixed surface heat flux. The body boundary conditions are based on human heat exchange with the environment. Under steady-state conditions, the metabolic heat production M is equal to the heat loss from a human body, Q_m, which consists of heat loss from skin surface Q_s and that caused by respiration Q_{res}. Q_s is composed of sensible heat loss Q_t and latent heat loss E_s. Sensible heat loss Q_t consists of convective Q_c and radiative Q_r heat loss, and these can be described by the following equations:

$$M = Q_m = Q_s + Q_{res} \tag{2.15}$$

$$Q_s = Q_t + E_s \tag{2.16}$$

$$Q_t = Q_c + Q_r \tag{2.17}$$

In most simulations without consideration of moisture transfer from the skin surface, we can obtain a sensible heat transfer Q_t from the skin surface to the environment by excluding the heat loss caused by respiration Q_{res} and evaporation E_s according to the equations from Fanger (1970) and ASHRAE 1989:

$$Q_{res} = 1.7 \times 10^{-5} M (5867 - P_a) + 0.0014 M (34 - t_a) \tag{2.18}$$

$$E_s = 3.05 \times 10^{-3}(5733 - 6.99M - P_a) + 0.42(M - 58.15) \qquad (2.19)$$

Where

P_a =vapor pressure, pa;

t_a =ambient air temperature, ℃.

The mean skin temperature t_s under thermal neutrality may be estimated by the following equation according to Fanger (1970):

$$t_s = 35.77 - 0.028Q_m \qquad (2.20)$$

In numerical studies, the body temperature is usually set in the range from 31℃ (SØrensen and Voigt 2003) to 33.7℃ (Murakami et al. 1999). And the convective heat transfer rate is usually set in the range from 20W/m^2 (Hayashi et al. 2002a) to 25W/m^2 (Brohus and Nielsen 1996). In other experimental studies, a third kind of boundary condition for the human body was used. Tanabe et al. (1994) assumed vapor pressure P_a to be 1.5kpa, which was equivalent to typical indoor air conditions at 24℃ and 50% relative humidity. Then the following equation could be derived from Equation (2.15) to (2.19):

$$Q_m = 1.96Q_t - 21.56 \qquad (2.21)$$

By replacing the term Q_m in Equation (2.20) with Equation (2.21), the following equation was obtained:

$$t_s = 36.4 - 0.054Q_t \qquad (2.22)$$

The skin surface of a thermal manikin was controlled to satisfy Equation (2.22), which implied that the skin temperature and heat loss at different segments of the human body were coupled and neither were set at constant values. However this kind of skin surface boundary condition has still not been realized in CFD studies. The

inherent fault of control Equation (2.22) when it is applied to each body part is that this equation is deduced from the heat balance of the whole body. The thermal regulation of the human body and the physiological difference at individual segment are not taken into account for studying the local thermal comfort under a non-uniform thermal environment. To do this some multi-node heat-balance models would be required. The body should be divided into many segments with each segment having its own boundary condition. For example, we may expect that the skin temperature of the feet and the breasts is not the same. Usually the temperature of the feet is much lower than that of the breasts. It is possible to couple a multi-node thermal regulation models, such as Berkeley thermal comfort model (Huizenga et al. 2001) with CFD calculation of the surface radiative and convective heat transfer by iteration method. Initial surface temperatures T_i are assumed as the boundary conditions to calculate the airflow field, room temperature field, and humidity ratio. Then using the resultant air conditions near the human body we can predict the skin surface temperatures T_c at each segment with the help of the thermal regulation model and then by replacing T_i with T_c, such calculation can be repeated until the difference of T_c between each iteration is small enough. A brief review of the thermoregulation models is given in Section 2.3 and the use of this coupling method will be presented Chapter 5.

If the respiration process is taken into account in the simulations, the flow rate and respiration cycle under light physical work should be studied. Different researchers (Hayashi et al. 2002a; Murakami 2002; Zuo 2003; Hyun and Kleinstreuer 2001) have used different curves to approximate the change of the inhaled and exhaled air flow rate with time (Figure 2.9). The real respiration characteristics of humans may vary a

little according to age, race, gender, activity level, etc. The exhaled air condition is not completely constant. The mean exhaled air temperature depends mainly on inhaled air condition (Höppe 1981). At an ambient temperature of 20℃, the mean temperature of exhaled air through the nose is approximately 32℃. The molecular composition of exhaled air is different from that of atmospheric air. Therefore the density of exhaled air is not the same as the density of the atmosphere, which will impact on the buoyancy function. BjØrn (1999) has given out the density of exhaled air at different exhalation temperatures.
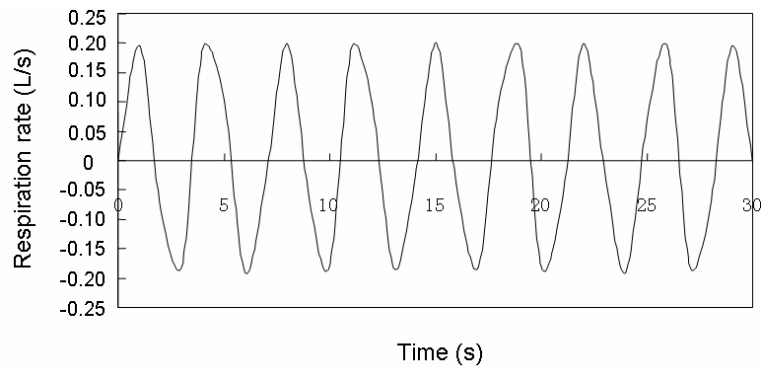
Figure 2.9a. The sinusoidal curve of human respiration according to Zuo (2003)
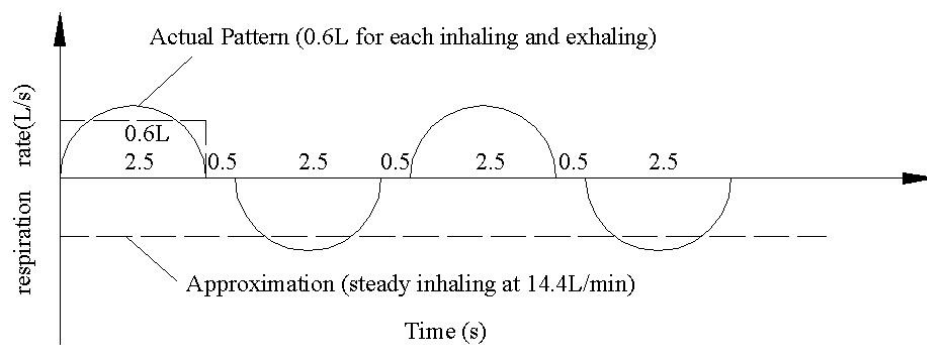
Figure 2.9b. Assumed model for steady inhalation by Hayashi et al. (2002a)
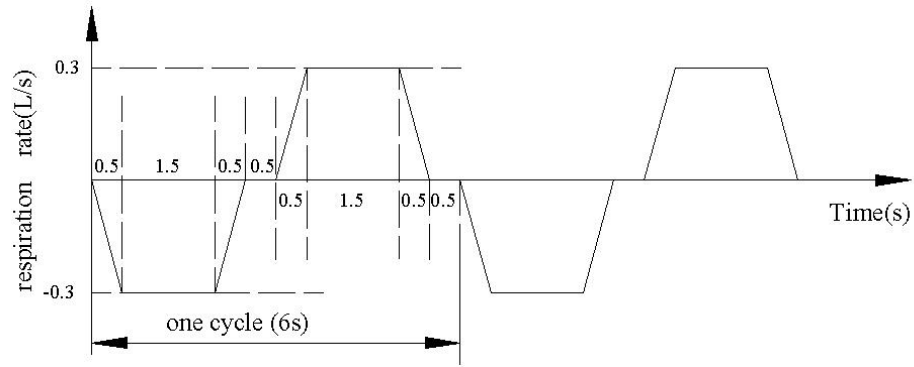
Figure 2.9c. Modelling of respiration by Murakami (2002)
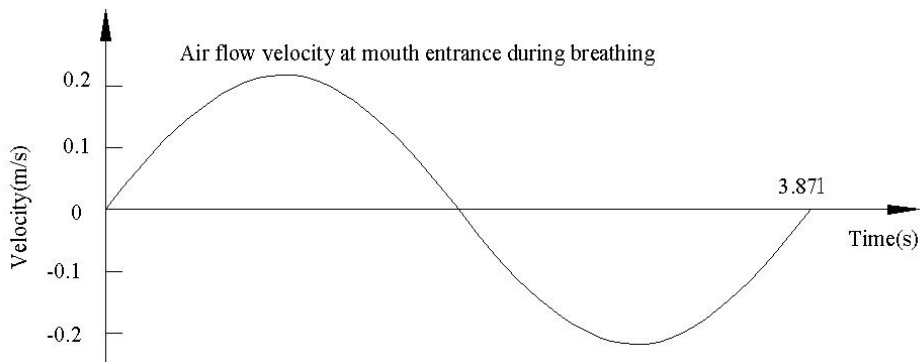
Figure 2.9d. Breathing waveform by Hyun and Kleinstreuer (2001)

Figure 2.9 Curves modeling inhalation and exhalation

2.2.8 Radiative heat transfer

To construct a comprehensive model of human thermoregulation and predict thermal comfort by numerical methods, radiative and convective heat transfer coefficients of individual body segments need to be known. Especially with the recently developed personalized air supply systems, local heat transfer at specific body regions varies greatly because human body is set in an asymmetric and non-isothermal environment. Experimental research on local radiative and convective heat transfer has been reported by de Dear et al. (1997).

Recently, some numerical research has been carried out (Table 2.4) (SØrensen 2002; SØrensen and Voigt 2003). In order to calculate the radiative heat transfer from a human body to a room wall and between body segments, an NTM with accurate and

40

detailed representation of the human body is necessary. Furthermore radiation is affected by the posture of the human body. Infinite combinations of human body postures will lead to different values of the radiative heat transfer rate. Usually the seated and standing postures are simulated. In the calculation of radiation heat transfer, the emissivity of the human body has been set about 0.95. The value of $4.7W/m^2℃$ has been widely accepted as a reasonable whole body estimate of the radiative heat transfer coefficient for general purposes (ASHRAE 1993) and is used as a reference value to evaluate calculation results. The radiation from a human body to room walls is surface to surface radiation. The calculation of view factors is computationally very expensive when there are a large number of radiating surfaces. In models with detailed representation of the human body the skin surface is constructed from thousands or even tens of thousands of patches. The calculation of view factors needs considerable computational time as well as high storage capacity. Experimental data for the radiative heat transfer coefficient for individual segments of a standing human body have been measured (Table 2.5) (de Dear et al. 1997; Ichihara et al. 1995). However no corresponding numerical data are reported. Murakami et al. (2000) simulated the radiative heat transfer using a simplified geometry of the human body in a standing posture. In their research no radiative heat transfer coefficient of individual segments was reported: their mean value for the radiative heat transfer rate was $38.3W/m^2$.

Table 2.4 Radiative heat transfer coefficient for different segments of a seated human body

Body Segments	Calculation by SØrensen et al. (2003) (W/m^2℃)	Experiment by de Dear et al. (1997) (W/m^2℃)
Foot	5.36	4.2
Leg	5.12	5.4
Thigh	4.61	4.6
Hand	4.12	3.9
Arm	4.30	5.2
Shoulder	4.63	4.8
Pelvis	5.01	4.8
Head	5.22	3.9
Chest	4.73	3.4
Back	5.07	4.6
Whole body	4.83	4.5

Table 2.5 Radiative heat transfer coefficient for different segments of a standing human body

Body Segments	Experiment by Ichihara et al. (1995) (W/m^2℃)	Experiment by de Dear et al. (1997) (W/m^2℃)
Foot	7.3	3.9
Leg	4.8	5.3
Thigh	4.2	4.3
Hand	3.7	4.1
Arm	4.0	4.9
Shoulder	4.0	5.2
Pelvis	3.9	4.2
Head	4.3	4.1
Chest	3.8	4.5
Back	3.6	4.4
Whole body	4.3	4.5

2.2.9 Convective heat transfer

The convective heat transfer coefficients reported by different researchers vary largely because the convective heat transfer from a human body to its surroundings is affected by air velocity, air flow direction and turbulence intensity (Table 2.6). The widely accepted expression of natural convective heat transfer coefficient is the following equation (Fanger 1970):

$$h_c = 2.38(t_s - t_a)^{0.25} \text{ W/m}^2 \text{°C} \tag{2.23}$$

Table 2.6 Comparison of the mean convective heat transfer coefficients h_c of a human body in still air

Researchers	Method	Posture	Ambient air speed (m/s)	h_c (W/m^2°C)
Murakami et al. (1995)	CFD	standing	<0.12	3.9
Murakami et al. (1995)	CFD	standing	<0.12	4.3
SØrensen and Voigt (2003)	CFD	seated	stagnant	3.13
Topp et al. (2002a)	CFD	seated	0.05	7.4
Voigt (2001)	CFD	seated	0.025	6.1
Brohus (1997)	Experiment	standing	<0.05	3.86
de Dear et al. (1997)	Experiment	standing	<0.1	3.4
de Dear et al. (1997)	Experiment	seated	<0.1	3.3

In still air the human body is enclosed by a rising thermal plume due to the temperature difference between the body surface and ambient air. The thickness of this boundary layer around the human body increases with height, and is similar to the flow around a vertical heated flat plane. Its thickness is about 8cm at the foot height level and 15cm at the head region (Murakami et al. 1997). The maximum air velocity above the head given by different researchers also differs greatly. The value of 0.23m/s has been given for a standing human body (Murakami et al. 1997; 1999)

and more than 0.5m/s for a seated human body (SØrensen and Voigt 2003). The value of 0.23m/s is consistent with that from earlier experiments (Homma and Yakiyama 1988). This rising warm thermal plume around the human body has a great impact on convective heat transfer and inhaled air quality. If the thermal plume is broken due to a high velocity of airflow impinging the human body the heat transfer coefficient increases greatly.

Murakami et al. (2000) simulated a standing human body with metabolic heat production of $100.4W/m^2$. In their simulation $29.1W/m^2$ was released to the surroundings by convection, $38.3W/m^2$ by radiation, $24.3W/m^2$ by evaporation and $8.7W/m^2$ by respiration. That is, 43% of sensible heat was lost by convection and 53% due to radiation. In the simulation by SØrensen and Voigt (2003), 40% of sensible heat was lost by convection and 60% by radiation. The results from Murakami et al. (2000) and SØrensen and Voigt (2003) are in agreement.

In still air the convective heat transfer coefficients of different body segments vary greatly (Silva and Coelho 2002; Yang et al. 2002) (Table 2.7). The feet and hands have large convective heat transfer coefficients since they are exposed to a cold rising airflow where the thermal plume is not fully developed. The convective heat transfer coefficient of the back is small because it is enclosed by a warm thermal plume.

Table 2.7 Convective heat transfer coefficients for different segments of a seated human body in a stagnant air flow field

Body Segments	Calculation by SØrensen and Voigt (2003) (W/m²℃)	Experiment by de Dear et al. (1997) (W/m²℃)	Experiment by Silva and Coelho (2002) (W/m²℃)	Experiment by Yang et al. (2002) (W/m²℃)
Foot	4.66	4.2	6.2	5.6
Leg	3.04	4.0	5.7	6.2
Thigh	3.18	3.7	4.4	3.9
Hand	4.50	4.5	4.4	5.9
Arm	3.82	3.8	6.0	6.3
Shoulder	2.71	3.4	4.6	5.9
Pelvis	2.80	2.8	3.4	3.1
Head	3.62	3.7	0.6	6.2
Chest	2.38	3.0	2.7	3.8
Back	2.23	2.6	2.1	2.4
Whole body	3.13	3.3	3.9	4.4

2.2.10 Contaminant distribution

Contaminant distribution around the human body has an important impact on inhaled air quality. Since the human body is enclosed by a warm rising thermal plume, air quality at the breathing zone is affected by this rising airflow. The essential question is whether inhalation and exhalation are taking place within this rising airflow. If we assume that (1) A person has a respiration of 0.6 l per inhalation. (2) Each inhalation lasts about 2.5s. (3) Air is inhaled from a hemisphere. Then air velocity at a distance of 8cm from the nose is about 0.006m/s. The effect of the inhalation on the surrounding air will be very small. Since the thickness of the thermal plume at the height level of the nose can reach 15cm the inhaled air will consist mostly of the air from the rising thermal plume (Figure 2.10). However from the results of an

experimental study on a living person and a thermal manikin (Hyldgaard 1994), the exhalation air jet can always penetrate through the thermal plume around the human body.

Figure 2.10 Path line showing origin of inhaled air in a stagnant ambient environment

It is important to evaluate the effect of entrainment of air from the lower zone to the breathing zone since inhaled air comes from the rising thermal plume. Brohus and Nielsen (1994) proposed the effective entrainment ratio η_e of lower air to the inhaled air:

$$\eta_e = \frac{C_{ref} - C_{inhalation}}{C_{ref} - C_{floor}} \tag{2.24}$$

where

C_{ref} =contaminant concentration at the breathing height apart from the body;

$C_{inhalation}$ =contaminant concentration of inhaled air;

C_{floor} =contaminant concentration at the floor level.

The rising thermal plume may have a positive or negative influence on inhaled air quality which depends on where the contaminant source is so long as the envelope of the warm rising airflow is not broken by the ambient room air movement or other invading flows. For example, if the contaminant is emitted from the floor, the rising airflow will draw up the contaminant to the breathing zone. In contrast in a displacement ventilated room, if the contaminant source is above the head, the rising airflow will entrain the fresh air to the breathing zone.

In the simulation of contaminant distribution around the human body, attention should be paid to the geometric model of the NTM and the posture of the body. If detailed information is required in the breathing zone such as in the evaluation of the performance of personalized ventilation systems, the presence of mouth, nose and ears will be required. Models with these facial extremities will require an increased number of grids and be computationally expensive. Brohus and Nielsen (1996) found great difference in the contaminant concentrations at the breathing level of two simplified models of the human body with different geometry. If the human body faces a horizontal airflow, the gap between the legs will allow air to flow across the lower body and affect the entrainment of the rising airflow which therefore affects different contaminant concentration at the breathing level. Simplified NTMs obtained by reducing legs to a solid extension of the torso may not predict the transport of pollutants accurately. The inhaled air quality is also affected by the posture of the body. Hayashi et al. (2002a) considered the human body in different postures: standing, sitting and sleeping and analyzed the inhaled air quality numerically. In the standing position the volume from which air will be inhaled

extends to the floor. The occupant inhales air from the volume that was close to the floor at the front of the body. The scenario is similar for a seated occupant. When an occupant is lying on the floor, air is drawn horizontally from both sides to the head.

2.3 A brief review of thermoregulation models

The studies on personalized ventilation illustrate that there is a lack of knowledge on human thermal sensation under an asymmetric environment. The non-uniform thermal environment created by personalized ventilation creates a demand for a local thermal comfort model. But the two most frequently cited thermal sensation models are Fanger's PMV (Fanger 1970) model and the TS and DISC indices calculated from ET* and skin wittedness in Gagge's two-node model (Gagge et al. 1970). These two models are based on a uniform, steady state energy balance, and the thermal sensation is described by the heat load on the whole body. None of them is suitable for assessing personalized ventilation. Although equivalent homogeneous temperature (EHT) and the upper and lower comfort bounds for each body segment have been developed to characterize the non-uniform environment, this approach is limited to the clothing and metabolic rate tested in steady state conditions (Wyon et al. 1989, Nilsson and Holmér 2003).

Recently, Guan et al. (2003) summarized that a complete heat-balance-type thermal comfort model should include three components: a physical heat exchange model and a clothing model, a physiological thermoregulation model, and a physiological thermal sensation model. The heat exchange model provides information on heat and mass transfer between the human body and the surrounding environment. The thermoregulation component takes account of the physiological reaction to the environment. Based on subject tests and statistic methods, the physical parameters

obtained from the previous two models are bridged with human thermal sensations. The human thermoregulatory system is very complicated due to the large number of variables involved and the feedback in many control loops. Also it is very expensive and time-consuming to conduct subject tests to set up a psychological thermal comfort model. In spite of these difficulties, in the past decade some advanced thermal comfort models were developed. The Smith-Fu finite element thermoregulation model (Smith 1991, Fu 1995) and the 65-node thermoregulation model (Tanabe et al. 2002) are designed to predict three-dimensional body temperature distribution, local sweat rates, and latent and sensible heat loss from the body surface. Fiala's dynamic model (Fiala 1998) and Wang's model (Wang 1994) are able to predict the transient thermal sensation based on pre-existing human subject test data, but these models are still based on a uniform environment. Huizenga et al. (2001) did further work to be able to predict human physiological and psychological response to transient, non-uniform thermal environments. Based on Stolwijk's 25-node model of human thermal regulation (Stolwijk 1971), Huizega et al's model allows an unlimited body segments, each of which consists of four body layers (core, muscle, fat, and skin tissues) and a clothing layer. Countercurrent heat exchange between the artery and vein, as well as heat exchanges between the blood vessels and the contacting tissues are simulated (Figure 2.11). A separate series of nodes represent blood and provide for conductive and convective heat transfer between segments and tissue nodes (Figure 2.12).
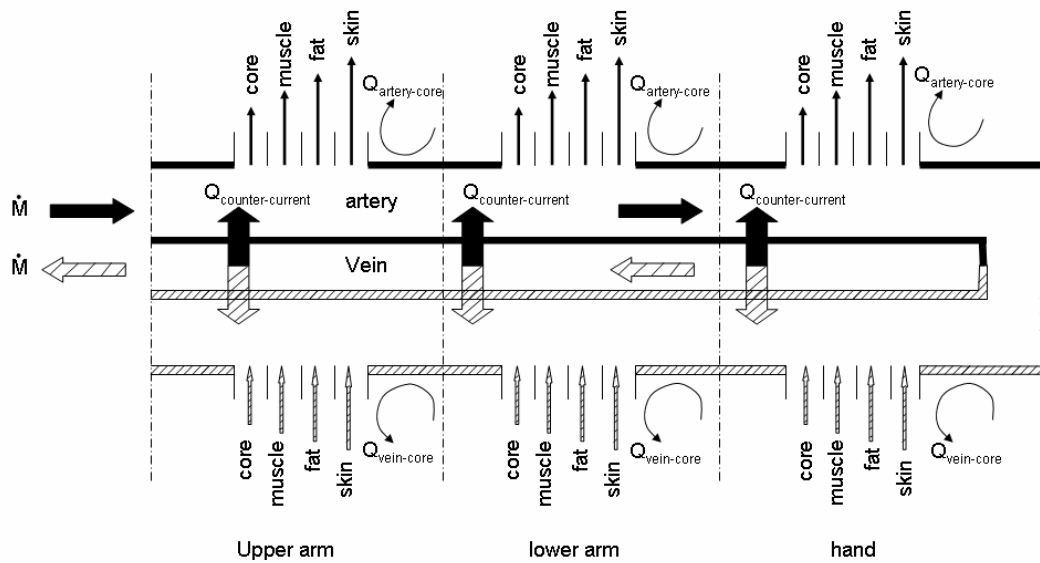
Figure 2.11 Blood flow model for an arm (Huizenga et al. 2001)
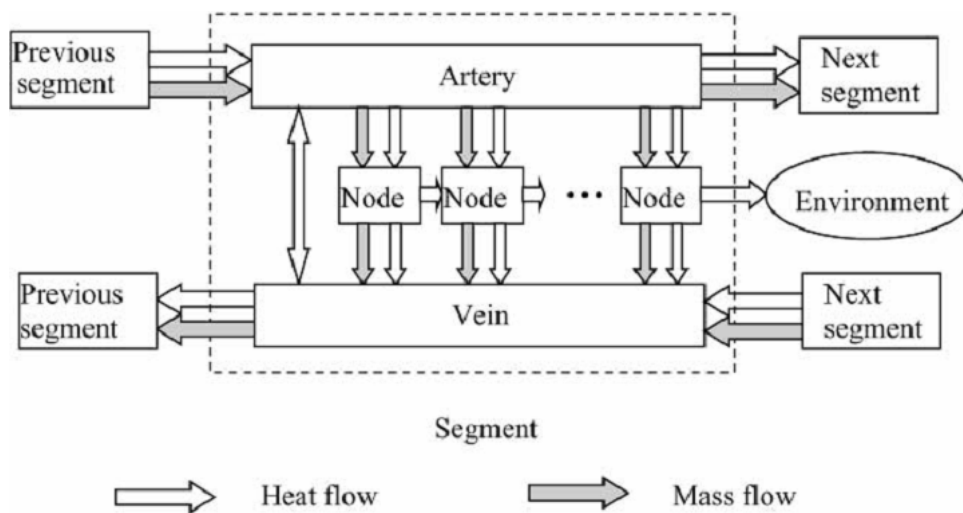
Figure 2.12 Blood flow model segment and node schema (Huizenga et al. 2001)

The model calculates heat transfer between each node using a standard finite-differencing algorithm with variable time-stepping to optimize computational resources while preserving numerical stability. Built into the model are the clothing node to model heat and moisture capacitance and heat transfer by conduction to surface in contact with the body, improved convective and radiant heat transfer coefficients, explicit radiant heat transfer calculation using angle factors, and a

unique blood flow model including counter-current heat exchange. This model also incorporates individual physiological differences by deriving the necessary physiological data (body density, metabolic heat production, body type, blood flow rate, body segment lengths, countercurrent blood vessel length in extremities, thermal capacitance, thermal conductance, skin surface area, and skin solar absorption) from readily available body characteristics: height, weight, body fat, gender, skin color, and body type. Validations of this model through several steady-state conditions and three transient environments show that it is able to predict both core and skin temperatures with a reasonable accuracy under a range of environmental conditions. More detailed information can be found in Huizenga et al. (2001).

More recently another comprehensive thermal sensation and comfort model has been set up by Zhang (2003) for transient and asymmetry conditions based primarily upon 109 tests with human subjects in the controlled environmental chamber at the University of California-Berkeley. In these tests, local body segments of the subjects were independently heated or cooled while the rest of the body was exposed to a warm, neutral, or cool environment. Based on the physiological and subjective parameters (skin and core temperature and their change rates, and perceptions of local and overall sensation and comfort), the following sensation and comfort predictive models were developed (Figure 2.13):

- A local sensation model for each of the 19 body parts
- A local comfort model for each of the 19 body parts
- An overall thermal sensation model
- An overall thermal comfort model
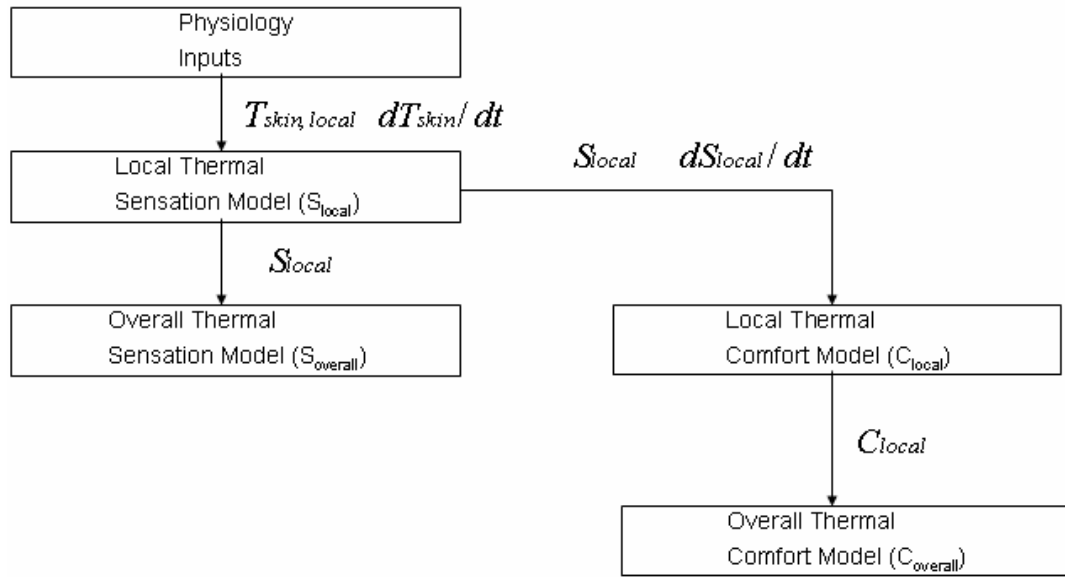
Figure 2.13 Flow chart of model relationships

Local skin temperature controls the local thermal sensation, which is also influenced by overall thermal state of the body represented by core temperature or mean skin temperature. In order to reflect the smaller range of tolerable skin temperatures above the setpoint compared to below the setpoint, the model is not symmetric to warm and cool conditions. Overall thermal sensation is the sum of local sensations multiplied by their weights. These weights are determined by the segment size, thermal sensitivity, and the sensation gap between the local part and the rest of the body. Local comfort is expressed as a function of local and overall thermal sensation. It is also asymmetric since the shifts to cold and warm are not equal. The overall comfort model is derived from local comfort restricted by a set of complaint rules. The thermal sensation scale used is a continuous scale and can be translated into the numerical values, i.e., "very cold" is -4, "cold" is -3, "cool" is -2, "slightly cool" is -1, "neutral" is 0, "slightly warm" is 1, "warm" is 2, "hot" is 3, "very hot" is 4. The thermal comfort scale ranges from very uncomfortable (-4) to very comfortable (+4).

In the middle the scale is broken between "just uncomfortable (-0)" and "just comfortable (0)". These models have been validated by the data from Delphi wind tunnel tests. The results show that they can predict subjects' votes very well. More detailed information can be found in Zhang (2003). Huizenga et al's model and Zhang's model are here called CBE thermoregulation model and CBE comfort model, respectively.

On the other hand, some preliminary investigations on virtual thermal comfort engineering, which couples CFD and the thermoregulation models, have been conducted (Huang 2002). Murakami et al. (2000) combined Gagge's two-node model with room air flow simulation. The sensible and latent heat losses from the human body were calculated, but the physiological difference of body parts was not included. Xue et al. (1999) coupled a three-dimensional flow field and a modified 25-node model of human thermoregulation. Distributions of air velocity, temperature, and moisture content were demonstrated in a crowded enclosure with 280 people sitting in 4 blocks. But the geometry of the human body was very simple. In more complicated methods, the multi-layer and multi-node thermoregulation model and surrounding environment simulation should be coupled together in an iteration loop on the premise of powerful software. In the experience of Currle (1997) normally 3-5 iterations are sufficient to get a converged result.

2.4 Research gaps

Personalized ventilation has been widely studied for its ventilation effectiveness. However, as a novel local air-distribution method, the knowledge on PV is far from sufficient. The air terminal device plays a role in determining ventilation

effectiveness, denoted by pollutant exposure reduction, air change effectiveness, etc. Numerous locations of air terminal devices relative to the human body cause various characteristics of ventilation effectiveness as a function of personalized air flow rate. In the micro-environment surrounding the body equipped with a PV system, personalized airflow may destroy the natural convection from the body and interact with room airflow, rebuilding a new local air field. This new air field throws the occupant into a non-uniform thermal environment, making our knowledge on thermal comfort unprecedentedly lacking. Furthermore, in the course of exploring the potentials of PV, such as improved occupant satisfaction and productivity, and accommodation of individual thermal preference, human response to PV is less studied. Whether the occupant will accept the locally applied personalized airflow or not is of practical meanings in journey of pursuing massive applications of PV.

2.5 Summary

This Chapter gives a review on the development of personalized ventilation and discusses several questions on CFD simulations of airflow around a human body and heat transfer from the body to the environment. Since a figurative representation of a human body is geometrically complex and it is heated the CFD study of the micro-environment around the body has some special characteristics:

- The geometry of an NTM has an impact on local airflow around the body but almost no influence on global flow. Simplified geometric models of a human body have their advantages through simplifying grid generation, reducing computational cost, and the need for memory storage for view factor calculations, etc. However models that accurately represent the human body can yield more detailed information on local areas around the body.

- K-ε turbulence models are usually used in the calculations with NTMs. When a human body is located in still air, the airflow around it is buoyancy-driven flow which transits from laminar flow to turbulent flow. The standard k-ε turbulence model has an inherent fault in modeling transitional flow and the low Reynolds k- ε turbulence model with a buoyancy term may has problems in convergence.

- Body-fitted coordinates or unstructured grids should be used to discretize the computational domain.

The results of a number of simulations are reviewed in this Chapter. Due to the variable nature of the parameters used for simulations the results show differences in airflow velocity, radiative heat transfer coefficient, convective heat transfer coefficient, and contaminant distribution. The techniques are still developing and we can expect further advances in NTM simulations. These may include:

- At the present time it is difficult to do an overall combined simulation which connects the heat and mass transfer from the human body to the environment with human thermoregulation. This specialized kind of simulations would have use in the prediction of local thermal comfort. Latent and sensible heat transfer from body segments needs to be taken into account. Coupling of mass and heat transfer from the inner-body to the outer-body at different body segments is the key to solving this problem. A simplified version of this coupling is demonstrated in Chapter 5.

- Simulations of transient inhalation and exhalation process with accurate geometric representation of the human body would be useful in the study of personalized ventilation. At the present time the respiration cycle is reduced

to a steady inhalation process by many researchers. Including exhalation makes the calculations more complex. It affects the inhaled air quality because some exhaled air will penetrate the thermal plume and the rest will mix with the rising warm air around the body and be re-inhaled.

Chapter 3

Experimental study on a chair-based personalized ventilation system

3.1 Introduction

In the experimental study reported here, the ventilation effectiveness of the chair-based personalized ventilation system (Figure 2.3) was measured at a flow rate of 0.4-2.5 l/s. Both isothermal and non-isothermal conditions were investigated. The personalized air was supplied at a temperature either equal to or 4-7℃ lower than the room mean temperature. Subjective measurements were also conducted to evaluate the human response to this ventilation method. Perceived air quality, irritation of the eyes, nose, and lips, thermal sensation at body parts, and overall thermal comfort were surveyed.

3.2 Ventilation performance measurement

3.2.1 Experimental methods

3.2.1.1 Experimental facilities and conditions

The experiments were conducted at the Hong Kong Polytechnic University in a laboratory used as a test chamber (Figure 3.1).
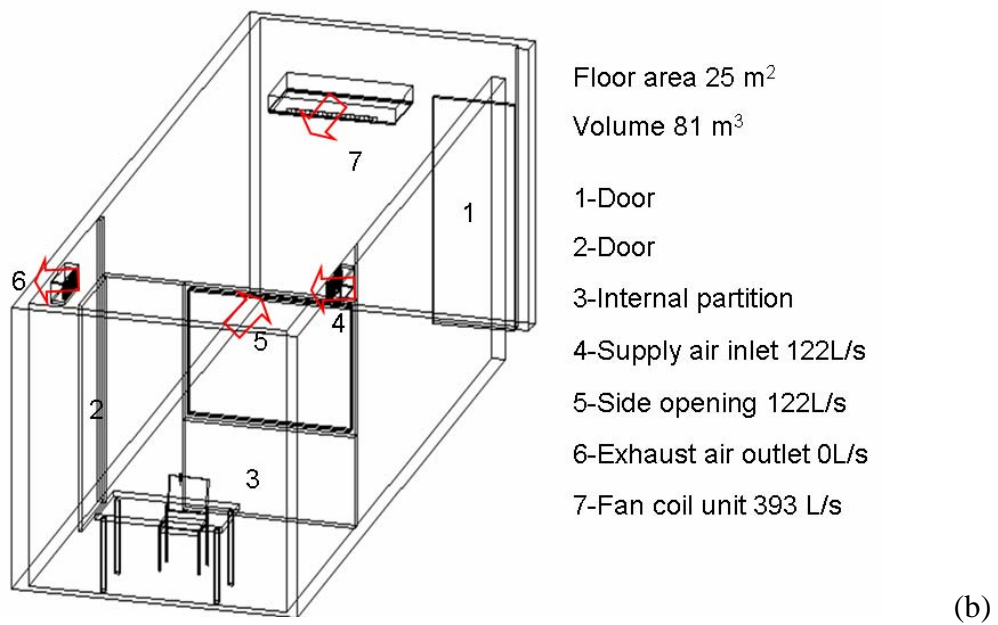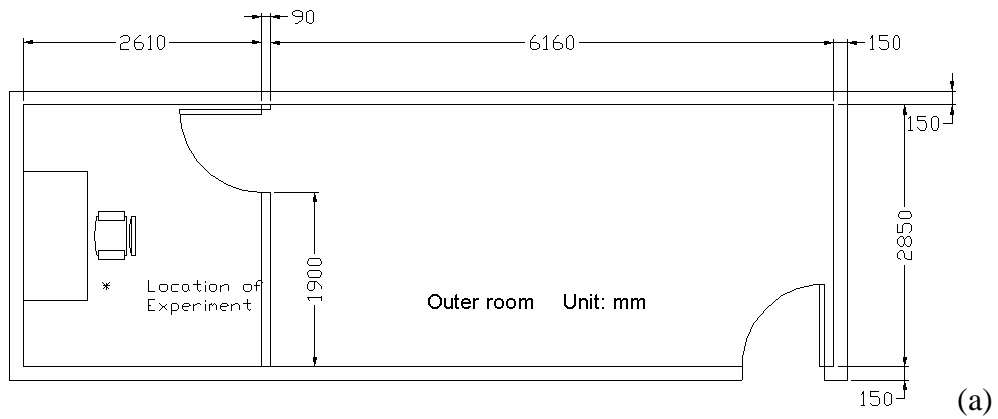
Figure 3.1 Plan view of the experimental chamber

A conventional mixing ventilation system operated to maintain a relatively uniform thermal environment in the occupied zone with a room air temperature of 22℃ and a relative humidity of 60%. The room air inlets and outlets were at the ceiling level. The personalized air system is illustrated in Figure 3.2(a). The personalized air terminal device (ATD) was located at the microphone position, as shown in Figure 3.2(b). In the previous experiments (Zuo 2003), four rectangular nozzles and four circular nozzles were developed and tested (Figure 3.3). Among them one circular nozzle named SCN exhibited a better performance than others. Therefore it was

selected in present experiments. The personalized air flow rate ranged from 0.4 l/s to

2.5 l/s. The temperature of personalized air ranged from 15-22℃.
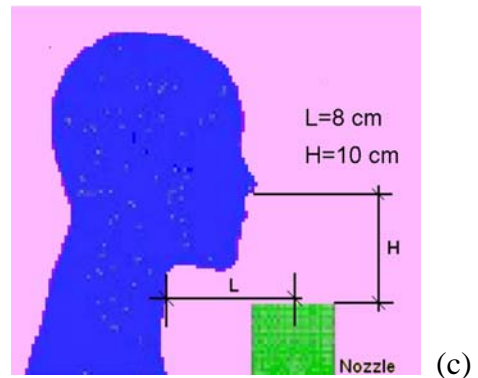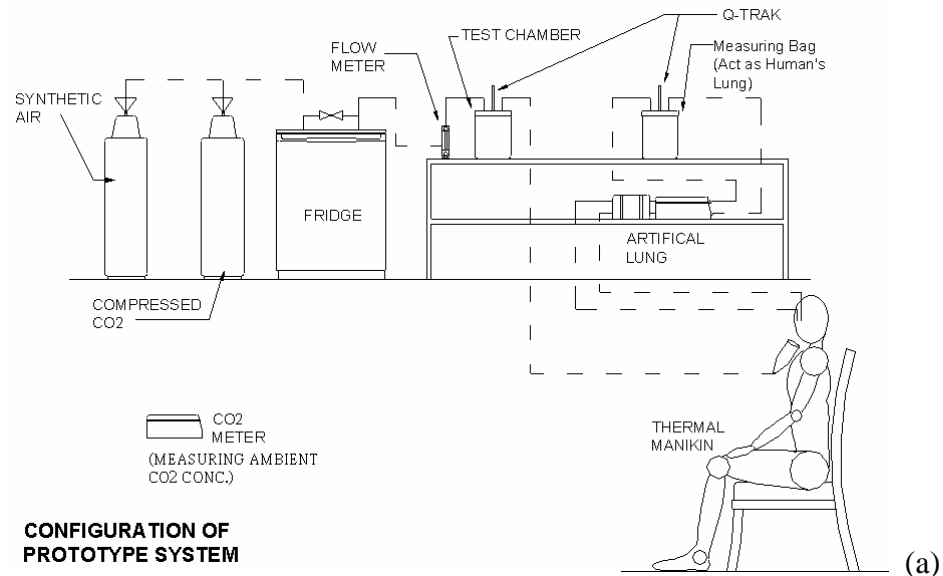
Figure 3.2 Schematic diagram of the personalized ventilation system

Nozzle Name	L1 (mm)	L2 (mm)	a1 (mm)	b1 (mm)	a2 (mm)	d1 (mm)	d2 (mm)
LSRN	230	270	150	70	30	28	–
MSRN	150	200	100	50	30	28	–
SSRN	150	200	100	30	30	28	–
FSRN	150	200	120	30	30	28	–
LCN	230	270	120	–	–	30	28
MCN	150	200	100	–	–	30	28
SCN	150	200	80	–	–	30	28
SSCN	150	200	60	–	–	30	28
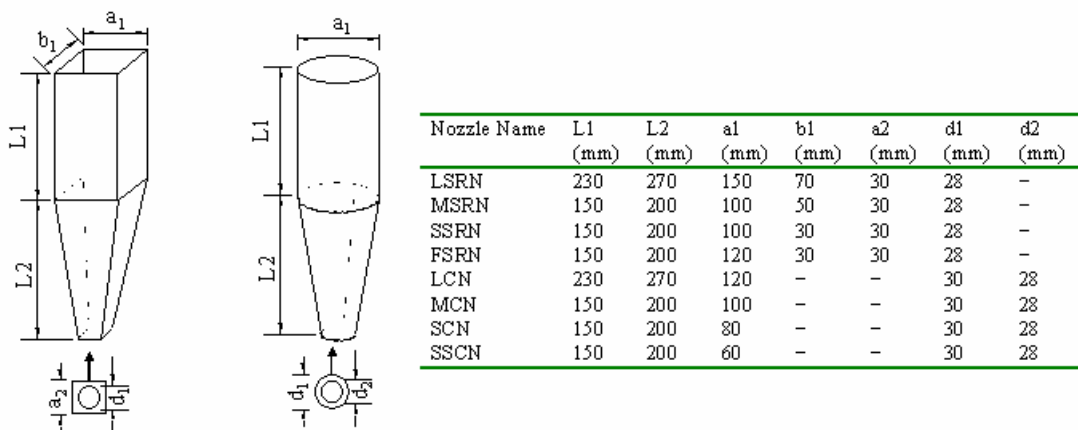
Figure 3.3 Geometry of personalized air supply nozzles (Zuo 2003)
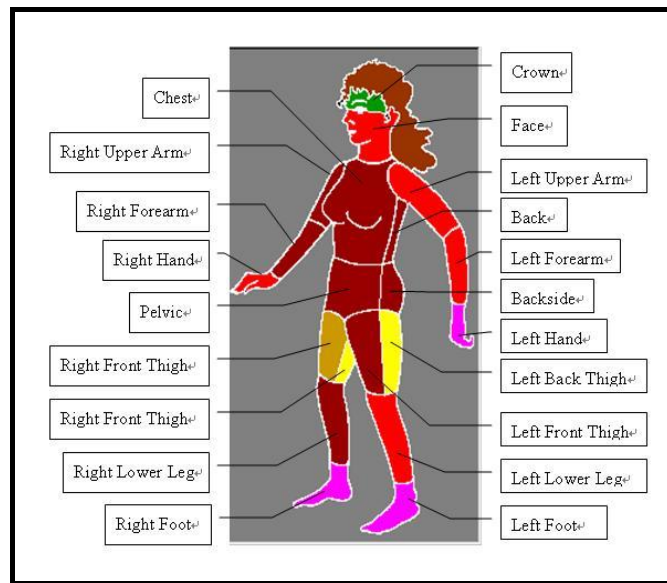
Figure 3.4 The 20 body segments of the manikin

A thermal manikin equipped with an artificial lung was used to simulate a "breathing human" (Figure 3.4). The manikin was a female model with 38 size and 168 cm height. She was made of fiberglass-armed polystyrene. This material gave a light and strong mechanical construction with a small thermal conductivity and thermal capacity. She had movable junctions in the neck, shoulder, hip and knee, so that she was able to stand and sit in a natural position. During the experiments, she was seated on a chair. The manikin was divided into 20 body segments that could be heated and individually controlled in order to maintain a surface temperature that was equal to the skin temperature of an average person in thermal comfort at a given actual level of activity (Melikov et al. 2000). Under the skin surface of the manikin were nickel wires of 0.3 mm diameter at a maximum spacing of 2 mm. The wires were covered by a protective shield. The heating elements were placed close to the surface to give the manikin a very small time constant (less than five minutes). The thermal manikin can be controlled by three methods: Comfort, PI (fixed skin

temperature) and Locked Power. In the experiments, locked power mode was applied, which specified the decided power to be transmitted to the manikin. Table 3.1 summarizes the powers specified for and the surface skin temperatures of the 20 body segments of the manikin. These heat fluxes were calculated based on the convective and radiative coefficients from de Dear et al. (1997). If the temperature reached maximum (40℃) for one or more segments of the manikin, the electrical heating power would be turned off in this/these part(s) to prevent overheating.

Table 3.1 Heat fluxes and skin surface temperatures of the 20 body parts

	Manikin segment		Heat Flux (W/m^2)	Skin temperature (℃)
1	Foot	Left	75.6	28.2
2	Foot	Right	75.6	28.8
3	Lower leg	Left	84.6	30.6
4	Lower leg	Right	84.6	31.5
5	Thigh	Left front	74.7	30.6
6	Thigh	Left back	74.7	34.4
7	Thigh	Right front	74.7	32.0
8	Thigh	Right back	74.7	34.8
9	Pelvis	-	90.5	31.6
10	Backside	-	64.8	30.4
11	Face	-	68.4	29.6
12	Crown	-	90.5	32.1
13	Hand	Left	75.6	27.7
14	Hand	Right	75.6	29.8
15	Forearm	Left	81.0	29.9
16	Forearm	Right	81.0	31.2
17	Upper arm	Left	73.8	29.0
18	Upper arm	Right	73.8	30.7
19	Chest	-	78.5	31.8
20	Back	-	76.9	31.3

The artificial lung was designed to realistically simulate the breathing function of a human being and to assess the quality of inhaled air. The air transporting system, which consisted of two pumps and two valves, controlled the frequency of breathing including the duration of inhalation and exhalation, e.g., the simulated pulmonary ventilation. For an average Asian person who was performing a light physical work, according to Huang (1977), the frequency of breathing was regulated to 15 times per minute by two connected digital timers (inhalation 2 seconds and exhalation 2 seconds), with a breathing volume in one cycle of 0.312 liter (Figure 3.5).
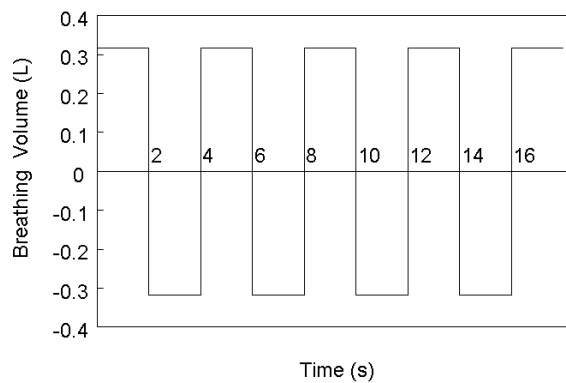
Figure 3.5 Breathing cycle operated by the pump controller

3.2.1.2 Measuring procedure

Tracer gas CO_2 was used to characterize the ventilation efficiency. The CO_2 concentration of personalized air (about 2000ppm~4000ppm) was fixed during one air flow rate and was far higher than that of ambient room air (about 400ppm~500ppm). The CO_2 concentration of personalized air, ambient air, and inhaled air were measured using a Q-Trak real time CO_2 monitor (Model 8551 from TSI), which had a detectable range of 0~5000ppm with an accuracy $\pm$ 3% at 25℃.

The measurement interval of CO_2 was 30 s, which was longer than the respiration cycle. Therefore, the monitored CO_2 concentration could be considered the time-average value. For each testing condition five data points were collected and the mean value was used.

Before conducting the measurement, the ambient air condition in the laboratory, such as air temperature and relative humidity, were measured. Then, the thermal manikin was connected to the computer with all the power inputs determined in Table 3.1. After the skin temperatures of the manikin were steady, the artificial lung and the PV system were operated. The synthetic air was adjusted to the tested flow rate. If the tested condition required the supply air temperature to be lower than room air temperature, PA needed to pass through the fridge to undergo heat exchange. Until the tested condition was steady, CO_2 concentrations of personalized air, inhaled air as well as ambient air were measured simultaneously. For each condition, five measurements were recorded.

3.2.2 Results and discussion

Previous tests in the same chamber (Zuo 2003) have revealed the effect of thermal plume and ATD geometry on the performance of PV. Two main findings are: 1). In comparison with using non-heated thermal manikin, the warm plume surrounding the heated manikin could increase the portion of ambient room air in inhaled air, and thus decrease PER. 2). In the supply range of 0.1-3.0 l/s, the nozzle with an outlet area of about 0.005 m^2 works better than the others. In the current experiments, the attention was focused on the influence of PA flow rate and temperature (Table 3.2).

Table 3.2 CO$_2$ concentration measured at ambient air (C$_a$), personalized air (C$_f$), and inhaled air (C$_i$), the values of η_{PER} and η_u for all experiment conditions

Flow rate (l/s)	CO$_2$ conc. (ppm)	Personalized air temperature (℃)		
		15	18	22
0.4	C$_f$	2138	2057	2214
	C$_i$	911	1040	1110
	C$_a$	454	446	449
	η_{PER}	0.271	0.369	0.375
	η_u	0.106	0.144	0.146
0.8	C$_f$	3075	2827	2136
	C$_i$	1520	1512	1479
	C$_a$	442	443	428
	η_{PER}	0.409	0.448	0.615
	η_u	0.080	0.087	0.120
1.2	C$_f$	3745	2053	2208
	C$_i$	2036	1309	1585
	C$_a$	456	440	429
	η_{PER}	0.480	0.539	0.650
	η_u	0.062	0.070	0.085
1.6	C$_f$	2400	2745	2152
	C$_i$	1498	1784	1623
	C$_a$	474	432	472
	η_{PER}	0.532	0.585	0.685
	η_u	0.052	0.057	0.067
2.0	C$_f$	2569	2626	2755
	C$_i$	1712	1867	2163
	C$_a$	465	471	472
	η_{PER}	0.593	0.648	0.741
	η_u	0.046	0.051	0.058
2.5	C$_f$	3616	2366	2132
	C$_i$	2622	1875	1739
	C$_a$	435	441	438
	η_{PER}	0.688	0.745	0.768
	η_u	0.043	0.046	0.048

3.2.2.1 The effect of flow rate

Figure 3.6 shows PER increased with the flow rate. The maximum PER was 0.768 at 2.5 l/s and 22℃. It could be imaged that the increment of PER became marginal at a certain high flow rate although this characteristic was not evident in the current testing, since the maximum flow rate, i.e. 2.5 l/s, was not high enough. Both Zuo's (Zuo 2003) and our experiments argued that 100% of the personalized air in the occupant's inhalation can not be achieved. This result agrees with the investigation by Melikov et al. (2002). They showed that for the flow rates studied (up to 23 l/s) the air supply nozzles were not able to provide 100% of the personalized air in the occupant's inhalation. In our investigation, even if the supply nozzles were located at the microphone position, PER could not reach 1.

The fresh air utilization efficiency η_u decreased as the supplied air flow rate increased from 0.4 to 2.5 l/s (Figure 3.7). The maximum η_u was about 0.15 at a lower flow rate. The value declined to about 0.04 to 0.05 as the supply air rate increased to 2.5 l/s. This is still much higher than 1% – the maximum that can be achieved in conventional ventilation systems.

As can be seen from Figure 3.6 and Figure 3.7, the increase in air flow rate will lead to an increase in PER but a decrease in utilization efficiency η_u. PER represents the quality of inhaled air while utilization efficiency characterizes the air supply efficiency. This means that a higher air flow rate will produce a better quality of inhaled air but will reduce air supply efficiency. And both of the change tendencies level off when the air flow rate exceeds a certain value. Thus, there should be an optimal value of the flow rate considering inhaled air quality and air supply

efficiency. For the angle and distance of the ATD to the face in this experimental work, this optimal value should be in the range of 0.8 l/s to 1.6 l/s. However, the optimal flow rate should be limited by the facial thermal comfort, which will be discussed in the following sections.
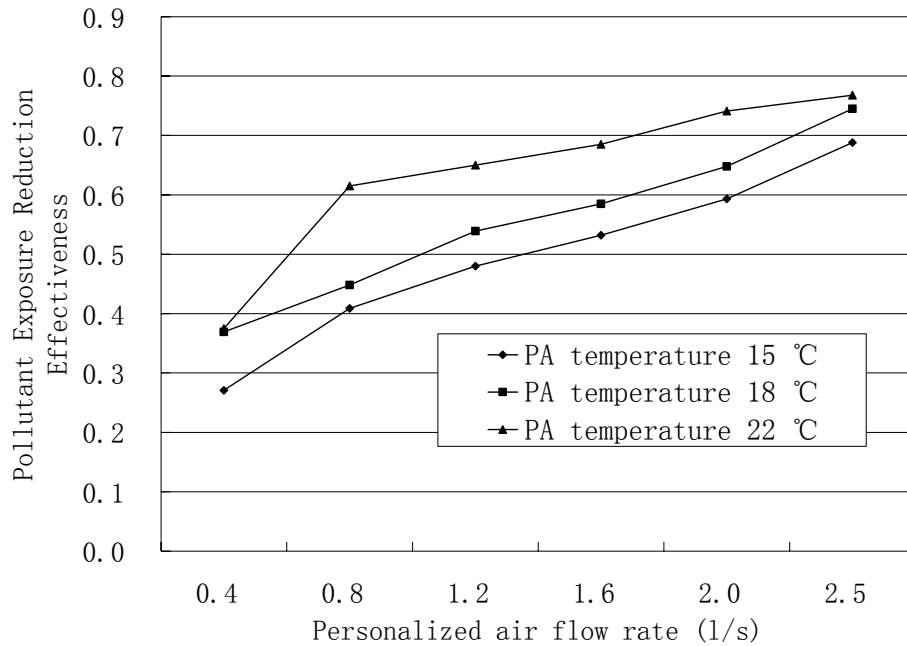
Figure 3.6 PER at different personalized air flow rate
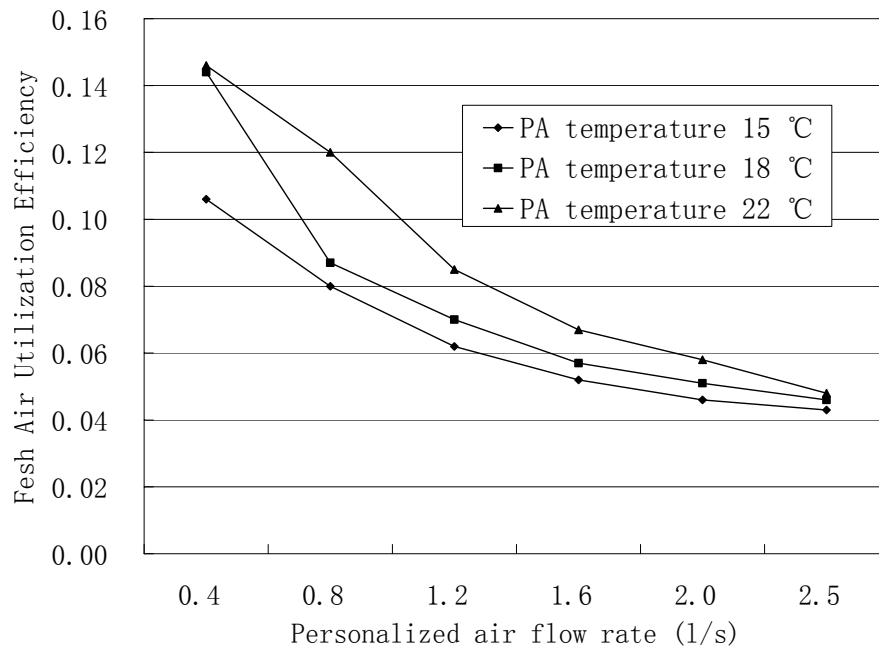
Figure 3.7 Fresh air utilization efficiency at different personalized air flow rate

3.2.2.2 The effect of PA temperature

In literature, studies on the effect of personalized air temperature are very scarce. As a consequence of the buoyancy effect, personalized air with a lower supply temperature may help to drop down before it reached the nose if personalized air was supplied beneath the face. When PA was supplied from the desk-edge, Faulkner et al. (2004) found that higher air change efficiency (ACE) at the breathing zone was measured with the supply air cooler than the room air. This result was contradicted with the expectation that the ACE should be higher under isothermal conditions reasoning that the warmer supply air would not drop, unlike the cooler air, and thus would be more easily caught in the thermal plume. Another available case from literature is the measurement by Melikov et al. (2002). Parts of the data are listed in Table 3.3. For VDG, supply air cooler than room air resulted in higher PERs at 5 and 10 l/s. However the temperature effect diminished at a high flow rate, i.e. 20 l/s, because at this flow rate the PERs were almost equal in isothermal and non-isothermal conditions. For HDG, PER was always lower in the non-isothermal condition. It can be seen that the effect of PA temperature is very complicated, depending on the location of ATD, PA flow direction, flow rate, body posture, and even dressing mode, etc.

In our experiments PER was higher at a higher supply air temperature. It was opposite to the simulation results in Chapter 4. Perhaps one portion of the reason was that in the experiment the supply jet flow was about 70^0 upward while in the simulation it was vertically upward.

Table 3.3 PER as a function of the airflow rate in isothermal and non-isothermal conditions (from Melikov et al. 2002)

Flow rate (l/s) ATD	Isothermal condition (room air 20 ℃ PA 20℃)				Non-isothermal condition (room air 26 ℃ PA 20℃)			
	5	10	15	20	5	10	15	20
VDG①	0.24	0.40	0.51	0.58	0.30	0.57	0.57	0.57
HDG①	0.36	0.37	0.38	0.39	0.24	0.21	0.20	0.20

① For the definition of VDG and HDG, see Figure 2.1.

3.3 Human response survey

3.3.1 Experimental methods

The human response to this chair-based personalized ventilation was studied with 18 combinations of personalized air temperature and flow rate. The personalized air temperature was regulated at 15℃, 18℃ and 22℃, with flow rates of 0.4, 0.8, 1.2, 1.6, 2.0, and 2.5 l/s. For each condition, the human subjects assessed the air with respect to thermal sensation, irritation, air movement, and acceptability.

3.3.1.1 Facilities and physical conditions tested

The experiments were conducted in the same climate chamber where the thermal manikin testing took place. In this mixing ventilated chamber, the mean indoor air temperature was controlled to 22 ℃ and the relative humidity about 50%. The thermal environment in the occupied zone could be regarded as relatively uniform, since the vertical temperature difference was no more than 1℃ and the air velocity less than 0.2 m/s. The mean radiant temperature was very close to the air temperature. There was no other source of heat in the chamber except the human body.

The personalized air supply system was identical with the one used to test PER except that to avoid odors, VOCs, and pollutants from the equipment itself in personalized air, a purification filter was installed just before the air supply nozzle. The relative humidity of personalized air was adjusted to be close to that of ambient room air (40-50%) through a humidifier. The ATD named SCN was selected for use in the subjective measurements.

During the period of the experiment, the outdoor air temperature ranged from 15 to 18 ℃ with a relative humidity of around 70%.

3.3.1.2 Subjects

Twelve untrained subjects (8 males and 4 females) were recruited to assess the air quality and thermal comfort provided by this chair-based personalized ventilation system. They were randomly selected university students living in the subtropics, aged between 22 and 28 and in good health. All of the subjects were volunteers who gave consent prior to the experiments. Before the experiments started the subjects were required to fill questionnaires on personal information, including sex, age, health condition, mode of dressing, and so forth. During the experiments, smoking was not allowed and the subjects were permitted to perform some common office work, such as reading and writing. The metabolic rate of the subjects was approximately 1.2 Met.

3.3.1.3 Experimental procedure

The experiments were conducted during weekdays in February and March 2005. Each subject participated in the survey separately on a weekday. Each survey was composed of 18 conditions and lasted for around 6 hours within a day. Prior to the

survey, the questionnaire was explained to each subject and he/she was then invited to the outer room to adapt to the room environment for about 20 minutes. The subjects were allowed to modify their clothing in order to feel thermally comfortable. The thermal insulation of the subjects' clothing ranged from 0.43 to 1.05 Clo. The subjects did not report any odors or make any complaints about poor indoor air quality at the start and the end of this 20-minute period. After the adaptation process, the subject was assigned to enter the experimental chamber and to sit at the workstation, with the ATD adjusted to the same position as in the manikin experiments. First, the personalized air was served at 22 ℃ and 0.4 l/s, and then the flow rate was increased and stabilized at five different levels of 0.8, 1.2, 1.6, 2.0, 2.5 l/s. The subjects were exposed to each flow rate for 15 minutes and were required to complete the questionnaire in the last 5 minutes. After the six flow rates at the temperature level of 22℃ were completed, the personalized air temperature was adjusted to 18℃, at which the six different flow rates were assessed, and finally the personalized air supply temperature was adjusted to 15 ℃. Therefore each combination of air temperature and flow rate was assessed based upon 15 minutes exposure of 12 subjects. Between two consecutive conditions there was a 5-minute break, both to allow the system to stabilize at a new operation condition, and for the subject to eliminate the thermal sensation in the previous condition, so that no carry-over effect between two experimental conditions was expected to occur. At the intervals of each air flow rate change, the subject could walk around or have a rest in the outer room, but he/she was not allowed to leave the laboratory.

The sequence of stepwise increased personalized air flow rates and decreased air temperatures was designed to capture the minimum air velocity and temperature at

which personalized ventilation would cause complaints. This progressively enhanced local cooling from personalized air may induce a decrease in thermal sensation votes, although a 5-minute break was set between two experimental conditions. Therefore, the results were somewhat conservative. Alternatively, the subjects could be exposed to high air velocities reduced step-by-step, or to randomized sequences. The best approach was to test one combination of air velocity and temperature per experiment. But this would have been too expensive and time consuming.

Part of the questionnaire is illustrated in Figure 3.8. All of the votes given between the two integers in the continuous scale were assigned with values according to the proportion of the line. In order to evaluate the subjects' feelings about the acceptability of personalized air, no neutral vote was allowed. Thus, the scale consisted of two parts, of which the upper part ranged from just acceptable to clearly acceptable, whereas the lower part was from just unacceptable to clearly unacceptable. Thermal sensation was assessed by the traditional seven-point scale (ASHRAE 1992). The feeling of irritation on the eyes, nose, and lips, the thermal sensation on the face, neck, upper body, and lower body, and the expectation of air movement were also recorded.
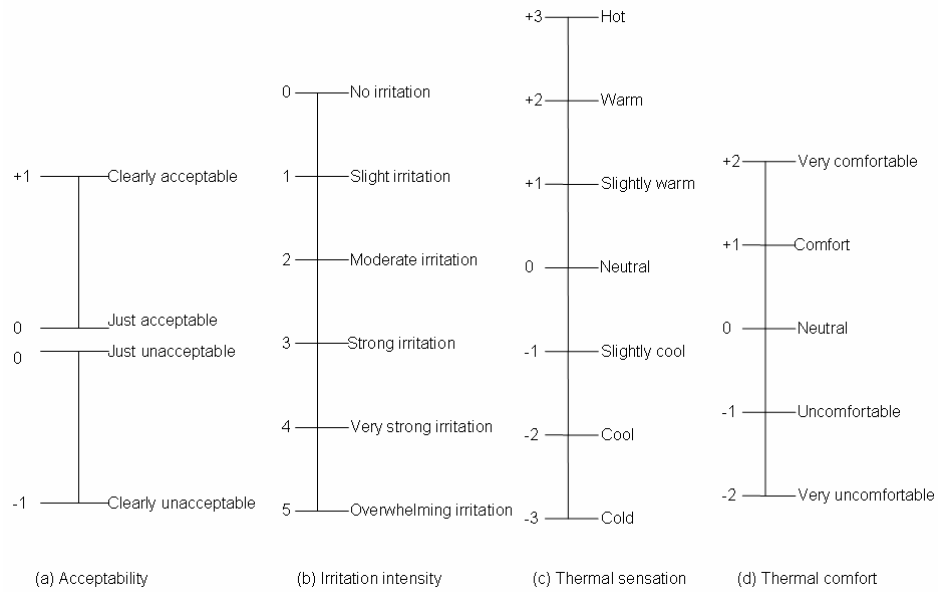
Figure 3.8 Scales used in the experiment for assessing perceived air quality and facial irritation as well as thermal sensation

Data obtained from subjective measurements were analyzed statistically. The normality distribution was tested using the Shapiro-Wilk method at the acceptable level of 5%. The average of the votes of all subjects on air acceptability, irritation, and thermal sensation were used. The P-values of the chi-square tests were reported.

3.3.2 Results and discussion

3.3.2.1 Perceived air quality

In Figure 3.19 the parabolic curve shows the relationship between perceived air quality and supply air flow rate. Perceived air quality increased as the flow rate increased within the range of 0.4 l/s to 0.8 l/s, and then decreased. This indicated that personalized air was effective at providing a satisfied feeling with inhaled air, and performed generally better at lower temperatures than at higher temperatures as illustrated by Figure 3.9, regardless of whether the personalized air was served isothermally or non-isothermally. At a flow rate of higher than 1.6 l/s, the perceived air quality decreased dramatically. One possible reason for the sharply lower

perceived air quality at a high personalized air velocity was the coupling of thermal sensation, including local drafts, irritation, and feelings of annoyance, with the acceptability of the inspired air, making it difficult for the subject to clearly distinguish between them. Li (2004) called this 'the coupling effect of thermal comfort and perceived air quality.' The influence of flow rate on perceived air quality is significant ($P<0.01$), while the influence of personalized air temperature is not distinct ($P>0.05$).
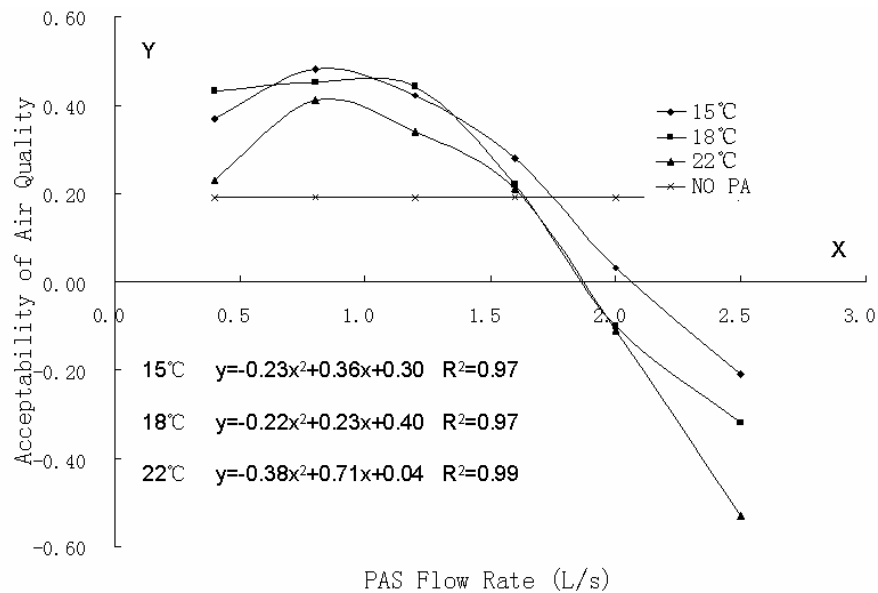
Figure 3.9 Perceived air quality under different personalized air conditions

Fang et al. (1998a, 1998b) found that the acceptability of air decreased significantly as temperature and humidity increased. They also generalized a linear relationship between acceptability and air enthalpy. It seems that sufficient cooling of the mucosa by the inhaled air due to convection and evaporation is essential for the perception of air quality if the temperature of inhaled air is below the mucosa temperature, which is normally in the range of 30 to 32℃. When the effect of respiratory cooling decreases to a certain level, the air will be perceived as being very poor even though

73

it is clean. No time course for the adaptation of air acceptability at different combinations of air temperature and humidity was found. Toftum et al. (1998) also consistently found that insufficient evaporative and convective cooling of the mucous membranes in the upper respiratory tract was the result of a course of local warm discomfort and a perception of poor air quality. They emphasized that the respiratory tract acted as an air-conditioning system that regulated the humidity level and temperature of the inspired air on its way from the nostrils, the nasal passage, and the nasopharynx, to the lungs; and this air-conditioning process was presumed to be decisive for the thermal perception of the inhaled air.

Therefore, in ventilated and air-conditioned spaces, not only the body surface but also the upper airway should be properly cooled to achieve overall thermal comfort and a pleasant perception of inhalation. Serving cool and fresh personalized air directly to the breathing zone is an effective way of achieving this. The results of the simulation (in the next Chapter) reveal that in total-volume ventilated spaces, the inhaled air temperature is usually slightly higher than the mean ambient air because of the natural convection around the human body. The chair-based personalized air is able to lower the inhaled air temperature by 2.5 to 3℃. A high flow rate could increase the value of PER, i.e. the percentage of personalized air in the inhaled air, and consequently decrease the inhaled air temperature much more.

Few studies on the influence of facial air velocity on perceived air quality have been reported. The old wisdom tells us that 'a person feels pleasant when a gentle breeze caresses his/her face.' It is reasonable to deduce that the effect of air velocity can also be related to the air cooling ability at the respiratory tract. A high air velocity

increases the value of the Reynolds number and, consequently, increases the Nusselt number and convective heat transfer coefficient. Therefore, it can be expected that proper facial air movement will be able to get rid of the feeling of stuffiness and improve the perceived air quality as long as there are no local drafts and feelings of irritation.

3.3.2.2 Irritation

Personalized air directed at the face may increase water loss in the eyes, lips, and upper respiratory tract. Therefore, the feelings of irritation on the subjects' eyes, nose, and lips were assessed. Only the results on the eyes are illustrated here (Figure 3.10), since the statistical characteristics and the fitness curve tendency for these three organs were similar, except that the intensities of irritation on the eyes were slightly higher than on the other areas.
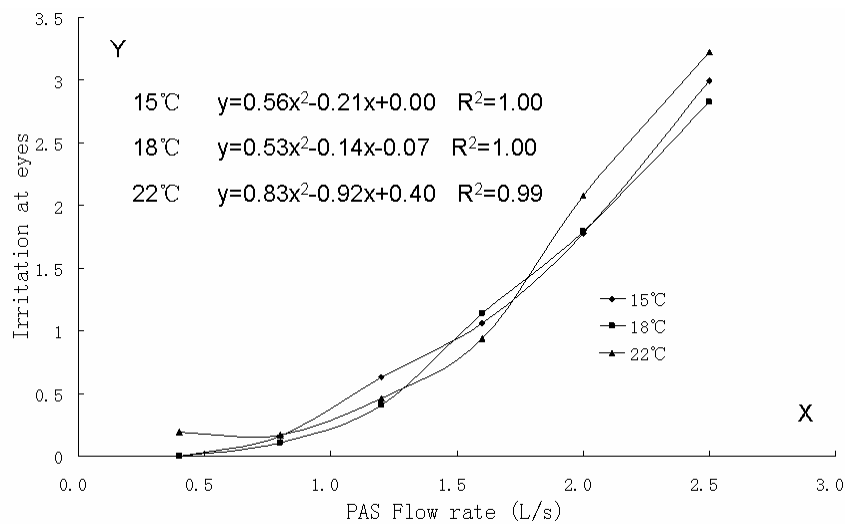
Figure 3.10 Feelings of irritation at the eyes under different personalized air conditions

It is known that precorneal tear film is responsible for protecting the ocular surface from environmental exposure. Blinking the eyes and secreting tears have proved to be essential for maintaining the tear film and mechanically removing deposited

particles. Based on studies on the stability of the tear film in office conditions, Sommer et al. (1994) found that in dry climates the breakup time of the tear film was reduced, causing 'office eye syndrome.' Wolkoff et al. (2005) summarized the view that eye symptoms could be the result of the precorneal tear film effect, such as dryness caused by: (1) an increased loss of water by evaporation due to thermal indoor environmental factors (for example, low relative humidity, high air temperature); (2) the stimulation of trigeminal nerve endings by indoor pollutants (for example, VOCs). Figure 3.10 shows that the feeling of irritation increased at a speed proportional to the square of the flow rate. If the flow rate exceeded 1.6 l/s, the feeling of irritation was unacceptable. The results showed that the influence of air velocity was significant (P<0.001). However, the influence of personalized air temperature was not significant (P>0.05). One reason could be that when personalized air reaches the face it has been heated to a certain degree due to the relatively small flow rate compared with other types of personalized ventilation and the mixing with ambient room air. A high facial air velocity strengthens the 'evaporation driving force,' leading to an unbalanced loss of water, i.e., dehydration. Though there are no mass-transfer coefficient equations available for air flow around human facial area, the mass transfer for turbulent flow past a flat plate can be taken as a reference (White 1991). The Sherwood number Sh could be correlated with the Reynolds number Re and the Schmidt number Sc for turbulent flow over a plate:

$$Sh = 0.0365 \, Re^{4/5} \, Sc^{1/3} \qquad\qquad (3.1)$$

This equation showed that the water loss rate at the eyes would be approximately proportional to the 0.8 power of the air velocity, which was much lower than the

square of the velocity. Perhaps subjective feelings of irritation were much more sensitive to the water loss rate.

The effect of humidity was not studied in this experiment. Survey results by Reinikainen and Jaakkola (2003) showed that, surprisingly, eye symptoms were not significantly associated with absolute and relative humidity. More studies of the human response at different levels of humidity in the field of personalized ventilation are needed.

3.3.2.3 Thermal sensation and comfort

The overall and local thermal sensations are shown in Figure 3.11. Both sensations decreased when the flow rate increased at different temperature levels. The influence of flow rate on thermal sensation was significant ($P<0.001$) except at the lower body part, while the impact of personalized air temperature was not remarkable ($P>0.05$). The sensation at the face and neck was below the overall thermal sensation, while the sensation at the upper and lower parts of the body was above. As the flow rate changed from 0.4 l/s to 2.5 l/s the sensation at the face and neck declined dramatically. There were at least two reasons for this. First, the face and neck are usually the parts of the body that are most sensitive to drafts and air movements, because, at least partly, these body parts are not masked by clothes and are directly exposed to air flows. Second, our investigations on local thermal sensations at the face and neck were performed with the thermal sensation of the whole body at neutral to slightly cool. Depending on the different clothing worn by the subjects, the value of PMV in the chamber without personalized ventilation is from -1 to 0. Previous results by Zhang (2003) indicated that local thermal sensation and comfort, even at the same local thermal environment, should be modified by the overall

sensation and condition of comfort. Furthermore, Toftum et al. (2003) found that, on average, a decrease in overall thermal sensation of 1 scale-unit from neutral to slightly cool resulted in a 2.5 to 3 times higher percentage of draft dissatisfied.

(a) T=15℃

(b) T=18℃

78
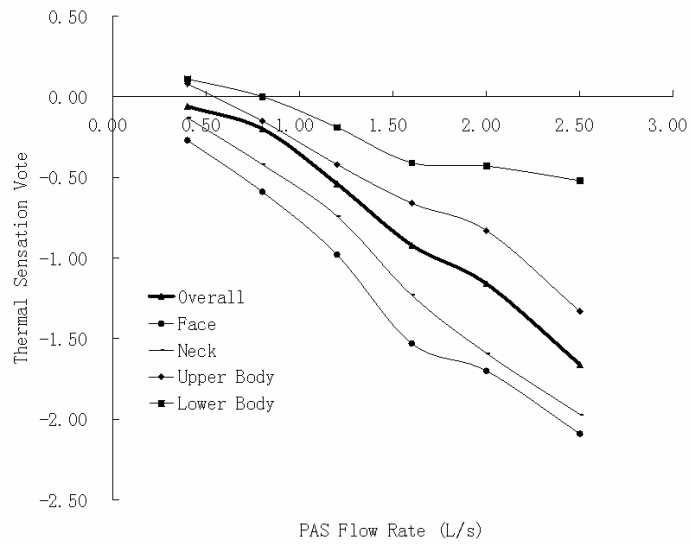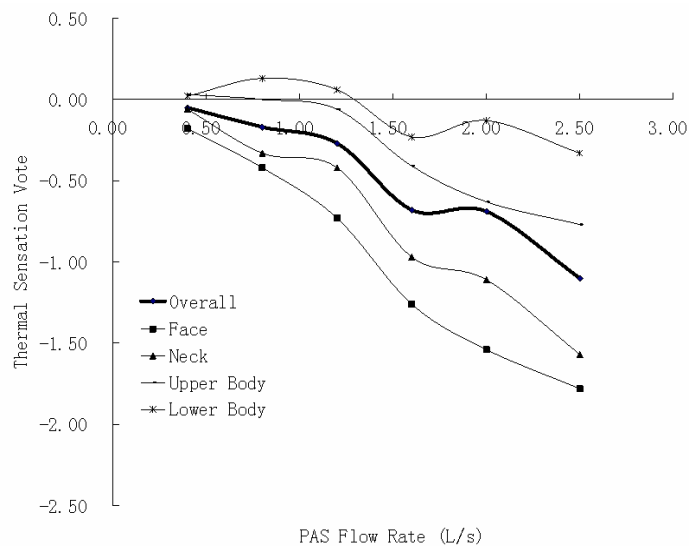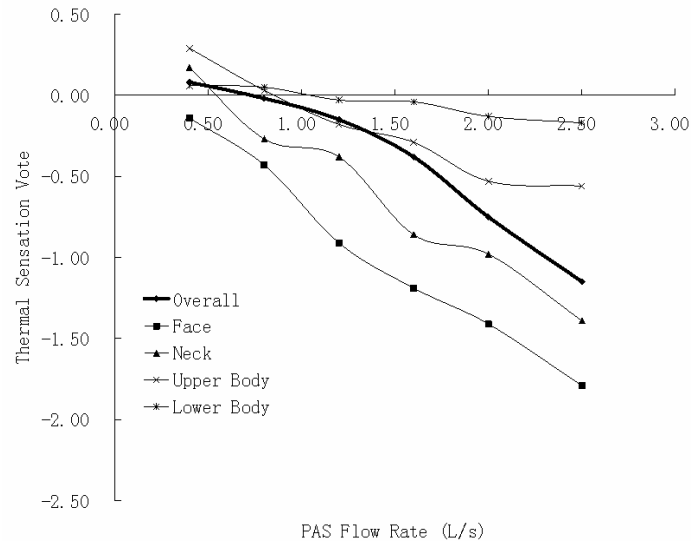
(c) T=22℃

Figure 3.11 Overall and local thermal sensations under different personalized air conditions

It was noticed that the thermal sensation at the lower part of the body was slightly lowered, although the physical thermal condition at this part was almost not influenced by personalized air. For example, at the personalized air temperature of 15℃ and flow rate of 2.5 l/s (corresponding to the most intensive cooling effect), the thermal sensation vote decreased from 0 to -0.5. This could, at least partly, be attributed to the psychological effect caused by personalized air supply as reviewed by Charles (2003). He thought that none of the studies on personalized ventilation adequately separated the effects of physical environment and psychological effects.

In the design of any types of personalized ventilation system, great efforts have been made to avoid the feeling of local drafts, while ensuring improved ventilation effectiveness. Fanger et al. (1988) defined a draft as 'an unwanted local cooling effect of the human body caused by air movement.' One method of evaluating local

79

comfort is the index of the predicted percentage of people who are dissatisfied (PPD), using Fanger's draft equation (Fanger et al. 1988):

$$PPD = (34 - t_a) \times (V - 0.05)^{0.62} \times (0.37 \times V \times T_u + 3.14) \tag{3.2}$$

where:

t_a = the local air temperature, ℃;

V = the local mean air speed, m/s;

T_u = the local turbulence intensity, %.

The percentage of those dissatisfied in the survey and the PPD values from Equation (3.2) if this equation were employed at face are listed in Table 3.4.

Table 3.4 Percentage of people dissatisfied (PPD) with local draft①②

	0.4 l/s	0.8 l/s	1.2 l/s	1.6 l/s	2.0 l/s	2.5 l/s
15℃	0(8.3)	0(22.2)	25.0(36.2)	50.0(51.2)	83.3(67.4)	100.0(89.4)
18℃	8.3(7.0)	8.3(18.7)	16.7(30.5)	50.0(43.1)	91.7(56.7)	100.0(75.3)
22℃	25.0(5.2)	8.3(14.0)	16.7(22.8)	50.0(32.3)	83.3(42.6)	100.0(56.4)

① The values listed in brackets were calculated from the Fanger's draft equation.
② The turbulence intensity was assumed to be 25%.

In the experiment, an air velocity was designated to cause a draft when the questionnaire was completed, so that a subject would feel unacceptable air movements locally and would feel cooler than neutral and uncomfortable at the exposed body parts. Generally, at a flow rate of lower than 1.2 l/s, the percentage of those dissatisfied was less than the PPD value from Equation (3.2), and at a higher flow rate the percentage of those dissatisfied was much higher. At a flow rate of 2.5 l/s, 100% of the subjects felt a draft and local discomfort. Here, subjects may have

included factors other than an unwanted local cooling effect into the concept of draft. Xia et al. (2000) suggested that the definition of draft should contain not only the cooling effect at lower temperatures, but also the annoying effect caused by the drying effect and air pressure at a higher temperature/velocity. Table 3.4 suggests that proper cooling from personalized air supplied at a flow rate of less than 1.2 l/s can not only prevent subjects from feeling a draft but also raise the comfort level. The subjects felt neutral to slightly cool but more comfortable. However, personalized air at a higher flow rate was definitely the source of the complaints about local drafts, annoying effects, and discomfort caused by wind pressure. This is further proved by Figure 3.12. With the increase in flow rate, although the overall thermal sensation was generally lowered step-by-step, the overall thermal comfort first rose and then declined, with a maximum value of about 1.3 to 1.5 at a flow rate of 0.8 l/s (The corresponding outlet velocity is 0.16 m/s). This is in line with the wisdom that people prefer a cool head and warm feet.
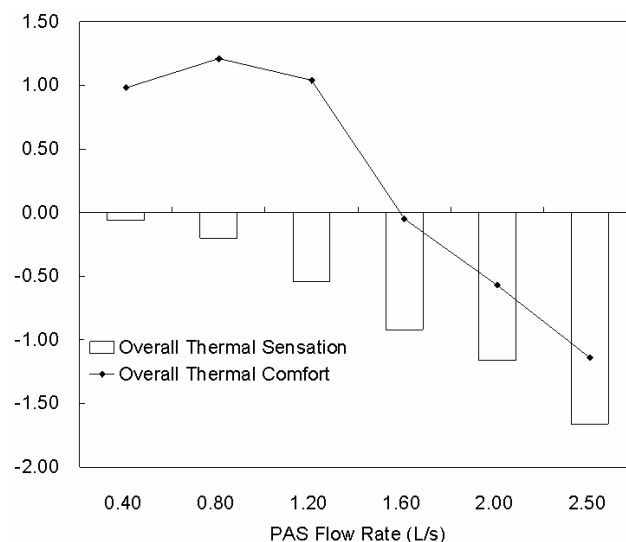
(a) T=15℃
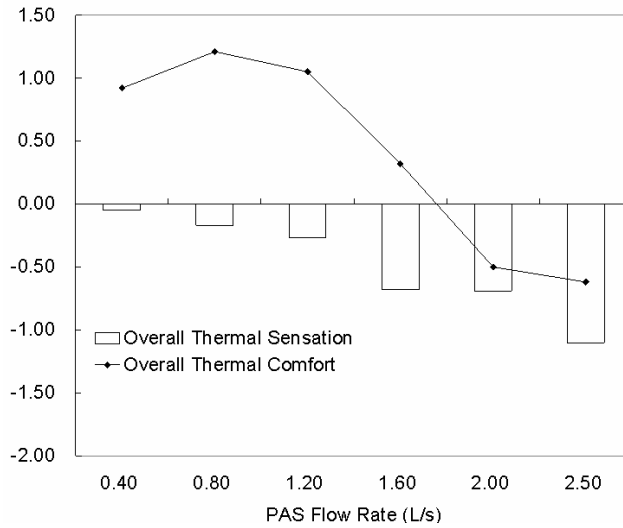
(b) T=18°C
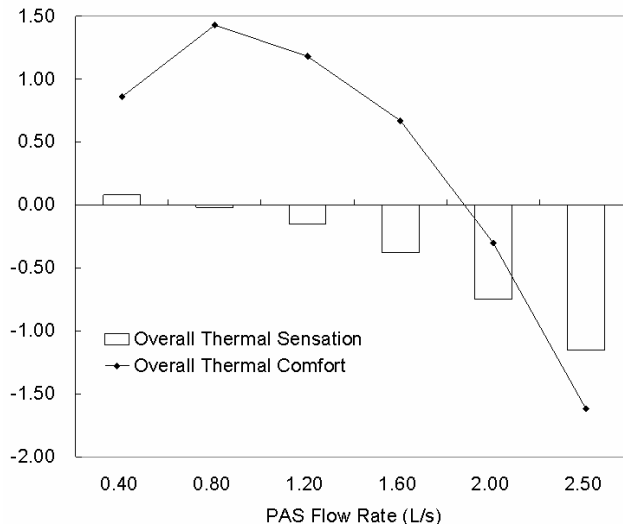
(c) T=22°C

Figure 3.12 Overall thermal sensation and thermal comfort under different personalized air conditions

In previous investigations of thermal comfort when a person was placed in a non-uniform thermal environment, such as the one caused by a vehicle HVAC system and personalized ventilation system, attempts were made to predict the overall thermal sensation and comfort by the local thermal sensation and comfort at different body parts (Zhang 2003, Li 2004). The following equation was usually employed:

$$\text{overall sensation} = \frac{\sum \text{weight}_i \times \text{local sensation}_i}{\sum \text{weight}_i} \qquad (3.3)$$

The weight for each body part was determined by the size of the body part, the sensitivity to warmth and cold, and the sensation of divergence from the rest of the body. Figure 3.13 shows the linear correlation between overall thermal sensation and every local sensation. No strong correlation was found. Perhaps a large sample in present experiments was required to deduce the relationship.
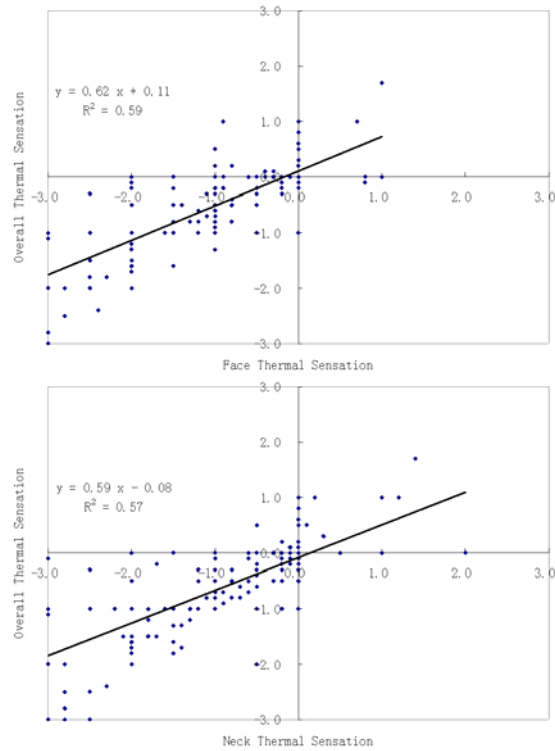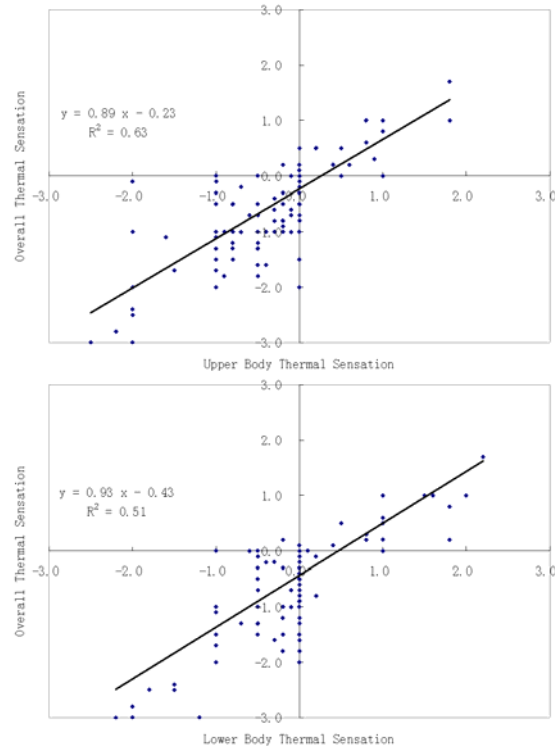
Figure 3.13 The correlations between overall thermal sensation and local thermal sensation

The survey results were limited to chair-based personalized ventilation, which supplied personalized air at the microphone position. The personalized air flowed upward across the human face. It was proved that even at equal air velocities the thermal sensation varied at different flow directions (Mayer and Schwab 1988). Zhou (1999) had shown that with the same air velocity, airflow from below resulted in the highest percentage of subjects dissatisfied due to draft, whereas airflow from the above resulted in the lowest percentage of dissatisfaction.

3.3.2.4 Preferences in air temperature and movement

The dissatisfaction about personalized air found in this study could be divided into two kinds. One was dry eyes, lips, noses, and/or disturbed breath caused by air movements. The other was a cooling draft at the face and neck caused by enhanced convective heat loss that combined the impact of air temperature and velocity. In

each of the experimental conditions, the preferred personalized air temperature and flow rate were collected. Three preferences for temperature (warmer, no change, and cooler) and three preferences for flow rate (higher, no change, and lower) were allowed for the subjects to choose from. It was believed that there was a close relationship between the preferred personalized air temperature with thermal sensation, while the preferred flow rate was associated with feelings of irritation and discomfort at the surface of the skin induced by air movements (Table 3.5).

Table 3.5 Expected air movement at different personalized air conditions

PAS System		Excepted Air Movement (%)			Excepted Air Temperature (%)		
Temperature (℃)	Flow Rate (L/s)	Lower	No Change	Higher	Cooler	No Change	Warmer
15	0.4	0	42	58	16	42	42
	0.8	0	75	25	0	58	42
	1.2	58	33	8	8	50	42
	1.6	75	25	0	25	25	50
	2.0	92	0	8	25	17	58
	2.5	92	0	8	25	17	58
18	0.4	8	50	42	16	42	42
	0.8	17	58	25	17	8	75
	1.2	25	67	8	25	42	33
	1.6	67	33	0	25	33	42
	2.0	92	8	0	17	17	66
	2.5	92	8	0	9	33	58
22	0.4	8	42	50	50	42	8
	0.8	17	75	8	0	83	17
	1.2	58	42	0	8	75	17
	1.6	67	33	0	16	42	42
	2.0	92	8	0	16	50	34
	2.5	100	0	0	0	50	50

A statistical analysis indicated that the expected air movement was greatly influenced by flow rate (P<0.01). More than half of the subjects wanted to reduce the supply flow rate when it exceeded 1.6 l/s. The influence of air temperature on the expected air temperature was not significant (P>0.05). Flow rate had no significant impact on the expected air temperature (P>0.05). This implies that the subjects were able to distinguish the effect caused by air movement and air temperature. Generally, more than 40% of the subjects wanted warmer personalized air when it was served at 15℃ and 18℃，even at a small flow rate.

3.4 Discussion

This work studied pollutant exposure reduction of a chair-based personalized ventilation system at various flow rates. It should be borne in mind that the ventilation effectiveness of personalized ventilation is under the control of many other factors, such as the exhalation process, body posture and movement, the background room air distribution method, etc. At a high personalized air flow rate it was found that the influence of exhalation was limited through the comparison of numerical and experiment results (Gao and Niu 2004). Fortunately, in a normal breathing process less than 16% of exhaled air is re-inhaled by the person himself/herself (Murakami 2004). It can be reasonably envisaged that serving personalized air can remove the exhaled air and reduce the re-inhalation ratio. So far, there have been few investigations in the field of personalized ventilation on the impact of body posture, and more studies are needed. Other types of personalized ventilation have been studied before throughout the world. The current results are particularly applicable to chair-based personalized ventilation, where the ATD is located at the position of the microphone. The situation will be completely different if the ATD is set at other positions, such as in the upper front of the face.

Generally, PER for different types of PV at various flow rates as shown in Figure 3.14 has three common characteristics: 1) PER is less than 1. 2) PER is zero when personalized air flow rate is zero and PER starts to ascend steeply at a certain flow rate, V_a. 3) the increase of PER becomes marginal at another flow rate, V_b. Ideally the operating flow rate of PV should be greatly higher than V_a and be as high as V_b. Therefore in the tests of air terminal devices (ATDs), finding the PER curve, at least V_a and V_b, is essential.
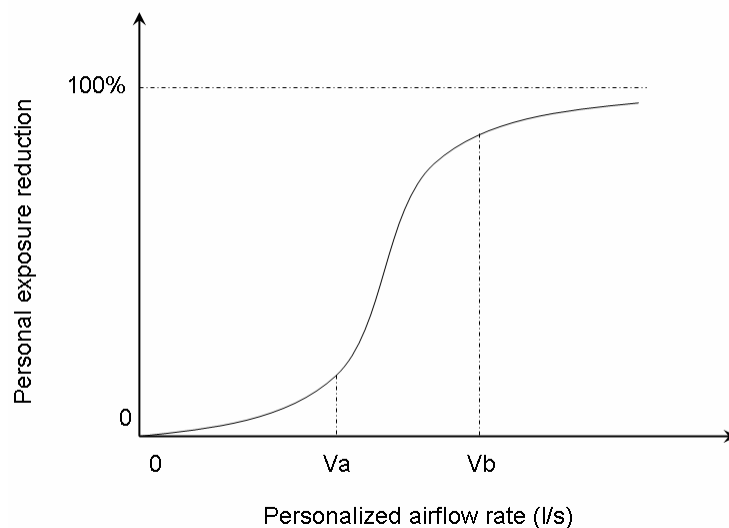
Figure 3.14 Schematic diagram of personal exposure reduction as a function of the personalized airflow rate

With PV the human exposure can be estimated by Equation (2.6). In mixing ventilation with a relatively uniform temperature and concentration field, personalized air can at all time dilute the pollutant concentration in inhalation if it is not directed against a pollution source. However the situation could be entirely different in displacement ventilation or under-floor air distribution (UFAD) where

vertical temperature and concentration stratification do exist. Temperature stratification inhibits the contaminant transport in the vertical direction. Ideally, contaminants generated in the upper recirculation zone could not be entrained into the lower occupied zone. The exhaled airflow (if it is a horizontal jet through the mouth) can be locked in the stratified layer at the breathing-zone height (BjØrn 2002). In this background supplying of personalized air from the front of the face breaks this stratification of temperature and concentration, and intensifies the transport of contaminants and the exhaled air. Cermak and Melikov (2003) compared the pervasion of the exhaled air from one manikin in a room conditioned by UFAD with and without personalized air supplied from the front of the face a little above the head. In their experiments the exhaled air was regarded as the source of the airborne infectious agents. The other manikin 1.65m away facing the polluting manikin was designated as the exposed person. They found the exposure to the exhaled air was higher if the polluting manikin was equipped with PV at the flow rate of 10 or 20 l/s. The exposure was the highest if both manikins were equipped with PV. This negative performance of PV was also testified by Melikov et al. (2003). Therefore PV has the risk of strengthening the spreading of respiratory epidemic diseases from person to person, such as SARS, common cold and flu. One expected promising scenario is that personalized air sweeping upward over the face carries the exhaled air to the upper recirculation zone. The upward airflow surrounding the body is assisted by personalized air if it is supplied below the chin. However this assumption should be validated in the future studies. In some special cases personalized air supply will enhance indoor contaminant transport, increase pollutant concentration level, and finally increase human exposure. Thus PV will not always guarantee a better inhaled air quality.

In the current survey of human responses to personalized ventilation, the position of the ATD was fixed and the subjects had no right to select their preferred location for the ATD. This deviated from the original design motivation of this chair-based personalized ventilation system, where the ATD is connected to the flexible "goose-neck' support that can be freely set by the user. Fixing the ATD position may imply the loss of potentially the greatest benefits of personalized ventilation, that is, the availability of personal control. Individual adjustment enables the occupant to 'design what he/she wants by himself/herself.' Therefore, further studies on user adjustment behavior are indeed necessary.

There are two perceived application strategies for personalized ventilation. The first is that the temperature of ambient room space is kept at 23-26 ℃ (comfort zone), and the second is to keep this temperature at about 26-29℃ and let the personal micro-environment be conditioned by personalized air in order to achieve energy saving. Can the spot cooling from personalized air accommodate individual preferences if the human body is placed in an environment in the comfort zone? Can the spot cooling of personalized ventilation bring thermal comfort to the whole body if the room air condition is out of the upper limit of comfort standards?

Kaczmarczyk's studies showed that at a room air temperature of 23-26 ℃ , personalized ventilation could improve the acceptability of and the occupants' satisfaction with the thermal environment without causing a drafty feeling, by adjusting the position of the air outlet, air flow rate, and air temperature (Kaczmarczyk 2003). A desk-edge mounted personalized ventilation device with a

supply flow rate of 3.5-7.1 l/s could bring individual control of range of equivalent homogeneous temperatures (EHT) up to $3℃$ based on thermal manikin testing (Tsuzuki et al. 1999). The cooling effect is strongly dependent on the air velocity, flow direction, temperature, turbulence, how much of the body is affected, and which parts. In physiological aspect, occupants can regulate local air conditions among the six factors in conventional thermal comfort theory (i.e., dry-bulb temperature, mean radiant temperature, air velocity, humidity, clothing insulation, and metabolic rate). In psychological aspect, individual control leads to a relaxation of expectations and a greater tolerance of temperature excursions (Brager and de Dear 1998).

It is well known that providing the occupants with locally controlled air movement can get back thermal comfort in warm environments. The higher the room air temperature, the higher the required local air velocity. The quantitative relationship of the trade-off between air temperature and velocity has been studied before (Fountain et al. 1994, Li 2004, Gong 2005) (Table 3.6).

Table 3.6 The models developed for local air movement in warm environment

Researchers	Equation	Remarks
Fountain et al. 1994	$PS = 1.13T_{op}^{0.5} - 0.24T_{op} + 2.7v^{0.5} - 0.99v$ (3.4)	This equation is only applicable in warm isothermal environments (24.5℃<Top<28.5℃), in which enhancing local air movement is proposed to bring overall thermal comfort. PS is the predicted percent satisfied. Top is operative temperature. v is air velocity. The air velocity is based on whole-body cooling calculations, and it is the average of air velocity at head- height, mid-body, and foot-level.
Li 2004	$TSV = 0.152t_a - 0.0726D_t - 0.676v_f - 3.15$ (3.5)	TSV-whole body thermal sensation t_a-ambient air temperature, 26-30℃ D_t-temperature difference between personalized air and room air, 0-6℃ v_f-local air velocity forced by PV, 0.4~1.4m/s It is developed for steady personalized ventilation.
Gong 2005	$PD = 0.001654(28 - t_a)^{1.25}(v_f - 0.05)(34 - T_f)$ $+ 0.0214T_u(v_f - 0.05)(34 - T_f)$ (3.6)	PD-the predicted percent dissatisfied t_a-ambient air temperature, 23.5~26℃ v_f-local air velocity forced by PV, <0.9m/s T_f-local air temperature of PA, 21~26℃ T_u-turbulence intensity, 0-60% This equation is developed from head cooling in a warm ambient environment.

The required local air velocity at the head (for most PV systems personalized air is directed at the head) is compared in an isothermal condition (Figure 3.15(a)) and a non-isothermal condition (Figure 3.15(b)) with a room air temperature of 26℃ since the intersection of the three models' application range is 26℃. In the comparison, PS is set to 90%, TSV 0, and PD 10%. The difference in required air velocities predicted by these models is relatively small. In a room with an ambient air temperature of 26 ℃, the local air velocity at the head used to offset elevated temperature is 1.19~1.26 m/s when personalized air is served also at 26℃, and 0.92~0.97 m/s when at 23℃. These velocities are reasonable in view of the fact that in the higher temperatures at about 30℃, very high air velocities up to around 1.6 m/s have been found to be acceptable (Toftum 2004). These data provide a useful foundation in determining the adjustable range of personalized air flow rate in the design stage. However it should be mentioned that these velocities are mean values based on the statistical results. The individual difference in preferred air velocity is wide (0.35~1.35 m/s at 28℃, and 0.55~1.85 m/s at 29.5 ℃) (Toftum 2004). Therefore individual control of personalized air velocity is very important.
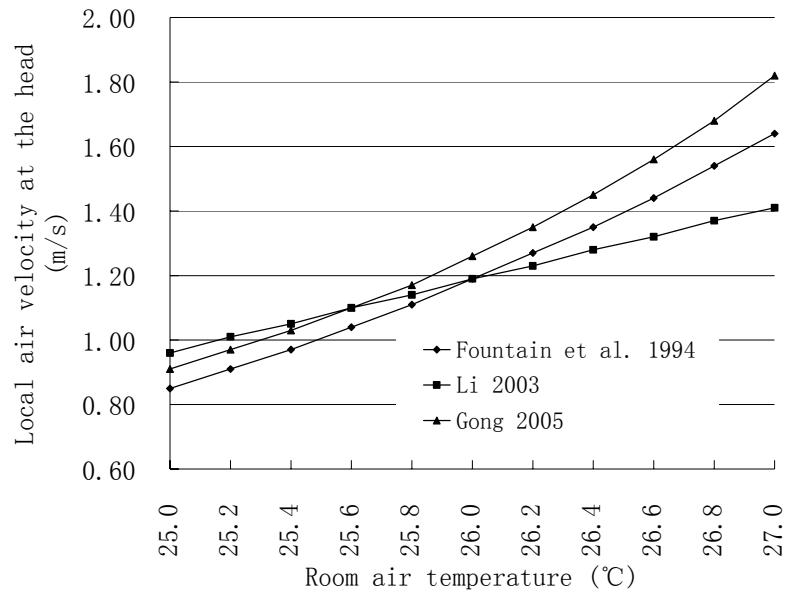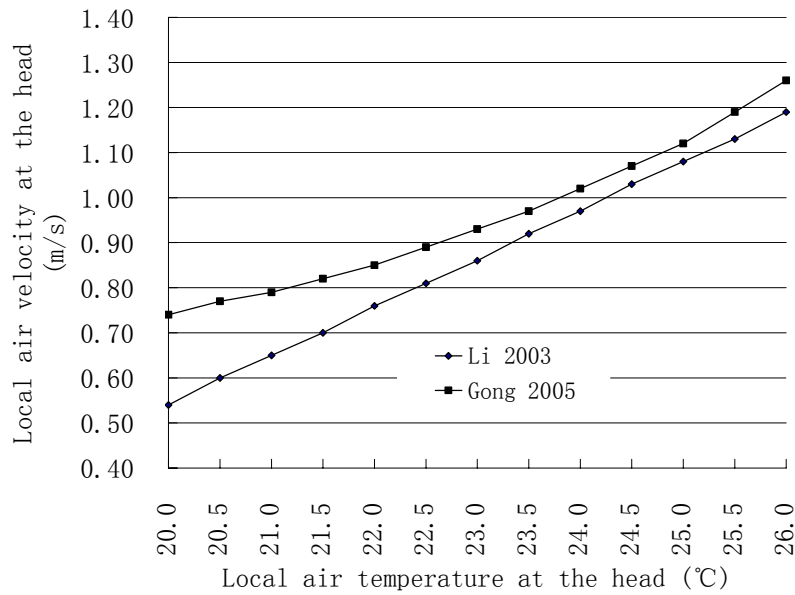
Figure 3.15 Comparison of different comfort models in an isothermal condition (a) and a non-isothermal condition (b)

In present experimental study of the chair-based personalized ventilation, the outlet area of PV is so small that the effective area of the human body under the control of personalized air will be consequently confined. The thermal sensation will then be

dominated more by ambient air than personalized air. Due to the small supply rate and outlet area, the author suggests that the ambient room space should be conditioned in a comfort zone and that personalized air is served primarily for better inhaled air quality.

3.5 Summary

The ventilation performance of a chair-based personalized ventilation system and the human response to it were studied by using a thermal manikin and subjective measurements.

One ATD of the personalized ventilation system (named SCN) was tested with regard to inhaled air quality and fresh air utilization efficiency. Supplying personalized air directly to the breathing zone of each individual made it possible to achieve a reduction of up to 76% in the level of pollutants in inhaled air. But even when the nozzle was located very close to the nose of the occupant, the inhaled air was still not completely composed of personalized fresh air. The quality of inhaled air improved with an increase in the supply air flow rate. The pollutant exposure reduction effectiveness reached a maximum value at a certain flow rate, whereas utilization efficiency of fresh air decreased as the flow rate increased. The influence of the PA temperature was also investigated. Taking into account both air quality and energy efficiency, a supply flow rate of from 0.8 l/s to 1.6 l/s was recommended.

Personalized air supply lowered inhaled air temperature and improved perceived air quality with temperatures ranging from 15℃ to 22℃. People were more sensitive to personalized air flow rate than to personalized air temperature. A higher flow rate than 1.6 l/s was not desirable since local drafts and intensive feelings of irritation

would result. Personalized air with temperatures below the room air temperature could bring 'a cool head' and a more comfortable feeling in comparison with mixing ventilation. Better inhaled air quality and thermal comfort could synchronously be achieved by personalized ventilation with a proper design.

Chapter 4

CFD study of the chair-based personalized ventilation system

During the last few years, CFD technology has progressed to the point where it is now possible to use it to analyze the micro-climate around a human body. Based on the review in Chapter 2 and encouraged by this progress, CFD techniques are employed to study the micro-environment around a human body in a PV system. As personalized fresh air is supplied directly to the breathing zone, it will modify the local airflow in the region close to the nose and mouth, the local heat flux, and the thermal sensation. The use of CFD techniques is essential for the visualization of the airflows in the breathing zone; the determination of the local temperature, velocity, and concentration fields; and the subsequent evaluation of the performance of the PV design.

4.1 CFD study of the micro-environment around a human body and personalized ventilation

4.1.1 Introduction

In this section, the airflow field and convective heat transfer around a seated human body with and without PV are simulated. The inhaled air quality improvement under different personalized airflow rates is studied. The respiration process is simplified to a steady inhalation process. The influence of other variables, such as the personalized air temperature, is numerically investigated in the next section.

4.1.2 Development of the numerical thermal manikin (NTM) and CFD methods

The geometry of the NTM in this study is a real and accurate representation of a nude seated female occupant whose arms are arranged in the posture of a person

seated behind a desk. Based upon an available thermal manikin (manufactured by P.T. Teknik, Denmark), all of the fine surface characteristics and extremities of the body can be obtained by using a 3-D laser scanning technique (Figure 4.1).
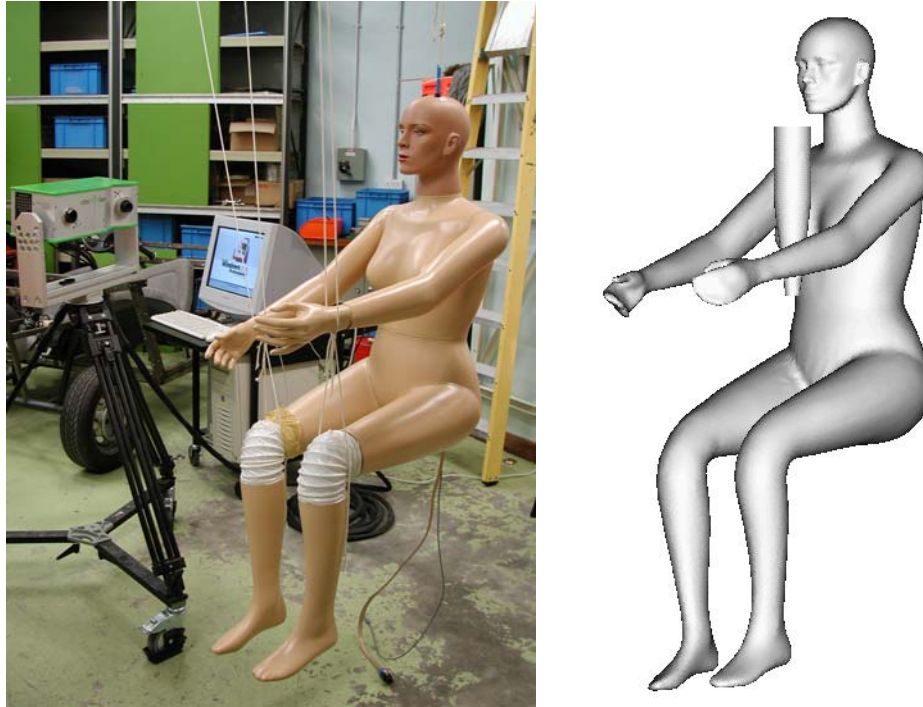
Figure 4.1 Geometry of the human body (left: thermal manikin in the laser scanning workshop; right: geometry of the numerical thermal manikin with the personalized ventilation device)

Openings at the nose and mouth are provided to simulate the breathing function. The shapes of hair and clothes are not included, as their correct description is too difficult. The surface of the NTM is composed of small patches that are discretized into triangular elements with an average length scale of 4 mm during grid generation. The patches are refined for certain special segments of the body, such as the face and hands. To save computational resources, the surface patches are coarsened at the back and abdomen. The total number of patches is about 2,000, and the surface area is 1.5696 m^2. This value is a little smaller than the surface area of 1.688 m^2 of the

numerical thermal manikin that was developed by Murakami et al. (1998) and the surface area of 1.594 m^2 of that developed by SØrensen and Voigt (2003).

The seated human body is placed in a displacement ventilated room (Figure 4.2). As illustrated in Figure 4.1, the personalized ventilation ATD is located at the microphone position beneath the chin. In this numerical simulation, a single ATD with a circular outlet, known as SCN (see Figure 3.3), is selected.
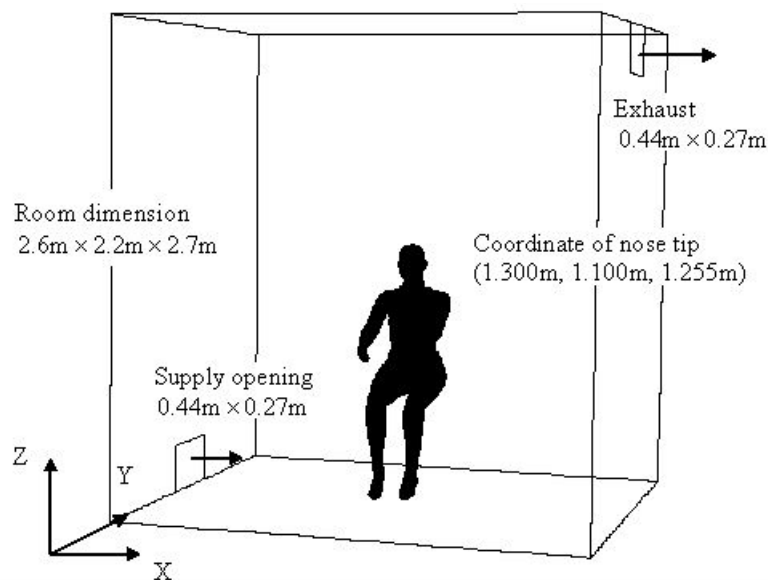
Figure 4.2 Thermal manikin in a displacement ventilated room

The ventilated room is divided into two parts: a cuboid that encloses the human body and the remaining room space. The cuboid is broken up into unstructured grids (tetrahedral cell topology), whereas the remaining room space is discretized with structured grids. In the region close to the body and the ATD the grids are refined. The total number of cells inside and outside the cuboid is 1,588,886 and 223,228, respectively (Figures 4.3 and 4.4).
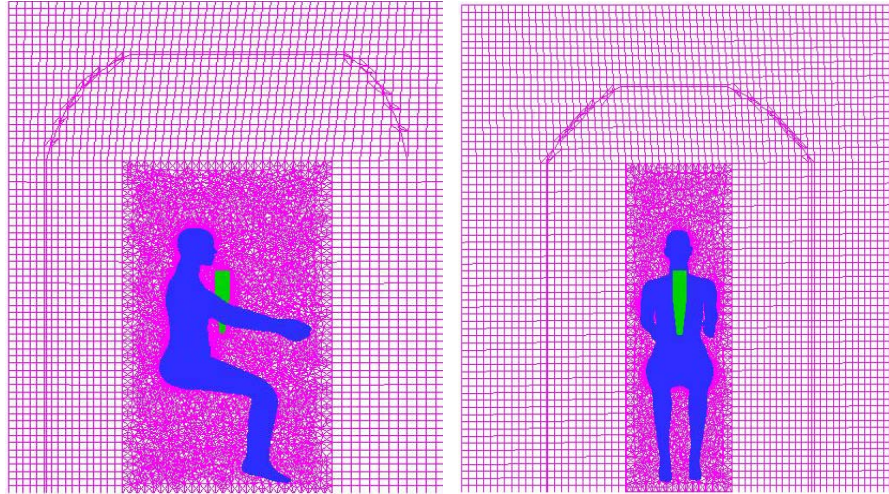
Figure 4.3 Side view and front view of the grid system
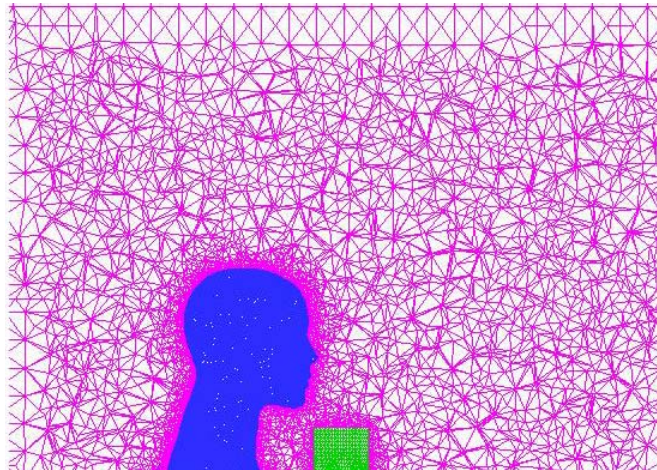
Figure 4.4 Grid distribution around the head and air terminal device

The standard k-ε model is applied in this simulation. As discussed in Chapter 2, as the airflow around a human body sitting in almost stagnant ambient air is under a transition regime that has not fully developed into turbulent flow, this selection is a compromise. The compromise of the standard k-ε model is based on the fact that the model is capable of simulating the convective heat transfer of buoyancy-driven airflow as long as a reasonable value of y^+ is achieved. The detailed numerical methods and boundary conditions are listed in Table 4.1 and Table 4.2. The real respiration process (see Figure 2.9a) is simplified to a steady inhalation process with

an inhaled air rate of 0.14 l/s. To characterize the quality of the inhaled air, the tracer

gas CO_2 is mixed with the room air and personalized fresh air supply. The radiation

is not taken into account at this stage, but is calculated in the thermal comfort

assessment in Chapter 5. The convergence is checked against the three criteria that

the ratio of the sum of the absolute mass residuals in each cell to the total mass

inflow is less than 0.1%, the ratio of the absolute energy residuals in each cell to the

total heat gain is less than 1%, and the sum of the normalized absolute residuals in

each control volume for all of the variables is maintained at less than 10^{-3}. Normally,

for each case less than 7,000-8,000 iterations are needed to achieve convergence if

the entire computational domain is initialized by setting the velocity to 0 and the

temperature to 22℃.

Table 4.1 Details of the numerical methods

Turbulence Model	Standard k-ε model
Numerical Schemes	Upwind second-order difference; PISO algorithm; Steady state with full buoyancy effect; Standard wall function.

Table 4.2 Boundary conditions

Room Air Inflow	$V = 0.12\text{m/s}$; $T = 22\ ℃$; $C = 500\text{ppm}$; $I = 5\%$; $D = 0.335\text{m}$.
Room Air Outflow	Pressure outlet
Room Wall	Adiabatic wall
Human Body	$T = 31\ ℃$;
Nose	$L = 0.14\text{l/s}$; $I = 0.5\%$; $D = 0.01\text{m}$ (velocity inlet)
ATD Boundary	Adiabatic wall
ATD Outlet	$L = 0 \rightarrow 3\text{l/s}$; $T = 20\ ℃$; $C = 4000\text{ppm}$; $I = 0.5\%$; $D = 0.08\text{m}$

4.1.3 Airflow field

Figure 4.5 shows the airflow around the body when the personalized airflow rate is 1.0 l/s. The human body is enclosed by a thermal plume, the thickness of which increases with height. The maximum air velocity that is due to buoyancy above the head is 0.25 m/s, which is in line with the value of 0.26 m/s that was established by Murakami et al. (1997).
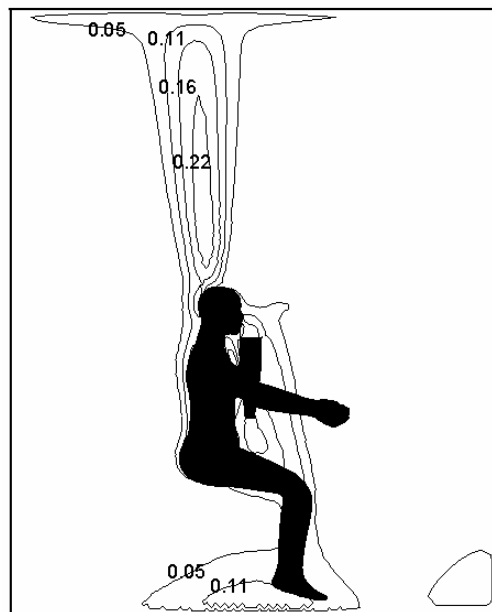
Figure 4.5 Airflow velocity (m/s) contour in the ventilated room at a personalized airflow rate of 1.0 l/s (at the surface x = 1.3 m)

The personalized air has an impact on the facial region, but almost no influence on the global flow in the room, as illustrated by Figure 4.6. The air speed in the facial region increases when the PV airflow rate increases.
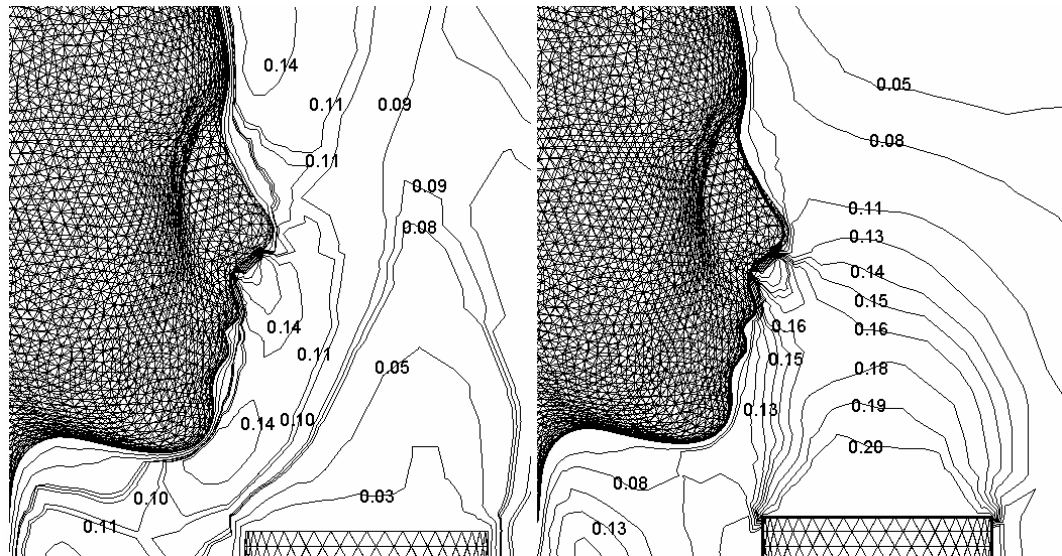
Figure 4.6 The air velocity (m/s) contour in the facial region at different PV supply rates (left: personalized airflow rate of 0 l/s; right: personalized airflow rate of 1.0 l/s)

It can be seen from Figure 4.7 that the buoyancy-driven airflow is able to draw contaminants from the floor region to the breathing region through the gap between the legs of the seated human body. Therefore, in the simulation of contaminant transport around a human body, the configuration of the legs is of great importance. The same result was reported by Brohus and Nielsen (1996).

Figure 4.7 Air path line at a personalized airflow rate of 1.0 l/s

4.1.4 Convective heat transfer

The room air temperature distribution is shown in Figure 4.8. The temperature stratification, which is a characteristic of displacement ventilation, can be clearly observed. The vertical temperature gradient below the height of the head ranges from 1.5℃/m below head height to about 0.7℃/m above the head. In agreement with the principle of displacement ventilation, the vertical temperature gradient in the occupied zone is large due to the heat that is generated by the human body, and is small in the upper zone due to the recirculation of the flow.
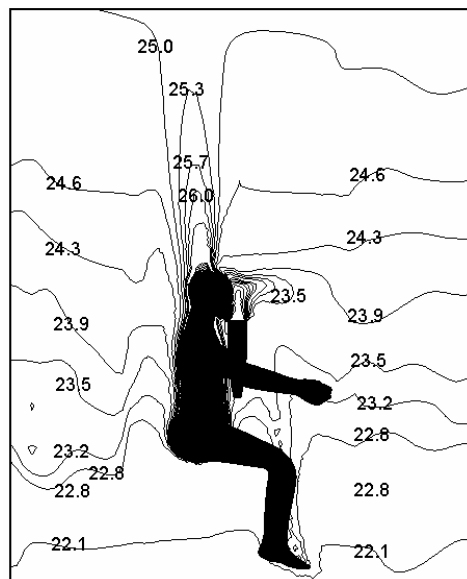
Figure 4.8 Room air temperature (℃) distribution at a personalized airflow rate of 1.0 l/s (at the surface x = 1.3 m)

Generally, the convective heat transfer from a human body to the surrounding environment is affected by several factors, including clothes, body posture, temperature difference, air velocity, turbulence intensity, and airflow direction. In this study, the nude seated human body is placed in almost stagnant air that has a

temperature difference of 7.5℃. The personalized air supply only serves to enhance the convective heat transfer in the facial region. The mean convective heat transfer coefficients of the body are almost the same at different personalized air supply rates. The convective heat transfer coefficient has a mean value of 4.79 W/(m^2℃), and ranges from 3.18 W/(m^2℃) at the shoulder to 7.14 W/(m^2℃) at the feet in the absence of PV. It has long been known that when the standard k-ε model is used in conjunction with the wall function, the calculated convection heat tends to be grid-dependent in the near wall region. A grid system with an inner domain grid size of 20 mm and an outer domain grid size of 40 mm is tested, and the total cell number is 212,973+278,196 = 491,169. The value of y$^+$ ranges from 4 to 25, and the convective heat transfer coefficient is 3.72 W/(m^2℃).

According to Equation (2.23) the convective heat transfer coefficient is 3.94 W/(m^2℃) at a temperature difference of 7.5℃. Some results from other researchers are listed in Table 4.3.

Table 4.3 Comparison of the mean convective heat transfer coefficient h_C of the human body[a]

Author	Position	Surface area[m^2]	Boundary condition	$t_{sk} - t_{am}$ [℃]	Ambient air speed [m/s]	h_C [W/(m^2℃)]
Topp et al. (2002) (CFD)	Seated	1.52	$q_C = 38$ W/m^2	5.1	0.05	7.4
Murakami et al. (1997) (CFD)	Standing	1.688	$q_C = 20$ W/m^2	4.0	<0.12	3.9
Murakami et al. (1997) (CFD)	Standing	1.688	$t_{sk} = 33.7$ ℃	7.7	0.25	7.1~12.8
Murakami et al. (2000) (CFD)	Standing	1.688	$q_t = 100.4$ W/m^2	6.8	<0.12	4.3
SØrensen and Voigt (2003) (CFD)	Seated	1.594	$t_{sk} = 31$ ℃	11.25	0.02	3.13
Brohus (1997) (Experiment)	Standing	1.62	$q_C = 25$ Wm^2	5.8	<0.05	4.32
de Dear et al. (1997) (Experiment)	Seated	1.471	$t_{sk} = 34$ ℃	12	<0.10	3.3
de Dear et al. (1997) (Experiment)	Standing	1.471	$t_{sk} = 34$ ℃	12	<0.10	3.4

[a] In Table 4.3, t_{am} is the ambient air temperature, q_C is the convective heat transfer from the human body to the environment, and q_t is the total heat loss from the body.

Comparing the results from Equation (2.23) and those from the experiments of de Dear et al. (1997), the mean convective heat transfer coefficient in the current simulation seems a little larger. There are two reasons for this. First, in this simulation the standard k-ε model, which is strictly only fit for fully developed

turbulent flows, is applied to the transition flow around the human body. Second, to describe the complicated geometry of the body, very fine unstructured grids are used in the computational domain close to the body, which leads to variation in the value of y^+ at the body surface boundary of between 1.5 and 25. This range seems a little smaller than the optimal range. As has been demonstrated, for the more coarse grid system near the body surface (the inner domain) where the y^+ value is between 4 and 25, the predicted h_c value improves from 4.79 to 3.72 W/(m^2 ℃). This again illustrates that caution should be exercised in locating the grids near the wall region.

4.1.5 Inhaled air quality

PV can create the effect of thermal sensation on the face, and thus a large PV airflow rate may cause local discomfort. According to Equation (3.2), assuming the PPD to be 20 and T_u to be 5%, the maximum mean air speed in the facial region should not be greater than 0.30 m/s. As the ATD in this study is located very close to the face, the mean air speed will reach 0.30 m/s in the facial region if the personalized airflow rate is 2.0 l/s. The value of the Reynolds number in the circular pipe of the ATD is 2,180 at a PV airflow rate of 2.0 l/s, which means that the airflow in the pipe is laminar if the flow rate is less than 2.0 l/s.
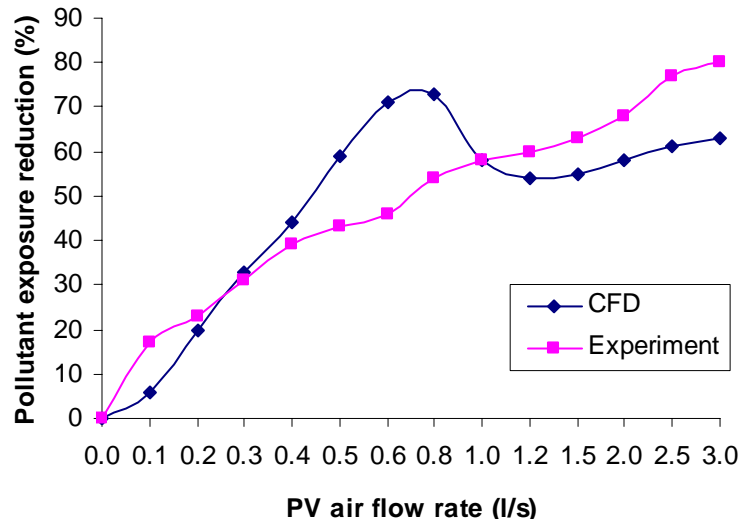
Figure 4.9 Pollutant exposure reduction obtained by CFD and experiment

The pollutant exposure reduction levels as a function of the PV airflow rate in the CFD and the experiment are compared in Figure 4.9. As the transient respiration process and the radiation are taken into account in the simulation, there is a difference between the two sets of results. In the experiment, the airflow from exhalation mixes with the personalized fresh air and is partly re-inhaled by the room occupants. Therefore, the replacement of dynamic breathing process with constant inhalation over-predicts the PER values. However, ignoring radiation may exaggerate the entrainment of the thermal plume, which will result in the under-prediction of the PER. The CFD result shows that an increase in the flow rate from 0 to about 0.8 l/s leads to an improvement in the quality of the inhaled air. The maximum PER is 73% at a flow rate of 0.8 l/s, and the PER decreases from 73% to 58% when the air supply rate increases from 0.8 l/s to 1.0 l/s. The slope of the curve becomes small and the PER reaches an almost steady-state value of 63% when the air supply rate is greater than 1.0 l/s. The occurrence of the maximum PER at a flow rate of 0.8 l/s can be explained by the local air velocity field and the CO_2 concentration distribution.

Although the ATD is located very close to the nose, the inhaled air does not all come from the PV system, but is composed of different airflows at different air supply rates. These airflows include air that is drawn up from the floor level through the gap between the legs of the occupant in the buoyancy function, air above the head, and personalized fresh air (Figure 4.10).
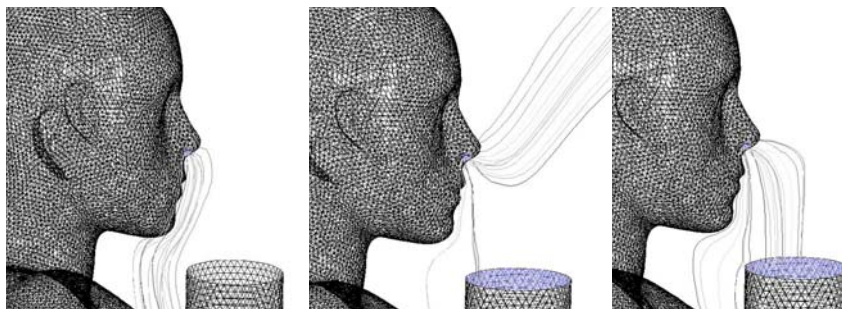
Figure 4.10 Path line of inhaled air (left: at a PV air supply rate of 0.1 l/s; middle: at a PV air supply rate of 0.4 l/s; right: at a PV air supply rate of 0.6 l/s)

The steady airflow around the nose is a potential flow. When the personalized airflow rate changes from 0 to 0.2 l/s, the jet flow from the ATD is too weak to penetrate the thermal plume. The potential flow is then enclosed by the thermal plume, because the plume is sufficiently strong at the height of the face. Therefore, all of the inhaled air comes from the warm rising flow. When the air supply rate increases from 0.2 l/s to 0.6 l/s, the thermal plume is penetrated by the jet flow, which means that the envelope of the potential flow is broken. At this stage, in addition to the warm rising air and the fresh air, some room air is drawn into the nose from the upper region. When the air supply rate increases continuously from 0.6 l/s to 0.8 l/s, the jet flow becomes strong enough to envelop the potential flow. No room air above the head can be drawn to penetrate this jet flow, and thus the inhaled air

consists of fresh air and the rising air in the thermal plume. The greater the air supply rate, the stronger the jet flow from the ATD and the higher the percentage of fresh air in inhalation. The increase in the air supply rate from 0 to 0.8 l/s results in the further extension of the core zone of the jet flow, in which there is a high concentration of fresh air. This proximity of this extension to the height of the nose explains the improvement in the inhaled air quality that occurs with an increase in the air supply rate. However, when the supply rate is greater than 0.8 l/s, the air speed of the jet flow exceeds 0.16 m/s, which is comparable to the air speed of the thermal plume at face height. This allows more rising air from the floor level to be entrained into the fresh air, which induces deterioration in the quality of the inhaled air. The same conclusion can be drawn from an inspection of the CO_2 concentration distribution in the facial region (Figure 4.11). The fresh air in the core zone of the jet flow reaches nose height at the supply flow rates of 0.8 l/s and 1.0 l/s, but the mean CO_2 concentration under the nose at 1.0 l/s is lower than it is at 0.8 l/s due to the entrainment function.
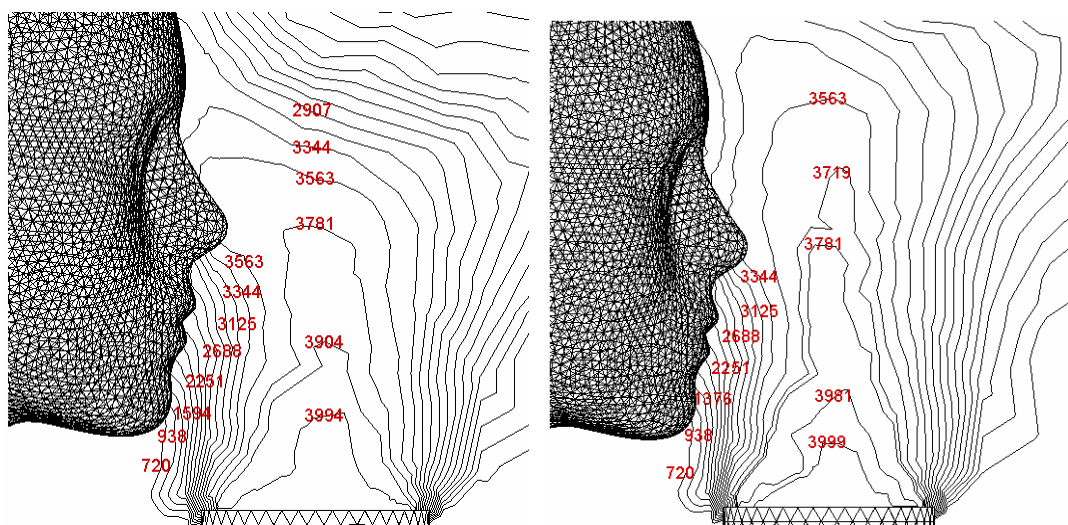
Figure 4.11 Local CO₂ concentration (ppm) contour (left: at a PV supply flow rate of 0.8 l/s; right: at a PV supply flow rate of 1.0 l/s)

4.1.6 Inhaled air temperature

Without PV, the inhaled air temperature is about 27.9℃. This is higher than the ambient temperature, because the inhaled air comes from the thermal plume. In the presence of a PV system, the inhaled air temperature decreases as the personalized air supply rate increases (Figure 4.12) when the temperature of the personalized air is 20℃. This drop in the inhaled air temperature has a positive effect on the perceived air quality, as discussed in Chapter 3. The minimum inhaled air temperature is 25.5 ℃ when the air supply rate is 0.8 l/s, but the temperature then climbs a little for the same reason, which leads to a decrease in the of PER from 0.8 l/s to 1.0 l/s.
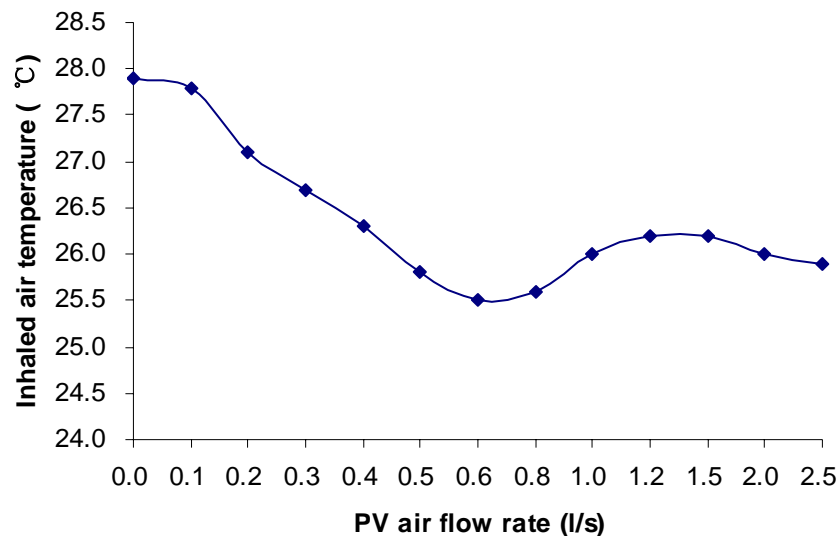
Figure 4.12 Inhaled air temperature at different PV airflow rates

4.1.7 Efficiency of the PV system

As illustrated in Figure 4.13, the maximum personalized air utilization efficiency is 16.6% at a personalized air rate of 0.6 l/s. This is much better than the 1%－ maximum value that can be achieved by conventional ventilation systems. There is a

large difference in the CFD and experimental results at low air supply rates, because exhalation plays an important role in the airflow field.
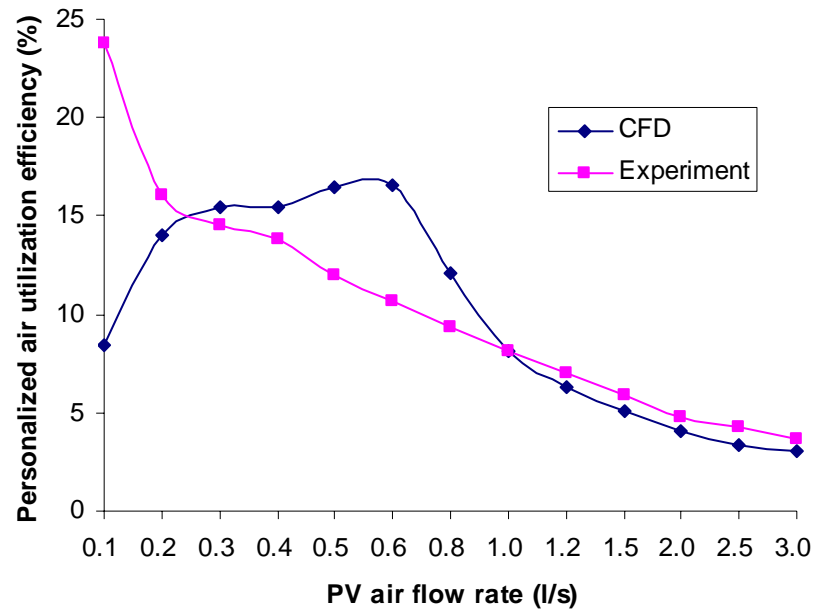
Figure 4.13 Personalized air utilization efficiency at different PV airflow rates

4.1.8 Summary

The micro-environment around a human body is simulated using the NTM. The performance of the selected ATD (SCN) is evaluated in terms of inhaled air quality, inhaled air temperature, and the efficiency of the PV system.

The maximum air speed in the thermal plume above the head of a seated human body is around 0.25 m/s. In the absence of the PV system, inhaled air is drawn up from the floor level to the facial region through the gap between the legs at the front. Therefore, in simulations that use a human body, the reduction of the legs to the torso may cause errors in the results. Temperature stratification in the ventilated room is observed. The mean convective heat transfer coefficient of the simulated seated human body is 4.79 W/(m^2℃). PV only increases the convective heat transfer from

the face to the surrounding environment, but has little impact on that of the overall body.

The maximum PER of the SCN in the numerical simulation is 73% at an airflow rate of 0.8 l/s, which is lower than the maximum airflow rate for local thermal comfort. In the steady-state simulation, the inhaled air temperature decreases as the personalized airflow increases from 0 to 0.8 l/s. At an room average temperature of around 23.5℃ and personalized air temperature of 20℃, the lowest temperature of the inhaled air is 25.5℃ when the maximum PER is achieved. The personalized air utilization efficiency, the highest value of which is 16.6% at an air supply rate of 0.6 l/s, first increases and then decreases as the personalized airflow rate increases. It can be seen from a comparison of the results from the CFD and the experiment that the exhalation process has an important influence on the PER at lower personalized airflow rates, because the strength of the exhalation airflow and the jet flow from the SCN are comparable at this stage.

4.2 Modeling the performance of personalized ventilation in different room air and personalized air conditions

4.2.1 Introduction

Based on the work in the previous section, simulation results using the renormalization k-ε model (Yakhot and Orszag 1986), which includes the low Reynolds number effect, are reported. The performance of the RNG k-ε model is compared to that of the standard k-ε model. The impact of changes in the room air rate, the room air movement, the personalized air temperature, and the turbulence intensity of the personalized air on the performance of PV are analyzed.

4.2.2 CFD method

The RNG k-ε model that includes a buoyancy term and a differential formula for effective viscosity to account for the low Reynolds number effect is combined with an enhanced wall treatment that integrates a two-layer model with an enhanced wall function, and is employed in this simulation using the CFD code Fluent (Fluent 6.1). The model is able to predict the heat and mass transfer in the viscous sub-layer of a solid surface, although with the drawback that finer grids are required near the wall. Using the RNG theory, the turbulence viscosity can be obtained by using the following differential equation.

$$d\left(\frac{\rho^2 k}{\sqrt{\varepsilon\mu}}\right) = 1.72 \frac{\hat{v}}{\sqrt{\hat{v}^3 - 1 + C_v}} d\hat{v}, \tag{4.1}$$

where $\hat{v} = \mu_{eff} / \mu$ and $C_v \approx 100$. Equation (4.1) is integrated to obtain an accurate description of how the effective turbulent transport varies with the effective Reynolds number, which allows the model to better handle low Reynolds numbers and near-wall flows. The enhanced wall functions are developed by smoothly blending an enhanced turbulent wall law with the laminar wall law. The whole domain is subdivided into a viscosity-affected region and a fully turbulent region. The two regions are demarcated by a wall distance based turbulent Reynolds number, Re_y, which is defined as

$$\text{Re}_y = \frac{\rho y \sqrt{k}}{\mu}, \text{ where} \tag{4.2}$$

$\text{Re}_y < 200$ is the viscosity-affected near-wall region.

The ventilated room is divided into two parts by structured and unstructured grids. Two boundary layers are created around the human body (Figure 4.14).
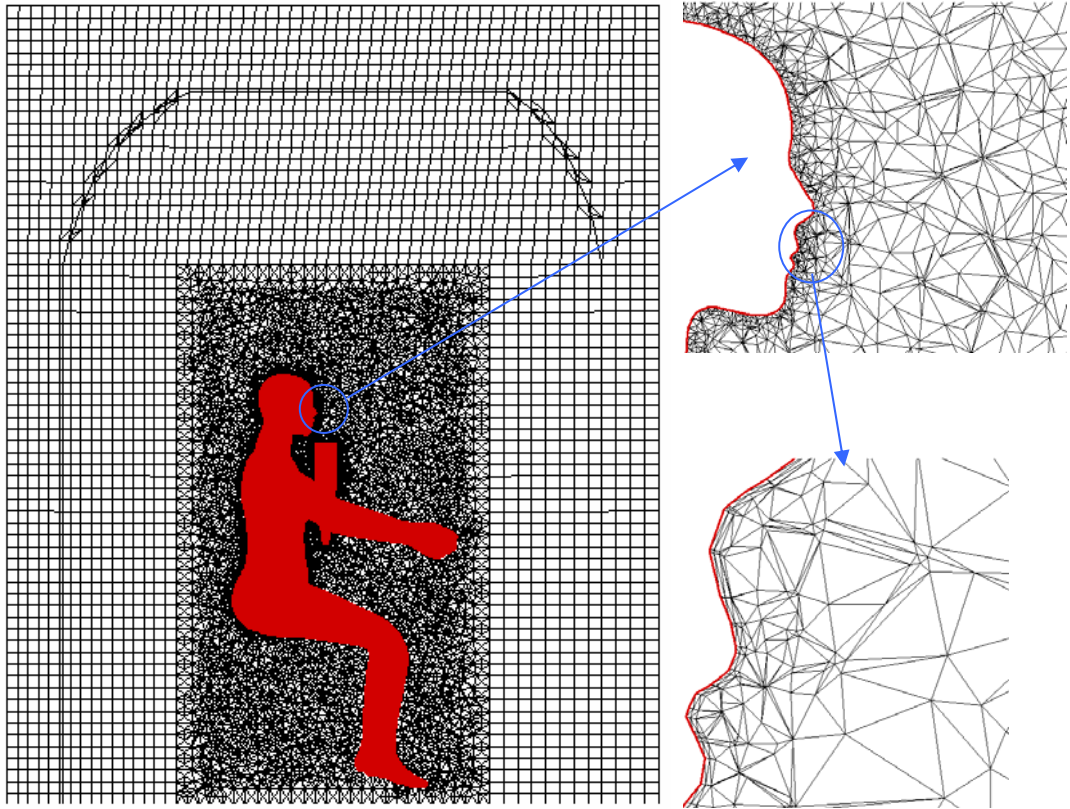
Figure 4.14 Grid system

The total number of cells inside and outside the cuboid is 1,062,900 and 223,228, respectively. At most body segments, the y+ values of the grids close to the human body are less than 1. A finer grid system with six boundary layers and a total of 1,745,857 cells is also tested, and the simulation results are similar. In total, 15 cases (Table 4.4) are simulated with different room air supply rates, PV airflow rates, temperatures, and turbulence intensity. The boundary conditions and numerical methods of Case 1-1 are listed in Table 4.5 and Table 4.6.

Table 4.4 Cases examined in the parametric study

Name	Room air supply method and velocity, m/s	PV airflow rate, l/s	PV air temperature, ℃	Turbulence intensity of PV air, %	Heat loss, W	PER, %
Case 1-1	From supply opening V = 0.12	0.8	20	5	43.5	74.4
Case 2-1	From supply opening V = 0.12	0.8	18	5	43.6	89.0
Case 2-2	From supply opening V = 0.12	0.8	22	5	43.5	46.4
Case 2-3	From supply opening V = 0.12	0.8	24	5	43.4	39.0
Case 2-4	From supply opening V = 0.12	1.6	20	5	44.0	55.6
Case 2-5	From supply opening V = 0.24	0.8	20	5	48.8	27.2
Case 2-6	From supply opening V = 0.24	1.6	20	5	48.9	46.2
Case 3-1	Left/right wall as room air inlet/outlet V = 0.02	0.8	20	5	49.4	18.1
Case 3-2	Left/right wall as room air inlet/outlet V = 0.2	0.8	20	5	76.7	0.01
Case 3-3	Front/back wall as room air inlet/outlet V = 0.02	0.8	20	5	49.8	20.8
Case 3-4	Front/back wall as room air inlet/outlet V = 0.2	0.8	20	5	74.5	47.0
Case 3-5	Back/front wall as room air inlet/outlet V = 0.02	0.8	20	5	48.5	18.1
Case 3-6	Back/front wall as room air inlet/outlet V = 0.2	0.8	20	5	75.1	55.5
Case 4-1	From supply opening V = 0.12	0.8	20	10	43.5	73.5
Case 4-2	From supply opening V = 0.12	0.8	20	20	43.5	71.0

Table 4.5 Details of the numerical methods

Turbulence Model	RNG k-ε model, including the low Reynolds number effect
Numerical Schemes	Upwind second-order difference; PISO algorithm; Steady state with full buoyancy effect; Enhanced wall treatment.

Table 4.6 Boundary conditions

Room Air Inflow	$V = 0.12 \text{m/s}$; $T = 22\,℃$; $C = 500 \text{ppm}$; $I = 10\%$; $D = 0.335 \text{m}$.
Room Air Outflow	Pressure outlet
Room Wall	Adiabatic wall
Human Body	$T = 31\,℃$;
Nose	$L = 0.14 \text{l/s}$; $I = 10\%$; $D = 0.01 \text{m}$.
ATD Boundary	Adiabatic wall
ATD Outlet	$L = 0.8 \text{l/s}$; $T = 20\,℃$; $C = 4000 \text{ppm}$; $I = 5\%$; $D = 0.08 \text{m}$.

4.2.3 Effects of the turbulence model

The airflow field, temperature field, and tracer gas concentration distribution are selected for the comparison of the two turbulence models. The magnitude of the air velocity just above the head is shown in Figure 4.15. In the experiment and simulation of Murakami (2002), the peak value of the overhead upward airflow is approximately 0.20 m/s. In the model in this study, the air speed is lower than 0.20 m/s. The reason for the difference is that the simulated body in Murakami's study is standing. The air speed above the head with the RNG k-ε model is a little higher than that with the standard k-ε model, although they are very close. This can be clearly observed by examining the room airflow field. As is illustrated in Figure 4.16, the core of the warm rising thermal plume with the maximum air speed does not occur right above the head due to the asymmetry of the seated body shape from back to

front. This phenomenon was validated in a simulation by SØrensen and Voigt (2003). The smooth vertical surface of the back is conducive to the formation of a warm upward flow that causes the flow direction above the head to deflect toward the back of the body. The warm flow above the head is thinner and stronger with the RNG k-ε model than it is with the standard k-ε model, although the maximum speed is the same at 0.26 m/s. This is because in the RNG k-ε model in this simulation of natural convection, the combined impact of the additional term R in the ε equation and other parameters, including C_1, $C_2, \sigma_k, \sigma_\varepsilon$, and C_μ, are different from those in the control equations of the standard k-ε model, which results in a decrease in the turbulent viscosity. Gan (1998) evaluated the performance of the RNG k-ε model and the standard k-ε model in predicting the turbulent buoyant flow, and found that the RNG k-ε model performed better than the standard k-ε model because of the inclusion of the rate-of-stain term R. Other modifications of the turbulence constants, such as C_2, σ_k, and σ_ε, also contributed to the improvement.
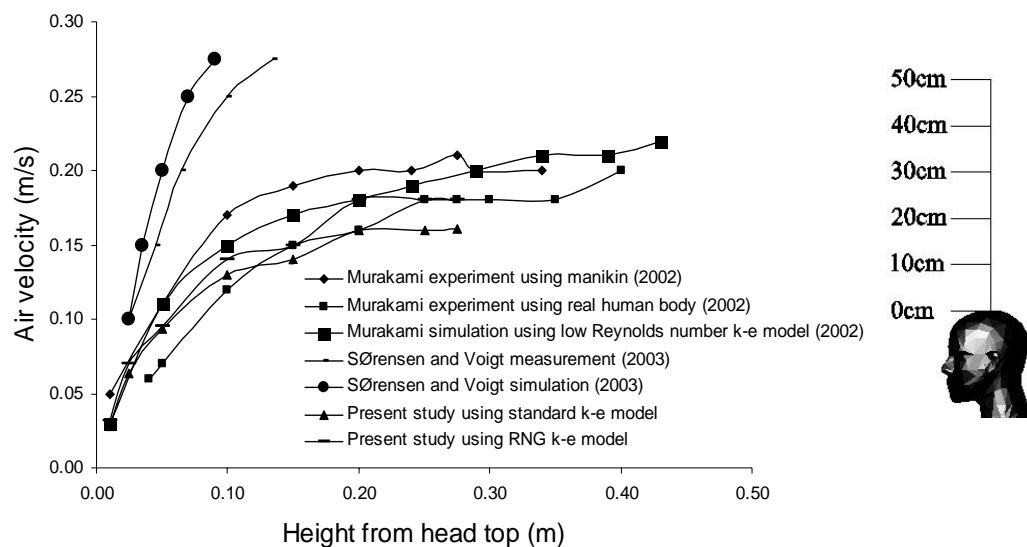
Figure 4.15 Comparison of air speeds above the head in calm ambient air
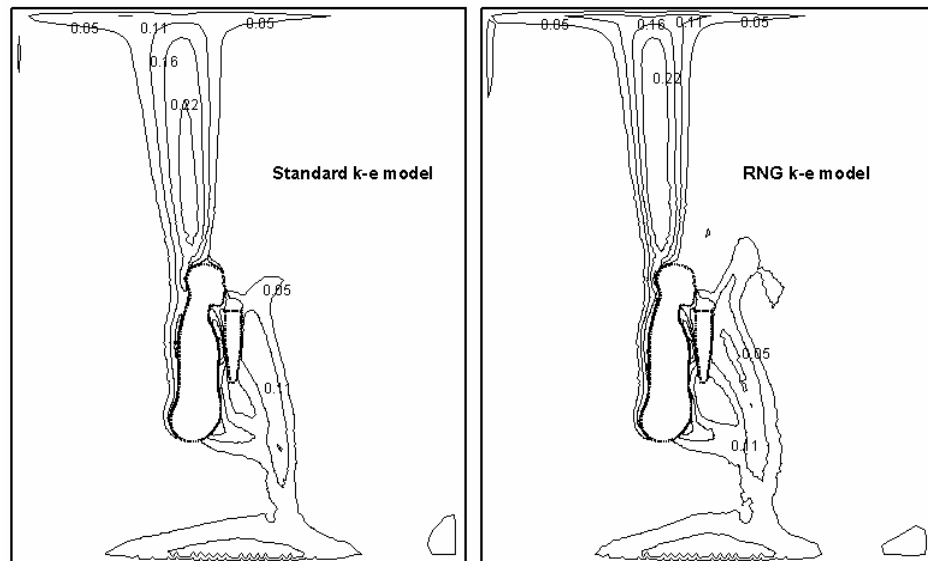
Figure 4.16 Air speed (m/s) contour at the middle surface (x = 1.3 m)

Figure 4.17 shows the air velocity boundary layer behind the human body in the neck region. The thickness of the velocity boundary layer is about 10 cm. In the simulation of a standing human body (Murakami et al. 1997), this thickness is 15 cm, whereas in the experiment investigating the effects of upward air movement at the neck of a seated human body it is 8-9 cm (Melikov and Zhou 1996), which is a little smaller than the value in the simulation. The maximum velocity in the boundary layer with the RNG k-ε model is larger than that with the standard k-ε model. This result was also found by Gan (1998) in a numerical investigation.

Figure 4.18 illustrates the concentration levels of the tracer gas CO_2 in the region around the nose and the outlet of the weak jet flow. The tracer gas concentration in the ambient room air and PV air supply is 500 and 4,000 ppm, respectively. It can be observed that large concentration gradients exist, and thus the accurate prediction of this concentration distribution is essential for the evaluation of PV performance. In contrast to the differing performance of the standard k-ε model and the RNG k-ε

118

model in the prediction of buoyant flow, the prediction by the two models of the gas concentration in the facial region is almost the same.
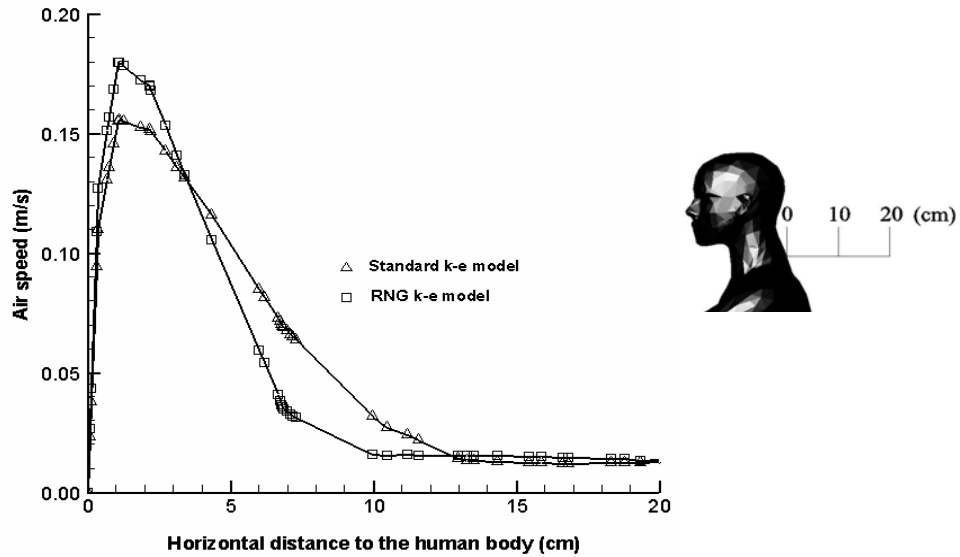
Figure 4.17 Magnitude of the air velocity at the neck level just behind the seated human body (at a height of about 1.10 m)
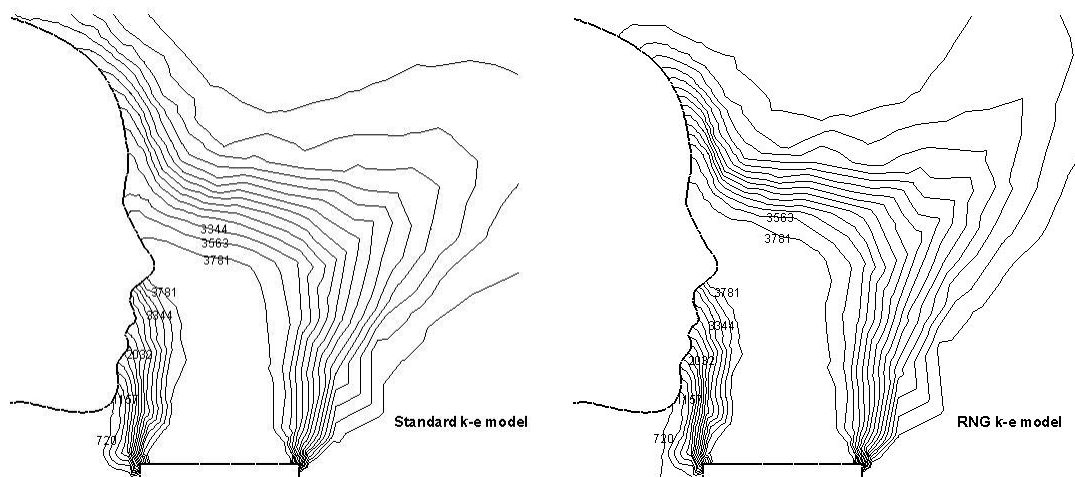
Figure 4.18 Tracer gas concentration contour (ppm) in the nose region (at the middle surface x = 1.3 m)

119

4.2.4 Effects of the room air change rate

Case 2-5 and Case 2-6 are designed to investigate the effects of the room air change rate per hour (ACH), in which the ACH rate is set to twice that in the standard Case 1-1. Generally, ACH has an impact on the room airflow pattern and room air temperature level if other factors, such as heat load and furniture configuration, are kept the same. Although the heat load differs a little between Case 1-1 and Case 2-5 because the human body is the only source of heat in the room and the boundary condition of the body surface is set to be isothermal, insight into the effects of ACH can still be obtained. In the displacement ventilated room, the ACH mainly affects the mean room air temperature (the temperature of the air at a height of 1.1m apart from the human body is assumed to be the mean room air temperature), since the change in the room air supply velocity from 0.12 m/s, as in Case 1-1, to 0.24 m/s, as in Case 2-5, results in little difference in the room ambient flow field. Therefore, attention should be focused on the mean room air temperature in studying the effect of ACH.

The room air and personalized air temperature have a combined influence on the thermal comfort, inhaled air quality, perceived air quality, and personal exposure reduction index.
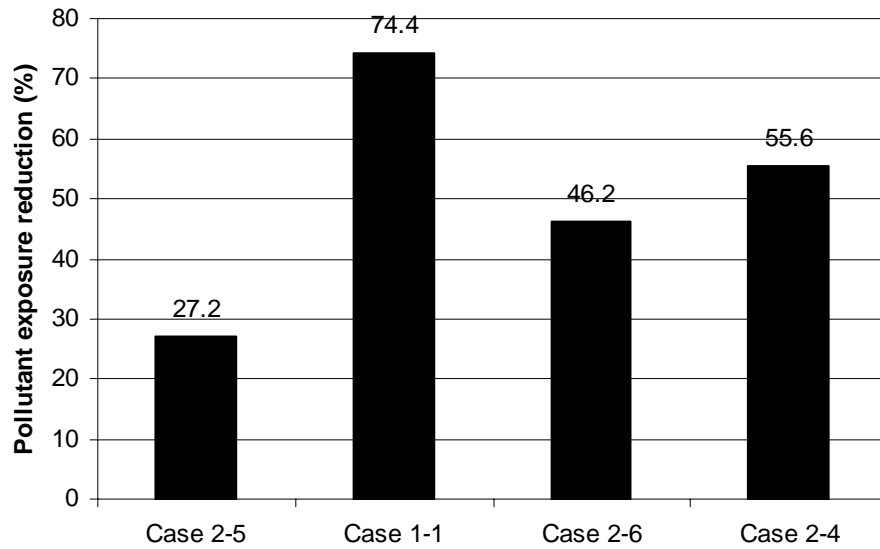
Figure 4.19 Comparison of the PER at different room air supply rates

Figure 4.19 shows the PER values in four cases when the room air is supplied at 0.12 m/s and 0.24 m/s and the personalized air is served at 0.8 l/s and 1.6 l/s. In the displacement ventilated room, the room air supply rate specifies the room air temperature level, which further determines the strength of the thermal plume around the human body (Figure 4.20 and Figure 4.21).
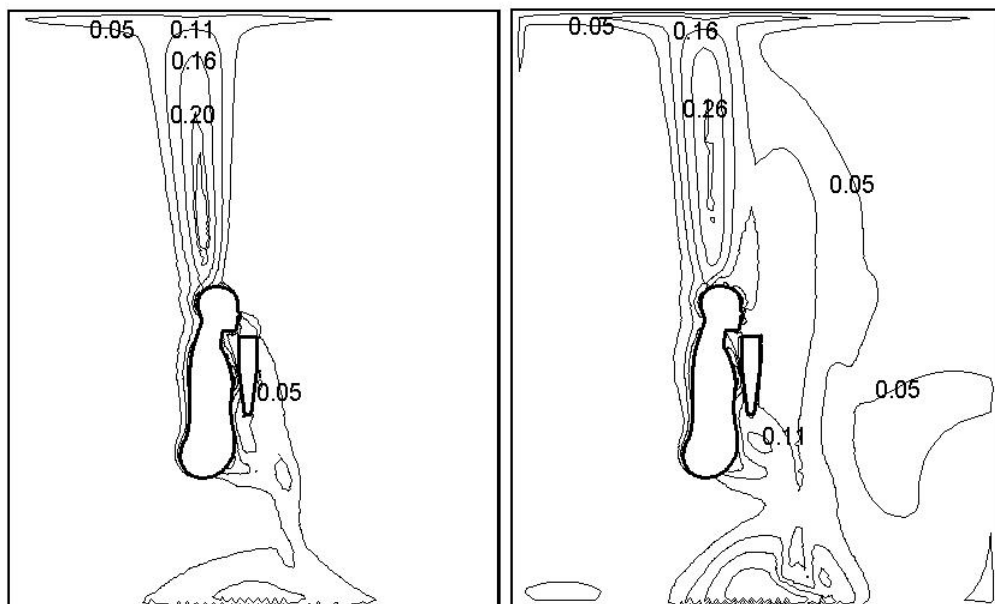
Figure 4.20 Air speed (m/s) contour at a room air supply velocity of 0.12 m/s (left) and

0.24 m/s (right) at the middle surface x = 1.3 m
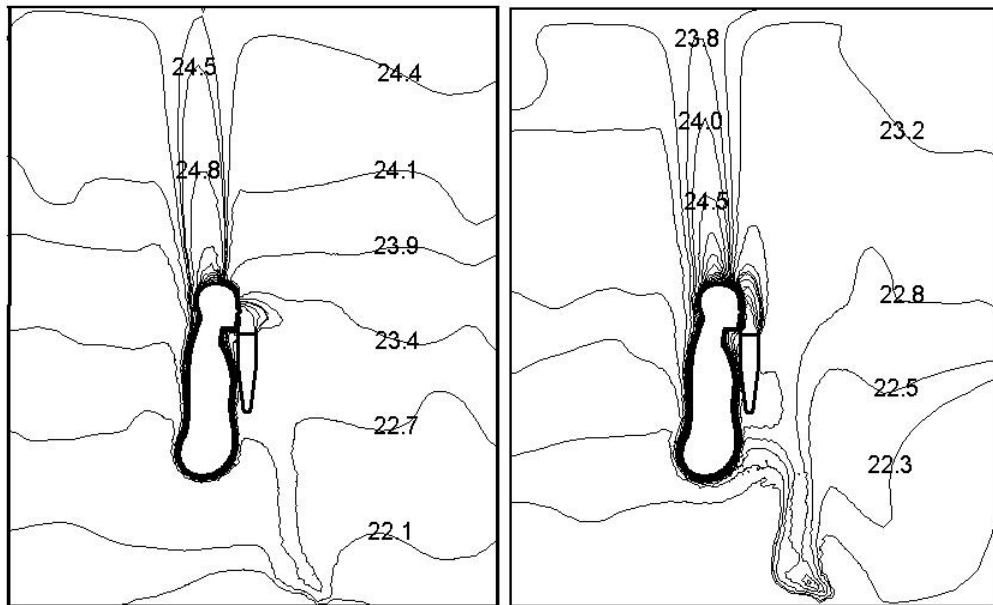
Figure 4.21 Temperature contours (℃) at a room air supply velocity of 0.12 m/s (left) and 0.24 m/s (right) at the middle surface x = 1.3 m

When the room air supply velocity increases from 0.12 m/s, as in Case 1-1, to 0.24 m/s, as in Case 2-5, the PER value decreases dramatically from 74.4% to 27.2%. This occurs at a personalized airflow rate of 0.8 l/s, and indicates that the PER value is very sensitive to the room air condition when the personalized air flow rate is low. When personalized air is served at a rate of 1.6 l/s, the PER changes from 55.6% to 46.2% if the room air inlet velocity shifts from 0.12 m/s, as in Case 2-4, to 0.24 m/s, as in Case 2-6. It appears that the weak jet flow is easily influenced by the thermal plume, and that the impact of the room air temperature on the PER is related to the strength of the personalized air jet flow. The higher the personalized airflow rate, the weaker the effect of the ambient air temperature, and vice versa. That the PER value in Case 2-5 is lower than that in Case 2-6 means that a higher personalized airflow rate brings better inhaled air quality, that is to say, a greater proportion of personalized air in the inhaled air. However, when the room air inlet velocity is 0.12

m/s, the PER value at a personalized air supply rate of 0.8 l/s is higher than that at the rate of 1.6 l/s, as reported in the previous section. Therefore, for this kind of PV system, in which personalized air is served at the microphone position at a low supply rate, the relationship between the PER and the personalized air flow rate is influenced by the ambient air condition.

It should be noted that in this simulation a fixed human body surface temperature is applied, and that under this boundary condition the plume around the body is affected by the average room air temperature. In reality, a human body at a moderate activity level may be better approximated by a fixed surface heat flux, with a convective thermal plume that is affected by both the radiant temperature and the room air temperature. Because of this, the impact of the room air temperature on the PER of PV may also depend on the radiant temperature, which, in turn, is determined by the background air conditioning system design. This deserves further investigation.

4.2.5 Effects of the temperature of the personalized air supply

As has been mentioned, the personalized air supply temperature and room air temperature have a combined effect on the performance of PV systems. Sekhar et al. (2003) tested one kind of desktop PV system, and found the ventilation effectiveness to be 1.84 and 1.6 at a personalized airflow rate of 15 l/s and personalized air temperature/room air temperature of 23/26℃, and 26/26℃. The combination of room air temperature and personalized air temperature that achieves the best inhaled air quality may be case dependent, as it is also related to other factors, such as the geometry and position of the ATD. Regardless of the PV design, it is important to ensure that the nose is in the core of the non-isothermal PV jet flow by taking

account of the personalized airflow trajectory deflection that is due to temperature difference. In some practical designs, the personalized air temperature can be controlled by adjusting the mixing ratio of the room air and the conditioned fresh outdoor air. This is not considered in this study, and the personalized air is assumed to be completely composed of fresh outdoor air.

Figure 4.22 shows the trend line of the PER when the PV temperature is gradually changed from 18℃ to 24℃. It is observed that increasing the personalized air supply temperature decreases the value of the PER. This is because the temperature of the personalized air determines the strength of the jet flow relative to the warm rising flow. Although the core of the fresh air reaches the mouth level, the concentration within the zone of less than 5 cm from the mouth differs greatly. It appears that a lower personalized air temperature results in less entrained room air in the inhaled air.
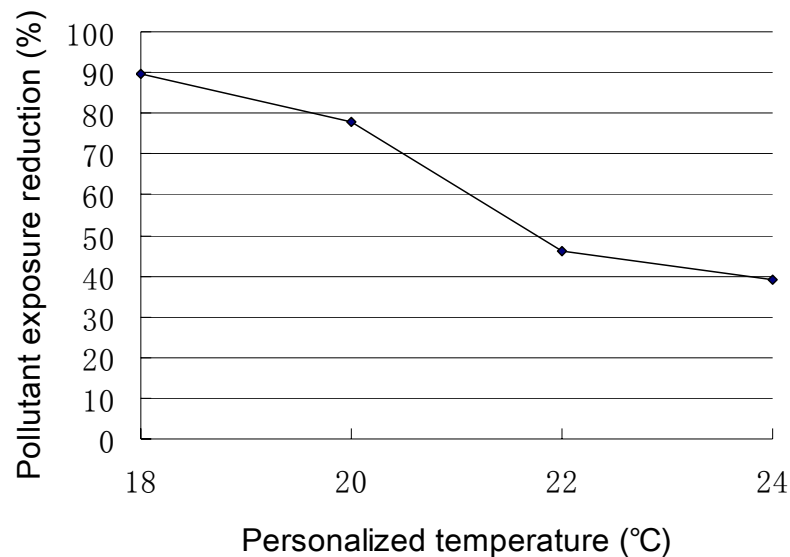
Figure 4.22 Pollutant exposure reduction at various temperatures of personalized air supply (personalized air is served at 0.8 l/s and the room air inlet velocity is 0.12 m/s)

4.2.6 Effects of room air movement

PV must be integrated into a background air conditioning system. However, the air movement that is caused by this secondary air conditioning system affects the micro-environment around the human body and the PV performance. Melikov et al. (2003) compared the ventilation effectiveness when PV is combined with mixing ventilation and when it is combined with displacement ventilation. In their experiments, the PV always protected the occupant from pollution when combined with mixing ventilation, but either improved or decreased the inhaled air quality when combined with displacement ventilation. Ambient air movement is of primary importance to the temperature and pollutant concentration field around the human body. Hyldgaard (1994) placed a thermal manikin as a pollutant source in a uniform horizontal airflow to study the pollutant transport and flow characteristics of respired air. He found that the horizontal uniform airflow at a speed of 0.05 m/s was able to remove the exhaled air. Even an airflow with a velocity of 0.05-0.10 m/s can prevent the buildup of the thermal plume on the windward side of the body, and if the back is turned against the uniform flow, then air can still be inhaled from the rising convection flow, as is the case in still ambient air. In the experiment of Melikov and Zhou (1996), it was found that an invading flow at a mean speed of 0.1 m/s with a turbulence intensity of 10% was able to penetrate the enclosing free convection flow.

In the numerical studies in this thesis, the human body is placed in a uniform airflow that approaches from the left, the front, and the back at velocities of 0.02 m/s and 0.2 m/s. Figure 4.23 shows the temperature field for Case 3-4 and Case 3-6. The warm rising flow on the windward side of the body is clearly torn away by the invading airflow, irrespective of the flow direction. On the leeward side of the body, a warm rising airflow still exists. However, when the body is located in a uniform airflow that has a speed of 0.02 m/s, the natural convection becomes stronger than in Case 1-

1 (displacement ventilated). This is because the mean room air temperature of the room that is ventilated by a plug flow at a speed of 0.02 m/s is lower than that of the displacement ventilated room in which the air supply velocity is 0.12 m/s.
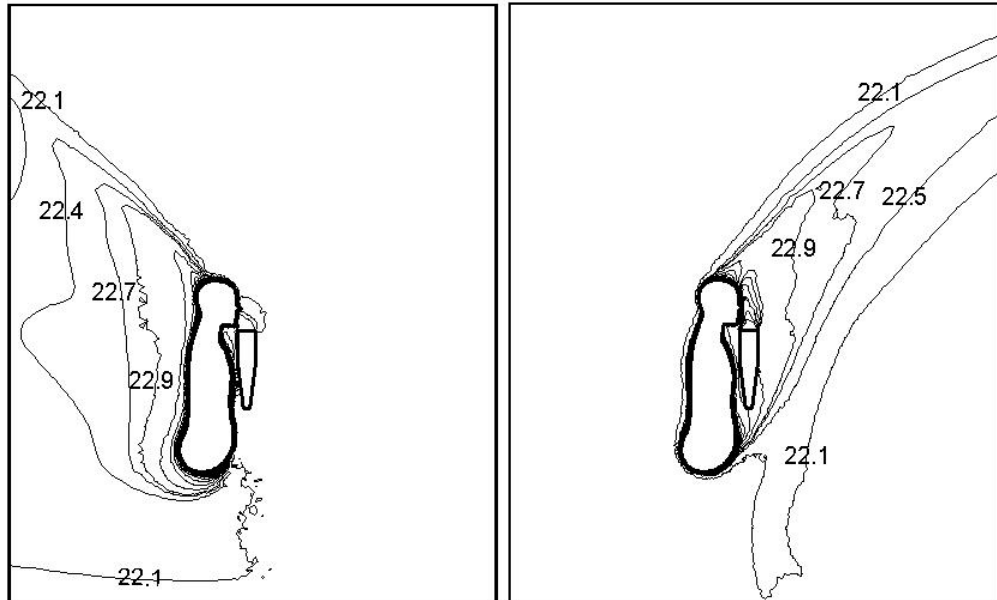
Figure 4.23 Temperature contours (℃) when a uniform airflow invades at a velocity of 0.2 m/s from the front (left) and back (right) at the middle surface x = 1.3 m
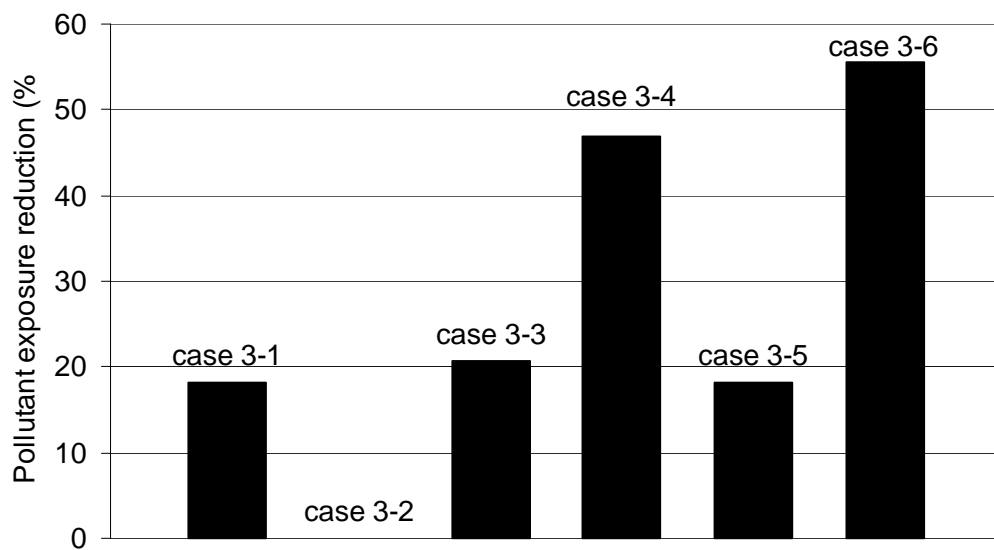
Figure 4.24 Comparison of the PER under different uniform airflows
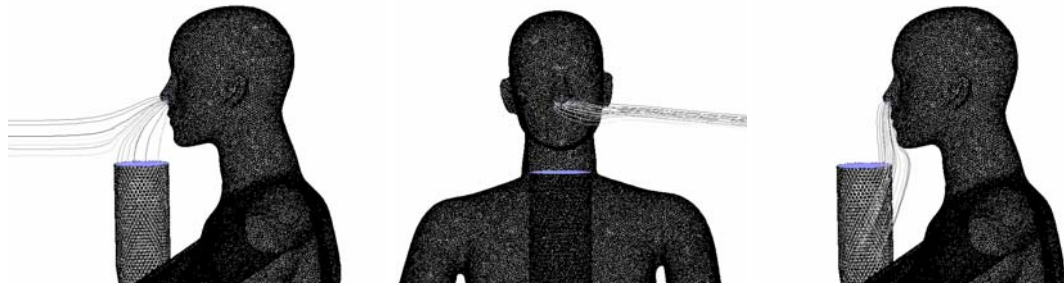
Figure 4.25 Path line of inhaled air when the human body is placed in a uniform airflow at a speed of 0.2m/s (left: airflow from the front; middle: airflow from the left; right: airflow from the back)
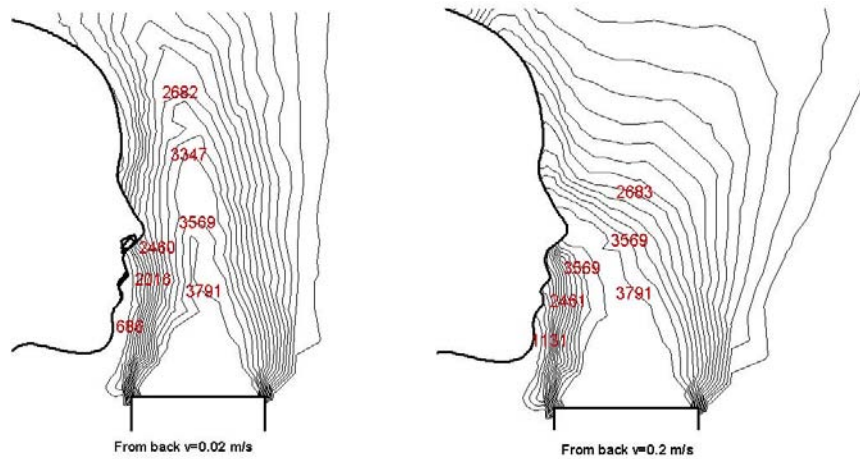
Figure 4.26 Tracer gas concentration distribution (ppm) when the airflow invades from the back at speeds of 0.02 m/s and 0.2 m/s

The PER values in Case 3-1 to Case 3-6 are compared in Figure 4.24. In Case 3-1, Case 3-3, and Case 3-5 the PER values are almost equal. This means that at the low air speed of 0.02 m/s, the flow direction has little impact on the inhaled air quality, because the airflow that invades from a different horizontal direction at a low speed has the same effect of strengthening the thermal plume around the body. In Case 3-2, Case 3-4, and Case 3-6, in which the uniform air speed is 0.2 m/s, the effect of the flow direction is more complicated. Rather unexpectedly, except for the cases in which the flow is lateral, the PER values are much higher at an air speed of 0.2 m/s

than at 0.02 m/s. Using the flow path lines, Figure 4.25 shows the composition of the inhaled air in Case 3-2, Case 3-4, and Case 3-6. When the human body faces the uniform airflow, the inhaled air comes partially from personalized air and partially from the invading airflow due to the breaking of the thermal plume on the windward side. The weak PV jet flow deflects to the face because of the impingement of the ambient airflow. Therefore, the PER in Case 3-4 is more than twice as high as that in Case 3-3. In Case 3-2, in which the ambient airflows from left to right at a speed of 0.2 m/s, the inhaled air comes almost totally from the uniform horizontal airflow. The PV jet flow is blown away. In this situation, the potential flow of the inhaled air is completely enclosed by the invading airflow. In Case 3-6, in which the uniform airflow comes from the back, the inhaled air is a mixture of air from the PV system and air from the thermal plume due to the protection of the warm rising flow on the leeward side that is provided by the human body. Surprisingly, the PER in Case 3-6 is much higher that in Case 3-5 (Figure 4.24). In Case 3-6, the room air flows through the gap between the legs, which confines the form of the thermal plume to the part of the body from the abdomen up to the head. Therefore, the air velocity of the warm upward flow at nose height in Case 3-6 is lower than that in Case 3-5. The tracer gas concentration distribution is shown in Figure 4.26. The stronger thermal plume in Case 3-5 when the inlet velocity of the plug airflow is 0.02 m/s induces two outcomes. First, the personalized air is drawn up to a higher level along the centerline of the PV jet, as the air speed of the thermal plume is higher than that of the jet flow at nose height. Second, the tracer gas concentration beneath the nose is lower, because more room air is entrained into this region.

4.2.7 Effects of the turbulence intensity of personalized air

Turbulence intensity has an influence on two aspects: the entrainment ability of the personalized air jet and facial thermal comfort. Distinct from some TAC systems, in which the rapid mixing of the local air supply and room air is desired to lessen the thermal asymmetry, PV aims to minimize this mixing process to achieve the best possible quality of inhaled air. In this simulation, the PER values are 74.4%, 73.5%, and 71.0% for the turbulence intensities of 5%, 10%, and 20%, respectively. It appears that the effect is significant, and therefore special consideration should be made of turbulence intensity in the selection of ATDs and personalized air conditions.

4.2.8 Summary

The RNG k-ε model and the standard k-ε model are compared, and it is found that for buoyant flow, the warm upward airflow above the head that is simulated by the RNG k-ε model is slightly thinner and stronger than that simulated by the standard k-ε model. For a jet flow, the tracer gas concentration distribution in the facial region that results from the interaction of the thermal plume and the PV airflow is almost the same in the two models.

At small volumes of personalized air supply, such as 0.8 l/s and 1.6 l/s, a larger temperature difference between the body surface and the room air causes a stronger thermal plume and a higher entrainment ability of the warm rising airflow, which decreases the fraction of personalized air in the inhaled air. However, the extent of this impact needs to be further investigated with different background air conditioning system designs, preferably with a fixed body surface heat flux condition. It is also found that the personalized air temperature specifies the intensity of the jet

flow, and that relatively lower personalized air temperatures bring the benefits of a higher PER and better perceived air quality.

Room air movement at a speed of 0.2 m/s is strong enough to tear away the protection of the thermal plume on the windward side of the body, and indeed, the orientation of the human body to the wind is of primary importance to the PER value. A uniform airflow from the left blows away the personalized air and leads to a PER value of almost 0. However, if the protection of the thermal plume is not broken by the invading airflow, then the horizontal movement of room air has no influence on the PER. Personalized air that has a high turbulence intensity mixes better with room air, and thus an air terminal device that can weaken the mixing process is desirable from the point of view of increasing the PER value.

4.3 Transient simulations of the human respiration process and inter-person exposure assessment

4.3.1 Introduction

The outbreak of SARS (severe acute respiratory syndrome) in over 25 countries around the world between November 2002 and June 2003 resulted in an unprecedented international effort to control the disease. Since the onset of the outbreak, there has been much debate as to the possible transmission modes of the disease. In general, infectious respiratory diseases, such as the common cold, influenza, and tuberculosis, are transmitted through droplets by the contact of a membrane with large pathogen-containing droplets, or through the air by the inhalation of fine droplets. The WHO consensus report (WHO 2003) is inclined toward the conclusion that the inter-person transmission of SARS occurs via large droplets. The current medical practice of infection control in hospitals differs for

diseases with these two transmission modes (ASHRAE 2003). However, in both cases, understanding the movement of the droplets that are generated in human respiration may lead to more effective control measures, such as better ventilation system design and operation and the correct use of personal protection equipment.

Li et al. (2005b) pointed out that most studies of the transport of human exhaled air are inconclusive. The dispersion and deposition of bio-aerosols as a result of breathing, coughing, and sneezing is a fundamental process that is not well understood. The more than one million droplets with a diameter of up to 100 μm that are generated by sneezing can travel a distance of up to 3 m in the initial few micro-seconds after the sneeze due to the inertia of the droplets. The diameter of the droplets decreases because of evaporation, and when the size is smaller than 5-10 μm the droplets can be suspended in the air, as the aerodynamic drag force, which is determined by Stokes' law (Vincent 1995), can easily overcome the force of gravity. As turbulence normally exists, these droplets can remain suspended in the air over prolonged periods. Zhao et al. (2004) showed that the concentration of the droplets that are created in the respiration process drops to below 0.001% of the initial concentration within 1 m of the human body, and that the droplets that are produced by sneezing or coughing may be horizontally transported over a distance of 3 m with an outlet velocity of 20 m/s.

In this section, the NTM is applied to study the transient airflow around the nose and mouth during respiration, the inhalation region, the exhaled air transport, and the sneezing process.

4.3.2 CFD method

Two human bodies that are represented by the NTM as facing each other are placed in a displacement ventilated room (Figure 4.27). One of the bodies is the polluting source and the other is exposed to the pollutant. The distance between the tips of the noses of the two bodies is about 1.2 m. The ventilation air is supplied from the sidewall at floor level at an inlet facial velocity of 0.2 m/s. The supplied air temperature is 22°C and the turbulent intensity I is assumed to be 20%. The ventilation rate is 0.024 m^3/s, which provides the room with 5.54 air changes per hour, approximating a practical displacement ventilation design. No other heat sources are present in this modeled room, except for the convection heat loss from the two human bodies. The exhaust grill is located at ceiling level. In this case, there is no strong buoyancy-driven convection flow, and thus the airflow pattern in this modeled room is close to a unidirectional flow, which is desirable for achieving better ventilation effectiveness. In reality, if there were other more intensive convection heat sources, such as office appliances and warm window or wall surfaces, then the hot plumes that would be generated by these sources would probably cause recirculation.
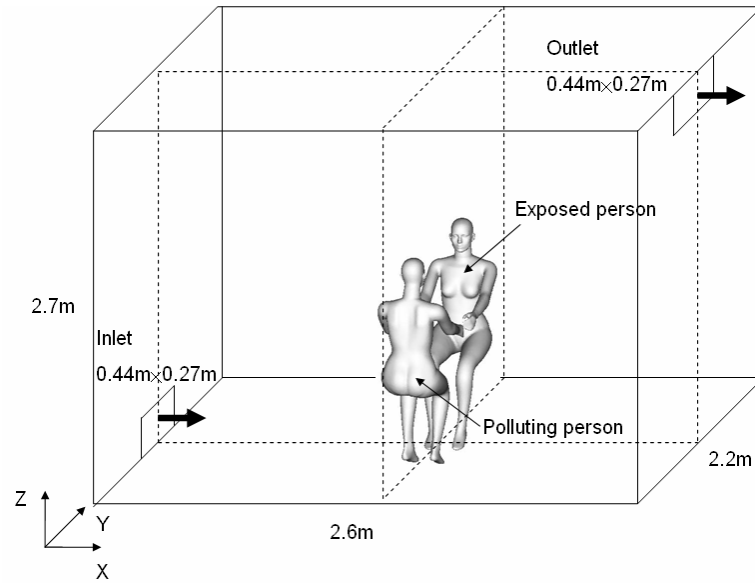
Figure 4.27 Schematic of the displacement ventilated room and the sitting positions of the two persons

The real respiration process of the polluting NTM is simulated (see Figure 2.9a). One breathing cycle lasts for 3.52 seconds. The transmission of the exhaled air is calculated by tracer-gas diffusion analysis. The tracer gas at a concentration C_{ex} of 1,000 ppm is added to the exhaled air and its transient spread across the room space is calculated based on the following governing conservation equation for chemical species.

$$\frac{\partial}{\partial t}(\rho\varphi) + div(\rho\vec{U}\varphi - \Gamma_{\varphi}grad\varphi) = S_{\varphi},\qquad(4.3)$$

where t is time, ρ is the air density, φ is the tracer gas concentration, $\vec{U}$ is a velocity vector, Γ_{φ} is a diffusion coefficient, and S_{φ} is the source term. Once the tracer gas concentration φ for a nodal point is obtained, the mass fraction f of the exhaled air can be calculated by using the following equation.

$$f = \varphi / C_{ex}.\qquad(4.4)$$

The mass fraction f is basically the fraction of exhaled air at that point.

133

The use of tracer-gas diffusion analysis for a normal breathing process is reasonable, as the number of droplets in the exhaled air is likely to be almost zero. In simulating droplet transport in the sneezing or coughing process using the concentration conservation equation, the shear stress, gravitational setting, and electrostatic force effect cannot be taken into account. In this regard, the simulated tracer gas movement in this study better approximates the movement of fine droplets, and especially those with an aerodynamic diameter of less than 2.5 μm. Modeling the movement of larger-sized particles requires the more complicated particle trajectory modeling approach, or the Eulerian approach, to take into account the gravity settling effects.

The transient process of the exposed NTM is simplified to a steady inhalation process with an inhaled air rate of 0.14 l/s. Three different cases of polluting NTMs that represent normal respiration through the nose or mouth and sneezing or coughing process are studied. The open area of the nose and mouth is 1.5 cm^2 and 2.5 cm^2 for the normal case and the sneezing or coughing case, respectively. The direction of the exhaled airflow from the nose and mouth is 30^0 downward and horizontal, respectively. The temperature of the exhaled air is 34℃ and the density is 1.15 kg/m^3 (Höppe 1981; BjØrn 2002). The assumed duration of sneezing is 1 second at a volume flow rate of 250 l/min (Badeau et al. 2002). For simplicity, only one sneezing process is modeled, although people may sneeze more than once in a cycle of sneezing or coughing.

4.3.3 The transient respiration process

Figure 4.28 and Figure 4.29 show the airflow vectors in the facial region when the occupant breathes through the nose and through the mouth, respectively.

(a) t = 7.04s   (b) t = 7.92s

(c) t = 8.80s   (d) t = 9.68s
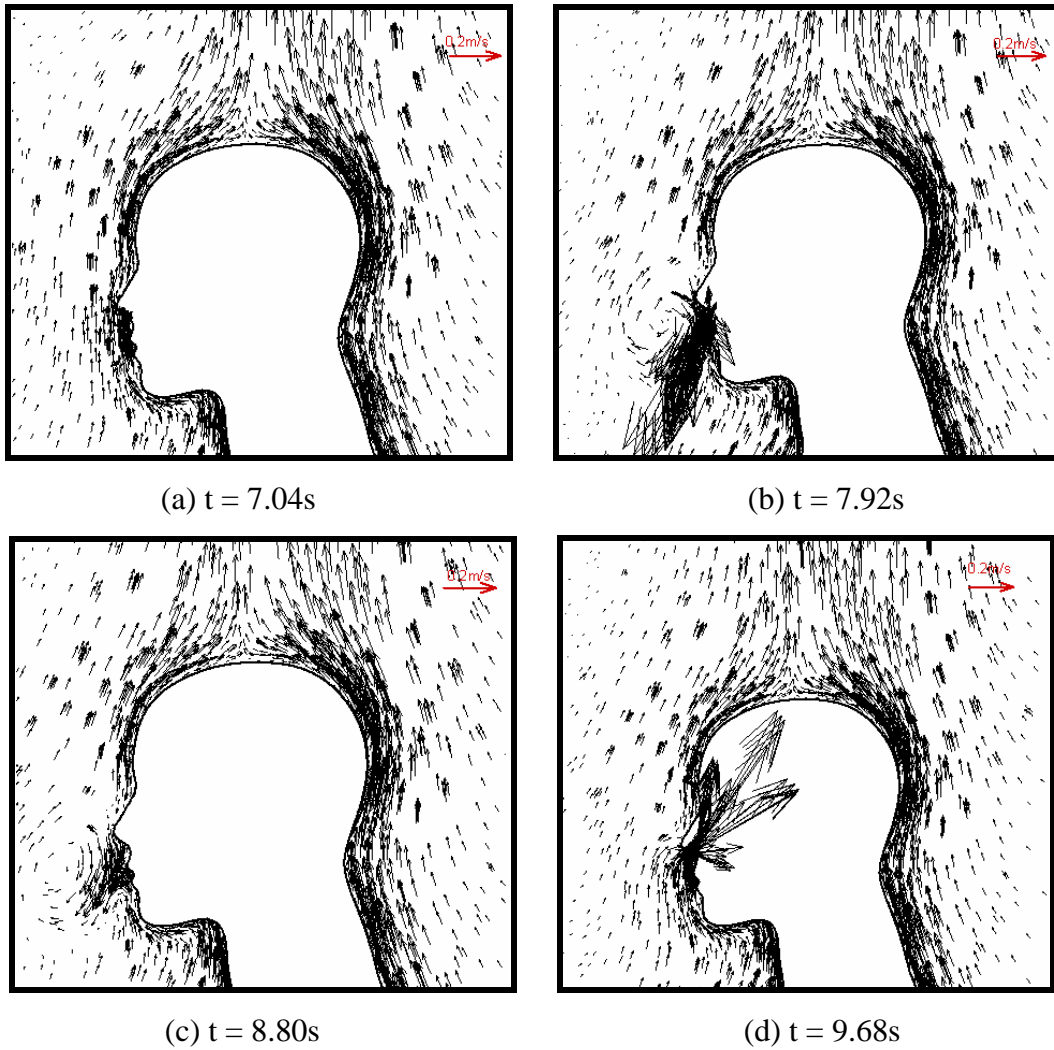
Figure 4.28 Velocity vector distribution in the respiration area around the nose

(a) t = 3.52s
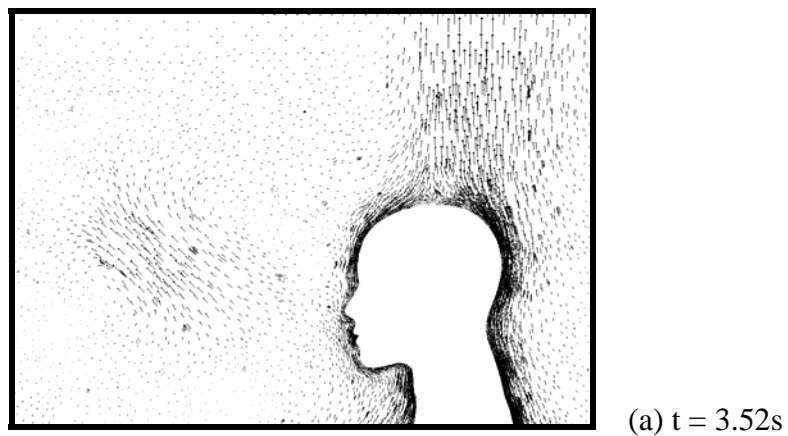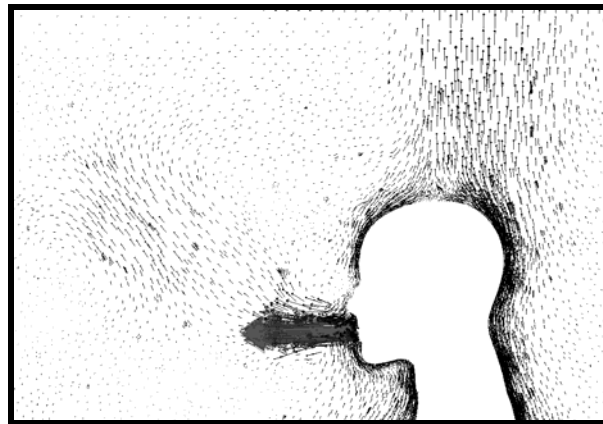
(b) t = 4.40s
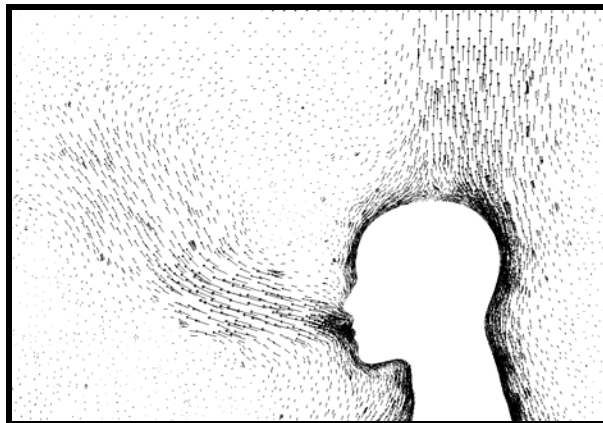
(c) t = 5.28s
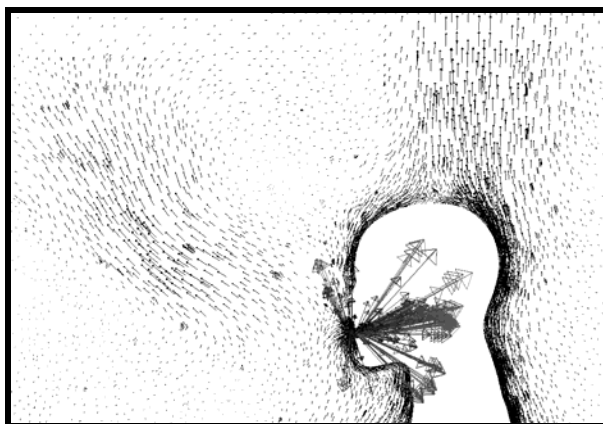
(d) t = 6.16s

Figure 4.29 Velocity vector distribution in the respiration area around the mouth

Due to the relatively small airflow rate of respiration, the inhaling and exhaling processes have almost no influence on the room airflow pattern. When breathing occurs through the nose only, the potential flow of inhalation is besieged by the natural convection surrounding the body, and small swirl flows are generated beside

the mainstream of the intermittent exhalation jet. When breathing occurs through the mouth only, the exhaled air gradually moves away in the direction of about 45^0 upward in front of the face. The tracer gas concentration in the room 0.8 m away from the head is almost zero, which indicates that human exposure to the air that is exhaled through the normal respiration of others is minimal in this displacement ventilated room. This result is in line with a previous investigation of the transport of exhaled droplets (Zhao et al. 2004). Figure 4.28 and Figure 4.29 show the three cycles of breathing that are simulated, although it can be expected that as time elapses the pollutants in the exhaled air may accumulate indoors and reach a quasi-steady concentration level. However, the distribution will strongly depend on the ventilation or air distribution method. With mixed ventilation, that is, when air is supplied from a high-velocity, high-entrainment diffuser that is located at ceiling level, the pollutant concentration in the room will be relatively uniform. In this simulation, the room has a quasi-unidirectional flow pattern, and the steady-state simulation indicates that high concentrations of exhaled air are only present above the occupied zone, which means that human exposure to the exhaled air of others is close to zero, since the exhaled air is promptly exhausted at ceiling level.

Figure 4.30 shows that the warm rising airflow under the jaw close to the body is diverted to the cheeks. Zhu et al. (2004) emphasized that the influence of the jaw cannot be ignored when examining the flow field in the respiration area.
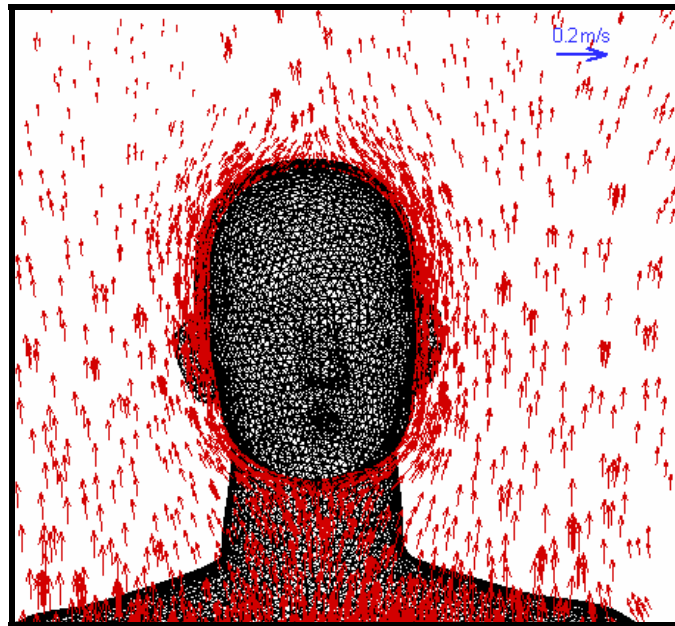
Figure 4.30 Velocity vector distribution in the jaw region

(a) Inhalation   (b) Exhalation
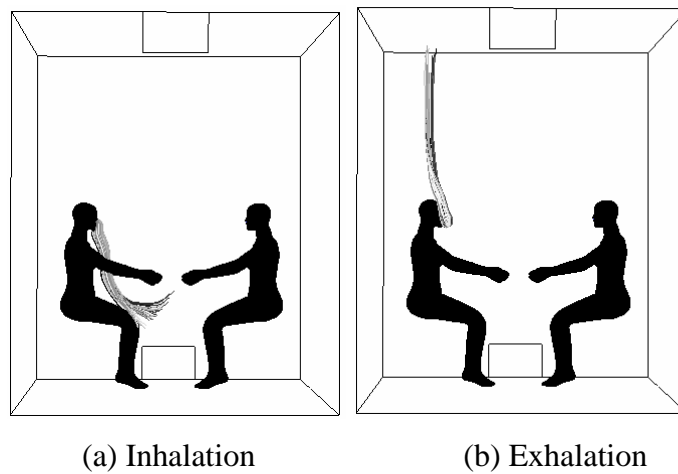
Figure 4.31 Path line descriptions of inhalation and exhalation through the nose only

(a) Inhalation   (b) Exhalation
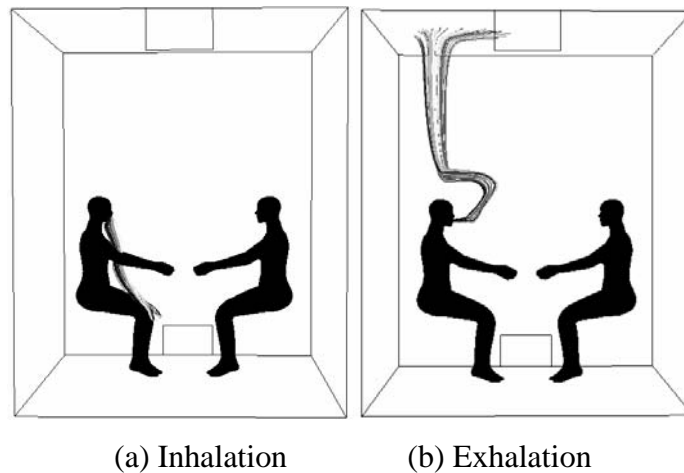
Figure 4.32 Path line descriptions of inhalation and exhalation through the mouth only

Figure 4.31 and Figure 4.32 illustrate the path line descriptions of the air that is inhaled and exhaled through the nose only and the mouth only, respectively. The air that is exhaled through the mouth is able to escape enclosure by the warm rising airflow around the human body because the exhaled flow is firmly horizontal at a high momentum level. In contrast, the air that is exhaled through the nose is entrained upward by the thermal plume because its downward direction reduces the momentum. In both situations, the inhaled air comes from the lower level of the displacement ventilated room in front of the body by natural convection. BjØrn and Nielsen (2002) pointed out that exhaled air stratifies at breathing height in a displacement ventilated room if the vertical temperature gradient is high enough, that is, if it is $0.5℃/m$ or above. However, this is not observed in this numerical study although the gradient is about $1℃/m$. It is presumably due to the fact that the air change rate per in present modeled room is 5.5, which is much higher than 0.71-1.77 in the experiments by BjØrn and Nielsen (2002).
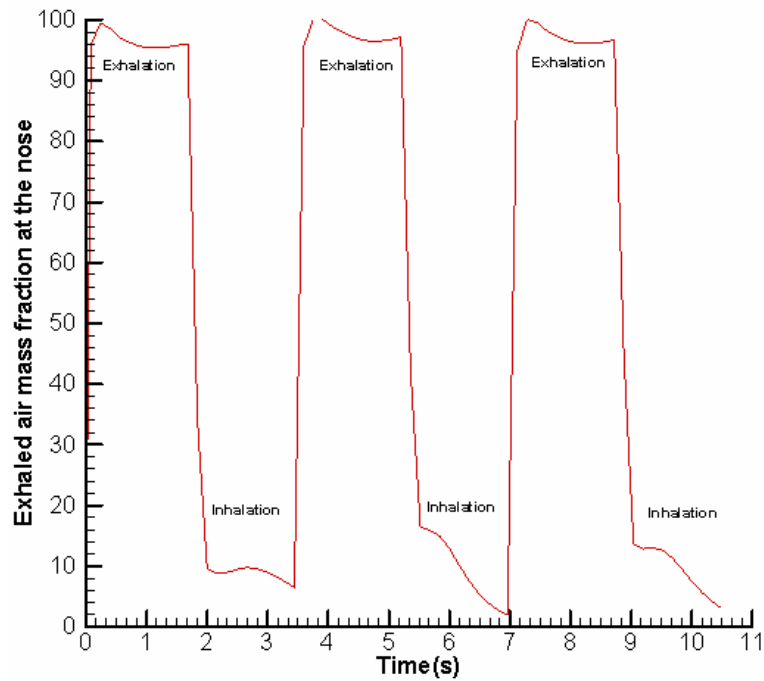
Figure 4.33 Temporal variation in the mass fraction *f* of the exhaled air when respiration occurs only through the nose (the value of *f* during the inhalation periods represents the re-inhalation of the previously exhaled air)
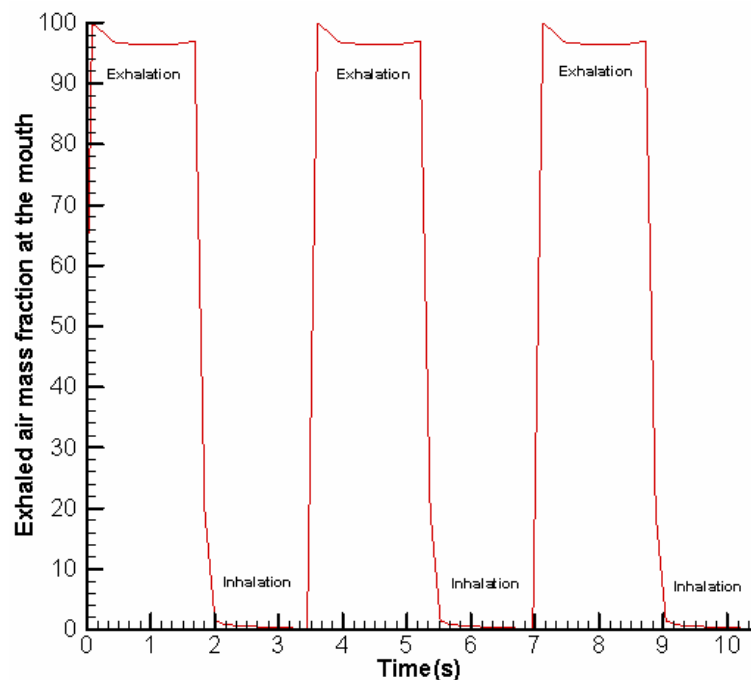
Figure 4.34 Temporal variation in the mass fraction *f* of the exhaled air when respiration occurs only through the mouth (the value of *f* during the inhalation periods represents the re-inhalation of the previously exhaled air)

Figure 4.33 and Figure 4.34 show the temporal variation in the mass fraction f at the nose and mouth when breathing occurs through the nose only and the mouth only, respectively. The results of three breathing cycles are shown. The mass fraction f during the exhalation periods is obviously 100% of the exhaled air, as it should be, and the mass fraction f during the inhalation periods is an indication of the percentage of the re-inhalation of a person's own exhaled air. Most of the exhaled air is removed, but a small portion is re-inhaled. When breathing occurs through the nose, the mean re-inhalation rate is about 10%, which is lower than the value of 16.2% in the simulation of a standing human body of Murakami (2004). This discrepancy may be due to a difference in parameter settings, such as the respiration frequency, exhaled air condition and direction, body posture, and nose/nostril area. When breathing occurs through the mouth the re-inhalation rate is almost zero. The reason for this is that the horizontal buoyant jet from the mouth penetrates the envelope of the thermal plume and is taken away by the room air.

4.3.4 The sneezing process

Figure 4.35 shows the spreading of exhaled air during and after sneezing. It is obvious that exhaled air is transported a long distance by sneezing or coughing. In the scenario under study, in which two occupants face each other at a distance of about 1.2 m, the air that is exhaled by sneezing approaches the other person in stages, but one second is enough for it to reach the breathing region of the exposed person. Because of its high velocity, the exhaled airflows almost horizontally, and is able to penetrate the protection of the boundary layer flow that encloses the exposed person. This proves that if the thermal plume is peeled off or penetrated, its positive function

of improving the inhaled air quality by drawing fresh air from the lower level of a displacement ventilated room disappears. Figure 4.35(g) indicates that the exhaled air travels across the body of the exposed occupant, hits the wall, and is finally exhausted. These simulation results correspond well with the results of the smoke visualization experiment of BjØrn and Nielsen (2002; Figure 4.35(h)). However, the smoke is shown to be rising above the head of the exposed occupant due to the buoyancy effect, and no smoke is blocked by the chest. This is because the exhaled air velocity is much lower in the smoke experiment, and consequently the value of Gr/Re^2 is higher than in the current simulation.

(a) t = 0.5s   (b) t = 1.0s

(c) t = 1.5s   (d) t = 2.0s
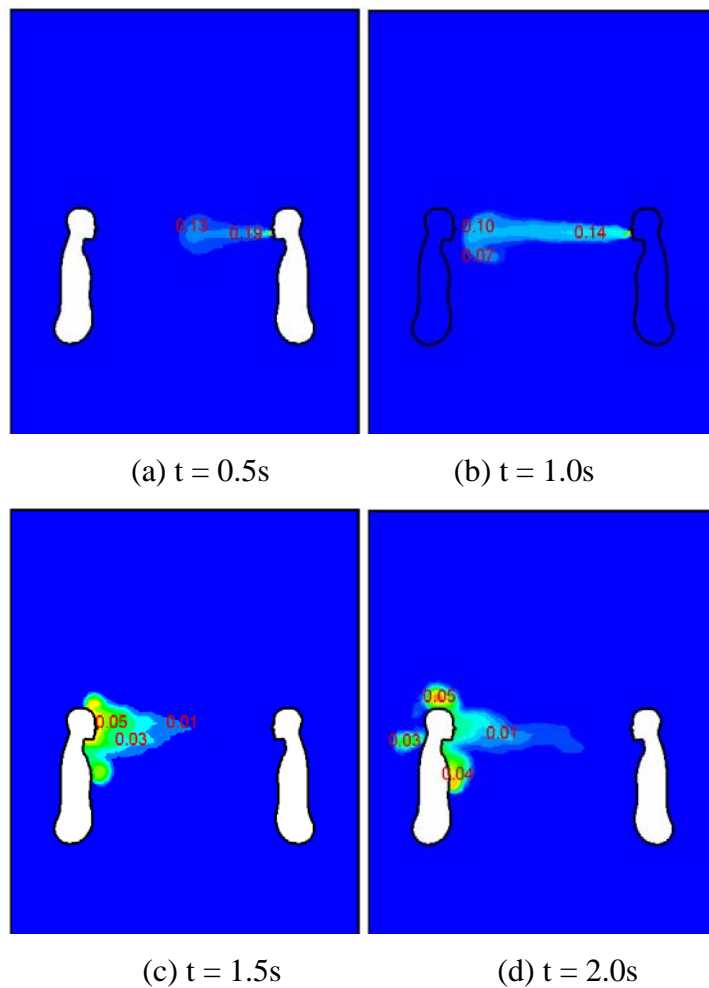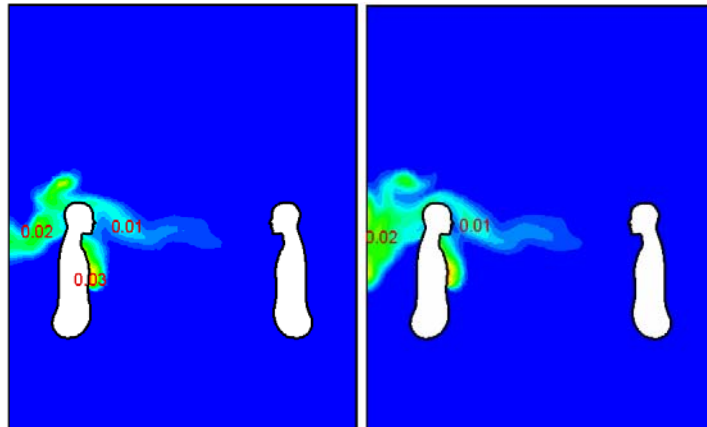
(e) t = 2.5s   (f) t = 3.0s
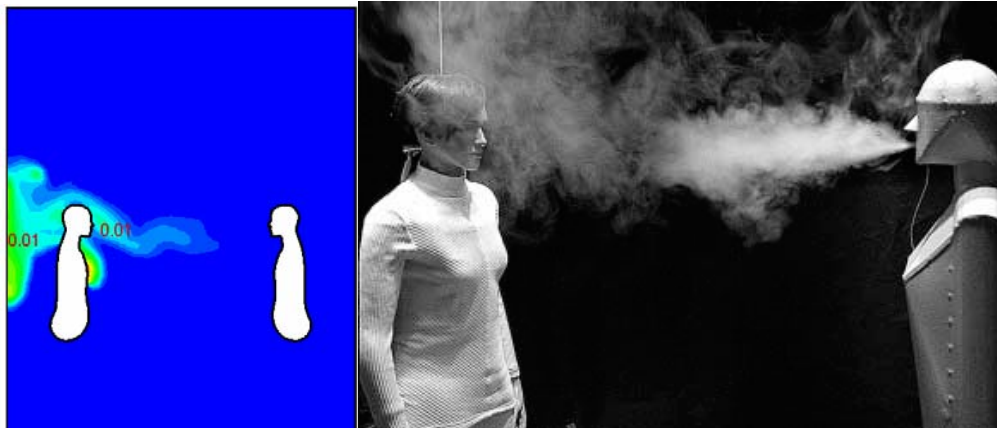
(g) t = 3.5s   (h) smoke visualization of the exhalation flow from the mouth (BjØrn and Nielsen 2002)

Figure 4.35 Distribution of the mass fraction of sneezed air during and after sneezing
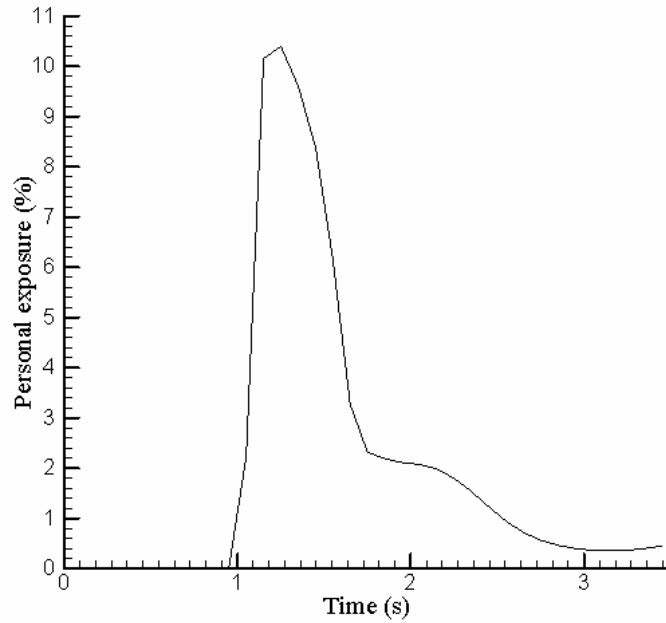
Figure 4.36 Mass fraction of sneezed air in the air inhaled by the exposed person during and after sneezing

Figure 4.36 shows the fraction of sneezed air in the inhaled air at different stages after sneezing. In the period from 1.0 s to 2.5s, the concentration of sneezed air in the inhaled air of the exposed person is greater than 1%. It is well known that the health impact of a gaseous pollutant to the human body is closely related to the received dose and exposure time. For example, the US EPA defines Acute Exposure Guideline Levels as the threshold concentrations of a single exposure over a certain period (US EPA 2001). Here, the conception of an "infection index" η is proposed in the following equation.

$$\eta = \int_0^\infty V_L \rho_{in} C dt ,\tag{4.5}$$

where V_L is the inhalation rate in m^3/s, ρ_{in} is the inhaled air density in kg/m^3, and C is the mass fraction of sneezed air in the inhaled air. In the current simulation, the value of η with regard to the exposed person is 800 µg. This value can be compared with the safety threshold, which is the maximum exposure that will not cause

infection. It is obvious that the value of the safe threshold will be different for different airborne infectious diseases. It should also be borne in mind that the adoption of the infection index must be accompanied by a measure of the concentration of a virus in the exhaled air. Toxicological studies have demonstrated that humans differ in sensitivity to every virus, and that the response spectrum follows a normal distribution (Li et al. 2005a). However, these issues are out of the scope of this study. The modeling that is presented here proves that the pollution that is created by sneezing may cause cross-infection in an indoor environment. Thus, the traditional courtesy of covering one's mouth with a handkerchief when sneezing may also have some merit in reducing infection. With regard to strategies to control the spread of disease, good personal hygiene habits, such as wearing a mask or having a personalized air supply, may be important. Further studies on the effects of such strategies in preventing the transmission of respiratory diseases are needed.

It should be noted that exposure to sneezing or coughing is highly directional. It can thus be envisaged that if a person is positioned behind a sneezing person, then the level of direct exposure will be much less. In the case that is simulated here of a room that is displacement ventilated, a large percentage of the pollutants can be exhausted by ventilation air quickly.

4.3.5 Summary

A three-dimensional NTM is applied to study the inhalation region, transmission of exhaled air, and personal exposure to the exhaled air of others. The following main conclusions can be drawn.

1. It appears that personal exposure to exhaled air from the normal respiration process of another person is very low in the room with displacement ventilation that is modeled. This conclusion agrees with the steady-state simulation, and also agrees with the notion that displacement ventilation is more effective than mixing ventilation. This result may well support the idea that a better ventilation system design in buildings could reduce the spread of infectious diseases.

2. The percentage of exhaled air in the next inhalation when respiration occurs only through the nose and only through the mouth is 10% and 0, respectively, which agrees with the conventional wisdom that one should inhale though the nose and exhale through the mouth.

3. When two people are facing each other, cross-infection may occur due to the long distances over which sneezed air can be transported, but this exposure is highly directional. The practical implication is that displacement ventilation may still have an effect in minimizing indirect exposure to pollutants in exhaled air.

This study demonstrates how CFD simulation can reveal the distribution mechanism of exhaled pollutants. Further studies are required to investigate how the inhalation region and exhalation transmission are influenced by the metabolic rate, breathing frequency and flow rate, exhaled air temperature and density, and body posture and orientation. Research on the dispersion of droplets that are generated by sneezing or coughing is also imperative, as such droplets, and especially those that are larger in size, have different aerodynamic behavior from that of gases.

Chapter 5

Coupling CFD and human body thermoregulation model for the assessment of personalized ventilation

5.1 Introduction

In this Chapter the NTM is equipped with a thermoregulation model to assess local thermal comfort. Through CFD and tracer gas techniques the ventilation effectiveness or PER is quantified. Then, based on the validated thermoregulation model for non-uniform and transient conditions developed by Zhang (2003), the physiological regulation mechanism and CFD are integrated to calculate the input data for the thermal sensation predicting model, which also takes account of a non-uniform thermal environment. Three application examples of this numerical method are demonstrated. One is for chair-based personalized ventilation and the other two are related to desk-based air supply. Finally with the help of this kind of coupling simulation, the performance of personalized ventilation in displacement ventilation (DV) and mixing ventilation (MV) is compared.

5.2 Modeling method

Detailed information of air temperature, humidity and air velocity can be calculated at each body segment by using an NTM. CFD assessment of thermal comfort with personalized ventilation requires the coupling of thermoregulation of the human body and the room airflow field, which means transferring data on the condition of the air into the thermoregulation model to obtain skin surface temperature, heat flux, and sweat loss. The iteration loop is shown in Figure 5.1. The following steps are the main components in this numerical method:

- Create a numerical thermal manikin with the real geometry of a human body

- Set up a thermoregulation model with multi-node function

- Establish a thermal sensation and comfort model for a non-uniform environment

- Obtain the environmental parameters, such as temperature, velocity, and pollutant concentration, using CFD

- Couple CFD and the thermoregulation model to obtain physiological data

- Use physiological parameters as inputs to predict thermal sensation and comfort

```
                        ┌─────────┐
                        │  Start  │
                        └─────────┘
                             │
         ┌───────────────────────────────────────┐
         │  Set metabolic heat, clo value, relative humidity │
         │       (assumed constant at 50%)        │
         └───────────────────────────────────────┘
                             │
      ┌──────────────────────────────────────────────┐
      │ Initialize skin surface temperature for each of the 16 segments T_sk │
      └──────────────────────────────────────────────┘
                             │
         ┌───────────────────────────────────────┐
         │  CFD calculation of flow, temperature fields (including │
         │       convection and radiation)        │
         └───────────────────────────────────────┘
                             │
         ┌───────────────────────────────────────┐
         │  Input the local air condition parameters into the CBE │
         │        thermoregulation model          │
         └───────────────────────────────────────┘
                             │
            ┌─────────────────────────────┐
            │   Obtain new skin temperature │
            └─────────────────────────────┘
                             │
              < |T_sk^n - T_sk^{n+1}| < ε ? >
                             │
                           End
```
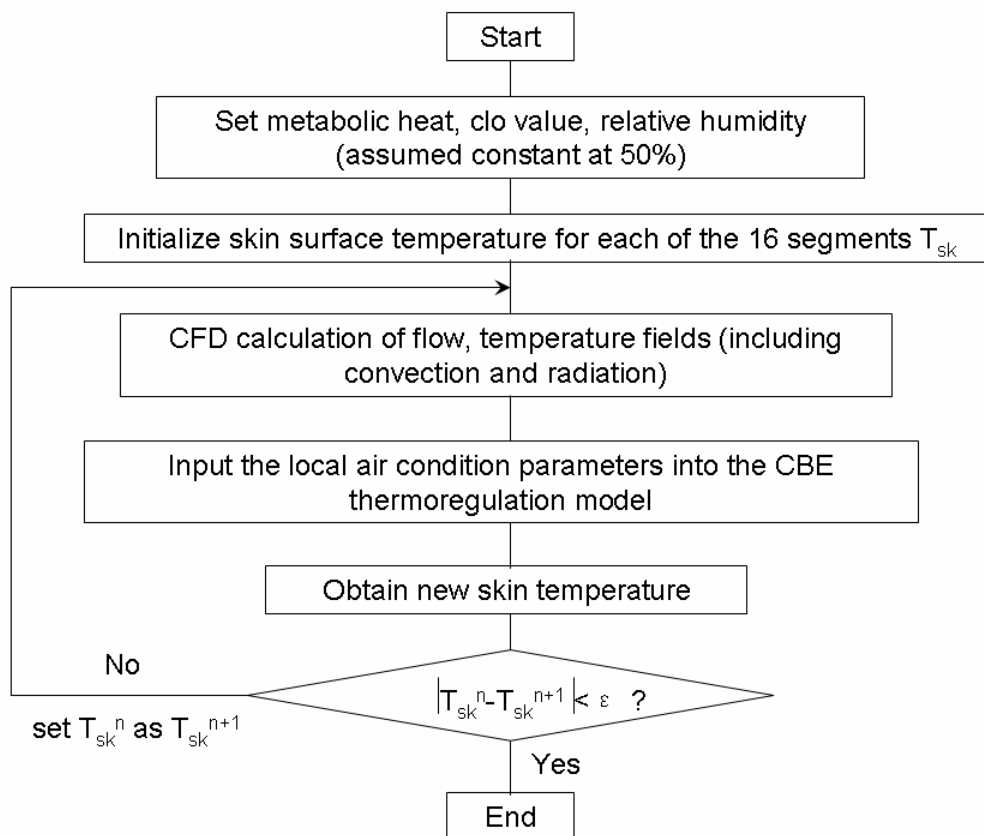
Figure 5.1 Coupling of CFD and the CBE thermoregulation model (ε controls the coupling accuracy and is set to 0.1 ℃ in present simulations)

No ... set T_{sk}^n as T_{sk}^{n+1}

$|T_{sk}^n - T_{sk}^{n+1}| < \varepsilon$?

Yes

5.2.1 Numerical thermal manikin (NTM)

The NTM body is divided into 16 segments. The surface area of each segment is listed in Table 5.1.

Table 5.1 Sixteen body segments and their areas

Number	Body part	Area (m^2)
1	L Foot	0.046
2	R Foot	0.046
3	L Low Leg	0.096
4	R Low Leg	0.096
5	L Thigh	0.170
6	R Thigh	0.177
7	Pelvis	0.176
8	Head	0.129
9	L Hand	0.040
10	R Hand	0.039
11	L Forearm	0.053
12	R Forearm	0.053
13	L Upper Arm	0.078
14	R Upper Arm	0.083
15	Chest	0.149
16	Back	0.138
17	Whole body	1.569

5.2.2 Evaluation indices

Melikov et al. (2002) proposed personal exposure effectiveness (PEE), ε_P, to quantify the improvement of inhaled air quality. The index ε_P is equal to PER, which is expressed as the percentage of personalized air in inhaled air. Faulkner et al. (2004) defined air change effectiveness (ACE) to quantify the benefits of personalized ventilation based on ages of air as follows:

$$ACE = \frac{\tau_n}{\tau_{avg}} \tag{5.1}$$

where τ_n is the nominal ventilation time constant and τ_{avg} is the average age of air at the breathing zone. An ACE value of 1.5 means a 50% increase in effective ventilation rate at the breathing zone relative to the perfect mixing with same amount of fresh air. The indices of PER and ACE are applied in this chapter in order to compare the simulated results with the experimental results.

5.3 Model validation

In the frame of the PMV model, a comfort zone is defined as $\left|PMV\right| < 0.5$, corresponding to 10% dissatisfaction of the whole-body thermal sensation. In the CBE Comfort Model the comfortable temperature range is defined as no appearance of whole-body and local discomfort (Figure 5.2). In both models the neutral temperature is almost the same, i.e. 24.6℃. This could be attributes to the fact that although the scales used are different in both models the neutral point is set on the heat balance of the body in a steady condition. The two models are in a good agreement in the cool side, but the CBE model predicts a much higher thermal sensation than the PMV model, shrinking the comfortable range by 1℃, at the warm side. It is unpractical to expect the predicted comfortable range from these two models to be identical since the CBE model estimates the comfort value directly using the 9-point comfort scale while the PMV theory is based on the percentage of dissatisfaction. Thermal sensation is symmetric at the neutral point in the PMV model, while not in the CBE model, which is more sensitive in the warm side in present cases (0.59 Clo, 50% RH, 0.15 m/s, 1.2 Met). One possible reason is that the CBE model is developed in summer conditions with a low value of Clo.
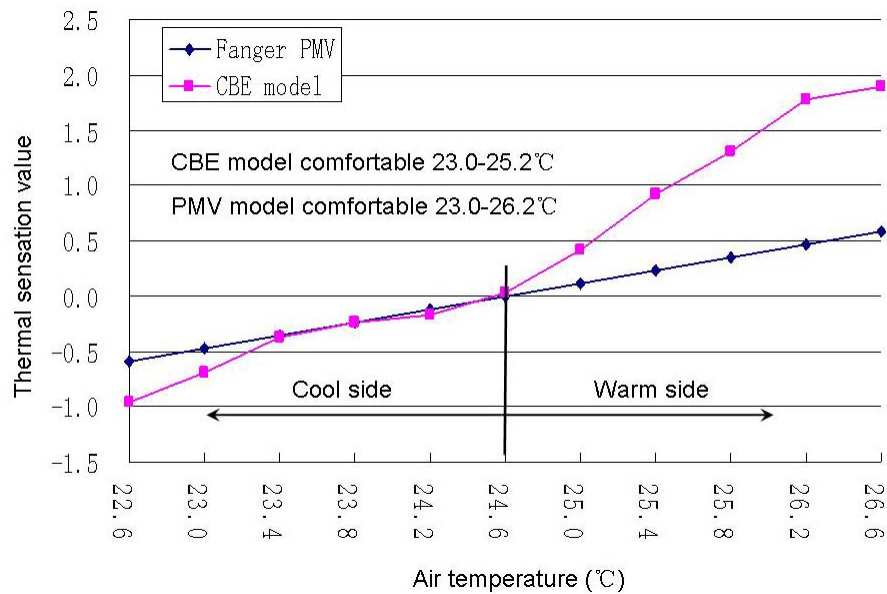
Figure 5.2 Thermal sensation and comfortable temperature range for a uniform environment (0.59 Clo, 50% RH, 0.15 m/s, 1.2 Met)

Besides in a uniform environment, the CBE model should certainly be validated in a non-uniform environment. Yamashita et al. (2005) studied thermal sensation and thermal comfort in summer during exposure to local airflow to face at a speed of 1m/s. The ambient temperature was maintained at 26.4℃ and the local airflow temperature ranged from 18 to 36℃. Eight male students were involved in their experiment. Figure 5.3 shows that the CBE model agrees well with the measurement. The important feature is captured by the model that if increasing local airflow temperature the overall sensation ascends linearly while the thermal comfort shows a peak at 30℃.
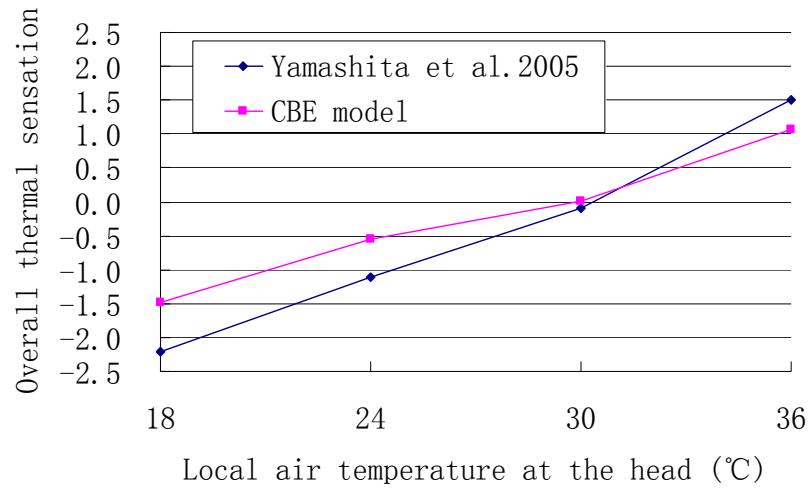
(a)
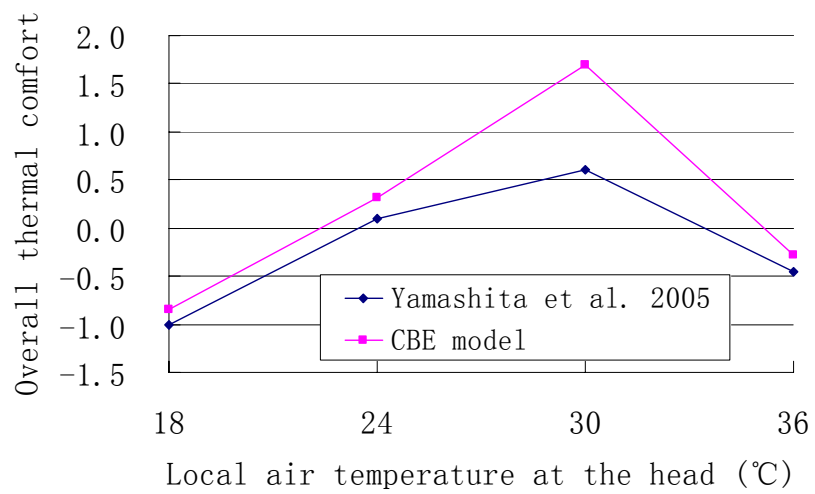
(b)

Figure 5.3 Comparison of measured thermal sensation (a) and thermal comfort (b) by Yamashita et al. (2005) with predictions from the CBE comfort model

5.4 Applications of the CBE Comfort Model

Turbulent air directed at local body parts, i.e. the face, the head, and the upper body, may cause draft feelings in cool-to-neutral conditions, while it can also relax thermal discomfort in neutral-to-warm environments. That is to say, the draft sensitivity is influenced by the general thermal sensation, or in other words, local thermal comfort in the same local micro-environment is affected by the overall thermal condition, i.e. ambient air temperature, velocity, humidity, and radiant temperature. Human subject

experiments by Toftum and Nielsen (1996) showed that significantly more persons feeling slightly cool perceived air movements as more uncomfortable than persons having a thermal sensation closer to neutral, provided the same air velocity. On the other hand, Sekhar et al. (2005) revealed that most subjects can achieve comfort with PV under warm experimental conditions with an ambient air temperature of 26℃.

Using CBE model as described in chapter 2, the author derived the head thermal sensation, head thermal comfort, overall thermal sensation, and overall comfort of a human body with a sitting posture in the situations where personalized air is directed at the head at different temperatures and velocity levels in a mixing ventilated and displacement ventilated room (Figure 5.4 and Figure 5.5). In mixing ventilation the uniform ambient air temperature is 26℃, and in displacement ventilation the vertical temperature difference from the feet to head is 4℃ with the temperature at the feet level of 24℃.
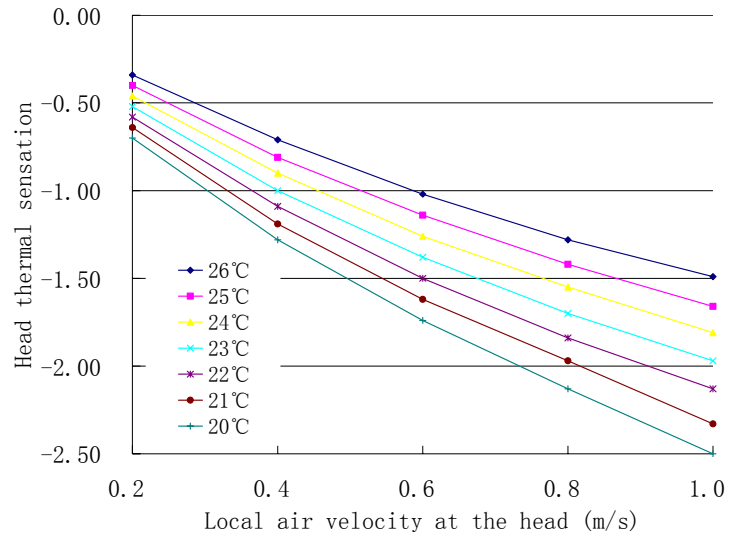
(a)
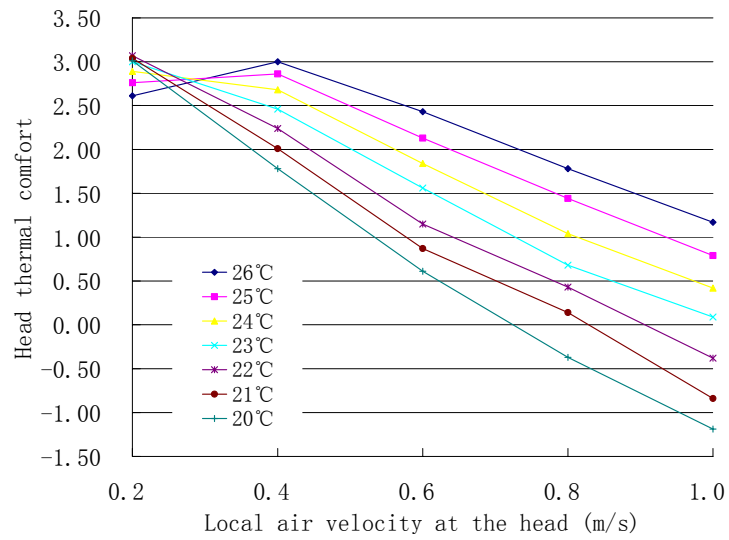
(b)
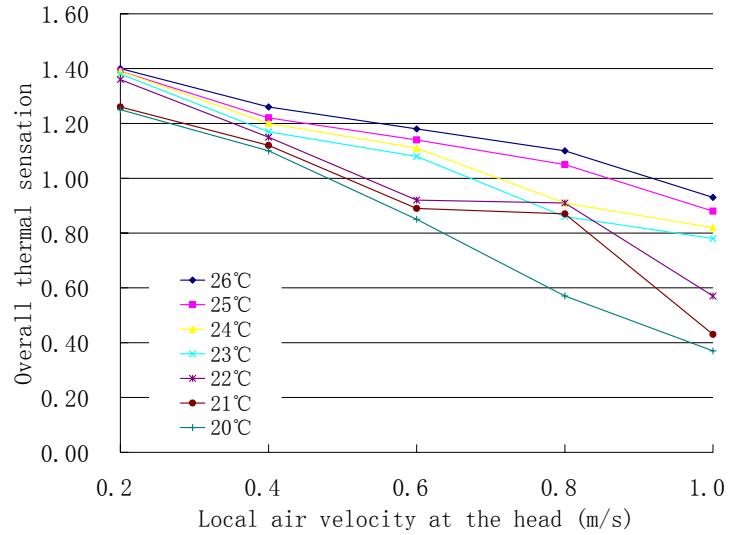
(c)
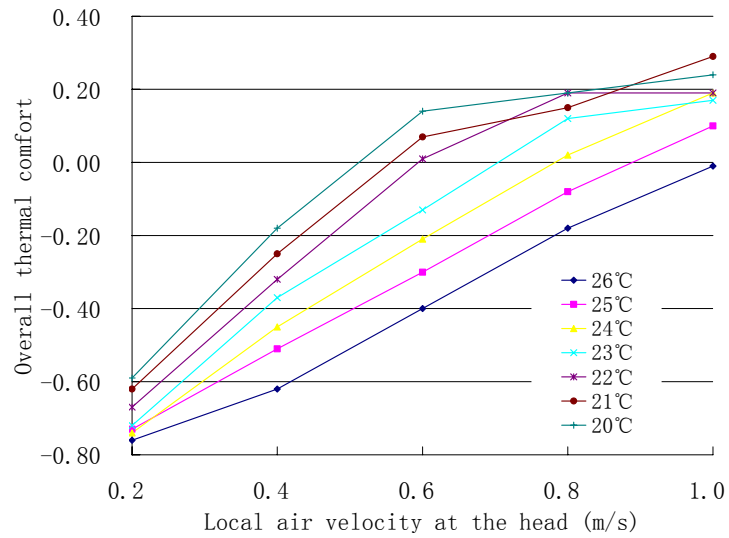
(d)

Figure 5.4 Head sensation (a), head thermal comfort (b), overall thermal sensation (c), and overall thermal comfort (d) with personalized ventilation in a mixing ventilated room

155

(a)

(b)

(c)
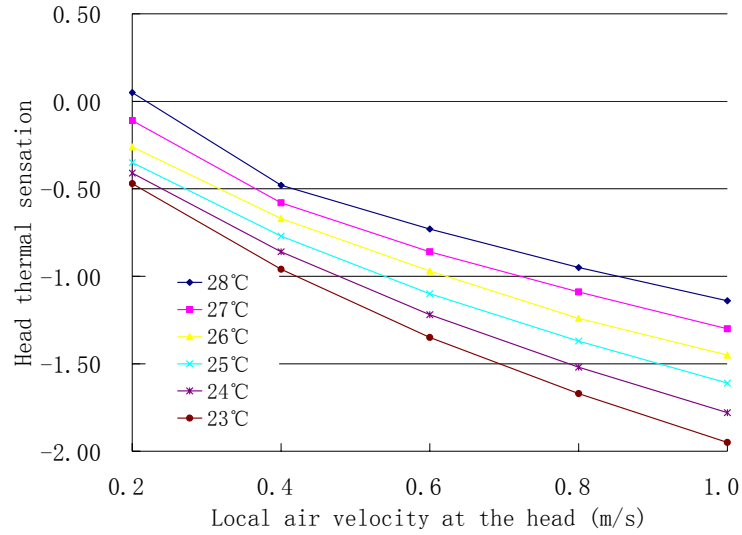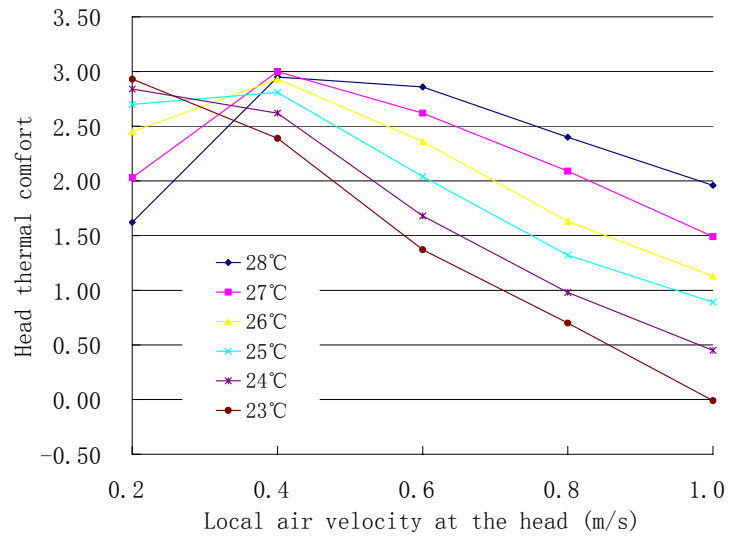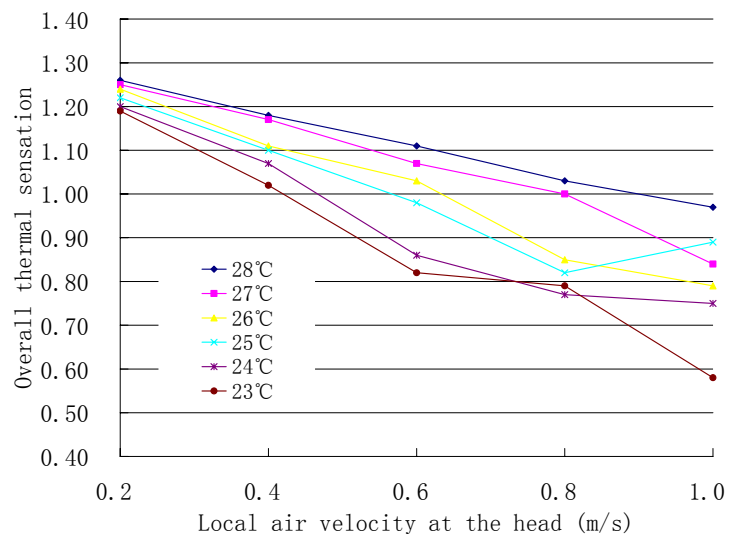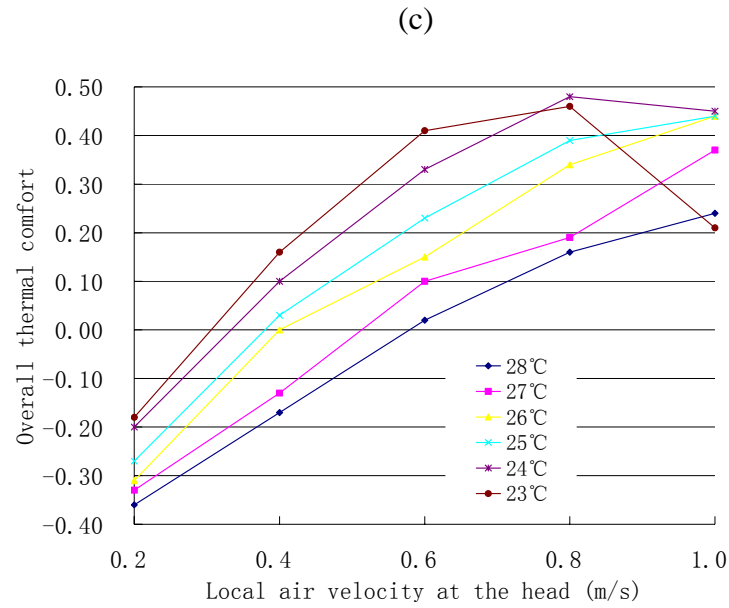
(d)

Figure 5.5 Head sensation (a), head thermal comfort (b), overall thermal sensation (c), and overall thermal comfort (d) with personalized ventilation in a displacement ventilated room

Generally personalized air supply can lower the head thermal sensation greatly and overall sensation relatively slightly in both mixing and displacement ventilation. The overall thermal comfort can be improved due to the released heat stress at the head by personalized air in warm ambient environments. It is again observed that the head sensation curve is linear while the head comfort curve is parabolic. This implies that the head sensation is proportionally decreased with the cooling capacity of personalized air. However the best head comfort level appears at a certain cooling capacity. Figure 5.6(a) indicates that people prefer to put their heads in a slightly cool condition (with the value of -0.50). With PV the overall thermal comfort could be obtained even when the overall sensation is in the warm side (with a value higher than 1.00) (Figure 5.6(b)). This phenomenon is also proved by Xia et al. (2000) who found the velocities people chose to achieve thermal comfort at high room temperatures were possibly lower than the ones required to restore thermal neutrality.

157

It shows a promising view in practical applications where the ambient room temperature can be increased in order to save energy while thermal comfort is still achieved.
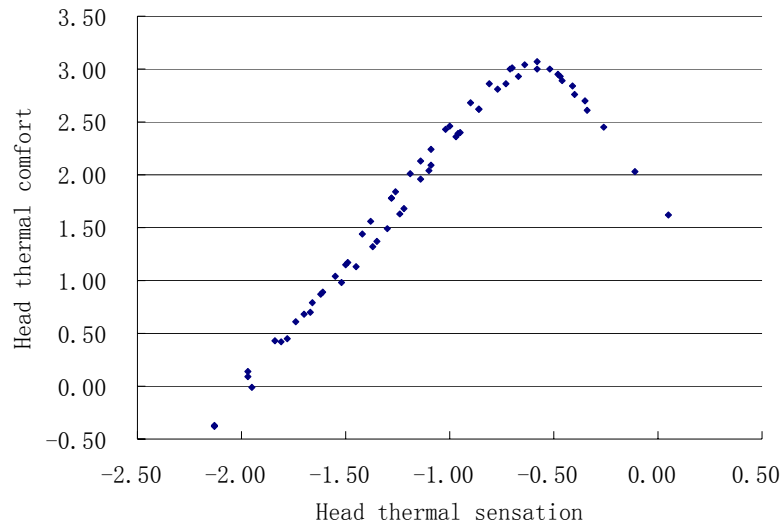
(a)
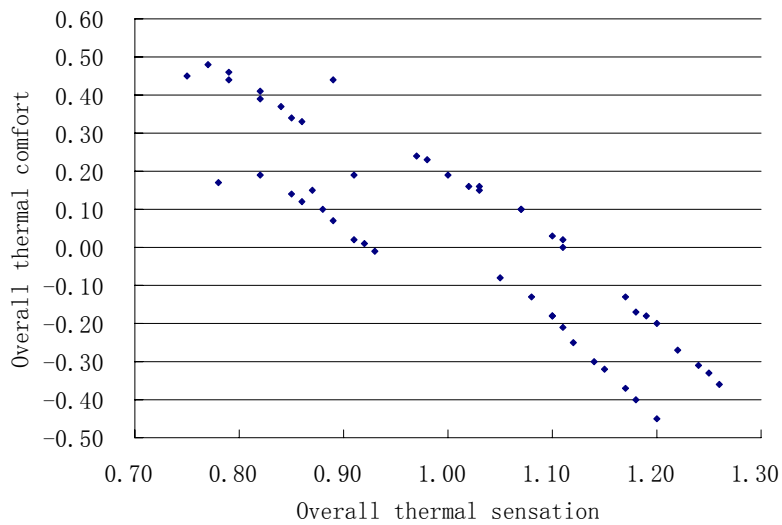
(b)

Figure 5.6 Head sensation VS head comfort (a) and overall thermal sensation VS overall comfort (b) (the data are from Figure 5.4 and Figure 5.5)

5.5 CFD simulation combined with the CBE Model-three examples

Application of the coupling method for the analysis of three types of PV systems is presented in this section.

5.5.1 Desk-edge-based personalized ventilation

Faulkner et al. (2004) tested the ventilation effectiveness of one personalized ventilation system in which personalized air is served at the desk edge and is directed upward, impinging firstly at the chest of the occupant (Figure 5.7(a)).

(a)

(b)

| 1-Room inlet |
| 2-Room outlet |
| 3-PV outlet |
| 4-Human body |
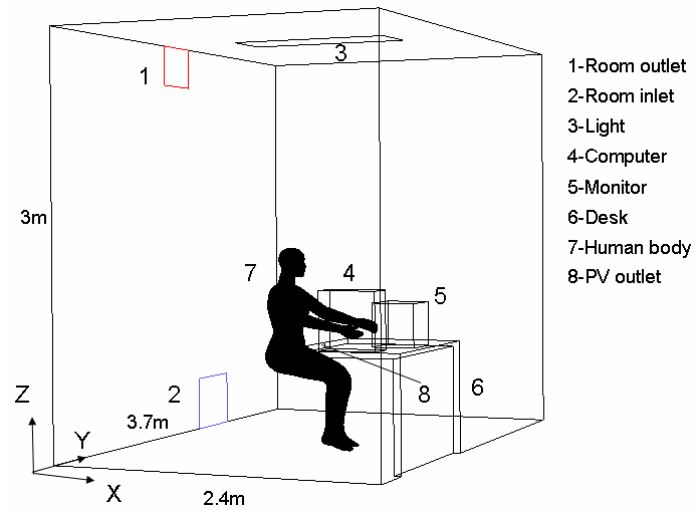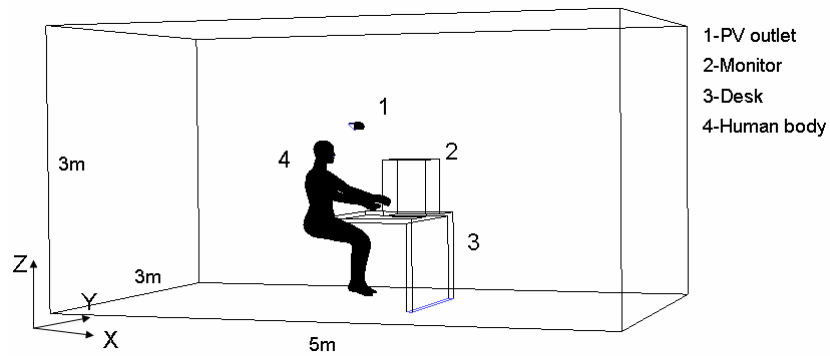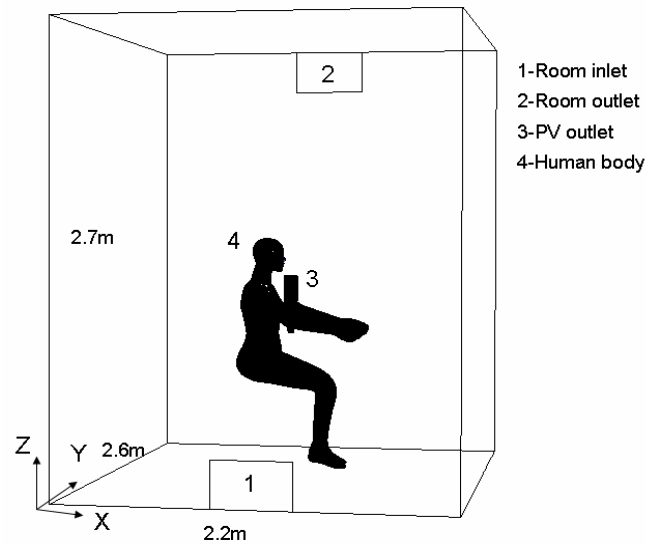
(c)

Figure 5.7 Configurations of different personalized ventilation (PV) systems: (a) desk-edge-based PV system from Faulkner et al. (2004); (b) movable panel PV from Melikov et al. (2002); (c) chair-based PV from Niu et al. (2004).

The cases where the personalized air is supplied in the direction of 45^0 upward are simulated. In the experiments (Faulkner et al. 2004), the room air was maintained at approximately 25℃ and personalized air was supplied iso-thermally at 25℃, or at a temperature about 5-6℃ less than the ambient room temperature, and at flow rates of 3.5, 4.8, 6.5 l/s. Personalized air was 100% outside air and the room supply air was 100% re-circulated air with an air flow rate of 33 l/s, equivalent to 4.4 indoor air volumes per hour. The ACE values were measured using a heated thermal manikin without the breathing function. Two interesting results were found. First, personalized air supplied isothermally at 25 ℃ resulted in lower ACE values than comparable tests in which PA temperature was 5-6℃ lower than the room air temperature at the same flow rate. It contradicted with the expectation that the ACE values would be higher under isothermal conditions since the warmer supply air

would not drop and would more easily be caught in the thermal plume of the body. Second, the ACE values tended to be higher at lower flow rates. The detailed ACE values from experiments and from present simulations are listed in Table 5.2.

Table 5.2 Air change effectiveness (ACE) values at personalized air (PA) flow rates of 3.5, 4.8, 6.5 l/s and personalized supply nozzle angle at 45^0

PA Temperature (℃)	PA Flow Rate (l/s)	ACE (simulation)	ACE (experiment)
20	3.5	1.85	2.2
25	3.5	1.32	2.0
20	4.8	1.68	1.9
25	4.8	1.39	2.7
20	6.5	1.58	1.7
25	6.5	1.46	-

Generally, the simulated values are lower than those of the experiments. This may be because that body posture in the experiments was not specified and the distance between the personalized air outlet and the head is not exactly identical in simulations and experiments. The simulation results are acceptable considering that in the repeated tests in experiments the ACE values at the nose differ, on average, by 0.3, with the largest difference at 0.7.

(a)

(b)

0.6 m/s

(c)

(d)

(e)

162
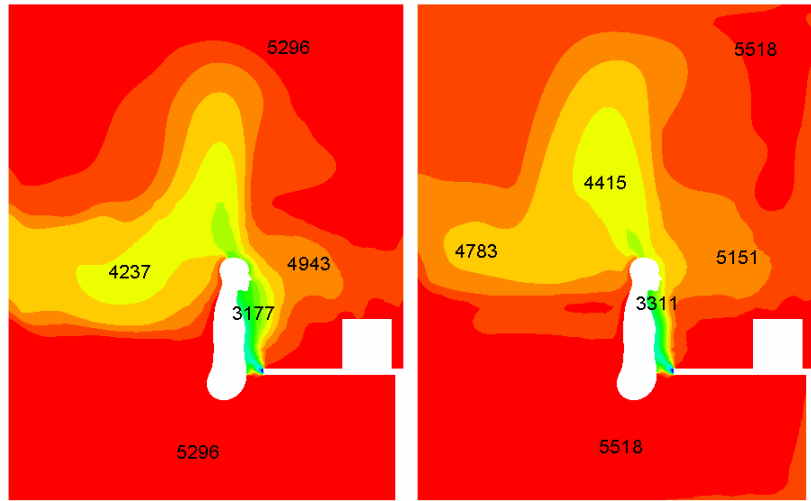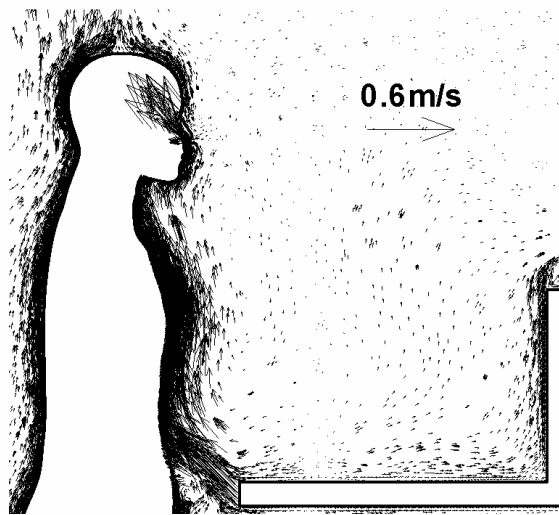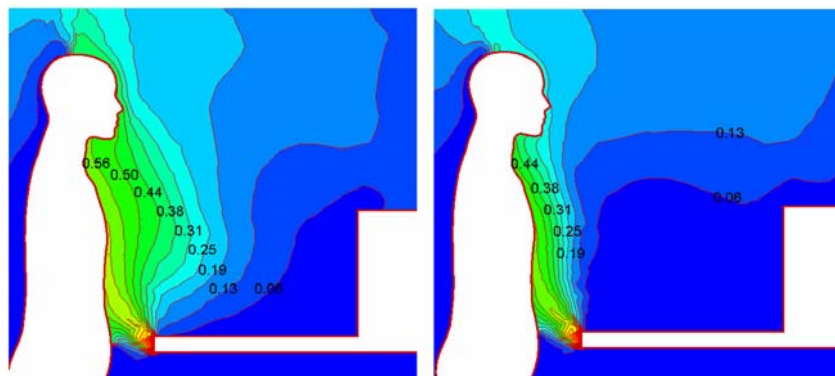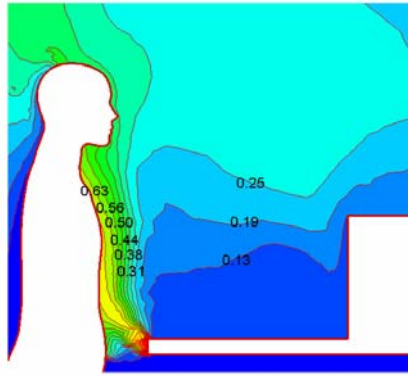
(f)

Figure 5.8 Distributions of age of air and tracer gas concentration at the iso-surface of y=0.54 m in the desk-edge based PV system: (a) Age of air when personalized air is served at 4.8 l/s and 20℃; (b) Age of air when personalized air is served at 4.8 l/s and 25℃; (c) Air velocity vector when personalized air is served at 4.8 l/s and 20℃; (d) Tracer gas distribution when personalized air is served at 3.5 l/s and 20℃ and the concentration in personalized air is set to 1. (e) Tracer gas distribution when personalized air is served at 3.5 l/s and 25℃ and the concentration in personalized air is set to 1. (f) Tracer gas distribution when personalized air is served at 6.5 l/s and 25℃ and the concentration in personalized air is set to 1.

The two interesting phenomena mentioned above are both found in the simulations. Figure 5.8(a) through (c) show the distributions of ages of air and air velocity vector. The age of air in front of the body is obviously lowered due to the personalized air supply. PA mixes with the thermal plume first and then climbs upward to the breathing height level. Tracer gas concentrations in front of the body are shown in Figure 5.8(d) through (f). One possible reason for the two phenomena is that personalized air at higher temperatures or higher flow rates results in increased upward velocity and, consequently, enhanced mixing with the room air. Since the nose is not located in the core of the personalized jet, this enhancement will lower inhaled air quality. A negative buoyancy effect induced by a lower supply temperature helps personalized air to spread above the desk and widen the upward

personalized airflow. The fact that the ACE values at 6.5 l/s are lower than at 3.5 l/s shows that there should be an optimum flow rate to achieve the highest ACE since the flow rate at zero will not cause an increase in ACE.

The PER values of this type of desk-edge-based personalized ventilation system are also calculated (Table 5.3). At 3.5 l/s and 20℃, almost one-half of the inhaled air is from personalized air. A numerical thermal manikin with steady inhalation through the nose at the rate of 0.14 l/s is also used in the simulations. No difference in the values of ACE and PER is found compared with the non-breathing manikin. It may be that transient simulation, including the inhalation and exhalation process, is imperative if the effect of respiration airflow on the performance of personalized ventilation is studied.

Table 5.3 Pollutant exposure reduction (PER) and inhaled air temperature difference (Δt_{inh}) in different personalized air (PA) supply systems[①]

Type	Room air Temperature (℃)	PA Temperature (℃)	PA Flow Rate (l/s)	PER	Δt_{inh} (℃)
Faulkner et al. 2004	25	20	3.5	0.48	-
	25	25	3.5	0.28	-
	25	20	4.8	0.48	-
	25	25	4.8	0.32	-
	25	20	6.5	0.42	-
	25	25	6.5	0.36	-
Melikov et al. 2002	20	-	0	-	22.6[②]
	20	20	5	0.775 (0.31)	-0.7
	20	20	10	0.856 (0.41)	-0.8(-0.3)
	20	20	15	0.865 (0.53)	-1.0
	20	20	20	0.875 (0.58)	-1.1(-0.5)
	26	-	0	-	28.8[②]
	26	20	5	0.589 (0.13)	-2.6
	26	20	10	0.590 (0.32)	-3.1(-3.2)
	26	20	15	0.855 (0.45)	-4.2
	26	20	20	0.877 (0.50)	-4.5 (-4.6)
Niu et al. 2004	23	-	0	-	27.7[②]
	23	20	0.8	0.684 (0.54)	-2.3
	23	25	0.8	0.348	0.4
	23	20	1.6	0.670 (0.65)	-2.4
	23	25	1.6	0.557	-0.1

① The values in bracket are from experiments.

② These are the temperature of inhaled air without personalized ventilation.

In the experiments, eleven subjects participated in the study of thermal comfort. Most (90%) of the subjects selected an overall thermal sensation between +1 and -1 on the ASHRAE thermal sensation scale (ASHRAE 2001). The supply air jet was

not objectionable since 67% of the subjects reported no change in air movement was wanted. Unfortunately, little information on the thermal comfort survey was reported by Faulkner et al. (2004), which makes a comprehensive comparison between simulations and experiments impossible.

Figure 5.9 shows that both the whole-body and the local thermal comforts are acceptable. No clear draft sensation is caused. The cooling is focused mainly at the head, chest, and arms and the sensations at the other body parts almost do not change (Figure 5.9(a)). Even at the strongest cooling condition (6.5 l/s and 20 ℃) personalized air only decreases the whole-body thermal sensation by 0.17 and thermal comfort 0.15 when compared with no personalized air supply. The clothing insulation at the chest makes the human body not so sensitive to personalized air cooling from the desk edge, as opposed to the case where personalized air is directed at the unclothed body parts, such as the head, from the desktop.

(a)

(b)
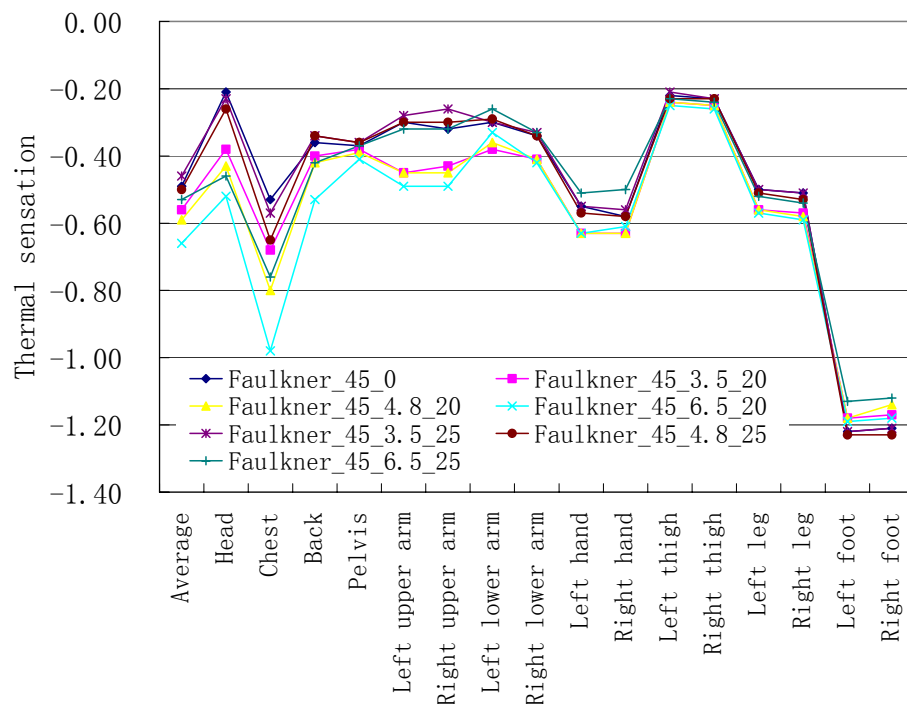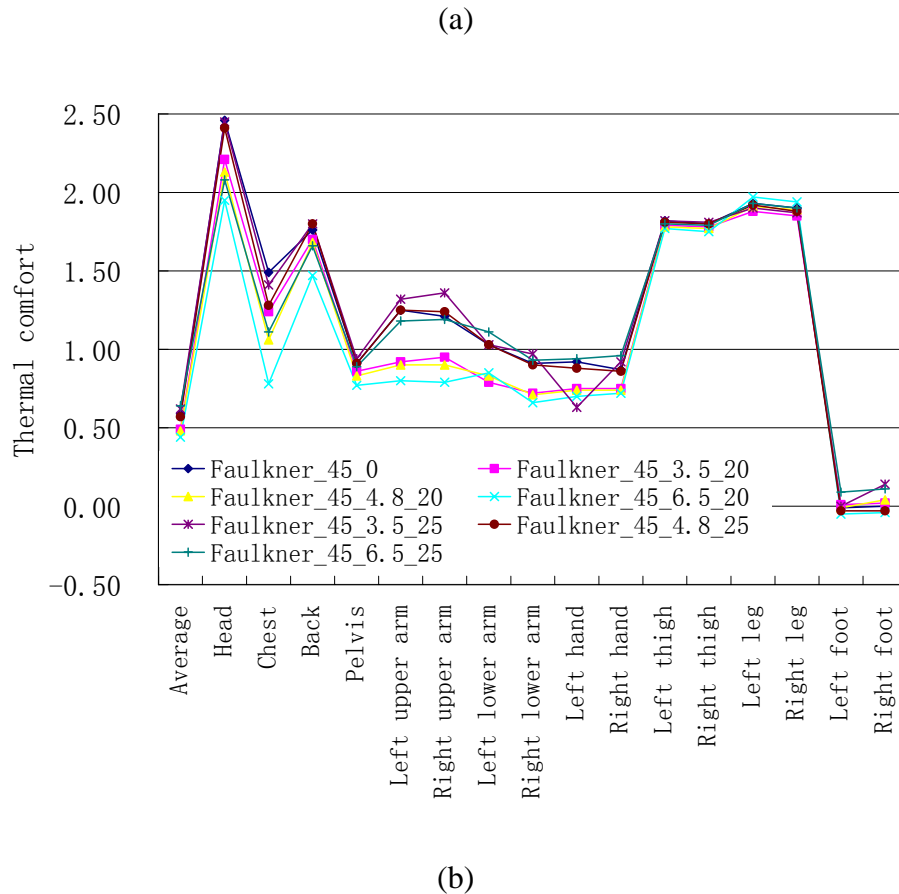
Figure 5.9 Thermal sensation (a) and thermal comfort (b) at different body segments in the desk-edge-based PV system. The legend shows the air supply angle, flow rate, and temperature. For example, Faulkner_45_4.8_20 means personalized air is served 45[0] upward at 4.8 l/s and 20 ℃.

Inspection on the ACE, PER, and thermal comfort reveals desk-edge-based personalized ventilation can improve inhaled air quality without causing draft.

5.5.2 Personalized ventilation using a movable panel

Melikov et al. (2002) measured the PER values of five different air terminal devices (ATDs) using a breathing thermal manikin. One of them, called the movable panel (MP) with rectangular opening ($240mm \times 75mm$), is simulated (Figure 5.7(b)). Isothermal (winter) conditions with an indoor operative temperature of 20 ℃ and a personalized air temperature of 20℃ and non-isothermal (summer) conditions with

an operative temperature of 26℃ and a personalized air temperature of 20℃ are simulated. An upward plug-flow with a velocity less than 0.06 m/s supplied uniformly from the floor is formed to maintain the room air temperature. The ATD is positioned 0.2 m in front of the manikin's face and 0.3 m above its nose. The flow rate of personalized air is changed from 0 to 20 l/s.

The PER values and inhaled air temperature decreases caused by personalize air supply from simulations and experiments are compared in Table 5.3. For PER, a relatively great difference is found. PER increases as personalized air flow rate increases, and this positive relationship becomes marginal at a high flow rate. The following factors may explain the discrepancy: (1) Hair is included in the experiments. (2) Airflow from the perforated ATD is simplified in the simulation as a jet flow with the initial velocity of the flow rate divided by outlet area ($0.24 \times 0.075 m^2$). (3) Body posture is not identical. (4) The effect of clothing on airflow around the body is not considered by the unclothed NTM. (5) The transient respiration process is simplified as steady inhalation. (6) There are test errors in the experiments. Part of the reason may also be attributed to unstructured grids and numerical errors. Although two boundary layers (Figure (5.13)) are created surrounding the body, a high quality of tetrahedral elements is difficult to be guaranteed due to the complexity of the geometry.
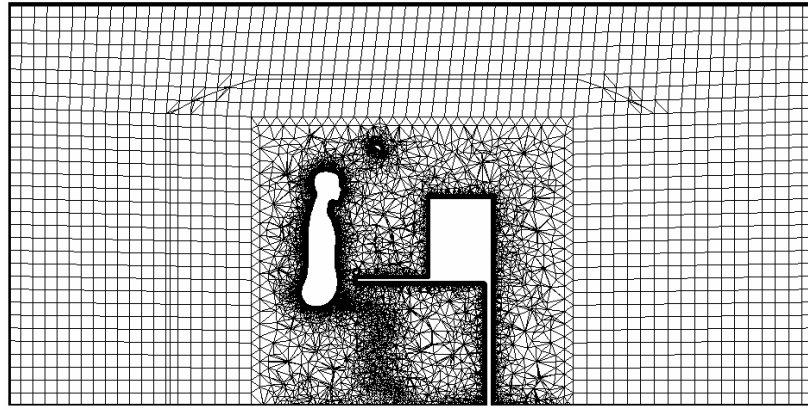
(a)
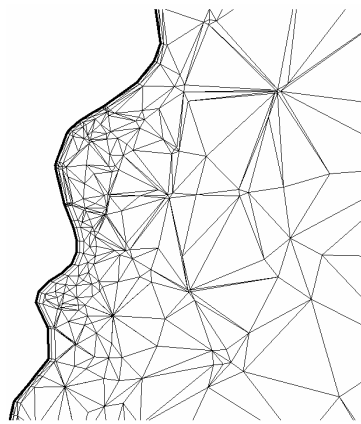
(b)

Figure 5.10 Grids system (a) in the case of Melikov et al. (2002) and the grids close to the nose (b)

In isothermal (winter) conditions, PER improvement is small ($\Delta PER = 0.10$) from 5 l/s to 20 l/s while it is remarkable ($\Delta PER = 0.29$) in non-isothermal (summer) conditions. As can be seen from Figure 5.11(d) and (e), the core of the isothermal jet flow of personalized air is able to reach the nose at 5 l/s, while it can not reach it at 10 l/s in non-isothermal cases due to the negative buoyancy effect. Measurement by Kaczmarczyk (2003) also shows that the nose is in the core regions of the isothermal jet flow from MP if flow rate exceeds 5 l/s. Figure 5.11(a) illustrates that without personalized air, the body is enclosed in a thermal plume that has a maximum

velocity of 0.24 m/s. This rising thermal plume can be peeled off by personalized air at a flow rate higher than 10 l/s in both isothermal and non-isothermal conditions (Figure 5.11(b) (c)). The inhaled air temperature without personalized ventilation is 22.6℃ at room air temperature of 20℃ and 28.8℃ at room air temperature of 26℃, which are 21.6℃ and 28.1℃, respectively, in the experiments (Melikov et al. 2002). The temperature of the inhaled air decreases with an increase of personalized air flow rate. In non-isothermal conditions, this decrease is much more substantial. The deviations from experiments in isothermal conditions are obvious, at least part of which are attributed to the fact that re-inhalation of the exhaled air of a temperature about 34 ℃ is not taken into account in the simulations.

(a)   (b)

(c)   (d)
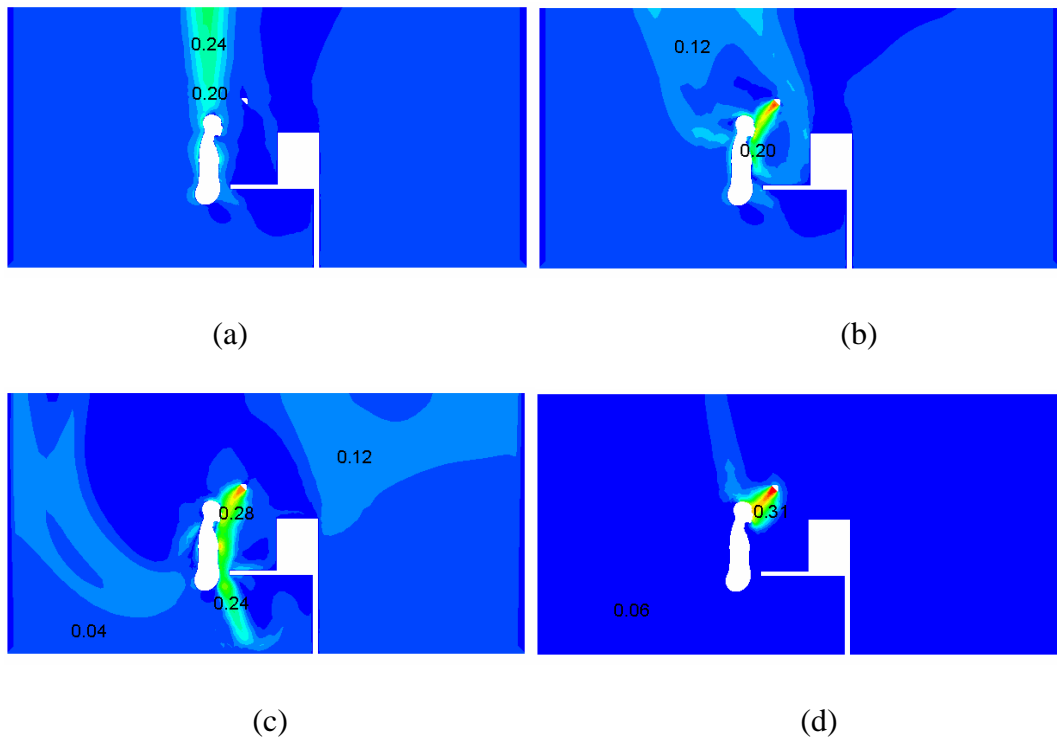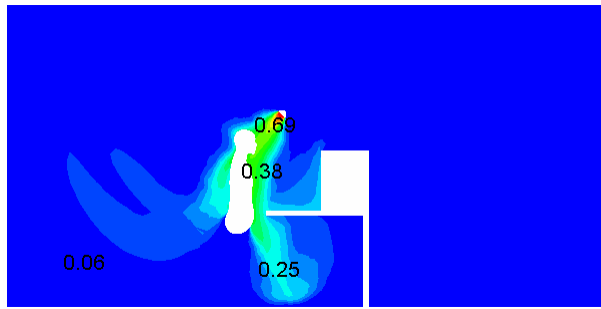
(e)

Figure 5.11 Distributions of air velocity and tracer gas concentration at the iso-surface of y=1.5 m in the PV system with movable panel (MP): (a) Side view of air velocity (m/s) when room air is supply from the floor at 26℃ and no personalized air is served; (b) Side view of air velocity (m/s) when room air is supply from the floor at 20℃ and personalized air is served at 10 l/s; (c) Side view of air velocity (m/s) when room air is supply from the floor at 26℃ and personalized air is served at 10 l/s; (d) Side view of tracer gas concentration when room air is supply from the floor at 20℃ and personalized air is served at 5 l/s; (e) Side view of tracer gas concentration when room air is supply from the floor at 26℃ and personalized air is served at 10 l/s.

Thermal sensation and thermal comfort in summer and winter conditions are shown in Figure 5.12. Clearly, the cooling is focused at the head and chest, which are directly exposed to personalized air. In both summer and winter conditions, personalized air can bring a "cool head" (Figure 5.12(a), 5.12(c)) and improve the comfort level at the head and the overall thermal comfort (Figure 5.12(b), 12(d)) when the flow rate is in the range from 5 l/s to 15 l/s. It is in line with the survey results that most subjects selected the local air velocity in a wide range from below 0.15 m/s (about 3 l/s) up to almost 0.8 m/s (about 15 l/s) if room air temperature was 23℃ and personalized air temperature was from 20℃ to 23℃ (Kaczmarczyk 2003).
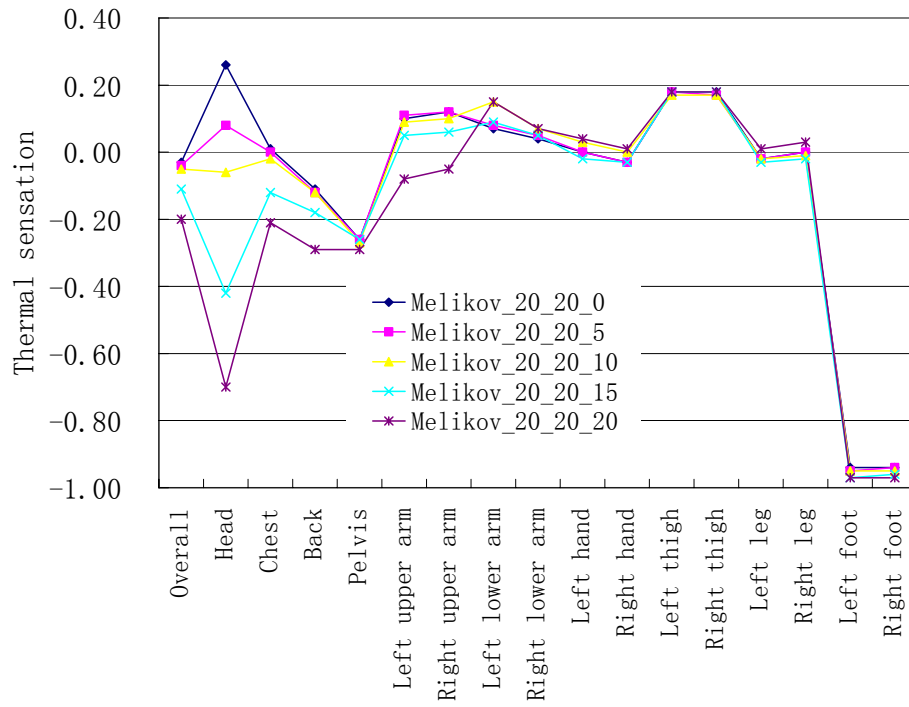
(a)
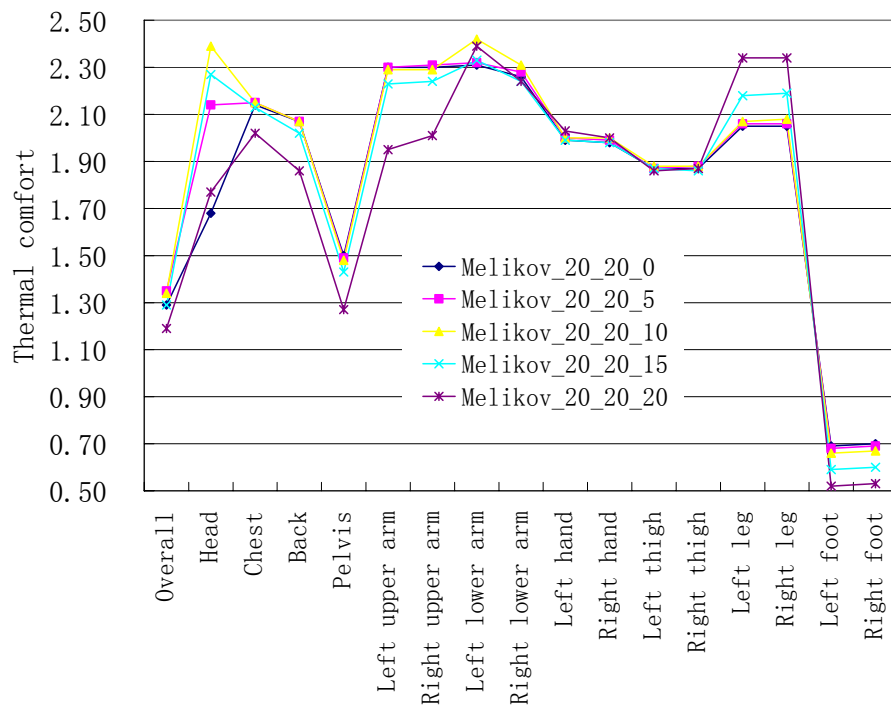
(b)
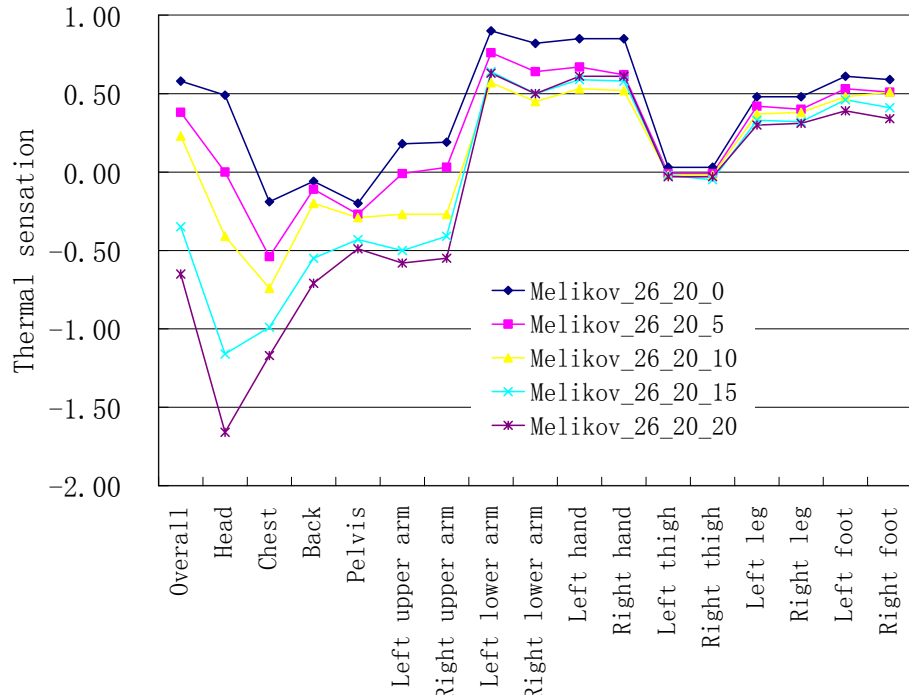
(c)
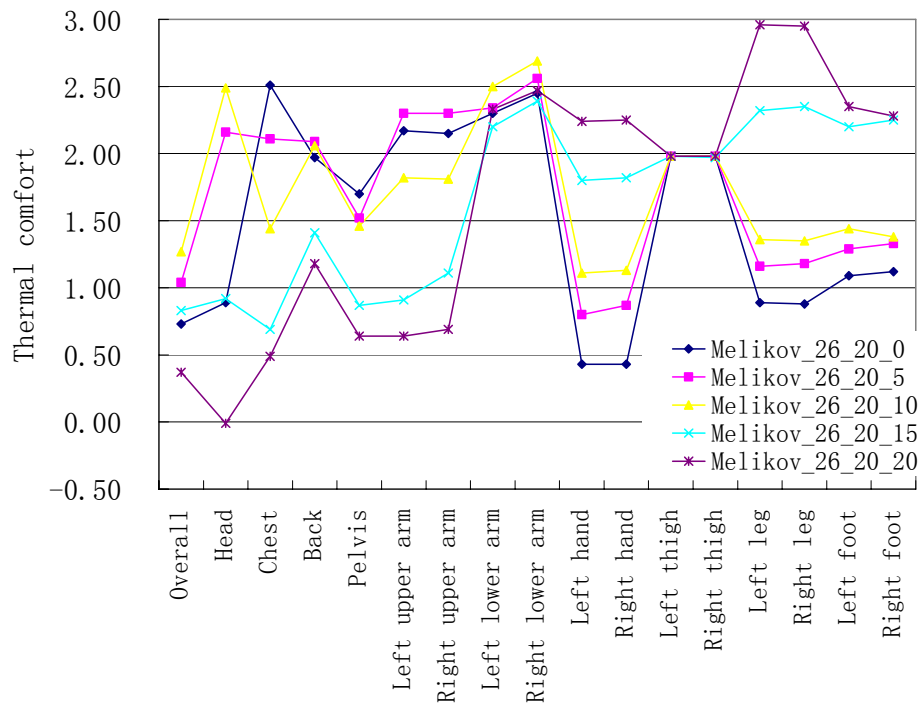
(d)

Figure 5.12 Thermal sensation and thermal comfort at different body segments in the PV system with movable panel when room air is replenished from the floor at 20℃. The legend shows personalized air temperature, flow rate, and room air temperature. For example, Melikov_26_20_10 means personalized air temperature and flow rate is 20 ℃ and 10 l/s individually and room air temperature is 26 ℃.

173

Table 5.4 Convective and radiative heat transfer coefficients for different body segments when the human body is placed in a uniform thermal environment with air temperature and mean radiation temperature of 26℃[①]

Body segment	Area (m²)	Convection			Radiation		
		Simulations [W/(m²℃)]	Experiments [W/(m²℃)]	Deviation (%)	Simulations [W/(m²℃)]	Experiments [W/(m²℃)]	Deviation (%)
Whole Body	1.568	3.09	3.3	-6.8	4.96	4.5	9.3
Head	0.118	4.00	3.7	7.5	5.43	3.9	28.2
Chest	0.153	2.96	3.0	-1.4	4.74	3.4	28.3
Back	0.166	2.47	2.6	-5.3	5.58	4.6	17.6
Pelvis	0.188	2.69	2.8	-4.1	5.00	4.8	4.0
Left upper arm	0.074	3.59	3.4	5.3	4.48	4.8	-7.1
Right upper arm	0.075	3.38	3.4	-1.0	4.55	4.8	-5.5
Left lower arm	0.055	2.95	3.8	-28.8	4.86	5.2	-7.0
Right lower arm	0.056	2.94	3.8	-29.3	4.80	5.2	-8.3
Left hand	0.036	3.21	4.5	-40.2	4.42	3.9	11.8
Right hand	0.037	3.22	4.5	-39.8	4.71	3.9	17.2
Left thigh	0.177	3.14	3.7	-17.8	4.85	4.6	5.2
Right thigh	0.178	3.23	3.7	-14.6	4.87	4.6	5.5
Left leg	0.085	3.23	4.0	-23.8	5.21	5.4	-3.6
Right leg	0.080	3.21	4.0	-24.6	5.13	5.4	-5.3
Left foot	0.045	3.94	4.2	-6.6	5.37	4.2	21.8
Right foot	0.045	3.88	4.2	-8.2	5.37	4.2	21.8

① The experimental values are from de Dear et al. (1997). The deviation is relative to the calculated values.

The heat loss at each body segment plays a key role in determining thermal sensation and comfort. The calculated heat transfer coefficients are compared with the

experimental values of a seated thermal manikin from de Dear et al. (1997) (Table 5.4).

Reasonable agreement is achieved for most body segments. Part of the deviations can be explained by the fact that the segmentation, body posture, and boundary conditions are not exactly the same in simulations and experiments. As to radiation, a large difference is found at the head, chest, feet, and hands. However at these segments the present simulated values are very close to the calculated values by SØrensen and Voigt (2003). The mean radiative heat transfer coefficient for the whole body is higher than the experimental one. However the simulated value is in line with the widely accepted value of 4.7 W/(m^2℃). With regard to convection, generally good agreement, with deviations less than 10%, is found except for the segments such as the arms, hands, legs, and thighs. Also, the natural convective heat transfer coefficient can be calculated from the empirical Equation (2.23), which results in 3.51 W/(m^2℃) for the average body surface temperature of 30.75℃ and ambient air temperature of 26℃. Present simulated value is slightly smaller than but much closer to the calculated one, i.e. 3.13 W/(m^2℃) by SØrensen and Voigt (2003). Previous numerical simulations (Murakami et al. 2000; SØrensen and Voigt 2003) found that in the dry heat loss from the human body, convection and radiation take up about 40% and 60%, respectively. In present investigation, 38.4% of dry heat is lost by convection and 61.6% by radiation.

5.5.3 Chair-based personalized ventilation

The chair-based personalized ventilation (ventilation seat) is also modeled (Figure 5. 7(c)). The room air is supplied at the low level of one sidewall with a flow rate of 14.3 l/s and a temperature of 20℃. The room air exhaust is at the ceiling level. The

human body equipped with a personalized ventilation system is placed at the center of the room, and no other heat source exists. Four cases where personalized air is served at 20℃, 25℃ and 0.8 l/s, 1.6 l/s are studied. The design flow rate of the chair-based personalized ventilation system is expected to be up to 3.0 l/s.

The PER values and inhaled air temperature decreases are shown in Table 5.3. The maximum PER is 0.684 at 0.8 l/s and 20℃, and the highest decrease of inhaled air temperature is 2.4℃ at 1.6 l/s and 20℃. PER at 0.8 l/s is higher than at 1.6 l/s. Low supply air temperature ensures high PER.

With regard to thermal comfort (Figure 5.13), only the head is affected. Personalized air at 0.8 l/s seems to have no thermal effect on the head, providing that personalized air velocity at the face is less than 0.15 m/s. At 1.6 l/s and 20 ℃ the thermal sensation is lowered by 0.52. The overall thermal comfort at both flow rates changes less than 0.2. Since the mean ambient air temperature in the occupied zone at the height of 1.1 m is about 23℃ and the clothing value is set in summer condition, the overall thermal sensation without personalized ventilation is -1.06 and the overall thermal comfort is -0.48. It is found that the body thermal conditions are mainly under the control of PA flow rate, not PA temperature. This agrees well with previous subject tests, which demonstrates that the influence of flow rate on thermal sensation is significant ($P<0.001$) at the head while the impact of personalized air temperature is not remarkable ($P>0.05$). The survey results also exhibit that personalized air at 0.8 l/s and 1.6 l/s can improve the overall thermal comfort since it brings a "cool head" and the overall thermal sensation without personalized air is neutral.
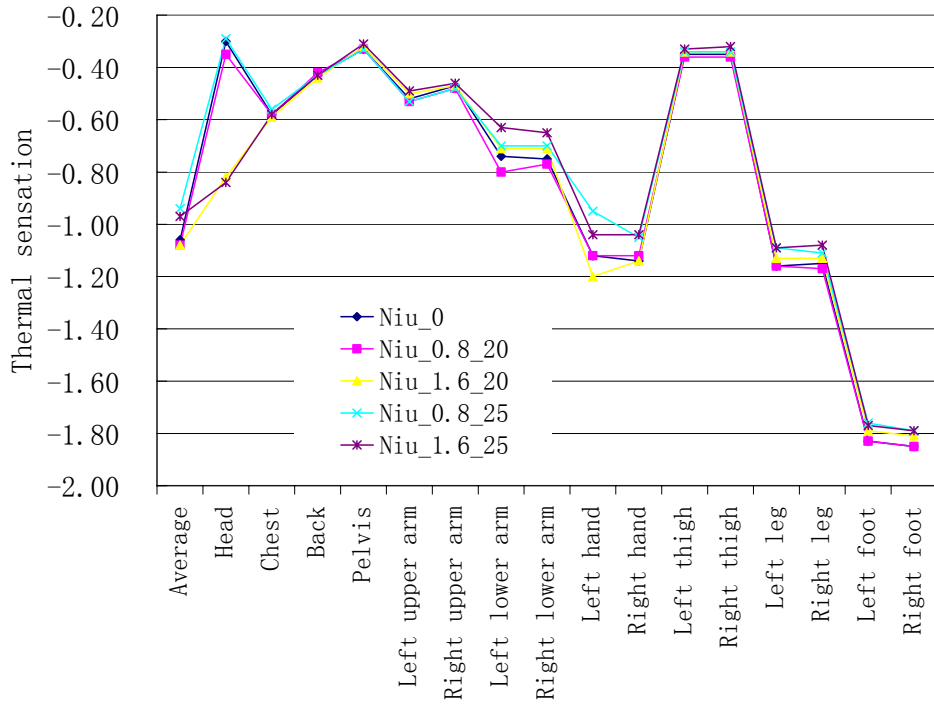
(a)
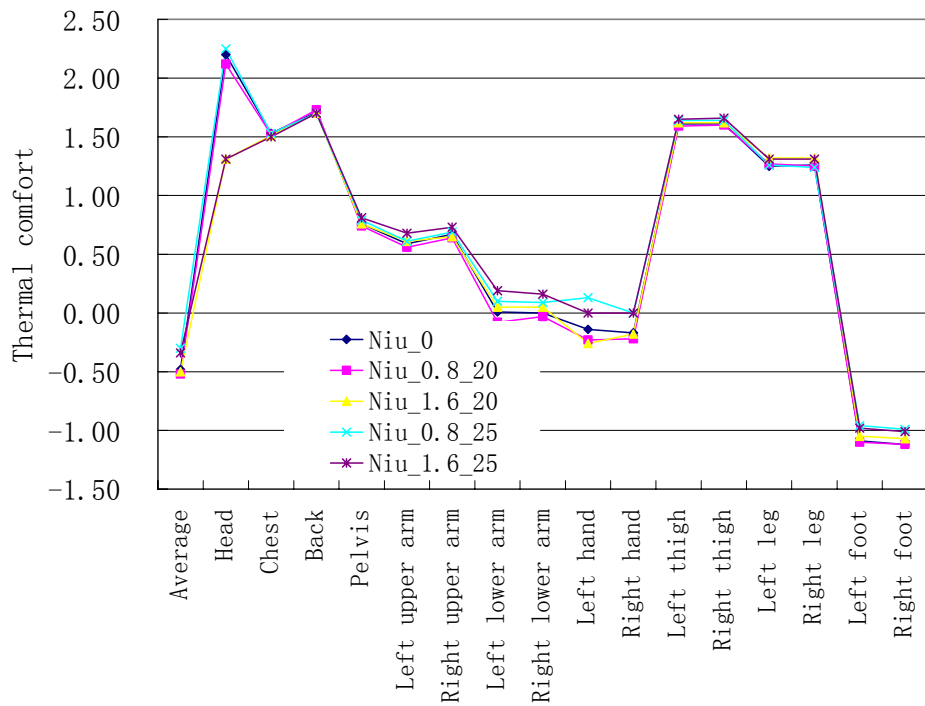
(b)

Figure 5.13 Thermal sensation (a) and thermal comfort (b) at different body segments in the chair-based PV system. The legend shows personalized air temperature and flow rate. For example, Niu_0.8_25 means the personalized air flow rate is 0.8 l/s and the temperature is 25 ℃.

Based on present simulations and the previous survey, it is recommended a supply airflow rate less than 2.0 l/s and a supply air temperature lower than room air temperature for chair-based personalized ventilation with the ATD at the microphone position. However the situation will be different if the occupant set the ATD at the other positions for his/her preference.

5.5.4 Results and discussion

In the development of personalized ventilation, three key issues have to be addressed, namely, ventilation efficiency or effectiveness, thermal comfort, and human acceptance and use patterns. The present simulations demonstrate applications of numerical thermal manikins in helping to understand the first two issues. An NTM is able to "tell" us the ventilation effectiveness, thermal sensation, and thermal comfort with reasonable confidence. On the other hand, deviations from experiments do exist. The ventilation efficiency of personalized ventilation is not only affected by the air supply rate and temperature, but is also sensitive to the body posture and movement and the location of the air terminal device. Transient respiration plays a key role at a relatively low supply flow rate. Accurate prediction of PER using CFD requires taking into account these factors more accurately. It also should be pointed out that, in the current coupling of CFD and a thermoregulation model for thermal comfort evaluation, the relative humidity is assumed to be 50%. The thermal comfort model used is established on the predicted skin and body core temperatures and their changing rates over time. It is well known that human comfort is also affected by the wind velocity at the eyes, lips, and nose, and irritations and dry feelings may be aroused by facial air movement. These factors have not been included in the current numerical models and final assessment of an HVAC system design by field surveys and subjective measurements are indeed necessary.

5.6 Comparison of the performance of personalized ventilation in displacement ventilation and mixing ventilation

This study aims at investigating the performance of PV when it is applied in conjunction with two different total-volume ventilation systems, namely mixing and displacement ventilation systems.

Another purpose is to examine the acceptable vertical thermal stratification when personalized air is served. ASHRAE Standard 55 (1992) limits the vertical air temperature difference between the head and ankle levels no more than $3\,℃$. However studies have revealed that the operative temperature is a stronger stimulation of discomfort than thermal stratification, and a higher temperature difference up to $6℃$ is acceptable (Kawahara et al. 1999; Wyon and Sandberg 1996; Zhang et al. 2005). It is believed that the discomfort is mainly aroused by the warm head or cold feet (Wyon 1994). Therefore it is reasonable to eliminate this discomfort by 'cooling head' via personalized air. Thus the operative temperature level and the vertical temperature difference can be loosed, suggesting energy savings.

5.6.1 Research method

The NTM is seated in a room with the dimensions of 4.0m (length) $\times$ 3.0m (width) $\times$ 2.7m (height) (Figure 5.14).
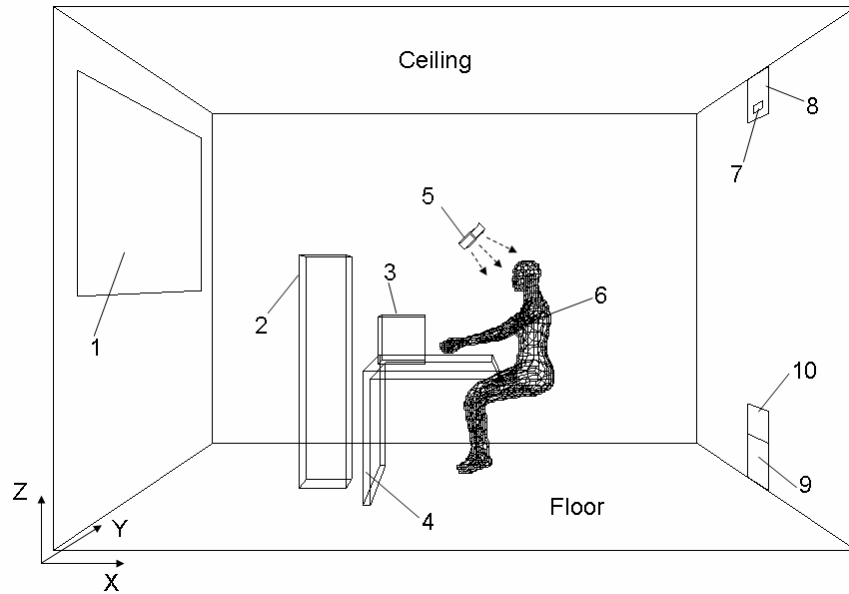
Figure 5.14 Configuration of the simulated office (room length (X) 4m, width (Y) 3m, height (Z) 2.7m; 1-window; 2-vertical heat source; 3-computer; 4-table; 5-personalized ventilation air terminal device (a circular outlet with a diameter of 20 cm); 6-human body; 7-mixing ventilation inlet $0.2\text{m}\times0.05\text{m}$; 8-displacement ventilation outlet $0.4\text{m}\times0.3\text{m}$; 9-mixing ventilation outlet $0.4\text{m}\times0.3\text{m}$; 10-displacement ventilation inlet $0.4\text{m}\times0.5\text{m}$)

Two types of background ventilation systems are installed, i.e. mixing and displacement ventilation systems. With displacement ventilation, a large wall-mounted diffuser is located at the floor level to supply cool air at a low speed, and an exhaust at the ceiling level. For mixing ventilation, an inlet diffuser with a small opening is set at the upper level, and an outlet at the floor level. The workplace is equipped with a personalized ventilation system. For simplicity only the circular air terminal device with a diameter of 20 cm is taken into account in the set-up.

The total heat released from the window, a computer, the vertical heat source, and the human body is about 445W, corresponding to a heat load of 37 W/m^2. The total amount of air supplied to the room via PV plus DV or MV systems is maintained

constantly at 51 l/s. The air change rate per hour is 5.7. The performance of PV is investigated at three airflow rates, i.e. 10, 15, and 20 l/s. The supply air temperature is 20℃, 19℃ and 17℃ for PV, DV, and MV respectively. In order to study the effect of vertical thermal stratification, the vertical heat source power is varied. In all 19 cases are simulated (Table 5.5).

Table 5.5 The setting parameters for the 19 cases

Number	Air distribution method	PV supply rate (l/s)	Room air supply rate (l/s)	Room air supply temperature (℃)	Vertical heat source (W)
Case 1A	DV	0	51	19	100
Case 1B	DV	10	41	19	100
Case 1C	DV	15	36	19	0
Case 1D	DV	15	36	19	100
Case 1E	DV	15	36	19	200
Case 1F	DV	15	36	19	300
Case 1G	DV	15	36	20	100
Case 1H	DV	15	36	21	100
Case 1I	DV	20	31	19	100
Case 2A	MV	0	51	19	100
Case 2B	MV	15	36	17	100
Case 2C	MV	15	36	17	200
Case 2D	MV	15	36	18	100
Case 2E	MV	15	36	19	100
Case 2F	MV	10	41	17	100
Case 2G	MV	20	31	17	100
Case 2H	MV	15	36	17	0
Case 2I	MV	15	36	17	300
Case 2J	MV	0	51	17	100

Table 5.6 The details of numerical methods

Turbulence Model	Standard k-ε model
Numerical Schemes	Upwind second order difference for the convection term; SIMPLEC algorithm
Window	Uniform heat flux 150W
Floor, ceiling, sidewalls	Adiabatic wall
Vertical heat source	Uniform heat flux 0～300W
Human body	Fixed skin temperatures of the 16 body parts from the coupled calculation
Computer	Uniform heat flux 120W
Table	Adiabatic wall
PV inlet	Airflow rate 0～20l/s, turbulence intensity 20%, turbulence length scale 0.014m
MV inlet	Airflow rate 31～51l/s, turbulence intensity 30%, turbulence length scale 0.005m
DV inlet	Airflow rate 31～51l/s, turbulence intensity 15%, turbulence length scale 0.03m
MV/DV outlet	Velocity and temperature: free slip
Nose	Steady inhalation, respiration rate 8.4 l/min, turbulence intensity 20%, hydraulic diameter 0.01m

An additional governing equation of tracer gas with the same physical property as that of air at the standard condition (273K, 101KPa) is solved in the testing of indoor air quality. Three plane sources of pollutants are considered: the ceiling, the floor, and the four sidewalls. It could mimic the situations in which the volatile organic compounds (VOCs) are released from the painted ceiling and sidewalls, and the dust is generated from the floor. The contaminant concentration is normalized by the value in the exhaust air. The details of the numerical methods are given out in Table 5.6.

5.6.2 Indoor air quality

5.6.2.1 Comparison of IAQ in DV and MV

Figure 5.15 shows the air velocity, temperature and concentration fields in DV and MV when personalized air is delivered at 15 l/s. As expected in DV the cool supplied air spreads over the floor and then is drawn up by the heat sources. Vertical temperature stratification appears whose gradient is steeper in the occupied zone than in the upper recirculation zone. The temperature difference between the ankle and head levels is about 3℃. In MV a strong supply jet attaches the ceiling, and then drops into the occupied zone. A relatively uniform temperature field is observed. The human body is enclosed by a thermal plume in DV solely (the figure is not shown here) while this phenomenon is not evident in MV. This plume is able to be peeled off by personalized air (Figure 5.15 (1a)). Although the supply air temperature is 2℃ lower in MV, the temperature level in the occupied zone is still a little higher than in DV, also accompanying a higher velocity level.

(1a)   (2a)
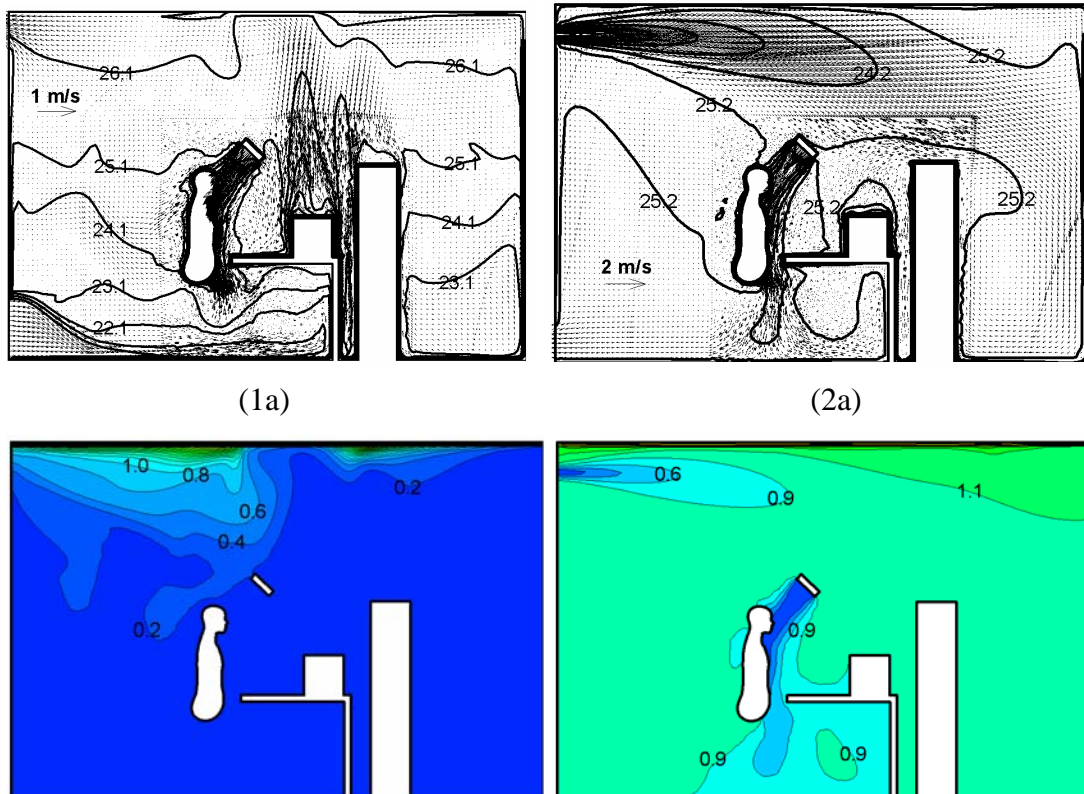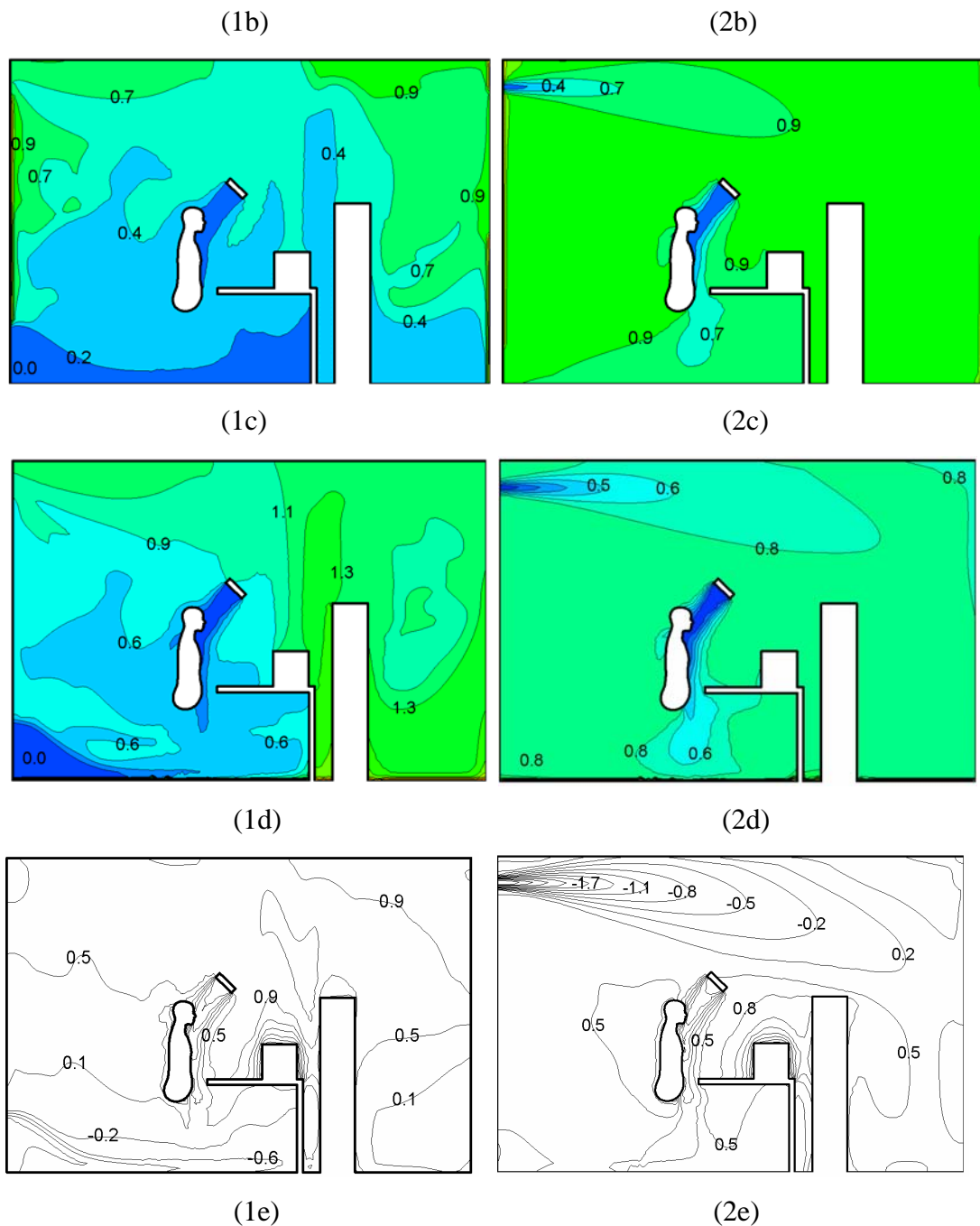
Figure 5.15 Temperature and velocity distribution (a); Concentration distribution, source from the ceiling (b); Concentration distribution, source from the sidewalls (c); Concentration distribution, source from the floor (d); PMV distribution (e) in case 1D (1) [DV 36 l/s 19℃, PV 15l/s 20℃, and vertical heat source 100W] and case 2B (2) [MV 36 l/s 17℃, PV 15l/s 20℃, and vertical heat source 100W]

In DV without PV concentration stratification is also observed when the contaminant is generated from the ceiling (The figures are not shown). The convection of the

contaminant from the upper to the lower is prevented by the temperature stratification. Since the room air outlet is located at the ceiling level the contaminant can be quickly exhausted before it is transported into the occupied zone. Theoretically the contaminant can be refined in the recirculation zone and it is better to reduce the height of this zone from the view point of indoor air quality. Here the concentration stratification height is higher than the thermal stratification height, depending on the location of the pollutant source. When the contaminant is produced from the floor the concentration indoor is more uniform than from the ceiling. The contaminant is transported from the floor to the upper by the displacement airflow. The concentration at the breathing zone is almost the same as that at the exhaust opening. It is in line with the experimental findings (He at al. 2005). Figure 5.15 (1d) well illustrates the following description by Cermak and Melikov (2006): 'the concentration of pollutants in the air spreading along the floor increases with the distance from the supply terminal. The highest concentration is found at the opposite wall.' When the contaminant is sent off from the four sidewalls its transport in horizontal direction into the occupied zone is restricted to some degree since the main indoor airflow is upward.

In MV without PV the concentration fields are always uniform. Human exposure in different cases is compared in Figure 5.16. Generally human exposure is lower in DV than in MV. However both ventilation methods are comparable in regard to floor pollution, which is also proved by experiments using a breathing thermal manikin (Cermak and Melikov 2006). A little discrepancy in the inhaled air quality in three MV cases without PV may be triggered by the combination of airflow pattern and pollutant source location, which results in different paths: supply jet → pollutant

source$\rightarrow$ occupied zone$\rightarrow$ exhaust, and supply jet$\rightarrow$ occupied zone$\rightarrow$ pollutant source$\rightarrow$ exhaust.
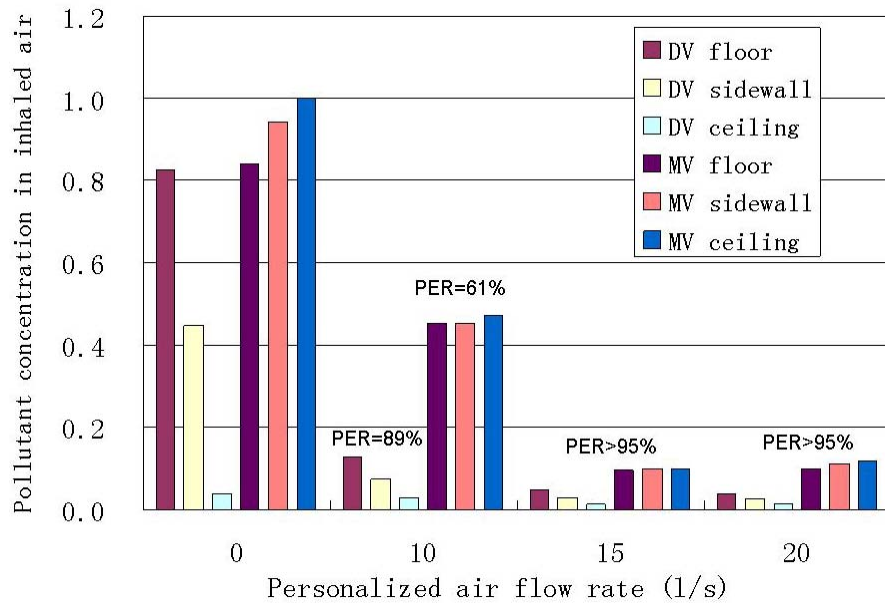
Figure 5.16 Pollutant concentrations in inhaled air (normalized by room exhaust air) at various personalized ventilation rate in a displacement ventilated (case 1D) and mixing ventilated (case 2B) room

5.6.2.2 Benefits from personalized air

Equipment of a personalized ventilation system is able to increase inhaled air quality greatly, in spite of the same total-amount of supply air rate (Figure 5.16). At a PA flow rate of 10l/s, the value of PER is 89% and 61% for DV and MV respectively. Adding tracer gas into personalized air and inspection of the concentration field indicate that since the temperature level is higher in MV than in DV, the non-isothermal jet flow from the personalized air terminal device (ATD) drops down in front of the face and the core of the jet does not reach the nose, resulting in a lower PER. Therefore in the design of PV it is crucial that its performance is dependent on the background ventilation method. At flow rates of 15 and 20 l/s, the jet is strong

enough to overcome the effect of temperature difference. PER is above 95% in both DV and MV.

The contaminant concentration in inhalation $C_{inhalation}$ can be calculated from the following equation:

$$C_{inhalation} = (1 - PER) \times C_{room}$$ (5.2)

where C_{room} is the mean concentration level indoor. As long as PER is not 100% inhaled air quality will also be determined by C_{room}. When the flow rate exceeds 15l/s the human exposure levels off at a low value. The results for floor pollution agree well with the experimental measurement (Melikov et al. 2003). Melikov et al. (2003) found ventilation effectiveness to be 7.0 and 19.1 in MV and DV, respectively, when personalized air was provided at 15 l/s. The corresponding values in present simulation are 10 and 21, respectively.

5.6.3 Thermal comfort

5.6.3.1 Thermal comfort in DV and MV, and the effect of cooling head

Thermal comfort in DV and MV is of different stories (Figure 5.17). Usually the most possible discomfort in DV is local draft, including cool feet or warm head. In current case where room air is supplied at 19℃ without PV a neutral overall sensation and a comfort value higher than 1.0 are achieved. No local discomfort is found. Servicing personalized air at 20℃ from 10l/s to 20l/s can remarkably lower the head sensation to around -1.3, and consequently cause a relatively small decrement of overall sensation from neutral to slightly cool. The overall comfort level descends but is still acceptable. It can be seen that the sensations of the body parts which are directly exposed to personalized air, such as the head, and the chest,

decrease greatly, while the sensations of the other parts change a little. Using PV the
sensation at the legs rises by around 0.5 since personalized air supply temperature is
1℃ higher than the room replenishment temperature and room air temperature at the
feet level ascends when applying PV at 20l/s (Figure 5.17(a)). This is the reason why
PV working at 10l/s leads to almost the same overall sensation and comfort
compared with the situation in DV solely. In this scenario a cooler head compensates
warmer legs. At the maximum PA flow rate, i.e. 20l/s, the head comfort value is 0.61.
It suggests that even though the whole body feels slightly cool (the overall sensation
value is -0.39), the occupant still prefers a cool sensation at the head.

(a)

(b)

(c)

189
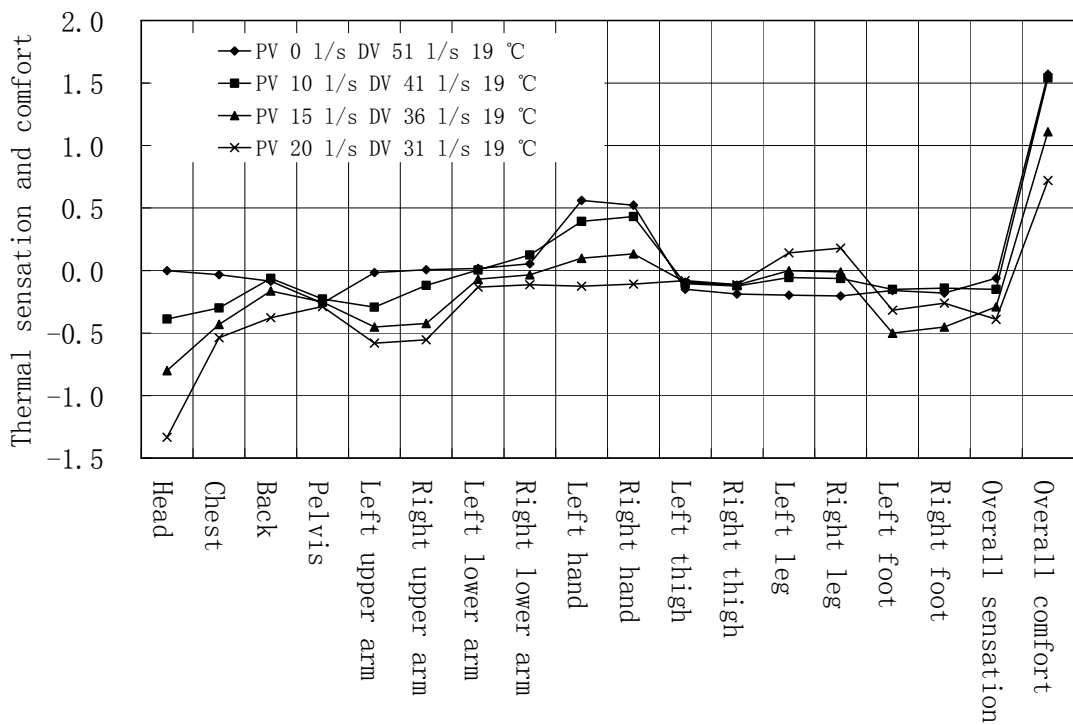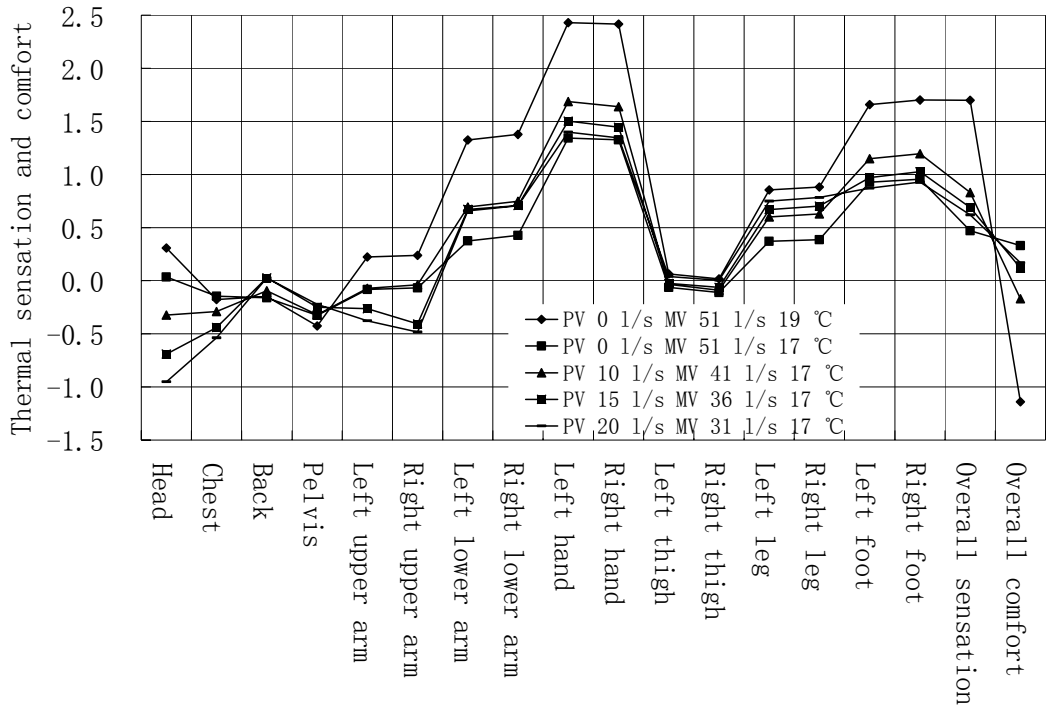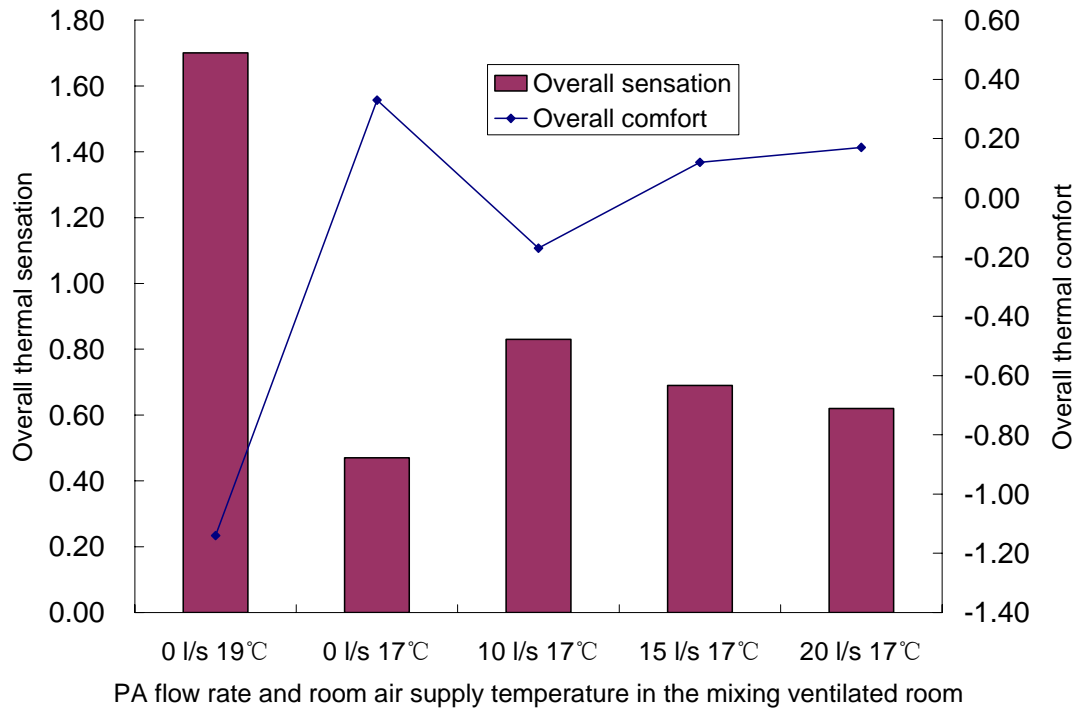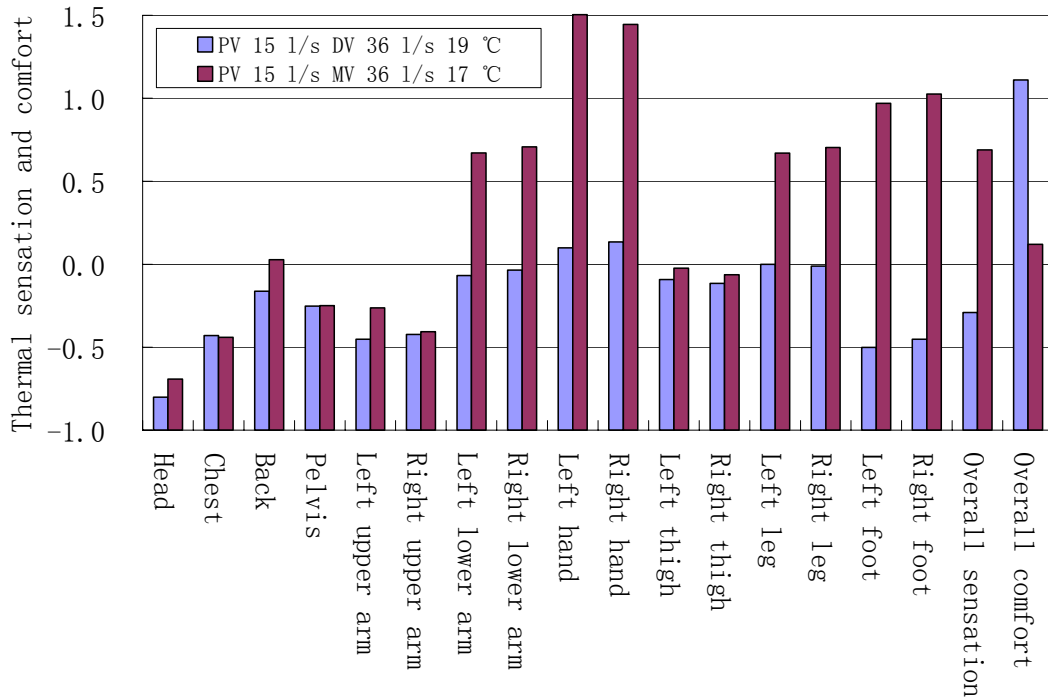
(d)

Figure 5.17 Thermal sensation and overall thermal comfort calculated from the CBE
model

In MV solely (Figure 5.17b, 5.17c), thermal comfort is unacceptable if room air is supplied at 19℃. In contrast to DV, MV equalizes the room air temperature by increasing it in the occupied zone and decreasing it in the upper zone. Therefore MV is not as energy-efficient as DV. The overall sensation is also higher in MV than in DV even though the supply temperature decreases to 17℃. It is further proved by Figure 5.15(1e), (2e), and Figure 5.17(d). In DV the PMV value rises from -0.5 to 0.5 from feet to head. However it fixes at 0.5 around the body in MV. Using the CBE model the overall sensation is 0.69 and -0.29 in MV and DV individually (Figure 5.17(d)). The two models here are in line.

Figure 5.17(c) shows an interesting tendency. Varying personalized air flow rate from 0 to 20 l/s step by step, the overall sensation firstly increases at 10l/s and then decreases gradually. At 10l/s it is uncomfortable. Due to a temperature difference of 3℃ between personalized air and room supply air, displacing air supply from room inlet to personalized ATD at the rate of 10l/s makes a warmer feeling at the body parts which are not directly exposed to personalized air. These sensations dominate the whole-body sensation when counteracting the effect of cooling head. However further enhancing personalized airflow from 15l/s to 20l/s turns the intervention between the head and the lower body parts into opposite direction. The whole body feels cooler and is brought back into comfort condition. Thus it is important to remember that the room ambient air temperature is comparably important. In the course of making use of the 'local cooling' via PA, the room ambient air temperature is expected to be increased in order to save energy. Present result indicates that this increment should be carefully inspected. This result matches well with the survey by Tham et al. (2003). They concluded that both indoor ambient temperature and PV supply airflow rates had strong effects on the thermal sensation of subjects.

5.6.3.2 Limitation of vertical temperature stratification

Present strict limitation of vertical temperature stratification can be loosed by releasing thermal stress at the head. Here the heat generation form the vertical heat source is strengthened in order to increase vertical temperature difference (Figure 5.18). In MV room temperature level rises almost uniformly by 1.6℃ if adding heat load of 100W. In DV the temperature increment at the height of 1.1m is around 1.0-1.2℃ per 100W. The temperature difference in the occupied zone (0-1.8m) ascends up to more than 6℃ at the load of 200W. The floor temperature is approximately 3℃

higher than the neighboring air because the adiabatic floor returns to air the absorbed

heat via radiation from the heat sources and the ceiling.
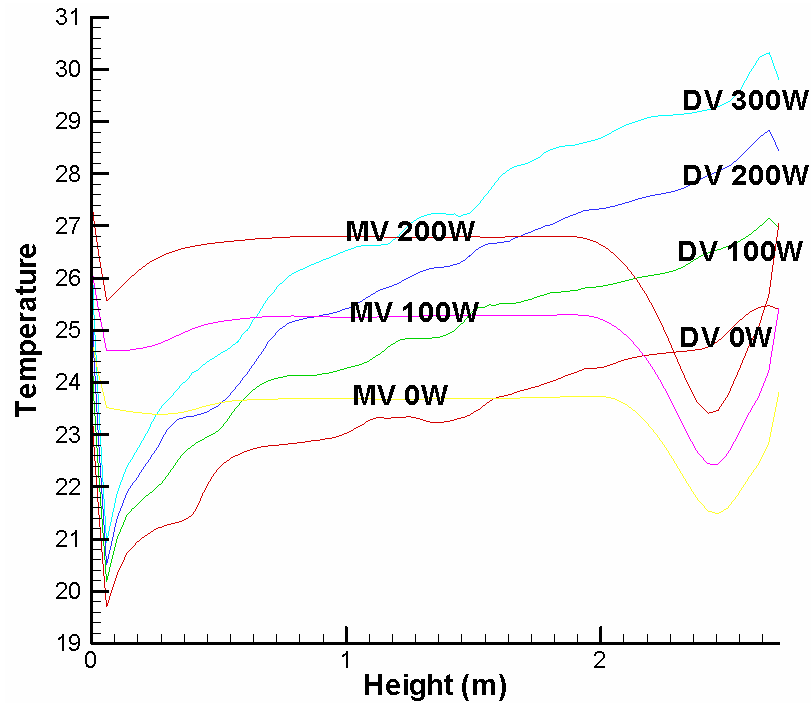
Figure 5.18 Vertical temperature distributions when changing the heat source power

Figure 5.19 shows the effectiveness of providing air movement at the head. In DV

increasing heat load from 0 to 300W makes overall sensation go up linearly, while a

maximum thermal comfort value exists, implying a parabolic relationship. In the case

of load at 200W, where the temperature at 1.1m is around 25.5℃ and the

temperature difference is above 6℃, the comfort level is still acceptable (0.21).
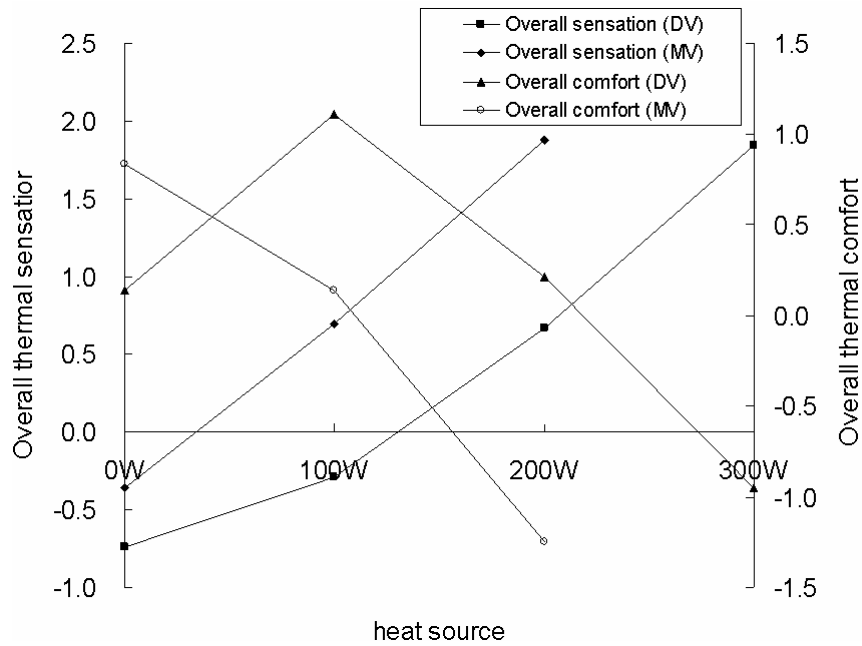
Figure 5.19 Thermal sensation and overall thermal comfort when changing the vertical heat source power

5.6.4 Summary

DV provides better inhaled air quality than MV except in the situation where contaminants are emitted from the floor. Serving personalized air to the breathing zone can greatly improve the inhaled air quality. But the degree of this improvement also depends on the room average pollutant concentration level. DV is more energy efficient than MV since it is only aimed at conditioning occupied zone. Equipped with PV the whole body sensation and comfort are controlled not only by personalized air but also by the indoor temperature level. Air movement at the head forced by PV can increase acceptable stratification up to 6℃.

Chapter 6

Conclusion and recommendations for future work

As concluding remarks are given at the end of each chapter, only the main points are highlighted in this section.

6.1 CFD simulation of the micro-environment around a human body

Recently, a database of benchmark tests for a numerical thermal manikin was established (see www.cfd-benchmarks.com). As a human body blocks airflows, generates heat and pollutants, and also breathes and moves, international efforts are being made to undertake CFD simulations of the human body (ASHARE winter meeting 2006). It must be recognized that in most cases simplifying the body as a cuboid is enough to obtain reasonable simulation results, as long as the focus is the global airflow field and an appropriate heat transfer boundary for the body is prescribed. However, to clarify the interaction of various airflows in the breathing zone with PV, an NTM with a real geometry is necessary. The representation of the skin surface of the extremities in this complicated type of NTM increases the number of computational grids that are needed up to a magnitude of millions, and makes almost structured grids impossible. Using two-equation models with wall functions also causes difficulties in capturing grid-independent results and accurate convective heat transfer coefficients. Few CFD practices have been reported that take account of the effects of human thermoregulation and the respiration process. The current practice in the simulation of a seated body in an almost stagnant environment shows the following.

1. The maximum upward air velocity in the plume above the head is around 0.22-0.24 m/s, and the thickness of the plume at the neck is about 10 cm.

2. A horizontal airflow at a speed of 0.2 m/s in free stream is strong enough to peel off the enclosing plume.

3. With PV, the inhaled air consists of room air and personalized air. The ratio of these two types of air is dominated by the relative strength of the warm rising flow and the personalized jet flow. A target velocity at the nose of less than 0.1 m/s of the personalized jet is able to break the plume envelope, which results in a promising PER value. However, the weak jet flow can be easily removed by a horizontal invading airflow such that it misses the nose or mouth, even at velocities of less than 0.2 m/s.

4. The temperature of a resting occupant' inhaled air is typically higher than that of room ambient air in a room ventilation system without PV. However, this study finds that with PV, the temperature of inhaled air can be lowered by around 2.7℃.

5. A transient simulation of breathing indicates that personal exposure to the air that is exhaled by others through the normal respiration process is very low in a displacement ventilated room. However, if two occupants are facing each other, then the risk of cross-infection through sneezing or coughing is much higher.

6.2 Experimental study of a ventilation seat

The performance of a particular kind of personalized ventilation – a ventilation seat – is measured. This ventilation seat has potential applications in cases in which the occupant of a seat is likely to be seated for a prolonged period. An air terminal device named SCN is tested using a heated breathing thermal manikin with an artificial lung. The two evaluation indices of the pollutant exposure reduction (PER) and the utilization efficiency are used. When operated at a flow rate of less than 2.5-3.0 l/s (corresponding PV outlet velocity 0.50-0.60 m/s), the ventilation seat achieves

a reduction of up to 76% in the level of pollutants in inhaled air. Based on a series of tests, a supply rate of 0.8~1.6 l/s (corresponding PV outlet velocity 0.16-0.32 m/s) is recommended.

Subjective measurements are carried out to investigate whether this ventilation seat will cause the sensation of a local draft. The statistical results show that people are more sensitive to the flow rate of personalized air than to its temperature. Personalized air is thus able to greatly improve the perceived air quality, and creates the sensation of a "cool head." The correct enhancement of the movement of air on the face can eliminate the feeling that a room is stuffy. However, a flow rate of higher than 1.6 l/s causes a local draft to be felt.

6.3 Coupling CFD and a human body thermoregulation model

The method of using an NTM to predict local thermal comfort may be a burgeoning area of HVAC research. Such prediction can be pursued in two directions. The first is the use of equivalent homogeneous temperatures to characterize the local heat loss at each body part. The second is the setting up of physical thermoregulation models and subjective local thermal comfort models, then continuously regulating the surface temperatures in the CFD boundary conditions through an iterative process, and finally using the converged skin thermal parameters to predict the thermal comfort level. The second method is that which is used in this study. Validation against three experimental studies proves the thermal comfort predictions from the coupling simulations to be acceptable. The method may be a useful tool for visualizing local thermal comfort at certain stages in the design of HVAC systems in which the application of PMV theory is questionable.

An example of the application of the method is exhibited by studying PV performance in a displacement ventilation system and a mixing ventilation system. It is found that effects of the background air conditioning and ventilation system on PV performance should be interpreted with caution. The whole-body sensation and comfort level can be determined by the personalized air and room air conditions, although the head has a higher weight than the other segments in determining the whole-body sensation. Air movement at the head that is caused by PV can increase the acceptable thermal stratification by up to 6 ℃ in a displacement ventilated space.

6.4 Recommendations for future work

1. Other aspects of the chair-based personalized ventilation system, such as first investment, operation cost, system control strategy, human use habits, and so forth, need to be clarified before the system is put to widespread use. Furthermore, the possible advantages of personalized air in improving human productivity and reducing Sick Building Syndrome are worth addressing.

2. Terrorism in the form of airborne chemical and biological warfare agent attacks, the outbreak of SARS, and the threat of avian flu have all caused concern about the transmission of particles or droplets in built environments. The advantage of PV in minimizing the exposure of building occupants to aerosolized pollutants and its disadvantage of maximizing the dispersion of fine droplets from a sick person merit further study.

3. With PV, the entire air conditioned space is split into task zones and an ambient zone, and heat transfer occurs between adjacent zones. If the ambient room air is supplied by displacement ventilation or UFAD, then temperature stratification will occur. These factors make energy modeling much more complicated.

Conventional HVAC energy modeling approaches are not suitable, as they assume the temperature of the conditioned space to be constant. To thermally model PV systems, the total building space could be divided into many well-mixed cells, with the heat and airflow among the cells being taken into account (Glicksman and Taub 1997) (Figure 6.1a). The use pattern of PV units would need to be established first, as this determines the thermal behavior of the cells that correspond to the task zones. For example, there is a heat gain in air that is supplied from concrete slabs and raised floor panels (Figure 6.1(b)). Due to the vertical temperature gradient, the floor is heated by radiation from the ceiling, and part of the heat is transferred to the room air through convection. At the moment, these particular thermal modeling factors are not embedded in the current energy analysis tools, such as EnergyPlus. The accurate modeling of the energy consumption of PV requires these factors to be fully addressed.

(a)   (b)
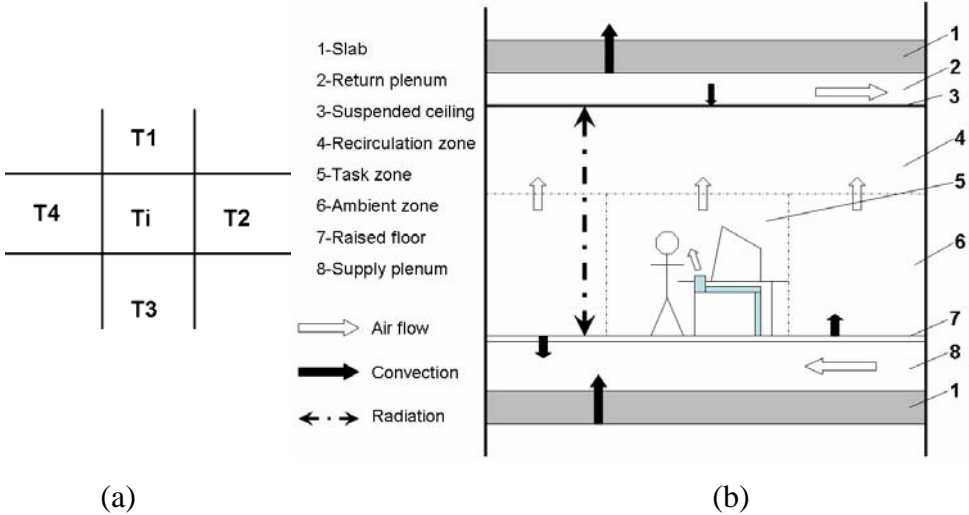
Figure 6.1 Schematic diagram of the heat transfer in a room with a PV system in (a) the horizontal direction (b) the vertical direction

References

[1]   Aalborg University and International Center for Indoor Environment and Energy, http://www.cfd-benchmarks.com.

[2]   Akimoto, T., Lee, Sueng-jae., Iesaki, N., Yokota, T., Hayashi, J., Tanabe, S. 2003. Impact of non-isothermal conditioning system on thermal comfort. *Proceedings of Healthy Buildings 2003*, Singapore, pp. 776-782.

[3]   Akimoto, T., Bauman, F.S., Benton, C.C., Arens, E.A. 1996. Field study of desktop-based task conditioning system. *Journal of Architecture Planning and Environment Engineering*, (490): 35-46.

[4]   Arens, E.A., Xu, T.F., Miura, K, Zhang, H., Fountain, M., Bauman, F. 1998. A study of occupant cooling by personally controlled air movement. *Energy and Buildings*. 27(1): 45-59.

[5]   Arens, E.A., Fountain, M.E., Xu, T.F., Miura, K., Zhang, H., Bauman, F.S. 1995. A study of occupant cooling by two types of personally controlled air movement. *Proceedings of PAN Pacific Symposium on Building and Urban Environmental Conditioning in Asia*, Nagoya, Japan, pp. 427-441.

[6]   ASHRAE. ANSI/Standard 55-1992, Thermal environmental conditions for human occupancy. Atlanta: American Society of Heating, Refrigeration and Air-Conditioning Engineers, Inc. 1992.

[7]   ASHRAE. ASHRAE handbook of fundamentals, Chapter 8, American Society of Heating, Refrigerating and Air-Conditioning Engineers, Inc. Atalanta, 1989.

[8]   ASHRAE. Physiological principles and thermal comfort; In ASHRAE handbook of fundamentals. American Society of Heating, Refrigerating and Air-Conditioning Engineers, Inc. Atalanta, 1993.

[9]   ASHRAE. ANSI/Standard 62-2001, Ventilation for acceptable indoor air quality. Atlanta: American Society of Heating, Refrigeration and Air-Conditioning Engineers, Inc. 2001.

[10]   ASHRAE. HVAC design manual for hospital and clinics, ASHRAE Special Project 91, American Society of Heating, Refrigerating, and Air-conditioning Engineers, 2003.

[11]   Awbi, H.B. 1996. A CFD study of the air quality at the breathing zone. *Proceedings of INDOOR AIR'96, the 7th International Conference on Indoor Air Quality and Climate*, Nagoya, Japan 1996; 2:1009-1014.

[12] Awbi, H.B. 1998. Calculation of convective heat transfer coefficients of room surfaces for natural convection. *Energy and Buildings* 28(2):219-227.

[13] Badeau, A., Afshari, A., Goldsmith, T., Frazer, D. 2002. Preliminary prediction of flow and particulate concentration produced from normal human cough dispersion. *Proceedings of the Second Joint EMBS/BMES Conference*, Houston, TX, USA, pp.23-26.

[14] Bauman, F.S. 1999. Giving occupants what they want: guidelines for implementing personal environmental control in your building. *Proceedings of World Workplace 99*, October 3-5, Los Angeles, CA.

[15] Bauman, F.S., Arens, E.A., Fountain, M., Huizenga, C., Miura, K., Xu, T., Akimoto, T., Zhang, H., Faulkner, D., Fisk, W., Borgers, T. 1994. Localized thermal distribution for office buildings, final report-phase Ⅲ, Center for Environmental Design Research, University of California, Berkeley, July, 115pp.

[16] Bauman, F.S., Arens, E.A. 1996. Task/ambient conditioning systems: engineering and application guidelines. Research Report. Center for Environment Design Research, University of California, Berkeley.

[17] Bauman, F.S., Arens, E.A., Tanabe, S., Zhang, H., Baharlo, A. 1995. Testing and optimizing the performance of a floor-based task conditioning system. *Energy and Buildings* 22(3): 173-186.

[18] Bauman, F.S., Carter, T.G., Baughman, A.V., Arens, E.A. 1998. Field study of the impact of a desktop task/ambient conditioning system in office buildings. *ASHRAE Transactions*, 104(part 1b): 1153-1171.

[19] Bauman, F.S., Johnston, L.P., Zhang, H., Arens, E.A. 1991. Performance testing of a floor-based, occupant controlled office ventilation system. *ASHRAE Transactions* 97(part 1): 553-565.

[20] Bauman, F.S., Webster, T. 2001. Outlook for underfloor air distribution. *ASHRAE Journal* 43(6): 20-25.

[21] Bauman, F.S., Zhang, H., Arens, E.A., Benton, C.C. 1993. Localized comfort control with a desktop task conditioning system: laboratory and field measurements. *ASHRAE Transactions* 99(part 2): 733-749.

[22] Berglund, L., Cain, W.S. 1989. Perceived air quality and the thermal environment. *Proceedings of IAQ'89: The Human Equation: Health and Comfort*, San Diego, pp. 93-99.

[23] Betts, P.L., Dafa'Alla, A.A. 1986. Turbulent buoyant airflow in a tall rectangular cavity. *ASME Winter Annual Meeting*, Anaheim, California, HTD-vol.60, pp.83-91.

[24] BjØrn, E. 1999. Simulation of human respiration with breathing thermal manikin. *Proceedings of Third International Meeting on Thermal Manikin Testing*, Stockholm, Sweden, 1:78-81.

[25] BjØrn, E. 2002. Dispersal of exhaled air in stratified surroundings-CFD studies. *Proceedings of ROOMVENT2002*, Copenhagen, Denmark, pp.285-288.

[26] BjØrn, E., Nielsen, P.V. 1998. CFD simulation of contaminant transport between two breathing persons. *Proceedings of ROOMVENT'98*, 1998; 1:133-140.

[27] BjØrn, E., Nielsen, P.V. 2002. Dispersal of exhaled air and personal exposure in displacement ventilated rooms. *Indoor Air* 12:147-164.

[28] Bluyssen, P.M., Lemaire, T. 1992. The distribution of perceived air quality in an office space-computer simulations and sensory evaluations. *Proceeding of ROOMVENT'92, Air Distribution in Rooms*, Aalborg, Denmark, 3:195-211.

[29] Bolashikov, Z., Nikolaev, L., Melikov, A., Kaczmarczyk, J., Fanger, P.O. 2003. New air terminal devices with high efficiency for personalized ventilation application. *Proceedings of Healthy Building 2003*, Singapore, pp. 850-855.

[30] Brager, G. S., and De Dear, R. J. 1998. Thermal adaptation in the built environment: a literature review. *Energy and Buildings* 27(1): 83-96.

[31] Brohus, H. 1997. Personal exposure to contaminant sources in ventilated rooms. Ph.D. thesis, Aalborg University, Denmark.

[32] Brohus, H., Nielsen, P.V. 1995. Personal exposure to contaminant sources in uniform velocity field. *Proceedings of Healthy Buildings'95, the 4th International Conference on Healthy Buildings*, Milan, Italy, 3:1555-1560.

[33] Brohus, H., Nielsen, P.V. 1996. CFD models of persons evaluated by full-scale wind channel experiments. *Proceedings of ROOMVENT'96, the 5th International Conference on Air Distribution in Rooms*, Yokohama, Japan, 2:137-144.

[34] Brohus, H., Nielsen, P.V. 1996. Personal exposure in displacement ventilated rooms. *Indoor Air* 6: 157-167.

[35] Brohus, H. and Nielsen, P.V. 1994. Contaminant distribution around persons in rooms ventilated by displacement ventilation. *Proceedings of ROOMVENT'94*,

The 4th International Conference on Air Distribution in Rooms, Krakow, Poland, pp. 294-312.

[36] CEN. 1998. Ventilation for Buildings: Design Criteria for the Indoor Environment, Brussels, European Committee for Standardization (CR 1752).

[37] Cermak, R., HolsØe, J., Meyer, K.E. Melikov, A.K. 2002a. PIV measurements at the breathing zone with personalized ventilation. *Proceedings of ROOMVENT 2002*, September 8-11, Copenhagen, pp. 349-352.

[38] Cermak, R., Majer, M., Melikov, A.K. 2002b. Measurement and prediction of inhaled air quality with personalized ventilation. *Proceedings of Indoor Air 2002*, pp. 1054-1059.

[39] Cermak, R., Melikov, A.K. 2003. Performance of personalized ventilation in a room with underfloor air distribution system: transport of contaminants between occupants. *Proceedings of Healthy Buildings 2003*, Singapore, pp. 486-491.

[40] Cermak, R., Melikov, A.K. 2006. Air quality and thermal comfort in an office with underfloor, mixing and displacement ventilation, submitted to Journal of Ventilation.

[41] Chang, H., Kato, S., Chikamoto, T. 2004. Effects of outdoor air conditions on hybrid air conditioning based on task/ambient strategy with natural and mechanical ventilation in office buildings. *Building and Environment* 39(2): 153-164.

[42] Chang, S.K.W., Gonzalez, R.R. 1991. Air velocity mapping of environment test chambers. *ASHRAE Transactions* 97(1):31-37.

[43] Chang, S.K.W., Gonzalez, R.R. 1993. Air velocity profiles around the human body. *ASHRAE Transactions* 99(1):450-458.

[44] Charles, K.E. 2003. A review of occupant responses to localized air distribution systems. *Proceedings of Healthy Buildings 2003*, Singapore, pp. 305-310.

[45] Chen, Q. 1995. Comparison of different k-ε models for indoor airflow computations. *Numerical Heat Transfer, Part B* 28:353-369.

[46] Chen, Q., Srebric, J. 2002. A procedure for verification, validation, and reporting of indoor environment CFD analysis. *HVAC&R Research* 8(2):201-215.

[47] Cho, S.H., Kim, W.T., Zaheer-uddin, M. 2001. Thermal characteristics of a personal environment module task air conditioning system: an experimental study. *Energy Conversion and Management* 42: 1023-1031.

[48] Currle, J. 1997. Numerical simulation of the flow in a passenger compartment and evaluation of the thermal comfort of the occupants. SAE Technical Paper Serials 970529.

[49] Davidson, L., Nielsen, P.V. 1995. Calculation of the two-dimensional airflow in facial regions and nasal cavity using an unstructured finite volume solver. ISSN 1395-7953 R9539, Department of Building Technology and Structure Engineering, Aalborg University, Denmark.

[50] de Dear, R.J., Arens, E., Zhang, H., Oguro, M. 1997. Convective and radiative heat transfer coefficient for individual human body segments. *International Journal of Biometeorology* 40(3):141-156.

[51] Dennis, S. 2001. Underfloor air distribution, Engineers newsletter of Trane Company.

[52] Dunnett, S.J. 1994. A numerical study of the factors affecting worker exposure to contaminant. *Journal of Aerosol Science* 25(Suppl.1):481-482.

[53] Fang, L., Clausen, G., Fanger, P.O. 1998a. Impact of temperature and humidity on perception of indoor air quality. *Indoor Air* 8: 80-90.

[54] Fang, L., Clausen, G., Fanger, P.O. 1998b. Impact of temperature and humidity on perception of indoor air quality during immediate and longer whole-body exposures. *Indoor Air* 8(4): 276-284.

[55] Fang, L., Clausen, G., Fanger, P.O. 2000. Temperature and humidity: important factors for perception of air quality and for ventilation requirements. *ASHRAE Transactions* 106(1): 503-510.

[56] Fanger, P.O. 1970. Thermal comfort: analysis and application in environmental engineering. Copenhagen, Danish Technical Press,.

[57] Fanger, P.O. 2000. Indoor air quality in the 21st century: search for excellence. *Indoor Air* 10: 68-73.

[58] Fanger, P.O. 1999. Human requirement in future air-conditioned environments: A search for excellence. *Proceedings of ISHVAC'99*, Shenzhen, China, pp. 86-92.

[59] Fanger, P.O. 2001. Human requirements in future air-conditioned environments. *International Journal of Refrigeration* 24: 148-153.

[60] Fanger, P.O., Banhidi, L., Olesen, B.W., Langkilde, G. 1980. Comfort limits for asymmetric thermal radiation. *ASHRAE Transactions* 86(2):141-156.

[61] Fanger, P.O., Christensen, N.K. 1986. Perception of draught in ventilated spaces. *Ergonomics* 29(2): 215-235.

[62] Fanger, P.O., Ipsen, B.M., Langkilde, G., Olesen, B.W., Christensen, N.K., Tanabe, S. 1986. Comfort limits for asymmetric thermal radiation. *Energy and Buildings* 8(3):225-236.

[63] Fanger, P.O., Melikov, A.K., Hanzawa, H., Ring, J. 1988. Air turbulence and sensation of draught. *Energy and Buildings* 12(1): 21-39.

[64] Faulkner, D., Fisk, W.J., Sullivan, D.P., Wyon, D.P. 1999. Ventilation efficiencies of desk-mounted task/ambient conditioning systems. *Indoor Air* 9: 273-281.

[65] Faulkner, D., Fisk, W.J., Sullivan, D.P. 1993. Indoor air flow and pollutant removal in a room with desk-top ventilation. *ASHRAE Transactions* 99(2): 750-758.

[66] Faulkner, D., Fisk, W.J., Sullivan, D.P. 1995. Indoor air flow and pollutant removal in a room with floor-based task ventilation: results of additional experiments. *Building and Environment* 30(3): 323-332.

[67] Faulkner, D., Fisk, W.J., Sullivan, D.P., Lee, S.M. 2004. Ventilation efficiencies and thermal comfort results of a desk-edge-mounted task ventilation system. *Indoor Air* 14(suppl 8): 92-97.

[68] Fiala, D. 1998. Dynamic simulation of human heat transfer and thermal comfort. PhD dissertation, Institute of Energy and Sustainable Development, De Montfort University, Leicester.

[69] Fisk, W.J., Faulkner, D., Mcneel, P.J. 1990. Indoor air flow and pollutant removal in a room with task ventilation. *Proceedings of the AIVC Conference on Ventilation System Performance*, September 18-21, Belgirate, Italy, pp. 79-99.

[70] Fisk, W.J., Faulkner, D.P., McNeel, P., Bauman, F., Arens,E. 1991. Indoor air flow and pollutant removal in a room with task ventilation. *Indoor Air* 1(3): 247-262.

[71] Fluent Inc. Fluent 6.1 User Manual, 2003.

[72] Fountain, M., Arens, E., de Dear, R., Bauman, F., Miura, K. 1994. Locally controlled air movement preferred in warm isothermal environments. *ASHRAE Transactions* 100(2): 937-952.

[73] Fu, G. 1995. A transient 3-D mathematical thermal model for the clothed human. PhD dissertation, Kansas State University, Manhattan, Kansas.

[74] Fukao, H., Oguro, M., Hiwatashi, K., Ichihara, M. 1996. Environment evaluation in an office with floor-based air-conditioning system in an office building-Thermal environment and IAQ in comparison with ceiling-based air-conditioning system. *Proceedings of ROOMVENT'96, the 5th International Conference on Air Distribution in Rooms*, pp. 315-322.

[75] Gagge, A.P., Stolwijk, J.A.J., Nishi, Y. 1970. An effective temperature scale based on a simple model of human physiological regulatory response. *ASHRAE Transaction* 77(1): 247-262.

[76] Gan, G.H. 1994. Numerical method for full assessment of indoor thermal comfort. *Indoor Air* 4: 154-168.

[77] Gan, G.H. 1998. Prediction of turbulent buoyant flow using an RNG k- ε model. *Numerical Heat Transfer, Part A* 33(2): 169-189.

[78] Gan, G., Awbi, H.B., Croome, D.J. 1993. CFD simulation of the indoor environment for ventilation design. *Presented at the ASME 1993 Winter Meeting-Paper No. 93-WA/HT-49*, New Orleans, USA.

[79] Gao, N.P., Niu, J.L. 2004. CFD study on micro-environment around human body and personalized ventilation. *Building and Environment* 39(7): 795-805.

[80] Gao, N.P., Niu, J.L. 2005. CFD study on the thermal environment around a human body: a review. *Indoor and Built Environment* 14(1):5-16.

[81] Genter, R.E. 1989. Air distribution for raised floor offices. *ASHRAE Transactions* 95(2): 141-146.

[82] Glicksman, L. R., and Taub, S. C. 1997. Thermal and behavioral modeling of occupant-controlled heating, ventilation and air conditioning systems. *Energy and Buildings* 25(3): 243-249.

[83] Gong, N. (2005). Human perception of local air movement in the tropics. PhD thesis, Department of Building, National University of Singapore.

[84] Grivel, F., Candas, V. 1991. Ambient temperatures preferred by young European males and females at rest. *Ergonomics* 34(3): 365-378.

[85] Guan, Y.Z., Jones, B.W., Hosni, M., Gielda, T.P. 2003. Literature review of the advances in thermal comfort modeling. *ASHRAE Transactions* 109: 908-916.

[86] Gwosdow, A.R., Nielsen, R., Berglund, L.G., Dubois, A.B., Tremml, P.G. 1989. Effect of thermal conditions on the acceptability of respiratory protective devices on humans at rest. *American Industrial Hygiene Association Journal* 50(4):188-195.

[87] Hanzawa, H., Nagasawa, Y. 1990. Thermal comfort with underfloor air-conditioning systems. *ASHRAE Transactions* 96(2): 696-698.

[88] Hayashi, J., Akimoto, T., Lee, Sueng-jae., Iesaki, N., Yokota, T., Tanabe, S. 2003. Thermal preference of task environment and its influence on productivity. *Proceedings of Healthy Buildings 2003*, Singapore, pp. 783-790.

[89] Hayashi, T., Ishizu, Y., Kato, S., Murakami, S. 2002a. CFD analysis on characteristics of contaminated indoor air ventilation and its application in the evaluation of the effects of contaminant inhalation by a human occupant. *Building and Environment* 37:219-230.

[90] Hayashi, T., Kato, S., Murakami, S., Yang, J.H. 2002b. CFD analysis on rising stream around a human body and its effect on inhalation air quality. *ASHRAE Transactions* 108(2):1173-1178.

[91] He, G., Yang, X., Srebric, J. 2005. Removal of contaminants released from room surfaces by displacement and mixing ventilation: modeling and validation. *Indoor Air* 15(5): 367-380.

[92] Hedge,A., Michael, A., Parmelee, S.L. 1990. Improving thermal comfort in offices. The impact of underfloor task ventilation. *Proceedings of the Human Factors Society 34th Annual Meeting - Orlando '90*, pp. 537-540.

[93] Heinemeier, K.E., Schiller, G.E., Benton, C.C. 1990. Task conditioning for the workplace: issues and challenges. *ASHRAE Transactions* 96(2): 678-689.

[94] Heinemeier, K., Bauman, F., Schiller, G., Benton, C., Arens, E. 1990. The implication of task conditioning for comfort and energy. *Proceedings of ACEEE Summer Study on Energy Efficiency in Buildings*, 3: 109-118.

[95] Heinsohn, R.J. 1991. Industrial ventilation: engineering principle. ISBN 0-471-63703-3, New York, John Wiley & Sons.

[96] Heiselberg, P., Murakami, S., Roulet, C.A. 1998. Ventilation of large spaces in buildings-analysis and prediction techniques. Annex 26: Energy efficient ventilation of large enclosures, Aalborg University, Aalborg, Denmark.

[97] Henkes, R.A.W.M., Hoogendoorn, C.J. 1995. Comparison exercise for computations of turbulent natural convection in enclosures. *Numerical Heat Transfer, Part B* 28(1): 59-78.

[98] Hiwatashi, K., Akabayashi, S., Morikawa, Y., Sakaguchi, J. 2000. Numerical study of a new ventilation tower system for fresh air supply in an air-conditioned room. *Proceedings of ROOMVENT2000*, UK, 1: 565-570.

[99] Homma, H., Yakiyama, M. 1988. Examination of free convection around occupant's body caused by its metabolic heat. *ASHRAE Transactions* 94:104-124.

[100] Höppe, P. 1981. Temperature of expired air under varying climatic conditions. *International Journal of Biometeorology* 25(2):127-132.

[101] Huang, D.Y. 1977. Physical diagnostics. China Commerce Publishing Co.

[102] Huang, L.J. 2002. Passenger thermal comfort model helps optimized HVAC systems. http://www.cfdreview.com/application/02/08/30/1422240.shtml.

[103] Huizenga, C., Zhang, H., Arens, E. 2001. A model of human physiology and comfort for assessing complex thermal environments. *Building and Environment* 36:691-699.

[104] Hyldgaad, C.E. 1994. Humans as a source of heat and air pollution. *Proceedings of ROOMVENT'94, 4th International Conference on Air Distribution in Rooms*, Krakow, Poland, pp. 413-433.

[105] Hyun, S., Kleinstreuer, C. 2001. Numerical simulation of mixed convection heat and mass transfer in a human inhalation test chamber. *International Journal of Heat and Mass Transfer* 44:2247-2260.

[106] Ichihara, M., Saitou, M., Tanabe, S., Nishimura, M. 1995. Measurement of convective heat transfer coefficient and radiative heat transfer coefficient of standing human body by using thermal manikin. *Proceedings of the Annual Meeting of the Architectural Institute of Japan*, 1:379-380 (in Japanese).

[107] ISO Standard 7730. 1993. Moderate thermal environments-determination of the PMV and PPD indices and specification of the conditions for thermal comfort, International Organization for Standard.

[108] Iwamoto, S. 1996. A study on numerical prediction methods of thermal environment around occupants. *Proceedings of INDOOR AIR'96, the 7th International Conference on Indoor Air Quality and Climate*, Nagoya, Japan, 1:299-303.

[109] Jeong, K. 2003. Thermal characteristics of a partition air supply system at a personal task area. *Proceedings of Healthy Buildings 2003*, Singapore, pp. 86-91.

[110] Jia, Q.X. 2000. Study on dynamization of air supply terminal. Ph.D. thesis, Tsinghua University (in Chinese).

[111] Jones, B.W. 1998. User interactive microclimate control. A new frontier: Environment for innovation. *Proceedings of International Symposium on Advanced Comfort Systems for the Work Environment*, Troy, NY: Rensselaer Polytechnic Institute, pp. 222-229.

[112] Kaczmarczyk, J. 2003. Human response to personalized ventilation, PhD thesis, Department of Mechanical Engineering, Technical University of Denmark.

[113] Kaczmarczyk, J., Zeng, Q.F., Melikov, A.K., Fanger, P.O. 2002a.. Individual control and people's preferences in an experiment with a personalized ventilation system. *Proceedings of ROOMVENT 2002*, September 8-11, Copenhagen, pp. 57-60.

[114] Kaczmarczyk, J., Zeng, Q.F., Melikov, A.K., Fanger, P.O. 2002b. The effect of a personalized ventilation system on perceived air quality and SBS symptoms. *Proceedings of Indoor Air 2002*, pp. 1042-1047.

[115] Kaczmarczyk, J., Melikov, A.K., Fanger, P.O. 2004. Human response to personalized ventilation and mixing ventilation. *Indoor Air* 14(suppl8): 17-29.

[116] Kato, S., Murakami, S., Zeng, J. 1996. Numerical analysis of contaminant distribution around a human body. *Proceedings of ROOMVENT'96, the 5th International Conference on Air Distribution in Rooms*, Yokohama, Japan, 2: 129-136.

[117] Kawahara, Y., Emura, K., Nabeshima, M., Bougaki, K., Kadoya, M. 1999. Air-conditioning with underfloor air supply: comfort in non-uniform thermal environment. *Building Services Engineering Research and Technology* 20(1): 1-7.

[118] Kim, S.W., Chen, C.P. 1989. A multi-time-scale turbulence model based on variable partitioning of the turbulent kinetic energy spectrum. *Numerical Heat Transfer, part B* 16(2): 193-211.

[119] Kohyama, M., Mizuno, M. 1996. Field measurements of the indoor environment of an office with task-ambient air conditioning system. *Proceedings of ROOMVENT96*, *the 5th International Conference on Air Distribution in Room*, July 17-19, pp. 141-148.

[120] Kubo, H., Isoda, N., Yanase, T. 1992. The effects of preferred air velocity on the human body in muggy conditions. *Journal of Architecture Planning and Environment Engineering*, no. 442.

[121] Lai, J.C.S., and Yang, C.Y. 1997. Numerical simulation of turbulence suppression: Comparison of the performance of four k-ε turbulence models. *International Journal of Heat and Fluid Flow* 18(6):575-584.

[122] Lam, C.K.G., Bremhorst, K. 1981. A modified form of the k-ε model for predicting wall turbulence. *Journal of Fluids Engineering* 103(3): 456-460.

[123] Launder, B.E., Spalding, D.B. 1974. The numerical computational of turbulent flows. *Computer Methods in Applied Mechanics and Engineering* 3(2): 269-289.

[124] Li, J. 2004. Characteristic of personalized ventilation and human thermal response, PhD thesis, Tsinghua University (in Chinese).

[125] Li, X., Yang, J., Sun, W. 2005a. Strategy to optimize building ventilation to aid rescue of hostages held by terrorists. Indoor and Built Environment 14(1): 39-50.

[126] Li, Y., Huang, X., Yu, I.T.S., Wong, T.W., Qian, H. 2005b. Role of air distribution in SARS transmission during the largest nosocomial outbreak in Hong Kong. *Indoor Air* 15(2):83-95.

[127] Loftness, V., Brahme, R., Mondazzi, M. 2002. Energy saving potential of flexible and adaptive HVAC distribution systems for office buildings, Research Report. Center for Building Performance and Diagnostics at Carnegie Mellon and Oak Ridge National Laboratory Air Conditioning and Refrigeration Technology Institute.

[128] Loomans, M.G.L.C. 1998. Measurement at and simulation of the (improved) desk displacement ventilation concept. *Proceedings of ROOMVENT'98*, June 14-17, Stockholm, 1: 241-248.

[129] Loomans, M.G.L.C. 1999. Study on the applicability of the desk displacement ventilation concept. *ASHRAE Transactions* 105: 759-768.

[130] Loomans, M.G.L.C., Rutten, P.G.S. 1997. Task conditioning + displacement ventilation, 1+1>2? *Proceedings of healthy buildings/IAQ'97*, Washington DC, USA, pp. 305-310.

[131] Loomans, M.G.L.C., Fabjen, J.R., Mook, van., Rutten, P.G.S. 1996. The introduction of the desk displacement ventilation concept. *Proceedings of ROOMVENT96*, Yokohama, Japan, pp. 99-106.

[132] Loudermilk, K.J. 2003. Temperature control and zoning in underfloor air distribution systems. *ASHRAE Transactions* 109(1): 307-314.

[133] Loudermilk, K.J. 1999. Underfloor air distribution solutions for open office applications. *ASHRAE Transactions* 105(1): 605-613.

[134] Matsunawa, K., Lizuka, H., Tanabe, S. 1995. Development and application of an underfloor air-conditioning system with improved outlets for a 'smart' building in Tokyo. *ASHRAE Transactions* 101(2): 887-901.

[135] Mayer, E., Schwab, R. 1988. Direction of low turbulent airflow and thermal comfort. *Proceedings of Healthy Buildings'88*, Stockholm, Sweden, 2: 577-582.

[136] Melikov, A.K. 1999. Design of localized ventilation. *Proceedings of 20th International Congress of Refrigeration, IIR/IIF*, Sydney, Vol.V (paper 746).

[137] Melikov, A.K. 2004. Personalized ventilation. *Indoor Air* 14(Suppl7): 157-167.

[138] Melikov, A.K., Kaczmarczyk, J., Cygan, L. 2000. Indoor air quality assessment by a "breathing" thermal manikin. *Proceedings of ROOMVENT2000*, pp. 101-106.

[139] Melikov, A.K., Cermak, R., Majer, M. 2001. Personalized ventilation: performance of different air terminal devices. *Proceedings of CLIMA*, CD-ROM, Napoli, Italy, pp. 101-106.

[140] Melikov, A.K., Cermak, R., Majer, M. 2002. Personalized ventilation: evaluation of different air terminal devices. *Energy and Buildings* 34: 829-836.

[141] Melikov, A.K., Cermak, R., Kovar, O., Forejt, L. 2003. Impact of airflow interaction on inhaled air quality and transport of contaminants in rooms with personalized and total volume ventilation. *Proceedings of Healthy Buildings 2003*, Singapore, pp. 592-597.

[142] Melikov, A.K., Halkjaer, L., Arakelian, R.S., Fanger, P.O. 1994a. Spot cooling-part 1: human responses to cooling with air jets. *ASHRAE Transactions* 100(2): 476-499.

[143] Melikov, A.K., Arakelian, R.S., Halkjaer, L., Fanger, P.O. 1994b. Spot cooling-part 2: recommendations for design of spot-cooling systems. *ASHRAE Transactions* 100(2): 500-510.

[144] Melikov, A.K., and Zhou, G. 1996. Air movement at the neck of the human body. *Proceedings of Indoor Air'96, the 7th International Conference on Indoor Air Quality and Climate*, Nagoya, Japan 1:209-214.

[145] Melikov, A.K., Pitchurov, G., Naydenov, K., Langkilde, G. 2005. Field study on occupant comfort and the office thermal environment in rooms with displacement ventilation. *Indoor Air* 15(3): 205-214.

[146] Mihira, K., Toda, H., Arai, H. 1997. Study on thermal manikin. *Japanese Journal of Human Factor* 13(2):47-53.

[147] Murakami, S. 1992. Prediction, analysis, and design for indoor climate in large enclosure. *Proceedings of the Third International Conference on Air Distribution in Rooms*, ROOMVENT'92, Aalborg, Denmark.

[148] Murakami, S. 1998. Overview of turbulence models applied in CWE-1997. *Journal of Wind Engineering and Industrial Aerodynamics* 74-76:1-24.

[149] Murakami, S. 2002. CFD study on the micro-climate around the human body with inhalation and exhalation. *Proceedings of ROOMVENT2002, the 8th International Conference on Air Distribution in Rooms*, Copenhagen, Denmark, 1:23-35.

[150] Murakami, S. 2004. Analysis and design of micro-climate around the human body with respiration by CFD. *Indoor Air* 14(Suppl7): 144-156.

[151] Murakami, S., Kato, S., Zeng, J. 1995. Development of a computational thermal manikin-CFD analysis of thermal environment around human body. *Proceedings of Tsinghua-HVAC'95*, Beijing, 2:349-354.

[152] Murakami, S., Kato, S., Zeng, J. 1996. CFD analysis of thermal environment around human body. *Proceedings of INDOOR AIR'96, the 7th International Conference on Indoor Air Quality and Climate*, Nagoya, Japan, 2:479-484.

[153] Murakami, S., Kato, S., Zeng, J. 1997. Flow and temperature fields around human body with various room air distribution, CFD study on computational thermal manikin-part Ⅰ. *ASHARE Transactions* 103:3-15.

[154] Murakami, S., Kato, S., Zeng, J. 1998. Numerical simulation of contaminant distribution around a modeled human body: CFD study on computational thermal manikin- part Ⅱ. *ASHARE Transactions* 104:226-233.

[155] Murakami, S., Zeng, J., Hayashi, T. 1999. CFD analysis of wind environment around a human body. *Journal of Wind Engineering and Industrial Aerodynamics* 83:393-408.

[156] Murakami, S., Kato, S., Zeng, J. 2000. Combined simulation of airflow, radiation and moisture transport for heat release from a human body. *Building and Environment* 35:489-500.

[157] Myers, J.B., Hosni, M.H., Jones, B.W. 1998. Interaction of air motion with the human body. *ASHRAE Transactions* 104(1B):863-882.

[158] Nakamara, Y., Mizuno, M. 1996. Study on thermal comfort and energy conservation of task-ambient air conditioning system. *Proceedings of ROOMVENT96, the 5th International Conference on Air Distribution in Room*, July 17-19, pp. 91-98.

[159] Nan, G., Sekhar, S.C., Cheong, K.W.D., Tham, K.W. 2003. Exploration of CFD models for personalized ventilation air terminal devices. *Proceedings of Healthy Building 2003*, Singapore, pp. 800-805.

[160] Nielsen, P.V. 1998. The selection of turbulence models for prediction of room airflow. *ASHRAE Transactions* 104(1B):1119-1127.

[161] Nielsen, P.V., BjØrn, E., Brohus, H. 2002. Contaminant flow and personal exposure. *Heating/Piping/Air conditioning Engineering* 74(8): 40-45, 63.

[162] Nielsen, P.V., Jacobsen, T.S., Hansen, R., Mathiesen, E., Topp, C. 2002. Measurement of thermal comfort and local discomfort by a thermal manikin. *ASHRAE Transactions* 108: 1097-1103.

[163] Nilsson, H.O. 2004. Comfort climate evaluation with thermal manikin methods and computer simulation models, PhD thesis, Department of Technology and Built Environment, University of Gälve, Sweden.

[164] Nilsson, H.O., Holmér, I. 2003. Comfort climate evaluation with thermal manikin methods and computer simulation models. *Indoor Air* 13: 28-37.

[165] Niu, J.L. 2005. Indoor ventilation system with personalized ventilation device and its method of usage. United States Patent No. US6, 910,921B2; date of patent: June 28, 2005 (Application No. 10/664,317, filed Sept.17, 2003).

[166] Niu, J.L., van der, Kooi.J. 1992. Grid-Optimization for k-ε turbulence model simulation of natural convection in rooms. *Proceedings ROOMVENT-92: Air Distribution in Rooms - Third International Conference*, 1: 207-223.

[167] Niu, J.L., Gao, N.P., Zuo, H.G. 2004. Ventilation efficiency of personalized ventilation: experimental study. *Proceedings of ROOMVENT2004*, 5-8 September, Coimbra, Portugal.

[168] Niwa, K., Murakami, S., Kato, S., Kondo, Y., Kitamura, N. 1996. Numerical analysis of flow and temperature field with local air conditioning by supply jets from the seats in hall. *Proceedings of ROOMVENT'96, the 5th International Conference on Air Distribution in Rooms*, Yokohama, Japan, 2:307-314.

[169] Nobe, T., Tanabe, S., Tomioka, Y. 2003. Task AC unit operating rate prediction in office. *Proceedings of Healthy Buildings 2003*, Singapore, pp. 725-730.

[170] Omori, T., Yang, J.H., Kato, S., Murakami, S. 2004. Coupled simulation of convection and radiation on thermal environment around an accurately shaped human body. *Proceeding of ROOMVENT 2004*, Coimbra, Portugal.

[171] Reinikainen, L.M., Jaakkola, J.J.K. 2003. Significance of humidity and temperature on skin and upper airway symptoms. *Indoor Air* 13(4): 344-352.

[172] Rodi, W. 1991. Experience with two-layer models combining the k-ε model with a one-equation model near the wall. *AIAA-91-0216, 29th Aerospace Sciences Meeting*, Reno, NV, 1991.

[173] Rohles, F., Konz, S., Jones, B. 1983. Ceiling fan as extender of the summer comfort envelope. *ASHRAE Transactions* 89(1): 245-263.

[174] Roos,A. 1998. The air exchange efficiency of the desk displacement ventilation concept. Theory, measurement and simulations. *Proceedings of ROOMVENT98*, Stockholm, Sweden, pp. 249-256.

[175] Schiller,G., Arens, E., Bauman, F., Benton, C., Fountain, M., Doherty, T. 1988. A field study of thermal environments and comfort in office buildings. *ASHRAE Transactions* 94(2).

[176] Seem, J, E., Braun, J.E. 1992. The impact of personal environmental control on building energy use. *ASHRAE Transactions* 98(2): 903-909.

[177] Sekhar, S.C., Ching, C, S. 2002. Indoor air quality and thermal comfort studies of an under-floor air-conditioning system in the tropics. *Energy and Buildings* 34: 431-444.

[178] Sekhar, S.C., Nan, Gong., Maheswaran, C.R.U., Cheong, K.W.D., Tham, K.W., Melikov, A., Fanger, P.O. 2003a. Preliminary findings of a pilot study of personalized ventilation in a hot and humid climate. *Proceedings of Healthy Buildings 2003*, Singapore, pp. 825-830.

[179] Sekhar, S.C., Nan, Gong., Maheswaran, C.R.U., Cheong, K.W.D., Tham, K.W., Melikov, A., Fanger, P.O. 2003b. Energy efficiency potential of personalized ventilation system in the tropics. *Proceedings of Healthy Buildings 2003*, Singapore, pp. 686-691.

[180] Sekhar, S. C., Gong, N., Tham, K. W., Cheong, K. W., Melikov, A. K., Wyon, D. P., Fanger, P. O. 2005. Findings of personalized ventilation studies in a hot and humid climate. *International Journal of Heating, Ventilating, Air-conditioning and Refrigerating Research* 11(4): 603-620.

[181] Silva, M.C.G., Coelho, J.A. 2002. Convection coefficients for the human body parts determined with a thermal mannequin. *Proceedings of ROOMVENT2002*, Copenhagen, Denmark, 1:277-280.

[182] Smith, C.E. 1991. A transient three-dimensional mode of human thermal system. PhD dissertation, Kansas State University, Manhattan, Kansas.

[183] Sodec, F., Craig, R. 1990. The underfloor air supply system-the European experience. *ASHRAE Transactions* 96(2): 690-695.

[184] Sommer, H.J., Johnen, J., Schongen, P., Stolze, H.H. 1994. Adaptation of the tear film to work in air-conditioned rooms (office eye syndrome). *German Journal of Ophthalmology* 3: 406-408.

[185] SØrensen, D.N. 2002. Radiation between segments of the seated human body. *Proceedings of ROOMVENT2002*, Copenhagen, Denmark, 1:317-320.

[186] SØrensen, D.N., Voigt, L.K. 2003. Modeling flow and heat transfer around a seated human body by computational dynamics. *Building and Environment* 38:753-762.

[187] Stolwijk, J.A.J. 1971. Mathematical model of physiological temperature regulation in man. NASA Contract Rep CR-1855.

[188] Tamblyn, R.T. 1995. Toward zero complaint in air conditioning systems. *HPAC Heating, Piping, Air Conditioning* 67(3).

[189] Tanabe, S., Arens, E.A., Bauman, F.S., Zhang, H., Madsen, T.L. 1994. Evaluating thermal environments by using a thermal manikin with controlled skin surface temperature. *ASHRAE Transactions* 100(1): 39-48.

[190] Tanabe, S., Kimura, K., Inoue, U. 1989. Proposal of evaluation method with thermal manikin. *Annual Meeting of Architecture Institute of Japan* 1:875-876.

[191] Tanabe, S., Kobayashi, K., Nakano, J., Ozeki, Y., Konishi, M. 2002. Evaluation of thermal comfort using combined multi-node thermoregulation (65MN) and radiation models and computational fluid dynamics. *Energy and Buildings* 34: 637-646.

[192] Tham, K.W., Sekhar, S.C., Cheong, D.K.W., Gong, N. 2003. Thermal sensation of tropically acclimatized subjects under fixed air flow of personalized ventilation. *Proceedings of Healthy Buildings 2003*. Singapore.

[193] Tham, K.W., Sekhar, S.C., Cheong, D.K.W., Gong, N. 2003. A case study of quantitative energy efficiency of personalized ventilation in the tropics. *Proceedings of ROOMVENT 2004*, 5-8 September, Coimbra, Portugal.

[194] Tjelflaat, P.O., Knott, R. 1996. A simulation model for thermal comfort of a person in a large enclosure. *Proceedings of INDOOR AIR'96, the 7th International Conference on Indoor Air Quality and Climate*, Nagoya, Japan, 2:1015-1020.

[195] Toftum, J. 2004. Air movement-good or bad? *Indoor Air* 14(Suppl7): 40-45.

[196] Toftum, J., Nielsen, R. 1996. Draught sensitivity is influenced by general thermal sensation. *International Journal of Industrial Ergonomics* 18(4): 295-305.

[197] Tofltum, J., Zhou, G., Melikov, A.K. 1997. Effect of airflow direction on human perception. *Proceedings of CLIMA2000*, September, Brussels.

[198] Toftum, J., JØrgensen, A.S., Fanger, P.O. 1998. Upper limits of air humidity for preventing warm respiratory discomfort. *Energy and Building* 28(1): 15-23.

[199] Toftum, J., Melikov, A., Tynel, A., Bruzda, M., Fanger, P.O. 2003. Human response to air movement-evaluation of ASHRAE's draft criteria (RP-843). *International Journal of HVAC&R Research* 9(2): 187-202.

[200] Topp, C. 2002a. Influence of geometry of a computer simulated person on contaminant distribution and personal exposure. *Proceedings of ROOMVENT2002, the 8th International Conference on Air Distribution in Rooms*, Copenhagen, Denmark, 1:265-268.

[201] Topp, C., Nielsen, P.V., SØrensen, D.N. 2002b. Application of computer simulated persons in indoor environmental modeling. *ASHRAE Transactions* 108(2):1084-1089.

[202] Tsuzuki, K., Arens, E.A., Bauman, F.S., Wyon, D.P. 1999. Individual thermal comfort control with desk-mounted and floor-mounted task/ambient conditioning systems. *Proceedings of Indoor Air 99*, Edinburgh, Scotland, August 8-13, 2: 368-373.

[203] US EPA. 2001. Proposed temporary acute exposure guideline levels (AEGLs). United States Environmental Protection Agency.

[204] Vincent, J.M. 1995. The motion of airborne particles. Oxford: Pergamon. Aerosol Science for Industrial Hygienists, pp. 72-113 [Chapter 4].

[205] Voigt, L.K. 2001. Navier-Stokes simulations of airflow in rooms and around a human body. Ph.D. thesis, Technical University of Denmark.

[206] Walsh, P.C., and Leong, W.H. 2004. Effectiveness of several turbulence models in natural convection. *International Journal of Numerical Methods for Heat & Fluid Flow* 14(5):633-648.

[207] Wang, X.L. 1994. Thermal comfort and sensation under transient conditions. Department of Energy Technology, Stockholm, The Royal Institute of Technology.

[208] Wargocki, P., Wyon, D.P., Baik, Y.K., Clausen, G., Fanger, P.O. 1999. Perceived air quality, Sick Building Syndrome (SBS) symptoms and productivity in an office with two different pollution loads. *Indoor Air* 9(3): 165-179.

[209] Wargocki, P., Wyon, D.P., Sundell, J., Clausen, G., Fanger, P.O. 2000. The effect of outdoor air supply rate in an office on perceived air quality, Sick Building Syndrome (SBS) symptoms and productivity. *Indoor Air* 10: 222-236.

[210] White, F.M. 1991. Heat and mass transfer, New York, Addison-Wesley.

[211] WHO. 2003. Consensus document of the epidemiology of sever acute respiratory syndrome (SARS), Department of Communicable Disease, Surveillance and Response, WHO/CDS/CSR/GAR/2003.11.

[212] Wolkoff, P., Nojgaard, J.K., Troiano, P., Piccoli, B. 2005. Eye complaints in the office environment: precorneal tear film integrity influenced by eye blinking efficiency. *Occupational and Environmental Medicine* 62(1): 4-12.

[213] Wright, N.G., Eason, G.J. 1999. Comparison of several computational turbulence models with full-scale measurements of flow around a building. *Wind and Structures* 2(4): 305-323.

[214] Wyon DP. 1994. Thermal gradients, individual differences and air quality, Proceedings of the Healthy Buildings, Budapest, Vol.2, pp 765-770.

[215] Wyon, D.P. 1996. Individual microclimate control: required range, probable benefits and current feasibility. *Proceedings of Indoor Air'96, the 7th International Conference on Indoor Air Quality and Climate*, Nagoya, Japan, pp. 1067-1072.

[216] Wyon, D.P., Sandberg, M. 1996. Discomfort due to vertical thermal gradients. *Indoor Air* 6(1): 48-54.

[217] Wyon, D.P., Larsson, S., Forsgren, B., Lundgren, I. 1989. Standard procedures for assessing vehicle climate with a thermal manikin. SAE Technique Paper Series 890049, pp. 1-11.

[218] Xing, H., Hatton, A., Awbi, H.B. 2001. A study of the air quality in the breathing zone in a room with displacement ventilation. *Building and Environment* 36:809-820.

[219] Xia, Y.Z., Niu, J.L., Zhao, R.Y., Burnett, J. 2000. Effects of turbulent air on human thermal sensations in a warm isothermal environment. *Indoor Air* 10(4): 289-296.

[220] Xu, Y.W. 1995. Fluid mechanics, pump and fan. China Architecture and Industry Press (in Chinese).

[221] Xue, H., Kang, Z.J., Bong, T.Y. 1999. Coupling of three-dimensional field and human thermoregulatory models in a crowded enclosure. *Numerical Heat Transfer, Part A* 36(6): 601-613.

[222] Yakhot, V., Orszag, S.A. 1986. A renormalization group analysis of turbulence. *Journal of Scientific Computing* 1(1):1-51.

[223] Yakhot, V., Orszag, S.A., Thangam, S., Gatski, T.B., Speziale, C.G. 1992. Development of turbulence models for shear flows by a double expansion technique. *Physics of Fluids, Part A Fluids Dynamics* 4(7): 1510-1520.

[224] Yamashita, K., Tochihara, Y., Kondo, Y., Takayama, S., Nagayama, H. 2005. Thermal sensation and comfort during exposure to local airflow to face or legs. *Journal of Physiological Anthropology and Applied Human Science* 24(1): 61-66.

[225] Yang, J.H., Kato, S., Hayashi, T., Murakami, S. 2002. Measurement of local convective heat transfer coefficients of the human body in outdoor and indoor

environments. *Proceedings of ROOMVENT2002*, Copenhagen, Denmark, 1:281-284.

[226] Yang, J.H., Kato, S., Chikamoto, T. 2004. Air flow measurement around human body with wide-cover personal air conditioning. *Proceedings of ROOMVENT 2004*, 5-8 September, Coimbra, Portugal.

[227] Yang, J.R., Kaczmarczyk, J., Melikov, A.K., Fanger, P.O. 2003. The impact of a personalized ventilation system on indoor air quality at different levels of room air temperature. *Proceedings of Healthy Building 2003*, Singapore, pp. 345-350.

[228] Yang, J.R., Melikov, A.K., Fanger, P.O., Li, X.T., Yan, Q.S. 2002. Impact of personalized ventilation on human response: comparison between constant and fluctuating airflows under warm condition. *Proceedings of ROOMVENT 2002*, September 8-11, Copenhagen, pp. 305-308.

[229] Zeng, Q.F., Kaczmarczyk, J., Melikov, A.K., Fanger, P.O. 2002. Perceived air quality and thermal sensation with a personalized ventilation system. *Proceeding of ROOMVENT 2002*, September 8-11, Copenhagen, pp. 61-64.

[230] Zhao, B., Zhang, Z., Li, X. 2004. Numerical study of the transport of droplets or particles generated by respiratory system indoors. *Building and Environment* 40(8):1032-1039.

[231] Zhang, H. 2003. Human thermal sensation and comfort in transient and non-uniform thermal environments, PhD thesis, CEDR, University of California at Berkeley.

[232] Zhang, H., Huizenga, C., Arens, E., Yu, T. 2005. Modeling themal comfort in stratified environment. *Proceedings of Indoor Air 2005*, September 4-9th, Beijing, China, pp 133-137.

[233] Zhang, Y. 2005. Effect of local exposure on human responses, PhD thesis, Tsing Hua University (in Chinese).

[234] Zhou, G. 1999. Human perception of air movement, PhD thesis ET-PhD-99-01, International Centre for Indoor Environment and Energy, Department of Energy Engineering, Technical University of Denmark.

[235] Zhou, W., Tham, K. W., Sun, W. 2005. Performance evaluation and comparison of two air terminal devices for personalized ventilation. *Proceedings of Indoor Air 2005*, Beijing, pp. 436-441.

[236] Zhu, J., Ito, H., Nakahara, N. 1995. Thermal comfort and energy saving of personal air-conditioning system using fluctuating air movement. *Proceedings of Indoor Air Quality-Ventilation and Energy Conservation in Buildings-The 2nd International Conference*, May 9-12, Montreal, Canada, pp. 785-792.

[237] Zhu, S., Kato, S., Murakami, S., Hayashi, T. 2004. Study on inhalation region by means of CFD analysis and experiment. *Building and Environment* 40(10): 1329-1336.

[238] Zuo, H.G. 2003. Experimental study of personalized air system for the reduction of pollutant exposure, Master thesis, Department of Building Services Engineering, The Hong Kong Polytechnic University.

[239] Zuo, H.G., Niu, J.L., 2002. Chan, D. Experimental study of facial air supply method for the reduction of pollutant exposure. *Indoor Air 2002-The Ninth International Conference on Indoor Air Quality and Climate*, Monterey, California, pp. 1090-1095.

List of publications

Journal publications

[1]   Gao N P and Niu J L (2004) CFD study on micro-environment around human body and personalized ventilation. Building and Environment, Vol. 39, pp.795-805.

[2]   Gao N P and Niu J L (2005) CFD study of the thermal environment around a human body: a review. Indoor and Built Environment, Vol.14, no.1, pp. 5-16.

[3]   Gao N P and Niu J L (2005) Modeling the performance of personalized ventilation under different conditions of room air and personalized air. Journal of HVAC&R Research, Vol.11, no.4, pp. 587-602.

[4]   Gao N P and Niu J L (2005) Transient CFD simulation of the respiration process and inter-person exposure assessment. Building and Environment, Vol.41, no. 9, pp. 1214-1222.

[5]   Niu J L, Gao N P, Ma P, Zuo H G (2005) Experimental study on a chair-based personalized ventilation system. Building and Environment, in press.

[6]   Gao N P, Niu J L, Zhang H (2006) Coupling CFD and human body thermoregulation model for the assessment of personalized ventilation. Journal of HVAC&R Research, Vol. 12, no.3, pp. 497-518.

[7]   Gao N P, Niu J L and Zhang H (2006) Investigating indoor air quality and thermal comfort using a numerical thermal manikin. Indoor and Built Environment, in press.

Conference publications

[1]   Niu J L, Gao N P, Zuo H G (2004) Ventilation efficiency of personalized ventilation: experimental study. Proceedings of ROOMVENT2004, Coimbra, Portugal.

[2]   Gao N P, Niu J L (2004) Ventilation efficiency of personalized ventilation: CFD study. Proceedings of ROOMVENT2004, Coimbra, Portugal.

[3]   Gao N P, Niu J L (2005) Modeling the performance of personalized ventilation under different room airflows. Proceedings of Building Simulation 2005, Montreal, Canada.

[4]   Gao N P, Niu J L (2005) CFD study on personal exposure with personalized ventilation system. Proceedings of Indoor Air 2005, Beijing, China.